ABSTRACT

Title of Document: ROLE OF BENZENE, TOLUENE AND XYLENE TO ACID GAS DESTRUCTION IN THERMAL STAGE OF CLAUS REACTORS

Salisu Ibrahim, Ph.D.

Directed By: Ashwani K. Gupta,
Distinguished University Professor,
Department of mechanical Engineering

Crude oil and natural gas often contain acid gases (H_2S and CO_2) and trace amounts of benzene, toluene and xylene (BTX) and these are all harmful to human health, environment and industrial equipment. Acid gases in chemical industry and vehicles cause corrosion to parts of engines, refinery equipment and catalysts deactivation in catalytic processes. Human exposure to H_2S, even in low concentrations, causes burning of eyes, headache, dizziness, dyspnea, and skin irritations. Inhalation of high doses of BTX may cause skin and respiratory tract irritation. Increased energy demand and exploitation of sourer feedstock have made

regulatory agencies worldwide to promulgate stricter regulations on sulfur emissions. US EPA requires a reduction of sulfur in gasoline from 30ppm to 10ppm by 2017. Crude oil and gas must be subjected to more efficient desulfurization processes. The separated acid gases and BTX is further processed in Claus process for chemical and energy recovery.

Currently, BTX poses several technical and operational problems that result in higher operational costs and increased toxic gas emissions in Claus plants. BTX destruction in the thermal stage of Claus process was identified as the solution. Acid gas and BTX combustion in thermal stage of Claus reactor, which provides simultaneous recovery of both sulfur and thermal energy, is the subject of this research. Effect of BTX in H_2S fueled flames on sulfur chemistry in thermal stage of a Claus reactor was characterized. Reactor conditions that promote BTX destruction are presented. Oxygen enriched combustion air for the destruction of BTX and acid gas is examined. Chemical kinetic pathways of BTX destruction under high temperature conditions of the Claus reactor are evaluated. Intermediate radicals and stable species formed during the combustion process are characterized using flame emission spectroscopy and gas chromatography (GC). Role of multiple contaminants, CO_2 and benzene, toluene or xylene in H_2S combustion is also investigated. Chemical kinetic pathways and reactor conditions that promote/hinder the formation of mercaptans (such as COS and CS_2) is addressed. The results presented here assist in the design guidelines of advanced Claus reactors for enhanced sulfur capture in the thermal stage and to mitigate environmental issues.

ROLE OF BENZENE, TOLUENE AND XYLENE TO ACID GAS DESTRUCTION IN THERMAL STAGE OF CLAUS REACTORS

By

Salisu Ibrahim

Dissertation submitted to the Faculty of the Graduate School of the

University of Maryland, College Park, in Partial Fulfillment

of the Requirements for the Degree of

Doctor of Philosophy

2015

Advisory Committee:

Professor Ashwani K. Gupta, Chair

Professor Jungho Kim

Associate Professor Nam S. Wang, Dean's Representative

Associate Professor Bao Yang

Associate Professor Ahmed S. Al Shoaibi

Dedication

This dissertation is dedicated to Almighty Allah for giving me the strength to complete this work, my parents (Ahmadu Ibrahim Guja and Mairo Ibrahim) for their mental support, my mentors for believing in my abilities, and all well-wishers.

Acknowledgments

This dissertation represents the result of my fruitful experience at the Combustion Engineering laboratory, University of Maryland College Park. I am sincerely grateful to Professor Ashwani K. Gupta for offering me the opportunity to work in Combustion Engineering laboratory. Professor Gupta's consistent demand for hard-work and productivity shaped my research aptitude and confidence that resulted in the timely completion of this dissertation. I am also very grateful to Associate Professor Ahmed S. Al Shoaibi of the Petroleum Institute Abu Dhabi who encouraged and supported me to join the PhD program at University of Maryland. Associate Professor Al Shoaibi has continued to inspire and support me throughout the course of my PhD program. He offered valuable contributions and supported in sourcing the finances used for this research investigation. My sincere appreciation also goes to members of my dissertation committee, Professor Jungho Kim, Associate Professor Nam S. Wang and Associate Professor Bao Yang for their efforts, advice and support.

I would like to extend my gratitude to the current and former team members of the Combustion Engineering laboratory. They offered me great support and valuable input, especially in setting up my experiments. The enormous gratitude to my parents cannot be expressed in words. It has been over a decade since I left them in pursuit of my academic and career development. I sincerely appreciate their relentless support and patience while away from them. Also, I would like to thank my fiancée, Zainab A. Auwal for her support and understanding during the most stressful

part of my PhD program. I would like to extend my gratitude to my friends for their support and encouragements. Finally, I acknowledge the research and financial support provided by The Petroleum Institute, Abu Dhabi, ADNOC and GASCO.

Table of Contents

List of Tables

List of Figures

Numenclature

Nomenclature

d	Burner outer diameter
D	Burner inner diameter
Φ	Equivalence ratio
W	Dimensionless axial distance

Subscripts

In	Inner
Jet	burner inner jet
Out	Outer

Chapter 1 Introduction

Sulfur is often present in the form of acid gases (H_2S and CO_2) in industrial and crude natural gas, which exists mainly as an undesirable by-product of gas processing in chemical industries (Nehlsen, 2006). Acid gases contain other impurities that include lower series of hydrocarbons (C_1-C_4), benzene, toluene and xylene (BTX), N_2, NH_3, CS_2 and COS (Deixonne et al., 2010; Gargurevich, 2012). The pernicious H_2S fumes that characterize many gas processing and operation sites of refinery and petroleum production represent a genuine threat to human health and our environment. Concentration levels of H_2S vary significantly depending on the source of supply. For instance, H_2S absorbed from amine treatment of natural gas or refinery gas, can contain 30-90% H_2S by volume or higher (Rameshni, 2010). Many other processes can produce H_2S with very small concentration, but in quantities that cannot be discharged into the atmosphere due to its hazardous effects (Tyndall & Ravishankara, 1991).

1.1 Environmental and Health Challenges of Acid Gas

The presence of H_2S, BTX and other impurities in crude oil and natural gas causes negative effects on the environment, human health and process equipment. Any fuel containing impurities cannot be used in chemical to thermal energy transformation due to the adverse effect of the byproducts generated.

From environmental perspective, acid gas, particularly H_2S and BTX have serious negative effects. This is because combustion of H_2S and BTX produces highly

toxic byproducts, such as sulfur dioxide, sulfuric acid, sulfurous acid, carbon monoxide, carbonyl sulfide, carbon disulfide, particulate matters (PM) and Polycyclic aromatic hydrocarbons (PAH). These byproducts affect air quality and are also considered major source of acidic precipitation (Kohl, 1997). Other formed sulfurous-carbonaceous compounds that include COS and CS_2 reach the stratosphere and generate sulfate aerosol layer, which affect the ozone concentration negatively (Crutzen, 1976). Sulfur compounds in chemical industry and vehicles also cause corrosion to parts of refineries and combustion engines because of the formation of oxy-acids of sulfur from combustion products. Also, sulfur compounds are undesirable in refining processes since they deactivate catalysts used downstream to upgrade fuel quality.

From Health perspective, acid gas causes numerous hazards to human health depending on the concentration and level of exposure. Low concentrations of H_2S can cause burning and tearing of eyes, headache, dizziness, dyspnea, and skin and throat irritations (Khol and Nielsen, 1997). High exposure to H_2S can cause asphyxiation, loss of consciousness and death (Nielsen, 1997). The particulate matter present in diesel exhaust can cause high levels of lung cancer in humans, aggravation of respiratory and cardiovascular diseases, existing asthma and chronic bronchitis (Nielsen, 1997; Wall, 2013). According to the health administration (OSHA), exposure to 10ppm or less of H_2S is classified as low-hazard, while greater than 10ppm and less than 30ppm exposures is considered medium-hazard, and H_2S exposures higher than 30ppm is designated as high-risk. On the other hand, BTX is not acutely toxic by inhalation, oral or dermal route of exposure. However, high

exposure to BTX vapors can cause central nervous system effects, such as drowsiness and lightheadedness and, based on data on some of the components, inhalation of very high doses of BTX may cause skin and respiratory tract irritation (Chevron Philips). Prolonged and repeated exposure to high concentrations of BTX may cause adverse effects in several organ systems, developmental toxicity and cancer (Chevron Philips).

1.2 Regulation on Sulfur Content in Fuels

In an effort to produce cleaner air with sulfur-bearing fuels, limits are placed on sulfur content in fuels and more stringent regulations on emission of pollutants from the combustion of H_2S and BTX are promulgated by various environmental regulatory agencies worldwide. The US EPA reduced the maximum allowable sulfur content in non-road diesel fuel from average of 3400ppm to 500ppm in 2007 and further to 15ppm in 2010. The highway diesel fuel was also reduced from current 500ppm down to 15ppm (per-gallon average) in June 2012 (Srivastava, 2012). More recently, the US EPA announced a new regulation that mandates oil and gas refiners to reduce sulfur content in gasoline from the current limit of 30ppm down to 10ppm by 2017 (Wall, 2013). A decade ago, the United States gasoline contained 300ppm of sulfur, but earlier regulations required refiners to cut the sulfur content by 90 percent, down to the current 30ppm.

The mobile source air toxics rules was also promulgated by the US EPA in 2007 to reduce benzene and other aromatics content in gasoline to further reduce hazardous air pollutants emitted by motor vehicles (Wall, 2013). The major air toxics

of concern are BTX and other hydrocarbons such as 1, 3-butadiene, formaldehyde, acetaldehyde, acrolein and naphthalene. Oil and gas refineries are facing major challenges to meet the new fuel sulfur specification along with the required reduction of aromatics content. These requirements are expected to be more stringent in the future, therefore putting pressure on oil and gas companies to develop deep desulfurization processes and more environmentally-friendly technologies. Some of the developed sulfur removal technologies include hydro-desulfurization (HDS), oxidative desulfurization (ODS), bio catalytic desulfurization (BDS) and amine extraction process.

1.3 Separation of Acid Gas from Crude oil and Gas

A brief summary is given on some of the technologies currently deployed to achieve deep desulfurization from crude oil and gas.

1.3.1 Hydro-Desulfurization

Hydro-desulfurization (HDS) is a commercially proven technology that uses catalytic chemical process to remove sulfur from natural gas and refined petroleum products that include gasoline or petrol, jet fuel, kerosene and diesel fuel. It also favors removal of nitrogen compounds and some metal impurities (Srisvastava, 2012). The HDS process involves catalytic treatment with hydrogen to convert the various sulfur compounds to H_2S and sulfur-free organic compounds. The HDS reactor is operated at elevated temperatures ranging from 573 to 673K and elevated pressures ranging from 30 to 130atm (Song, 2003; Srisvastava, 2012).

The catalysts consist of an alumina base impregnated with cobalt and molybdenum. In this process, sulfur is converted to H_2S, which is then removed from the flue gas by amine scrubbing. The H_2S resulting from the HDS reaction is eventually subjected to further treatment in a modified Claus process plants to recover elemental sulfur and energy. HDS is the primary desulfurization technology used today, although caustic washing to remove low molecular weight thiols is also in use (Song, 2003). It is desirable for refineries to desulfurize both distillate streams generated during direct distillation of crude oil and streams coming out from conversion units such as fluid catalytic cracking (FCC) and hydrocracker units. Although HDS can be performed either before FCC or after, depending on the refinery design, it must be performed before catalytic reforming process to prevent the poisoning of catalysts (Pt) by sulfur (Song, 2003).

HDS is an expensive technology that is energy intensive and requires huge amounts of high purity hydrogen as reactant (Bonde, 2000; Song, 2003). Interest in HDS was initially triggered by the availability of hydrogen from catalytic reformers (Nehlsen, 2006). However, it is also widely acknowledged that HDS helps improve the fuel properties, as it favors a higher distillate to residual fuel oil ratio, in addition to the sulfur removal from crude oils (Srivastava, 2012; Song, 2002; Wall, 2013). This makes HDS more attractive in the light of increasing requirements for deep sulfur removal.

1.3.2 Oxidative Desulfurization

Oxidative desulfurization (ODS) technology is used for the production of ultra-low sulfur diesel at low costs (Babich et al., 2003, Song et al., 2004). Pioneering

companies such as BP, Texaco, Shell have been developing suitable ODS technologies to obtain ultra-low sulfur fuels (BP, 2012; Srivastava, 2012). The ODS is typically a two stage process that include oxidation, followed by liquid extraction. In ODS, heavy sulfides are oxidized by adding one or two oxygen atoms to the sulfur using suitable oxidants to avoid breaking of any carbon–sulfur bonds. This results in the formation of sulfoxide and sulfone compounds that are then extracted or adsorbed from the light oil due to their increased relative polarity (Tam et al., 2002). In addition, it also facilitates their separation, not only by extraction, but also by distillation or adsorption (Otsuki et al., 2000). Refineries commonly use solvent extraction technology to remove sulfur and nitrogen compounds from light oil. The solvent is recovered and regenerated through distillation process (Guth and Diaz, 1974; De Souza and co-workers, 2009). Because of the minimal difference in polarity between sulfur and other aromatic hydrocarbons, solvent extraction causes associated loss of useful hydrocarbons along with sulfur removal (Babich et al, 2003). The sulfoxides and sulfones produced after ODS exhibit increased relative polarity and are preferentially extracted from light oil using a non-miscible solvent. The extraction efficiency depends on the solvent's polarity (Otsuki et al., 2000; Song, 2002). Other criteria for the selection of suitable solvents include boiling point, freezing point and surface tension. The solvent is separated from the oxidized compounds by simple distillation for recycling and regeneration. Some common water-soluble polar solvents used are dimethyl sulfoxide (DMSO), dimethylformamide (DMF) and acetonitrile. The former two solvents have a high extractability for sulfones, but also

have a high boiling point (573K). This is close to the boiling point of the sulfones, which creates difficulty in separation and regeneration for further extraction.

ODS process has more advantages when compared to HDS technology. The capital expenditure for ODS is less than that of HDS, as different fractions can be oxidized under low temperature and pressure conditions, and expensive hydrogen is not required (Babich et al., 2003, Song, 2002).

1.3.3 Bio-Catalytic Desulfurization

Bio-desulfurization (BDS) is a technological process that utilizes special protein-based biocatalysts to remove sulfur compounds from crude oil. This technology has drawn wide attention because of its green processing of fossil fuels for sulfur removal (Borge et al., 2003). The BDS process involves the use of a continuously fed, well stirred reactor to bring into contact mixtures of air, whole cell, oil and water to produce desulfurized oil stream free of water and biocatalyst cell (Armstrong et al., 1995; Gupta et al., 2005). BDS technology is cheaper than HDS, as the former requires less energy and hydrogen. The BDS reactor is operated under ambient temperature and pressure with high selectivity, which results in decreased energy costs, low emission and minimal formation of undesirable side products (Gupta et al., 2005).

1.3.4 Adsorptive Desulfurization (ADS)

Adsorption has been deployed in the oil and gas industry to achieve deep sulfur removal from sulfur-bearing fuels. The removal of sulfur compounds and dibenzothiophenes (DBT) has been studied over zeolites, aluminosilicates, activated carbon (AC), alumina and zinc oxide catalysts (Tarawa et al., 2001; Bezverkhyy et

al., 2008). The use of hydrogen during adsorptive desulfurization has also been identified as a suitable technique that combines the benefits of catalytic HDS with ADS (Tarawa et al., 2001). This process is called Reactive adsorption desulfurization (RADS). RADS technology is based on reactive adsorption, wherein sulfur is captured in the form of metal sulfides using metal-based adsorbents. The formed metal sulfide is then processed in a separate regeneration reactor. This technology is currently used to achieve deep diesel and gasoline desulfurization. ConocoPhillips is using a process called S-Zorb Diesel and S-Zorb Gasoline process for naphtha, which are based on RADS (Michael and Bruce, 1991). The S-Zorb for diesel contacts diesel fuel streams with a solid sorbent in a fluid bed reactor at relatively low pressures and temperature in the presence of hydrogen. The sulfur atoms of the sulfur-containing compounds adsorb onto the sorbent and then react. ConocoPhillips' S-Zorb Gasoline technology operates at low pressure and elevated temperatures.

Compared to HDS, the ADS process occurs at lower temperatures (Tarawa et al., 2001; Srivasta, 2012). Also, in RADS, the amount of hydrogen consumed in the process is low. While the adsorption process in ADS is highly effective, the development of adsorbents that is easy to regenerate, but also exhibit high adsorption capacity for sulfur compounds remain a major challenge (Hernandez and Yang, 2004).

1.3.5 Amine Extraction

Separation of acid gas from crude natural gas commonly takes place through amine extraction process (Tyndall & Ravishankara, 1991; Wayne, 1985; Jensen & Webb, 1995; El-Bhishtawi &Haimour, 2004). In this process, the sour gas is passed

over an aqueous solution of alkanolamines, wherein the CO_2 and H_2S (acid gases) are absorbed from the up flowing sour gas to produce sweetened gas stream (i.e., H_2S free natural gas). The concentration of H_2S and CO_2 is proportional to their partial pressures in the sour gas (Jensen and Webb, 1995). The alkanolamines used in the amine extraction process are organic chemical components that consist of at least one hydroxyl and amino groups. Each of these two groups has its own role in the process, wherein the hydroxyl group reduces pressure of the vapor in the aqueous solution in order to increase the water solubility. On the other hand, the amino group provides the required alkaline medium in this aqueous solution in order to increase the tendency of the acidic gases absorption. The most common, which have been widely used commercially are monoethanolamine (MEA), diethanolamine (DEA), and methyldiethanolamine (MDEA) (El-Bhishtawi & Haimour, 2004). Amines, which contain two hydrogen atoms attached to the nitrogen atom, are called primary amines such as (MEA), while amines which contain only one hydrogen atom attached to the nitrogen atom are called secondary amines such as (DEA), and the amines which contain no hydrogen atoms are called tertiary amines such as (MDEA) (Jensen and Webb, 1995).

1.4 Treatment of Acid Gas

As the need for deep sulfur removal gains more momentum, the volume of generated acid gas and associated impurities is expected to increase. Moreover, lighter feedstocks are becoming scarce, and increased amounts of sourer feedstock are exploited. The produced acid gas subsequently requires efficient treatment to recover

energy, sulfur and other valuable chemicals. Therefore, there is need to increase the processing capacity of existing gas-treating technologies, while developing alternative processes for valuable chemical and energy recovery from acid gas.

Claus process, shown in figure 1-1, is widely used to recover sulfur and thermal energy from acid gases (Khudenko et al., 1993; Clark et al., 2000). Beside the Claus process, many commercial processes based on adsorption, absorption, and wet oxidation are used. A comparative analysis of the different sulfur recovery processes in commercial operation was reported by John, 2012. Also, a novel chemical-looping process has been developed for converting sulfur dioxide (SO_2) in the flue gas generated from industries to elemental sulfur using oxygen carriers (such as Ca-based or Cu-based).

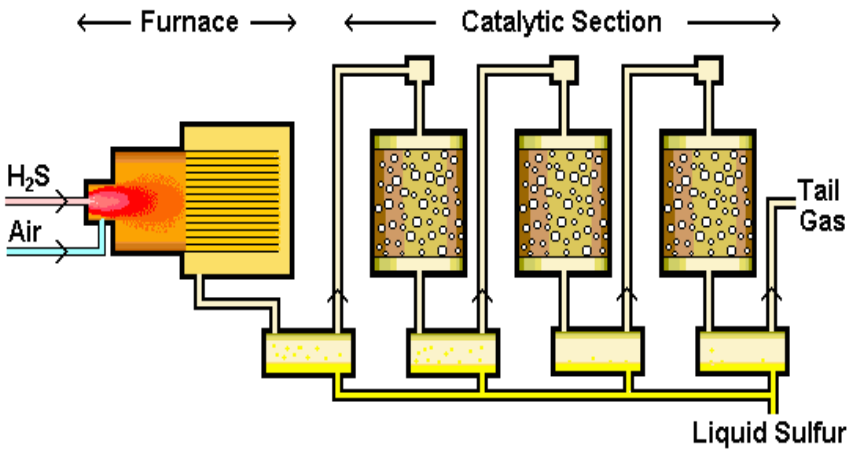

Figure 1-1. Claus Process (Sulfotech)

The selection of gas-treating process depends on many factors that include the volume, temperature and pressure of gas to be processed, required selectivity, sulfur recovery levels desired, types and concentrations of impurities present, emission regulations to be met, and capital and operating costs. The modified Claus technology

has the highest efficiency at 95% to 99.8%, as well as the least hazards. It is also a more reliable and mature technology when compared to other process types (Clark et al., 1998, 2000; John, 2002). The adsorption process is limited to low volumetric flow of acid gas. Only the Claus process can treat large amounts of feed gas with high H_2S concentration, and produce minimum ecological impact with a tail-gas treatment unit. Claus process is commonly divided into two stages; thermal stage and catalytic stage.

4.4.1 Claus Thermal Stage

In the thermal stage, reaction between H_2S and O_2 occurs in a Claus furnace, under rich conditions (Equivalence ratio of three) to form elemental sulfur (S_2) (Selim et al., 2011a, 2013). During this reaction, one-third of the H_2S is burned to form SO_2 (reaction 1-1). The reaction then continues between SO_2 and unreacted H_2S, in ratio 2:1 to produce sulfur (reaction 1-2), which is captured in liquid or solid state. The Claus furnace is operated at temperatures from 1027-1477K, and products from this step include: sulfur dioxide, water and unreacted H_2S and other byproducts.

$$H_2S + 1.5O_2 = H_2O + SO_2;\ Hr = -518\ kJ/mol \qquad (1\text{-}1)$$

$$2H_2S + SO_2 = 1.5\ S_2 + 2H_2O;\ Hr = 47\ kJ/mol \qquad (1\text{-}2)$$

Additionally, some of the sulfur dioxide produced here reacts with hydrogen sulfide inside the furnace to produce sulfur, and this accounts for the greater percentage of total sulfur production (reaction 1-2). The furnace products flow then into a waste heat boiler to condense the sulfur and produce high pressure steam for the Claus catalytic stages.

1.4.2 Claus Catalytic Stage

The remaining H_2S from the Claus furnace is reacted with SO_2 at lower temperatures (about 470-620K) over an alumina- or titanium dioxide-based catalyst to produce more sulfur. In the catalytic stage, mostly S_8 is produced, which is an exothermic reaction whereas in the thermal stage S_2 is the major product (Sassi & Gupta, 2008; Selim et al., 2012a). Other allotropes of sulfur may also be present in smaller quantities. About 60-70% of elemental sulfur, on the average, is produced from reaction 1-2 (Sassi & Gupta, 2008). Reaction 1-2 is exothermic and a cooling stage is needed following these steps in order to condense the sulfur produced. The condensed phase is then separated from the gas stream by draining it into a container.

The basic Claus process has a sulfur recovery efficiency of about 94% to 98% (Sulfotech). However, many improvements have been developed and the modified Claus process achieves 99+% of H_2S conversion efficiency. A tail gas clean-up process is often used (John, 2002). An example is the amine-based tail-gas clean-up process, which reduces all the sulfur compounds in the tail-gas leaving the front-end Claus sulfur plant back to H_2S, then uses selective amine absorption to remove the H_2S while allowing most of the carbon dioxide to slip. The H_2S and carbon dioxide removed by the amine are stripped from the amine and recycled back to the Claus plant, allowing an overall sulfur recovery in excess of 99.5% (El-Bishtawi & Hairmour, 2004).

The efficiency of Claus process and the quality of produced sulfur can vary significantly depending on the acid gas composition, rector design configuration and operational conditions (Slavens et al., 2010; Deixonne & Sharma, 2010; Rameshni,

2010). Acid gas composition varies significantly depending on the desulfurization unit. The variation could become wider as the world is shifting towards utilization of heavier and sourer feedstock with higher content of acid gas and other contaminants, due to depletion of light and sweet feedstock. As a result, there is significant demand for improved energy and sulfur recovery efficiency in both new and existing gas processing plants and refineries, while reducing health and environmental burden.

To improve the efficiency of Claus process, the understanding of reaction chemistry, especially in the thermal stage reactor is crucial (Gargurevich, 2005; Selim, 2012a&b; Clark et al., 2000). The chemistry of H_2S combustion is highly desirable for the optimization of Claus process plants. Other practical challenges associated with the non-uniformity of acid gas feed decrease the Claus process efficiency significantly and results in increased emissions (Salvens et al., 2010). Previous researchers have identified the chemistry of thermal stage reactor as the least understood, but yet most capable of improving the process efficiency (Clark et al., 2000). Considerable effort has been made to understand and elucidate hydrogen sulfide combustion with emphasis on the chemical kinetics and reaction pathways of hydrogen sulfide combustion under different conditions (Chin, 2000; Selim, 2012a,b&c). With the increasing drive to minimize environmental pollution from sulfur-bearing fuels, there is a renewed interest in increasing the capacity of Claus process plants, while developing alternatives ways of utilizing acid gas. Therefore, it is imperative to provide a unified review of existing studies on the reaction chemistry, and Claus process operation for sulfur recovery from acid gas.

1.5 Research Motivations

Crude oil and natural gas contain several contaminants that pose serious negative effects on the industrial process equipment, environment, human health, process conversion efficiency and increased operational costs. Typical crude oil and natural gas, most often contains contaminants such as acid gas (H_2S, CO_2), CS_2, COS and higher hydrocarbons. Some of the most common higher hydrocarbons that exist in crude oil and natural gas include benzene, toluene, and xylene (BTX). The combustion of crude oil and natural gas produces highly toxic and environmentally malignant byproducts, such as SO_2, SO_3, H_2SO_4, CO, COS, CS_2, particulate matter (PM) and polycyclic aromatic hydrocarbons (PAH). Therefore, the presence of contaminants in crude oil and natural gas requires highly efficient gas treatment process. These contaminants are separated from crude oil and gas in the form of acid gases and other associated impurities through highly efficient desulfurization processes. The separated acid gas is then subjected to further treatment in Claus process to recover energy and sulfur simultaneously. The impurities that accompany the separated acid gas significantly impact the conversion efficiency of the thermal stage of Claus process. This often results in increased processing costs, increased trace pollutants to directly impact the environment, increased number of catalytic stages and quality of sulfur produced. Also, some of these impurities (such as COS, CO and CS_2) are formed in the process, and in significant quantities that can adversely impact the process with increased operational costs and unwanted emissions of health hazardous compounds. Aside from the environmental impact associated with the above mentioned contaminants (CO_2, N_2, COS, CS_2 and BTX),

several technical problems occur during the treatment of these contaminants in a Claus process. For instance, the presence of high concentrations of CO_2 in the acid gas (lean acid gas) produces multiple problems in Claus process which include:

1. Insufficient high furnace temperature during the process which inhibits the proper destruction and combustion of higher hydrocarbons (BTX) present.

2. Lean acid gas provides the problems of flame stabilization in the Claus furnace.

3. Presence of BTX in the catalytic stages of Claus process deteriorates catalytic beds from the deposition of carbon/soot on the catalysts.

4. Decreases the thermal stage efficiency to require additional processing in the catalytic stages. This can require additional catalytic stages.

In view of the aforementioned motivations, the objectives of this study were formulated as discussed below.

1.6 Research Objectives

The aim of the proposed work is to understand the detailed sulfur chemistry with the presence of various contaminants (BTX) accompanying the acid gas stream, as well as the formation and destruction of COS and CS_2 in the thermal stage of the reactor. The goal is to establishing more favorable operating conditions of the reactor for improved efficiency of the thermal stage and reduced environmental burden. Detailed examination of these parameters for gas phase chemistry will assist in providing design guidelines for optimum operation over wide ranges of acid gas composition. The specific objectives include:

I. Examine the effect of trace amounts of benzene, toluene or xylene on the chemical kinetic pathways of H_2S combustion in a thermal stage Claus reactor

II. Characterize the effect of BTX and their amounts on sulfur chemistry and conversion efficiency of hydrogen sulfide at the thermal stage of Claus process

III. Determine the fate of BTX in a Claus reactor under various operational conditions with and without the presence of carbon dioxide. Identify conditions for their defined degree of destruction.

IV. Identify the conditions under which COS and CS_2 are formed in Claus furnace and identify conditions that mitigates their formation

Chapter 2 Literature Review

In this section, literature review related to the topic of this dissertation is presented. It is categorized into six sections. The first section covers reactions mechanisms of hydrogen sulfide combustion and the second section contains literature on experimental characterization of hydrogen sulfide combustion in flames. In the third and fourth sections, practical problems of sulfur recovery in the industry are highlighted, which is followed by alternative ways of utilizing acid gas to recover hydrogen and sulfur in the fifth section. In the sixth section, literature on BTX oxidation and pyrolysis is provided.

2.1 Reaction Mechanisms of H_2S Combustion

Several reaction mechanisms of hydrogen sulfide combustion have been proposed in open literature. Norrish et al., 1957 studied the mechanism of H_2S combustion, using kinetic spectroscopy and flash photolysis. They proposed a reaction mechanism consisting of 13 elementary reactions, and highlighted the significance of HS and OH radicals to H_2S combustion. This mechanism includes several steps; initiation, chain propagation and branching, and chain termination. Levy et al., 1965 examined $H_2S/O_2/N_2$ flames in a flat burner, and reported an extended version of the 13 elementary reaction mechanism proposed by Norrish et al., 1957 up to 18 elementary reactions. They also affirmed the importance of elementary reactions involving HS radicals in the overall chemistry of H_2S combustion. Muller et al., 1979, 1980 studied sulfur chemistry in fuel-rich $H_2/O_2/N_2$ flames with addition of

0.25, 0.5 and 1% of H_2S in the mixture. They used a quantitative laser fluorescence technique to quantify HS, S_2, SO, SO_2, and OH species, on the basis of which 36 elementary reactions mechanism was proposed. Frenklach et al., 1981 investigated experimentally the oxidation of H_2S and ignition delay using reflected shock waves. They reported a reaction mechanism for H_2S oxidation, consisting of 17 species and 57 elementary reactions.

Cerru and co-workers, 2005, 2006 proposed a more detailed reaction mechanism, consisting of 12 species and 70 elementary reactions for H_2S pyrolysis and oxidation in both laminar and turbulent flames. The mechanism under-predicted SO_2 by ~ 31% and ignition delay time by ~ 35%. They also reduced the detailed mechanism, using sensitivity analysis approach and implemented steady state assumption for minor species that include HSO, HOSO, $HOSO_2$, H_2S_2, and S. They obtained a 6-step reaction mechanism that was compared to their detailed mechanism and other experimental data from the literature and good agreement was obtained under most of the reaction conditions tested. Selim and co-workers, 2012a implemented error propagation approach to reduce the detailed reaction mechanism of Leeds University, 2002, which consists of 111 reactions and 41 species. Their comprehensive strategy reduced 111 detailed reaction mechanisms down to 19 reactions with maximum error of 16%.

Blitz et al., 2000 and Hughes et al., 2001, 2002 of Leeds University developed detailed reaction mechanisms of H_2S combustion. Blitz et al., 2000 examined the reaction between two important intermediate species of H_2S combustion (OH and SO). They calculated the reaction rate coefficient of OH reaction with SO over

temperature range of 295-703K, using laser flash photolysis coupled with laser-induced fluorescence (LIF). They revealed that reaction of OH/SO occurs in several steps, starting with the formation of HOSO and, which is most likely to produce SO_2 and H. Isomerization of HOSO results in the formation of HSO_2 that decomposes rapidly to form H and SO_2. The steps leading to the end-products of OH/SO reactions were ambiguous and needed further clarification. Hughes et al., 2002 determined numerically the reaction rate coefficients of all the intermediate steps that were ambiguous. They tested the reaction rate coefficients under a wide range of temperatures (300-2000K) and pressures (10^{-3}-10^{6} atm). In another paper (Hughes et al., 2001), they examined premixed methane flames doped with sulfur and nitrogen. They modified their initial sulfur mechanism until a final version consisting of 111 reactions and 41 species was compiled (Leeds University, 2002).

Zachariah et al., 1987 examined the flame structure of $H_2/SO_2/O_2$ at equivalence ratio from 1.35 to 2.4 and low-pressure condition using numerical and experimental methods. The numerical predictions were conducted using a reaction mechanism that consisted of 44 chemical reactions and 17 species, which showed good agreement with experimental data, except for H_2S mole fractions that was under predicted by ~35% and HS was over-predicted by ~ 60%. Chernysheva et al., 1990 investigated H_2S reaction with oxygen under stoichiometric conditions. They developed a detailed reaction mechanism of H_2S combustion that contained 201 reactions and 23 species. Their mechanism showed qualitative agreement with most of the experimental data. Sendt et al., 2002 reported a detailed mechanism for H_2–S_2–

H_2S system. This mechanism consists of 21 reactions and it was validated over a wide range of temperatures (873-1723K) and pressures (0.04-3 bar).

2.2 Experimental Characterization of H_2S Combustion

The combustion of H_2S has been investigated experimentally and reported in open literature. Merryman and Levy, 1967, 1968, 1971, 1972 & 1979 reported extensive studies on H_2S and CS_2 flames. They examined the oxidation of hydrogen sulfide in a flat flame burner under low pressures (0.1 and 0.05atm) and measured the active intermediate species using mass spectrometer (SO, S_2O, SO_2 and SO_3). Of particular interest, is the revelation that a change in equivalence ratio from stoichiometric to oxygen-rich conditions did not affect SO radical, whereas mole fractions of SO_2 showed considerable decrease. They emphasized that S_2O is formed slightly before SO formation under oxygen-rich conditions and suggested possible channels for SO formation in the reaction pool. They also examined formation of sulfur trioxide in staged combustion of CH_4/H_2S mixture in an effort to lower NO_x emission during combustion (Merryman and Levy, 1979). However, a major set-back was the high levels of CO produced in the first stage due to the lack of oxygen or low reaction temperatures. There was no significant increase in SO_3 formation in the second stage compared to single stage combustion process and, delaying the injection of secondary air reduced SO_3 formation considerably (Hedley, 1967). Merryman and Levy, 1969 also investigated COS combustion under low-pressure condition. They divided COS flame into two distinct reaction zones; CO and SO_2 were formed in the first stage, while in the second zone, CO oxidation to CO_2 occurred.

Azatyan and co-workers, 1969 used an electron spin resonance (ESR) technique and gas chromatography (GC) to elucidate key aspects of sulfur chemistry. They examined the chemistry of H_2S, CS_2, sulfur vapor and COS flames at low-pressure, and observed that H_2S combustion occurs through formation of H_2, SO_2 and SO in the first stage, and that SO_2 formation relies significantly on SO radicals. In the second stage, H_2 oxidation occurs and OH radicals are formed. Bernez-Cambot et al., 1981 studied H_2S diffusion flame and reported results that agree with those of Azatyan et al., 1969, except for the OH radicals which were not reported. Aztayan and co-workers, 1969 also examined sulfur flames. They used a separate reactor to generate sulfur vapor used in the experiments. It was observed that sulfur vapor oxidation produces significant amounts of atomic oxygen and SO in the reaction pool. Examination of COS combustion under low-pressure conditions further confirmed that COS combustion produced high amounts of atomic oxygen and SO. Sharma et al., 1967 and Liuti et al., 1966 examined the chemistry of CS_2 flames, and also observed that CS_2 combustion helps release large quantities of atomic oxygen and SO. It was observed that SO mole fraction reaches its maximum under stoichiometric conditions, while CS and atomic oxygen reached minimum mole fractions. They attributed this to the formation of intermediate compounds such as COS.

Another striking observation common to both Aztyan et al., 1969 and Bernez-Cambot et al., 1981 is that H_2S is an inhibitor to H_2 oxidation, which has also been confirmed in studies by Selim, 2012c. This observation was further explored in the work of Pierucci and co-workers, 2004, wherein they compared the contact times of pure H_2S, H_2 and CH_4, and their equimolar mixtures against the conversion of

different fuels at reactor temperature of 1500K. They affirmed that H_2S is more reactive than H_2 and CH_4.

Tsuchiya and co-researchers, 1999 studied H_2S oxidation using laser photolysis in a shock tube using atomic resonance absorption spectroscopy as the detection system. They focused on elementary reactions that play prominent role in H_2S oxidation (reactions 2-1 to 2-3):

$$SH + O_2 \rightarrow \text{products} \qquad (2\text{-}1)$$

$$S + O_2 \rightarrow SO + O \qquad (2\text{-}2)$$

$$SO + O_2 \rightarrow SO_2 + O \qquad (2\text{-}3)$$

They revealed that reaction (2-1) could yield several products that include HSO+O, SO+OH, SO_2+H, and HO_2+S. This is a very controversial reaction in most H_2S combustion mechanisms. They computed kinetic parameters for the three reactions, considering HSO+O as the products for reaction 2-1 and compared the Arrhenius plots with literature data. An adopted reaction mechanism of H_2S combustion, consisting of 30 elementary reactions was then obtained.

In an effort to further deepen the understanding of sulfur chemistry in flames, researchers also sought to understand the detailed role of intermediate species to the combustion chemistry of H_2S, and this provided significant insight into various reaction pathways involved. They used non-intrusive examination of excited species chemiluminescence. The phenomenon of chemiluminescence is the result of chemi-excitation process, which involves increasing the total energy of a molecule by means of a chemical reaction, and this causes light emission. Identifying the characteristic spectrum associated with various species (intermediate or stable) has proved to

significantly improve the understanding of flame chemistry especially in hydrocarbon combustion (Dagnall et al., 1969).

Lewis et al., 1939 examined HS absorption bands. They generated HS radicals by passing pulses of radiofrequency current to H_2S, and then synchronized the radiofrequency pluses to immediately precede the flashlight to be absorbed by HS. A band of HS absorbsion was detected at 323.7nm wavelength. Muller et al., 1979 then measured concentrations of HS, S_2, SO, SO_2, and OH radicals using quantitative laser fluorescence. Fuwa et al., 1963, 1969 used an atomic absorption instrument to detect the presence of SO_2 ultraviolet absorption bands. The setup consisted of a light source, absorption cell, burner, light dispersing elements and detectors. They showed the presence of strong absorption band of SO_2 within 200-230 nm and 250-300nm.

Toyoda et al., 1974 reported experimental data on the emission spectra of CS_2, H_2S and other non-sulfurous compounds. They used a heated tungsten filament as an electron source in a controlled electron beam to provide excitation of the species examined. The emission spectrums of CS_2 showed more intense bands at 282nm and 285nm, while strong bands of H_2S that appeared at 486, 434, 410, 397 and 389nm were attributed to hydrogen Balmer series. Folwer et al., 1931 examined the spectrum of carbon disulfide, sulfur and hydrogen sulfide flames and proved that CS_2 flame emissions extend from ultraviolet to blue wavelength. They attributed the formation of these bands to S_2 and SO species. Sulfur bands were found to be absorption bands, but they were obtained as emitting bands when a stream of oxygen was directed into the flame. They also examined sulfur and hydrogen sulfide flame spectra, which

showed similar spectrum as compared to that of CS_2 flame. They observed formation of OH bands in hydrogen sulfide flames.

Gaydon and co-workers, 1934, 1947, 1974 examined the spectra of hydrocarbon flames containing small amounts of SO_2 and SO_3. They reported band systems for SH, CS, S_2 and SO radicals, and elaborated on mechanisms of formation of observed species. A strong ultraviolet emission band observed in the flame spectra was attributed to the reaction of sulfur dioxide and atomic oxygen to form sulfur trioxide (Gaydon and Whittingham, 1947). They also made considerable effort to understand the continuum emissions from sulfur compounds, and were the first research group to report on the afterglow of sulfur dioxide in flames (Gaydon, 1934). It is one of the most famous spectrums in flames of sulfur compounds. In their work, sulfur dioxide afterglow was generated using a purified liquid sulfur dioxide and subjecting it to an intense discharge of two aluminum electrodes. As a result, a strong violet-blue afterglow was obtained in the range of 260-470nm with sulfur dioxide absorption bands superimposed on the continuum within a range of 280-315nm. They also found that the series of peaks superimposed on the afterglow continuum in the range of 382.8-469.9nm emanated from different excited species, and sulfur monoxide, sulfur dioxide, oxygen and elemental sulfur were the most prominent species responsible for those peaks. Afterglow of sulfur dioxide was further examined by Mulcahy and Williams, 1970 who examined sulfur dioxide afterglow from the reaction between sulfur dioxide with atomic oxygen. Afterglow of SO_2 started at around 280nm and diminished near 500nm. The occurrence of sulfur dioxide afterglow was attributed to the following group of reactions:

$$SO + O = SO_2^* \quad (2\text{-}4)$$

$$SO_2 + O + O = O_2 + SO_2^* \quad (2\text{-}5)$$

They reported that reaction (2-4) occur in two steps described below:

$$SO_2 + O + M = SO_3^* + M \quad (2\text{-}6)$$

$$SO_3^* + O = SO_2^* + O_2 \quad (2\text{-}7a)$$

$$SO_3^* + O = 3SO_2^* + O_2 \quad (2\text{-}7b)$$

The formation of singlet and triplet SO_2 afterglow were attributed to reactions (2-7a) and (2-7b) respectively. They also observed that the singlet SO_2 emissions represented the stronger part of the afterglow continuum at 350nm, while the triplet emissions were responsible for the weaker part of the afterglow near 425nm. Halstead and Thrush, 1966 also examined sulfur dioxide afterglow from reaction between sulfur dioxide and atomic oxygen. They defined the recombination reactions in SO_2 afterglow as shown in equations 2-8 and 2-9 and considered reaction 2-8 to be responsible for weaker part of the afterglow at around 425nm. They considered reaction 2-9 to be the dominant reaction that is responsible for SO removal.

$$SO_2 + O + M = SO_3^* \quad (2\text{-}8)$$

$$SO + O = SO_2^* \quad (2\text{-}9)$$

Selim et al., 2011b also observed SO_2^* afterglow in their examination of hydrogen sulfide flames. They examined the spectra of H_2S/O_2 under lean condition (equivalence ratio of 0.5), and showed strong absorption bands of SO_2 within 280-310nm and groups of superimposed peaks beyond 370nm. This was attributed to singlet (at around 365m) and triplet (beyond 400nm) excited afterglow of SO_2^*. Selim and co-workers emphasized that neutralization of SO_2 afterglow continuum is

crucial in order to detect the bands of sulfurous species in hydrogen sulfide flames. They successfully neutralized SO_2* afterglow by injecting trace amounts of H_2S into H_2/air flames under near stoichiometric condition to hinder formation of SO_2 in significant amounts. Their results revealed the formation of a strong bluish inner cone located near the flame base upon injection of trace amounts H_2S. The inner cone showed strong group of peaks between 320-470nm. These peaks were grouped into SO* band within 320-350nm, SO_3* and H* bands beyond 350nm and HS absorption bands at 324.03 and 328.62nm.

2.3 Practical Challenges of Sulfur Recovery

A review of literature on the existence of impurities in acid gas and their effect on the chemical kinetics and product distribution of hydrogen sulfide combustion is presented in this section. As mentioned earlier, acid gas contains several contaminants such as N_2, NH_3, CS_2, COS and hydrocarbons that include benzene, toluene and xylene, commonly known as (BTX). Some of these contaminants, such as COS and CS_2 are also formed in the Claus reactor. The presence of contaminants in acid gas, such as BTX, even in very small concentrations can alter the chemical kinetics of H_2S combustion significantly, resulting in reduced process efficiency and performance and increased operational cost (Slavens et al., 2010).

Numerical and experimental results have been reported on the role of contaminants (CO_2, N_2, CH_4 and mercaptans) to hydrogen sulfide combustion. Khudenko, Gitman and Wechsler, 1993 studied the effect of air enrichment with

oxygen and air enrichment by oxygen-air-water oxidizers on the treatment of acid gases (H_2S and CO_2). They found that oxygen enrichment reduces the equipment size and provides sufficiently higher sulfur recovery in comparison to the conventional Claus Process. Conversely, enrichment by oxygen-air-water oxidizers causes a decrease in sulfur recovery through dissociation of water into hydroxyl groups, which enhances SO_2 production.

Selim et al., 2008a&b, 2012a&b, 2013 reported extensive experimental results on the chemical kinetic pathways of acid gas (H_2S and CO_2) combustion under various conditions. They examined the effect of different contaminants (CO_2 and N_2) on the optimum operating temperature of Claus reactor in the thermal stage, both numerically and experimentally (Selim et al., 2008a&b, 2012b). The results revealed that carbon dioxide affects the reaction chemistry significantly, which impacts conversion efficiency. They showed that at low temperature, CO_2 and N_2 act as inert gases thereby reducing the optimum operating temperature by reducing the reactants partial pressure. Conversely, at high temperature CO_2 enhanced the oxidizing medium, which deteriorates the efficiency of Claus process considerably. However, nitrogen acted as an inert gas, wherein it reduced the reactants partial pressure, which did not affect the performance of Claus process significantly. Also, they examined the sulfur chemistry with the acid gas (H_2S and CO_2) addition in H_2/air flame at different equivalence ratio (Selim et al., 2014). They found that presence of CO_2 enhances the oxidizing medium of the reaction pool while simultaneously promoting formation of carbonaceous-sulfurous compounds (such as COS and CS_2). These compounds have negative effect on the performance of Claus process.

Selim, AlShoaibi & Gupta, 2011a also studied hydrogen sulfide combustion in methane/air flame at three different equivalence ratio of 0.5, 1 and 3 that represent fuel lean, stoichiometric and rich conditions respectively. They revealed that in the presence of oxygen, oxidation of hydrogen sulfide forms SO_2, while the depletion of oxidant (Claus conditions) favors formation of elemental sulfur. However, higher hydrocarbons were formed in trace amounts under Claus conditions wherein sulfur dioxide acted as a coupling catalyst, which enhanced the dimerization of CH_3 radical to form higher series of hydrocarbons. Under Claus conditions, sulfur deposits were formed in low temperature regions of the reactor including the sampling line. They analyzed the deposits using X-ray powder diffractometer that showed cyclo-S_8 (α-sulfur) with orthorhombic crystal structure. They attributed the formation of α-sulfur to the agglomeration of elemental sulfur (S_2) during its condensation at low temperatures. In another investigation, Selim et al., 2013 examined the effect of contaminants (CO_2, CH_4 and C_3H_8) on quality of sulfur deposits collected from hydrogen sulfide combustion under rich (Claus) and stoichiometric conditions. They collected Sulfur deposits from H_2S combustion under various conditions and analyzed them using X-ray powder diffraction and laser induced breakdown spectroscopy (LIBS). Results from LIBS experiments revealed that equivalence ratio of H_2S/O_2 flame did not have significant impact on the quality of captured sulfur. Similarly, presence of CO_2 in the acid gas stream showed insignificant effect on the deposited sulfur. However, sulfur deposits from combustion of hydrogen sulfide in methane and propane showed traces of carbon (soot). Compared to methane, concentration of carbon was higher with propane.

Arutyonov & co-workers, 1993a examined the oxidation of 10% CH_4 and 10% H_2S with 5% O_2 in diluted N_2 in a quartz reactor at temperatures lower than 800K and high residence time, in the order of tens of minutes. They found that H_2S was completely oxidized within a temperature range of 700 -800K while at lower temperatures incomplete conversion of H_2S was observed, but no quantitative analysis on methane conversion was reported.

Chin et al., 2000, 2001 studied the oxidation of H_2S and H_2S-CH_4 mixtures in a tubular reactor within a temperature range of 1273 – 1473K and residence time of 100 to 1200ms. They reported that H_2S consumption is faster in the presence of methane, while the amounts of SO_2 formation reduced. Their results also revealed that methane is less competitive for oxygen than H_2S, which results in methane reacting with other major sulfur containing species to form carbon disulfide. In the same paper, they examined the reaction of methane with sulfur dioxide to determine if this reaction is directly responsible for COS formation. They concluded that COS is not a direct product of reaction between methane and sulfur dioxide, rather methane is partially oxidized to CO which then provides the channel for COS formation.

Smith et al., 1982 examined CO/O_2/Ar flames with addition of trace amounts of SO_2. They determined the kinetic parameters of SO_3 elementary reactions. Glarborg et al., 1996 and Alzueta et al., 2001 reported experimental and numerical findings on the effect of SO_2 to CO oxidation, and later, Dagaut et al., 2003 examined NO and SO_2 addition effects to CO-H_2 mixtures. They conjectured that SO_2 inhibits oxidation of CO and CO-H_2 and the inhibition rate is more severe under fuel-rich condition. This was attributed to the observation that SO_2 acts as radical sink in the

reaction pool, wherein it favors radical recombination. They also compared their experimental results with numerical data, which was obtained using an adopted reaction mechanism that consisted of 67 elementary reactions and 23 species.

2.4 Challenges of COS and CS_2 in Sulfur Recovery

In Claus Process, COS and CS_2 are formed or present in the feed gas, and they cause negative impact on Claus reactor performance and efficiency. The formation of COS and CS_2 in Claus reactors often contribute to about 20 to 50% of the overall pollutants emission from the process plants (Luistra and D'Haene, 1989; Sames et al., 1990). These compounds also cause a decrease in catalyst activity due to sulfate formation. Thus, the global reactions responsible for COS and CS_2 formation/destruction in the Claus process have received some attention.

Luistra and D'Haene, 1989 used plant data analysis to prove that the concentration profile of COS increases with increase in temperature. Sames et al., 1990 have also proved that good relationship exist between the formation of COS and the presence of CO and sulfur. Sames & co-workers reported that up to 71% of COS is formed both in the reaction furnace and waste heat boiler. The high temperatures in Claus reactor support the dissociation of CO_2 to form CO and O_2 and the formed CO reacts with elemental sulfur to form COS. Chernysheva and co-workers, 1990 examined mechanistic pathways for the gas-phase oxidation of H_2S and CS_2. They developed CS_2 mechanism consisting of 70 elementary reactions. Gargurevich, 2005 reported novel mechanistic pathways for COS and CS_2 formation based on fundamental chemical laws.

Arutyunov and co-workers, 1991, 1992, 1993b studied the kinetics of reactions of SO_2 with hydrocarbons. In one of their papers, Arutyunov et al., 1992 examined the homogenous gas phase reaction of SO_2 with CH_4 in a quartz reactor within a temperature range of 1100-1350K and pressure of 53kPa, and measured the concentration of stable gases using IR spectra. They also examined the effect of SO_2:CH_4 ratio in the inlet gas. The results revealed that the rate of SO_2 conversion was dependent on the rate of CH_4 pyrolysis. At low ratio of SO_2:CH_4, the more favorable products were CO_2, H_2O and S_2 while at higher SO_2:CH_4 ratio, the more favorable products were CO, H_2O and H_2S. In a similar study, Arutyunov et al., 1993b examined the reaction of C_2H_2 with SO_2 under identical conditions and found that CS_2 and COS are the major sulfur containing species observed. However, formation of COS occurred at much later stage of reaction and was attributed to the oxidation of CS_2 by available SO_2. Within the temperature range examined, rate of SO_2 reduction by C_2H_2 was 3 to 5 times greater than the rate of SO_2 reduction by methane. Interestingly, the rate of SO_2 reduction by CH_4 was proportional to SO_2 concentration while no definite relationship was observed on the rate of SO_2 reduction by C_2H_2. This provided strong evidence that the reduction of SO_2 occurs through reactions with products of C_2H_2 pyrolysis.

Karan & co-workers, 1998a and 1998b studied the homogenous gas phase reactions of COS and CS_2 formation in a quartz tubular reactor placed in a furnace. They studied the kinetics of reaction of CO with S_2 to form COS within a temperature range of 873-1423K and residence time of 0.5-2s. They developed a kinetic model that accounted for both formation and decomposition of COS. It was observed that

the reaction of CO with S_2 to form COS is very rapid at temperatures exceeding 1273K. Karan & co-workers also reported experimental data on thermal decomposition of COS over a wide range of COS concentrations (0.20–2.33 mol%) and temperatures (1073-1373K), typically encountered in the modified Claus process. The experimental results revealed that COS conversion increases with temperature increase in the reactor and inlet concentration of COS. Karan and Behie, 2004 examined CH_4-S_2 and CH_4-H_2S reactions at high temperatures (1073-1523 K) in a flow reactor within a pressure range of 101-150kPa and residence times of 90-1400ms. The results proved that the reaction of CH_4 with S_2 to produce CS_2 is kinetically favored, and this reaction occurs rapidly. On the other hand, reaction of CH_4 with H_2S also forms CS_2, but the rate of CS_2 formation is limited by the H_2S thermal decomposition at the initial stage of reaction.

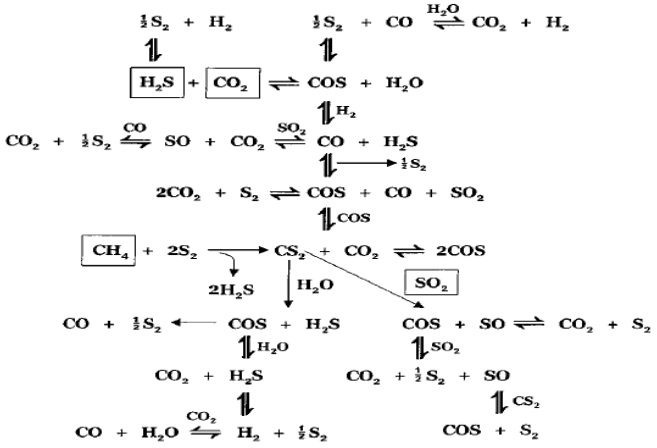

Figure 2-1. Mechanism of COS and CS_2 Formation/Decomposition in Claus Reactor (Clark et al., 1997, 2000)

Clark & co-workers, 1995, 1997, 1998, 2000 reported systematic studies on the mechanism of H_2, CO, COS and CS_2 decomposition and formation in the Claus

furnace (figure 2-1). They conducted experiments using an externally heated tubular reactor with variable quenching of the hot gases, and reported that CO_2 and sulfur species do not result in CS_2 formation, but hydrocarbons react with sulfur to produce CS_2. Under the partial oxidation conditions of the furnace, they found that H_2S is destroyed much faster than hydrocarbons in the feed gas due to the lower S-H bond energy as compared to C-H. New chemical pathways that involve the reaction of CS_2 and COS with major species such as SO_2, CO_2, and H_2 were also examined. They found that destruction of COS and CS_2 by reaction with water vapor occurs very rapidly, and CO_2 does not react with sulfur species to form CS_2.

2.5 Sulfur Recovery via H_2S Pyrolysis

In an effort to develop alternative ways of utilizing acid gas, studies on the non-catalytic thermal decomposition of H_2S to produce hydrogen and elemental sulfur (reaction 2-10) have been extensively examined (Reymont, 1974). Most studies have focused on the kinetics of both the forward and reverse reaction 2-10 over a wide temperature range. Several research groups derived chemical kinetics rate of H_2S dissociation under wide range of temperatures, residence times, and pressures (Harvey et al., 1998; Bishra et al., 1987; Binoist et al., 2003). Others studied hydrogen sulfide dissociation in the presence of catalysts (alumina or molybdenum) to favor higher conversion of the endothermic dissociation rates of H_2S (Fakuda et al., 1978; Raymont, 1974).

$$H_2S = H_2 + 0.5S_2 \qquad (2\text{-}10)$$

These studies were also partly motivated from the need to optimize sulfur recovery through modeling of the Claus reaction furnace and associated waste heat boiler (Hawboldt et al., 2000, Nasto et al., 1994). The kinetics of reverse reaction 2-10 was examined by Kaloidas and Papayannakos, 1989. They implicitly relied on the available kinetic models within the literature, wherein they used first-order kinetics for the H_2S decomposition reaction, and a form, $-d[H_2]/dt = k[H_2][S_2]1/2$, for the rate expression of the reverse H_2/S_2 reaction proposed by Aynsley et al., 1935 at lower temperatures. The high-temperature decomposition of H_2S was also reported by Randall and Bichowsky, 1918; Raymont, 1974; Fukuda et al., 1978 and Chivers et al., 1989. However, investigation of the direct reaction between hydrogen and sulfur is only reported in the literature at lower temperatures (Norrish and Rideal, 1923; Zel'venskii et al., 1961). It was noted that these studies did not show any agreement in the reported order of reaction. For instance, Darwent and Roberts (in Raymont, 1974) claimed a second order dependency on H_2S for the rate of decomposition reaction, whereas both Raymont, 1975 and Adesina et al., 1995 have suggested first-order kinetics. In light of the apparent lack of agreement on the kinetics of this system, a reevaluation of the kinetic data for the H_2/S_2 reaction reported in the study by Dowling & co-workers, 1990 was undertaken. They extended this study to Claus process conditions (high temperature range of 875-1700K and residence time between 0.03-1.5s), and reported first-order dependence on both hydrogen and sulfur for the reversible homogenous gas-phase kinetics of H_2S decomposition to produce hydrogen and sulfur. Dowling and co-workers, 1990 reported an experimental rate expression for reaction 2-10 ($-d[H_2]/dt = k[H_2][S_2]$), different from that used by Kaloidas and

Papayannakos, 1989. A reversible kinetic treatment of the system was also performed, which included the assumption of strict first order kinetics for H_2S decomposition and pseudo-first order behavior for the H_2/S_2 reaction. Dowling et al., also proved the feasibility of using a rapid thermal quench technique to minimize the reverse reaction of H_2S decomposition (reaction 2-10), and this was also suggested by Chen et al., 1986. Despite this type of scrutiny, the reported studies thus far, have failed to provide a unified picture of the overall kinetics within this system, often yielding conflicting results even as to the form of rate expressions and reaction order.

Hawboldt, Monnery and co-workers 2000, 2001 examined key reactions of H_2S under Claus process conditions. They studied the reaction between H_2S and SO_2, which is highly important in Claus process using an isothermal reactor under wide temperature range of 1123-1400K and residence times of 0.05-1.2s, and developed a kinetic rate expression for SO_2 reaction with H_2S. They similarly investigated the rate of pyrolysis and oxidation of ammonia in Claus process (Monnery et al., 2001).

Slimane at al., 2004 examined numerically the partial combustion of different acid gas compositions and oxidizers (20% H_2S, 80% N_2)/air, (20% H_2S, 80% N_2)/O_2, 100% H_2S/air, 100% H_2S/O_2, (25% H_2S, 75% N_2)/air, and (25% H_2S, 75% N_2)/O_2, under super-adiabatic conditions. The major focus of their work was to optimize the yield of H_2 under conditions examined. They revealed that high H_2 and low SO_2 yield were more favorable at equivalence ratios above 6.

Montoya et al., 2005 conducted quantum chemical calculations to study the interaction between H_2S and molecular oxygen. They used the chemical bond lengths

to define possible isomers from [H_2/S/O_2] that are favorable during H_2S and O_2 reaction. The possible pathways of H_2S reaction were described as follows:

$$H_2S + O_2 \leftrightarrow HO_2 + HS \quad (2\text{-}11)$$

$$H_2S + O_2 \leftrightarrow HSO + OH \quad (2\text{-}12)$$

$$H_2S + O_2 \leftrightarrow SO + H_2O \quad (2\text{-}13)$$

$$H_2S + O_2 \leftrightarrow SO_2 + H_2 \quad (2\text{-}14)$$

They determined the energy level of each isomer and found reaction (2-11) to be the most favorable pathway of H_2S/O_2 reaction. Binoist and co-workers, 2003 studied pyrolysis of H_2S in diluted argon using a continuous and perfectly mixed reactor, within a residence time of 0.4-1.6s and temperature range of 1073-1373K. They reported detailed kinetic mechanism for H_2S pyrolysis that consists of 22 reactions. Manenti et al., 2013 also reported detailed kinetic mechanism for pyrolysis and oxidation of sulfur compounds, and validated it against literature and industrial data acquired from different Claus plants. It was noted that this mechanism accounted for the presence of light hydrocarbons, ammonia and other species that are often present in acid gases.

2.6 BTX Thermal Decomposition

Benzene, toluene and xylene (BTX), originating from crude oil and natural gas wells are major components of practical hydrocarbon fuels, such as gasoline, diesel oil and kerosene (Natelson, 2010&2011). Presence of BTX in transportation fuels helps to suppress auto-ignition and reduce the chances of engine knock (Andrae, 2011). BTX causes severe technical and environmental problems to Claus process

plants. They are generally understood to play prominent role in soot and polycyclic aromatic hydrocarbon (PAH) formation during thermal oxidation and pyrolysis, most especially in rich flames. Soot and PAH are very harmful pollutants that hinder human health and environment (Andrae, 2011)). To improve the performance of hydrocarbon fuel engines and ensure cleaner air, development of comprehensive mechanistic models that help characterize the chemical kinetics of hydrocarbon fuels oxidation and pyrolysis is crucial. Most researchers have used BTX as key components of surrogate fuel to understand the characteristics and thermal decomposition of practical hydrocarbon fuels (Ji et al., 2012; Natelson, 2010).

The characteristics of benzene, toluene and xylene thermal oxidation and pyrolysis that include ignition delay times and laminar flame speeds have been widely examined (Ji et al., 2011). Ignition delay and laminar burning velocity are fundamental characteristic parameters of fuel combustion. Ignition delay is very important for describing auto-ignition, understanding the ignition mechanism and analyzing the chemical reaction pathway. Laminar burning velocity is an important fundamental property of a fuel that affects its burning rate. The burning rate is an intrinsic property of a combustible mixture. It has significant impact on the performance and efficiency of engines and emissions (Lovell et al., 1934; Ji et al., 2010, 2011). Therefore, both parameters are highly essential in building, validating and improving kinetic models. A wide spectrum of experimental and numerical work has been conducted on the oxidation and pyrolysis of BTX, including xylene isomers. Various models on the kinetics and product speciation of each aromatic compound;

benzene, toluene and xylene isomers have also been proposed and validated against different experimental data.

2.6.1 Xylene Thermal Decomposition

Xylene exists in three isomeric forms (o-xylene, m-xylene and p-xylene), unlike benzene and toluene. The relative characteristics of xylene isomers during thermal decomposition have been subject of previous investigations (Andrae, 2011). Xylenes are more suitable representatives of the aromatic fraction in jet or diesel surrogates when compared to benzene and toluene, because the molecular weights of xylenes are more comparable to practical hydrocarbon fuels. However, there are far more studies on thermal decomposition of benzene and toluene, compared to xylene isomers (Zhao et al., 2015). The relative behavior of xylene isomers during thermal oxidation and pyrolysis was reported by Lovell & Co-workers, 1934. They studied the auto-ignition characteristics of the xylene isomers in a single cylinder engine, and measured the critical compression ratio (CR), which is defined as the lowest CR at which knock occurs. The results revealed that at 600 revolutions per minute the CR increases from o-xylene (9.6), m-xylene (13.6) to p-xylene (14.2). Jackson, 1951 made similar revelation when they measured the spontaneous ignition temperatures of o-xylene, igniting at a much lower temperature (734 K), m-xylene (836 K) and p-xylene (838 K). Wright, 1960 examined the oxidation of xylene isomers in a sub-atmospheric quartz vessel and observed higher reactivity for o-Xylene, with activation energy for the oxidation process of 38kcal/mol, 1 and 2kcal/mol less than m-xylene and p-xylene. Barnard & Sankey, 1968a compared the slow oxidation of m-xylene and p-xylene in a static reactor at 733-785K. They observed nearly identical

behavior of the m-xylene and p-xylene isomers. Barnard & Sankey, 1968b further examined the oxidation of o-xylene under similar conditions, and observed a much higher reactivity of o-xylene than m-xylene and p-xylene.

Roubaud & co-workers, 2000a&b compared the characteristics of xylene isomers at low and intermediate temperatures. The most interesting revelation from their work is the observation that, on the basis of reaction kinetics, di-methyl and tri-methylbenzene with at least one adjacent methyl pair (e.g., *o*-xylene and 1, 2, 3-trimethylbenzene) exhibit a higher reactivity than those with isolated methyl substituents (e.g., *m*-xylene and *p*-xylene). They studied the stoichiometric oxidation of three xylene isomers in a rapid compression machine at 600-900K and 5-15atm (Roubaud et al., 2000a). The minimum auto-ignition temperatures reported are 679K (o-xylene at 12atm), 906K (m-xylene at 21atm) and 904K (p-xylene at 22atm). It was observed that the oxidation behavior of m-xylene is similar to p-xylene, which was much different from that of o-Xylene. The reactivity of o-xylene was similar to that of n-alkanes, while m-xylene and p-xylene exhibited reactivity resembling that of toluene oxidation. They conjectured that the proximity and length of the alkyl chains are two important factors in low temperature reactivity of xylenes. Roubaud et al., 2000b further examined low temperature branching pathways of o-xylene in a rapid compression machine. GC/MS and FID was used to detect 22 intermediate species and analyzed the reaction pathways accounting for the highest concentration of carbon atoms (2-hydroxybenzaldehyde, 2-methylbenzaldehyde and o-xylene oxide). The reaction pathways of o-xylene proceeded in the following sequential order: H-abstraction, molecular oxygen addition, isomerization to produce alkylhydroperoxy

radicals and decomposition producing the stable intermediates. This oxidation sequence leading to stable intermediates is similar to those observed during low temperature oxidation of n-alkanes.

Gaïl & co-workers, 2005, 2007 & 2008 further examined the oxidation of p-xylene at higher temperatures (900-1300K). They studied p-xylene oxidation in an atmospheric pressure jet-stirred reactor and equivalence ratios of 0.5-1.5 (Gaïl & Dagaut, 2005). The combustion generated species were measured using GC/MS equipped with flame ionization detectors (FID). Aromatic intermediates observed were benzaldehyde, toluene, benzene, cyclopentadiene, styrene and methylethylbenzene. Oxidation of m-Xylene was examined in another paper (Gaïl & Dagaut, 2007), under similar conditions. The results were overall similar, except for the slightly slower reactivity of m-xylene, compared to p-xylene. Gaïl et al., 2008 then investigated o-xylene oxidation under identical conditions. The reactivity of o-Xylene was observed to be much greater than the other isomers (m-xylene and p-xylene).

Battin-Leclerc & co-researchers, 2006 reported similar reactivity at much higher temperatures (1330-1800K). They examined oxidation of xylene isomers in oxygen/argon mixtures in a shock tube at pressures of 6.7-9atm and equivalence ratio range of 0.5-2. Their results did not show any significant difference in ignition delay of the three isomers under the conditions examined. This observation contradicted that of Roubauld & co-workers, 2000a&b. However, Shen & Oehlschlaeger, 2009a reported similar measurements at lower temperatures (941–1408K) and pressures range of 9 to 45atm, and conjectured that o-xylene is slightly more reactive than p-

and m-xylene. The results also showed that the ignition delay times of p- and m-xylene were similar to those of toluene under comparable conditions, and this is in good agreement with the findings of Roubaud & co-workers 2000a&b.

Da Silva & Bozzelli, 2010 attempted to reconcile the observed differences with a kinetic mechanism proposed to describes low-to-intermediate oxidation chemistry of xylene and tri-methyl-benzene. They used electronic structure calculations to prove that the oxidation of o-methyl-benzyl ($C_6H_4CH_3CH_2$) and o-methyl-benzoxyl ($C_6H_4CH_2OOHCH_2$) radicals could lead to the formation of an unstable double hydro-peroxide alkyl radical ($C_6H_4CH_2OOHCHOOH$) via reaction with oxygen, which undergoes chain-branching decomposition to produce two OH radicals. However, it has not yet been ascertained if the proposed mechanism by da Silva & Bozzelli, 2010 can explain similar behavior observed in laminar flames, wherein the overall burning characteristics is controlled by high-temperature reaction kinetics.

Farrell & co-workers 2004&2005 reported the laminar flame speeds for mixtures of benzene and several alkyl-benzenes with air in a constant volume combustion vessel, at 3atm and an unburned gas temperature of 450K. They observed that the laminar flame speed varies in a descending order from benzene, toluene to o-xylene and p-xylene. Won et al., 2011 examined the extinction strain rates of counter-flow non-premixed flames of toluene, 1, 2, 4-trimethylbenzene, and 1, 3, 5-trimethylbenzene. Toluene showed the highest flame extinction propensity while 1, 3, 5-trimethylbenzene preceded 1, 2, 4-trimethylbenzene.

Ji & co-workers, 2010&2011 reported systematic measurements of the laminar flame speeds and extinction strain rates of benzene, n-propyl-benzene, toluene, o-, m-, and p-xylene, and 1, 2, 4- and 1, 3, 5-trimethylbenzene in counter-flow flames with well-defined uncertainties. The experiments were conducted at an atmospheric pressure and unburned temperature of 353K for the unreacted fuel-containing stream. It was observed that benzene/air flame propagated much faster than xylene isomers and other alkylated derivatives. They also observed different H-shift energy barriers in the methyl-benzyl radical, which provides a logical explanation for the observed differences in the reactivity of o-, m-, and p-xylene flames. Their numerical data suggested that the aromatics flames are highly sensitive to fuel-specific chemistry and more specifically to the reaction kinetics of the first few intermediates in the oxidation process following the fuel consumption.

Emdee & co-researchers, 1990, 1991a&b examined the oxidation of xylenes at 1155 K and equivalence ratios from 0.69-1.7. They observed greater reactivity for o-xylene than m- or p-xylene, as other previous investigators. This was attributed to the pathway leading to formation of o-xylylene during simultaneous oxidation of the side chains. The o-xylylene isomerizes to form styrene, which then produces phenyl and vinyl radicals. Alternatively, a sequential oxidation route was considered, which produces o-tolualdehyde. This was further justified by measurement of o-tolualdehyde in substantial quantities.

Emdee et al., 1991a&b measured intermediate species generated during m-xylene and p-xylene oxidation in an atmospheric flow reactor at temperature range of 1093-1199K and equivalence ratio range of 0.47-1.7. The major aromatic

intermediates identified were benzene, toluene, methyl-benz-aldehyde, ethyl-toluene, benz-aldehyde, ethyl-benzene, styrene, methyl-benzyl alcohol, methyl-styrene, and 1, 2-ditolylethane, while the major aliphatic intermediates were methane, acetylene, ethene, cyclo-pentadiene and vinyl-acetylene. Simulation data proved that a side-chain H-abstraction to form methyl-benzyl (xylyl) radical accounted for 65-75% of the fuel consumption, while methyl group abstraction to produce toluene accounted for 20-30% of the fuel consumption. Oxidation of p-xylene occurred through sequential and simultaneous oxidation of the methyl side chains. Overall, the behavior of the isomers was similar, with p-xylene slightly more reactive than m-xylene, except for the formation of p-xylylene from p-xylene oxidation, which did not have an analogous pathway in m-xylene oxidation.

Loftus & Satterfield, 1965 examined partial oxidation of o-xylene in a flow reactor and identified o-xylene oxide (1, 3-dihydro-2-benzofuran, or phthalan) as the key intermediates. Eng et al., 1998 used time-resolved UV absorption at 265nm to measure the production of p-methyl-benzyl radicals produced by p-xylene oxidation at temperatures of 1050-1400K behind reflected shock waves. Gregory et al., 1999 also collected exhaust samples that were analyzed using GC/MS from the combustion of xylene isomers in a single cylinder engine operating at 1500 RPM. The major intermediates observed were toluene, benzene, styrene, and ethyl toluene.

2.6.2 Toluene Thermal Decomposition

Oxidation and pyrolysis of toluene has attracted several interests because it exists naturally in transportation fuels and is considered an important component in surrogate fuels of gasoline (Eng et al., 2002; Pengloan et al., 2001; Shen et al.,

2009b). A review of experimental data on toluene oxidation and pyrolysis was evaluated by Yuan et al., 2014. The vast amount of data includes global combustion parameters such as ignition delay times, laminar flame speeds and species profiles in shock tube, flow reactor and low pressure premixed laminar flames. However, some important aspects of toluene pyrolysis and oxidation data and proposed kinetic mechanisms are discussed.

Burcat & co-workers, 1979, 1986 conducted early work on the ignition delay times of toluene oxidation. They examined ignition delay of toluene oxidation behind reflected shockwaves between 2-8atm and temperatures of 1330-1820K, at equivalence ratio of 0.33-1. A kinetic model for toluene oxidation that consisted of 146 reactions was proposed. Davidson et al., 2005 then examined the ignition delay of toluene oxidation in a shock tube at relatively lower temperatures of 855-1269K but higher pressures of 14-59atm under fuel lean and stoichiometric conditions (equivalence ratios of 0.5 and 1.0). They observed pre-ignition energy release, which manifested as an increase in pressure prior to ignition. Sakai et al., 2007a&b and 2009 also used a reflected shock tube to measure the ignition delay of toluene within a temperature range of 1270-1755K and a reflected shock pressure of 2.4atm, at equivalence ratio of 0.5 - 1.5. Eng et al., 1998 studied toluene and xylene oxidation in shock tubes at temperatures of 1050-1400K and pressures of 2-4atm. They proposed a simplified reaction network, consisting of 4 reactions to predict oxidation of toluene and p-xylene. Vasudevan et al. 2005a&b measured the ignition delay of toluene in shock tubes at an atmospheric pressure and temperatures of 1430-1820K under stoichiometric condition. They measured the time history of OH radicals from toluene

oxidation and the resulting ignition delay data were compared to those from Burcat et al., 1979. Ignition delay data was modelled using kinetic models proposed by Dagaut et al., 2002 and Lindstedt & Maurice, 1996.

Roubaud & co-workers, 2000a&b measured ignition delay times in rapid compression machines for a variety of alkylbenzenes (including toluene) under stoichiometric condition, at a compressed gas pressure of 25atm and temperatures of 600-900K. The lack of necessary information to correct the pressure and temperature variations during the ignition period as a result of heat loss will make it difficult to model the experimental data. Mittal & Sung, 2007 also studied ignition delay in a rapid compression machine at compressed conditions of approximately 24.7 and 44.4atm and 920-1100K at different equivalence ratios (0.5 to 1.0), for which corrections reflecting heat loss are available. However, they did not observe any pre-ignition energy release, which contradicts the finding of Davidson & co-workers, 2005. Shen et al., 2009 attempted to reconcile the contradiction in the results of Mittal et al., 2007 and Davidson et al., 2005. They conducted high-pressure shock tube experiments using toluene/air mixtures at 1021-1400K and 10-61atm at equivalence ratios of 0.25, 0.5, and 1.0. Their results did not show pre-ignition energy release or reduced activation energy at stoichiometric condition as reported by Davidson and co-workers, 2005.

Vasu et al., 2010 observed that recent ignition delay time studies of toluene ignition, using shock tubes and rapid-compression machines have not achieved a strong consensus at intermediate temperatures (900–1200 K) and high pressures (near 50atm). They measured ignition delay times for toluene/air mixtures at high pressures

(near 50atm) over the temperature range of 966 to 1211K, using pressure and emission measurements behind reflected shock waves. The reported ignition delay time data were in good agreement with the data of Davidson et al., 2005 and Shen et al., 2009. Ignition delay time measurements were also compared with the predictions of several toluene reaction mechanisms, and updated reaction rate values were suggested to improve model performance.

Colket et al. 1994 characterized the concentration profiles from the products of toluene pyrolysis in a shock tube at a pressure of 10atm and temperatures of 1200-1850K. They proposed 19 reversible reactions to predict the pyrolysis of toluene. Eng et al., 2002 measured species concentration from pyrolysis and combustion of toluene in a shock tube at pressures of 1-2atm and temperatures of 1350-1900K. They proposed a simplified reaction network, consisting of 7 reversible reactions. Pamidimukkala et al., 1987 examined toluene pyrolysis in a shock tube at temperatures of 1150-2200K, pressures of 0.2-0.5atm and proposed 26 reversible reactions to simulate the pyrolysis of toluene. Braun-unkhoff et al., 1988 examined toluene and phenyl pyrolysis in a shock tube at pressures of 1.5-7.8atm and temperatures of 1300-1800 K. They measured product species concentration from the toluene pyrolysis process.

Zhang et al., 2009 examined toluene pyrolysis in a flow reactor at 10atm using synchrotron vacuum ultraviolet photoionization mass spectrometry. They reported that the mechanism of toluene pyrolysis proceeds via a free-radical mechanism, producing mainly benzene, methane, hydrogen and di-benzyl molecules. The formation of benzene resulted from ipso addition reaction followed by the elimination

of a methyl radical. The formation of methane or hydrogen involved H-transfer reactions, and the di-benzyl compounds were formed by a termination reaction.

Shukla et al., 2007 conducted mechanistic study of toluene pyrolysis at low pressures (8-15atm) and high temperatures (1136-1507K). The gas-phase reaction products were detected at constant residence time (0.56s) in an in-situ direct sampling mass spectrometric study, using a vacuum ultraviolet single-photon ionization time-of-flight mass spectrometry technique. They evaluated PAH formation under the examined conditions. The role of aromatic radical-radical and radical-molecule reactions were found to be dominant. Based on the experimental results, they proposed different reaction pathways on PAH formation, with a major emphasis on phenyl, cyclopentadienyl, benzyl, indenyl, and cyclopenta-fused PAH radicals. It was conjectured from this study that any one kinetic model alone could not explain perfectly the large PAH formation in toluene pyrolysis.

Lannuzel et al., 2010 examined the pyrolysis of toluene at high pressure. They revised earlier published reaction mechanism, comprising of 30 free-radical reactions, which was used to model the pyrolysis of toluene over a wider range of temperatures and pressures. They evaluated the mechanism of formation of major intermediate species during toluene pyrolysis. At high pressure ($P > 98atm$) and low temperature ($T < 723K$), a chemical analysis from this model showed that the bimolecular initiations are more important than the monomolecular initiations in the early stages of toluene pyrolysis. The formation of benzene from toluene occurred through ipso addition reaction followed by the elimination of a methyl radical and the formation of methane by H-transfer reactions. Bi-aromatic compounds were produced by the

additions of benzyl radicals to aromatic rings, and are major reaction products with benzene and methane. The di-benzyl compounds were formed by termination reaction. However, the experimental and simulation results did not give any evidence of aromatic ring rupture, in particular C_2H_2, which is the major product of a ring opening reaction.

Yuan et al., 2014 studied pyrolysis and oxidation of toluene in a flow reactor at higher pressures (5 to 760atm) and temperatures (1100 to 1730K). They detected a number of pyrolysis products, such as free radicals, isomers and PAH. Mole fractions of pyrolysis products as a function of heating temperature were reported. A kinetic model was then developed and validated against flow reactor pyrolysis and jet stirred reactor oxidation data, and used sensitivity and reaction path analysis to examine key reaction networks for the toluene pyrolysis and oxidation. In the flow reactor pyrolysis, toluene consumption occurred by H-atom abstraction and uni-molecular decomposition reactions, producing benzyl radical. The subsequent decomposition of benzyl radical produced C_7H_6, o-C_6H_4 and C_5H_6. These products either decomposed to smaller products or participated in the formation of PAH. It was conjectured that benzyl, C_7H_5, and C_5H_5 radicals, especially the two C_7 radicals play important roles in the formation of PAH. While in the jet stirred reactor oxidation, toluene consumption mainly took place through H-atom abstraction reactions by OH, H and O to produce benzyl radical. The effect of reactor pressure and reactants equivalence ratio was noticeable on the dominant consumption pathways of toluene and benzyl. Moreover, $C_6H_4CH_3$ radical did not play considerable role at 10atm than at 1atm, and its oxidation sequence ultimately lead to C_4H_4 and phenyl.

Significant studies have also been conducted to measure the laminar speed of toluene flames (Ranzi et al., 2012). The recent review by Ranzi et al., 2012 summarizes the experimental work on laminar flame speeds of toluene and several other hydrocarbon fuels. Hirasawa et al., 2002 investigated the atmospheric laminar flame speeds for the combustion of toluene-air and mixtures of air with ethylene, n-butane and their blends, both experimentally and computationally. They deployed digital particle image velocimetry (DPIV) to characterize the laminar flame speeds over a wide range of equivalence (0.8-1.3) and temperature of 298 K. A reaction mechanism that consists of 95 species and 621 elementary reactions was compiled to model the experimental data.

Johnston & Farrel, 2005 reported measurement of laminar burning velocities at 450K and 304atm and equivalence ratio range 0.80-1.4 for five aromatic fuels that included toluene. The laminar flame speed was determined using high speed schlieren visualization, which was used to monitor flame growth following ignition. Benzene exhibited the fastest speed, followed by ethyl-benzene, n-propyl-benzene, toluene, and then m-xylene. Kumar et al., 2007 examined the laminar flame speed of toluene at an atmospheric pressure and temperature of 400 K over an equivalence ratio of 0.7-1.4. Li et al., 2009, 2010 & 2011 studied the laminar premixed flame speeds of toluene at low pressure of 0.04atm and temperatures of 500-2200K, over an equivalence ratio of 0.75-1.9. A detailed reaction mechanism that consists of 176 species and 804 elementary reactions was used to model the experimental data.

Detilleux et al. 2009a&b, 2011 examined the laminar-premixed flames of toluene combustion at low pressure (0.47atm) and temperatures (500-1700K), over

equivalence ratio of 0.7-2. Dames et al., 2012 studied the laminar flame speed of toluene at temperature of 353K, atmospheric pressure and equivalence ratio of 0.7-1.4. Hui et al., 2012 also examined toluene laminar flame speed at atmospheric pressure within temperature range of 298-400 K and equivalence ratio of 0.7-1.4. The laminar flame speeds and extinction stretch rates were determined using experimental and numerical methods. The simulation results were in reasonable agreement with experimental data, and sensitivity analysis demonstrated that the flame phenomena are mostly sensitive to chain branching and heat release reactions.

Sileghem et al., 2013 measured laminar burning velocities of toluene and other fuels using the heat flux method on a flat flame adiabatic burner at an equivalence ratio from 0.7 to 1.3 and temperatures between 298K and 358K. The temperature dependence of the fuels was reported and the measurements are compared to literature data and simulations using reduced kinetic models.

Several detailed kinetic models have been proposed to support analysis of experimental results from the various experimental studies published in literature (Zhang et al., 2010; Metcalfe et al., 2011). A kinetic model was proposed by Klotz et al., 1998 for high temperature oxidation of neat toluene, neat butane, and toluene-butane blends in an atmospheric-pressure flow reactor. They focused on understanding the behavior of blended fuels. An extensive validation of the toluene mechanism was conducted and it was discovered that improvements were needed in the toluene model of Emdee et al., 1992. A kinetic model was proposed by Emdee et al., 1992 to predict experimental data from toluene and benzene oxidation in a flow reactor. The changes made to Emdee's model included addition of iso-butyl reactions,

which significantly improved predictions for 1, 3-butadiene and acetylene. Improvements were also made in the prediction of benzaldehyde since the experimentally measured benzaldehyde profiles were obtained with a gas chromatograph better configured to separate polar compounds than in previous studies. Klotz et al., 1998 then examined the tendency of kinetic models to accurately predict decomposition of blended fuels, and conjectured that when the chemical interactions between the various fuel components are limited to radical pool effects, the blended fuel oxidation process is more likely to be predicted when the blend model is properly configured to predict the oxidation processes of the neat fuel components.

Sivaramakrishnan et al., 2006a modified the earlier model proposed by Klotz et al., 1998 to simulate their high-pressure shock tube speciation measurements. Bounaceur and co-workers, 2005 proposed a detailed kinetic model on the basis of previous benzene sub-mechanism. This model predicted fairly well the experimental data from low-temperature jet-stirred reactor and higher temperature shock tube ignition delay data and the flow reactor data due to Brezinsky et al., 1992 and Klotz et al., 1998.

Lindsted & Maurice, 1996 proposed a detailed kinetic model for toluene combustion that consisted of 743 reactions and 141 species. They evaluated the assembled mechanism over a wide range of experimental data from counter-flow diffusion flames, plug flow reactors and premixed flames, and shock tube pyrolysis experiments. This kinetic mechanism represented a major attempt to develop a chemical kinetic mechanism that is applicable to intermediate and high temperature

oxidation. El Bakali et al., 2007 assembled detailed toluene kinetic model based on the detailed mechanism of Maurice & Lindsted, 1996 to simulate their experimental data. They examined temperature distribution and mole fraction profiles in laminar stoichiometric and premixed $CH_4/O_2/N_2$ and CH_4/1.5% $C_6H_5CH_3/O_2/N_2$ flames at low pressure (0.0519bars), using thermocouple, molecular beam/mass spectrometry, and gas chromatography/mass spectrometry technique. Good agreement between the model and experiments was observed and major reaction pathways in both flames were assessed.

Dagaut & co-workers, 2002 examined the oxidation of toluene in a jet-stirred reactor over a wide range of reactor conditions. Mole fractions of reactants, stable intermediates and final products were measured using on-line and off-line GC analyses. They also used a detailed kinetic reaction mechanism, featuring 120 species and 920 reactions, which was then used to simulate the ignition of toluene/oxygen/argon mixtures (Pengloan & Dagaut et al., 2001) and the burning velocities of toluene/air data reported by Davis et al., 1996&1998. Good agreement was obtained with ignition delay data and with flame speeds for rich condition. The results were interpreted using sensitivity and reaction path analyses, based on species rates of reaction. Toluene oxidation proceeded via formation of benzyl, by H-atom abstraction, and the formation of benzene, by H-atom displacement yielding methyl and benzene; benzyl oxidation yielded benz-aldehyde, that further reacted to yield phenyl whereas benzyl thermal decomposition yields acetylene and cyclopentadienyl; further reactions of cyclopentadienyl yield vinyl-acetylene.

Andrea et al., 2005, 2008 & 2013 developed a detailed kinetic model for the oxidation of n-heptane/toluene mixtures, in a series of studies. The toluene sub-model was validated against high-pressure shock tube ignition delay measurements and also compared the species concentration profile with the data reported by Sivaramakrishnan et al., 2004, 2005 & 2006a. They also validated this toluene sub-mechanism against experimental data in a more recent study (Andrea et. al., 2008), and revised some key reactions in the toluene sub-set based on quantum chemical calculations involving the benzylperoxy radical ($C_6H_5CH_2OO$) reported by Murakami et al., 2007 and the kinetic model by Sakai et al., 2007a,b & 2009. The revised model was also validated against experimental data from ignition delay in shock tube and rapid compression machine. Species profiles in flow, perfectly stirred reactors and laminar burning velocity were also compared with simulated data, using the revised kinetic model. This model featured 635 reactions and 137 species, and it improved the overall model predictions at lean fuel-air conditions for both neat toluene and toluene-blends.

Dagaut et al., 2002 studied toluene oxidation in a jet-stirred reactor over the temperature range of 1000-1375K at 1atm and equivalence ratio of 0.5-1.5. Concentration profiles of reactants, stable intermediates and final products were measured by probe sampling followed by online and off-line GC analysis. The experimental data were modeled using a detailed kinetic reaction mechanism, consisting of 120 species and 920 reactions. The kinetic scheme was used to simulate the ignition of toluene-oxygen-argon mixtures data by Burcat et al., 1986 and Eng et al., 1998, and the burning velocities of toluene-air mixtures data by Davis et al., 1996.

The proposed kinetic model showed good agreement with the experimental data set. However, this kinetic mechanism did not agree with previously proposed kinetic mechanisms by Emdee et al., 1992 and Davis et al., 1996. Sensitivity and reaction path analysis proved that toluene oxidation proceeds via formation of benzyl, by H-atom abstraction, and the formation of benzene, by H-atom displacement yielding methyl and benzene; benzyl oxidation yields benzaldehyde, that further reacts to yield phenyl, whereas benzyl thermal decomposition yields acetylene and cyclopentadienyl; further reactions of cyclopentadienyl yield vinyl-acetylene.

Sivaramakrishnan et al., 2006a examined ignition delay of toluene pyrolysis in a shock tube, at temperatures of 1200-1900K and pressure of 27atm. They proposed a reaction mechanism consisting of 87 species and 262 reactions. The detailed chemical kinetic model was used to simulate the stable species profiles (specifically toluene, benzene and methane) from the high-pressure pyrolysis data sets and shock tube-atomic resonance absorption spectrometry of H atom profiles, obtained from prior toluene pyrolysis experiments performed under similar high-temperature conditions and lower pressures from 1.5 to 8bar (Sivaramakrishnan et al., 2004 and 2005). A variety of stable species, ranging from small hydrocarbons to single ring aromatics (principal soot precursors such as phenyl-acetylene and indene) were sampled from the shock tube and analyzed using standard gas chromatographic techniques.

Bounaceur et al., 2004 & 2005 reported experimental data from a jet-stirred reactor with toluene concentrations from 1.4 to 1.7% diluted in helium, at equivalence ratios from 0.45 to 0.91, over a temperature range of 873-923K and pressure of 1atm. In both studies, reactant, product and many intermediate species were detected and

quantified. Bounaceur et al., 2005, also reported a detailed kinetic model based on a previous benzene sub-mechanism that predicted fairly well the experimental data from low-temperature jet-stirred reactor. This model was also validated against higher temperature shock tube ignition delay data and the flow reactor data due to Brezinsky et al., 1996 and Klotz et al., 1998. A kinetic mechanism, comprising 273 species and 1740 reactions was developed by Tian et al., 2011 to elucidate the low-pressure toluene flame speciation data reported by Li et al., 2009. This kinetic model accounted for the formation of poly-aromatic hydrocarbons. Zhang et al., 2010 proposed a detailed kinetic model consisting of 137 species and 530 elementary reactions to simulate toluene pyrolysis at low pressure, over a temperature range of 1270–1870K. They obtained satisfactory agreement between experimental and modeling results, including decomposition products and PAH up to phenanthrene.

Metcalfe et al., 2011, reported a detailed chemical kinetic model, featuring 329 species and 1888 elementary reactions to describe toluene oxidation. They validated their model over a wide range of experimental conditions which included flow reactor, shock tube; jet-stirred reactor and flame studies, and good agreement was obtained between the simulated and experimental data. Toluene thermal decomposition and radical attack reactions leading to oxygenated species were given particular attention. The benzyl radical sub-mechanisms was expanded to include isomerization and thermal decomposition reactions, which are important at flame temperatures, and a molecular oxygen attack path to form the benzylperoxy radical, which is found to be relevant at lower temperatures. The final toluene kinetic models resulted in acceptable fuel consumption profiles in both flames and plug flow reactors

and sensible predictions of the temporal evolution of the hydrogen radical and pyrolysis products in shock tube experiments. The evolution of major and intermediate species in plug flow reactors was well modelled and an excellent laminar burning velocity prediction was achieved.

Narayanaswamy et al., 2010 examined the oxidation of different aromatics that included toluene and xylene in a shock tube and plug flow reactor over wide range of conditions. Detailed reaction mechanism that consisted of 158 species and 1804 reactions was proposed. The detailed kinetic model was compared with previously published experimental data of Burcat et al., 1979 and 1986, Shen et al., 2009, Vasudevan et al., 2005, Sivaramakrishan et al., 2004, 2005 & 2006a, Klotz et al., 1998, Davis et al., 1996, Johnston & Farrel, 2005, Hirasawa et al., 2002, Emdee et al., 1992, Battin-Leclerc et al., 2004, 2005 & 2006 and Ji et al., 2012. These experimental data were obtained from studies conducted in shock tubes, plug flow reactors, and laminar burning velocities at moderate to high temperatures. The reported kinetic model agreed reasonably well with the experiments over wide range of temperatures and pressures. However, some differences were observed in the ignition delay times of certain species when compared to the high pressure data. The low temperature oxidation of ethyl-benzene involving the formation of peroxy radicals was found to be crucial in order to reproduce the experimental ignition delay time data at temperatures less than 1100K. The PFR data for all species showed good agreement for the fuel decay profiles and concentration of the major products and most of the intermediate species. The burning velocities computed for toluene were also in good agreement with the data reported by Davis et al., 1996 and Hirasawa et

al., 2002. However, when compared against the data of Johnston & Farrel, 2005, the burning velocities of toluene, ethylbenzene and m-xylene showed higher values than those reported experimentally.

2.6.3 Benzene Thermal Decomposition

Pyrolysis and oxidation of benzene has a critical role in the combustion chemistry of practical fuels. An evaluation of experimental data on benzene oxidation and pyrolysis was reported by Vourliotakis et al. 2011. Early studies on the development of benzene oxidation models were conducted by Bittker, 1991, who proposed a simplified mechanism to predict the ignition delay time measurements of Burcat et al., 1985 and the flow reactor data of Lovell et al., 1988. This mechanism was developed empirically by adjusting the rate constants of some important reactions to fit the experimental data. Brezinsky & coworkers, 1986, in a pioneering effort, proposed detailed reaction mechanism for benzene and toluene oxidation. This mechanism was the starting point of most subsequent modeling studies. Several other kinetic mechanism of benzene oxidation have been reported in open literature, most of which are on the basis of the flame data of Bittner and Howard.

Richter & Howard, 2002 on the basis of the work of Shandross et al., 1996 proposed a detailed kinetic model for the formation and consumption of single-ring aromatic hydrocarbons in premixed acetylene, ethylene and benzene flames. The model predictions were compared to experimental data reported by Bittner & Howard, 1981 and Grieco et al., 1998 for near-sooting and sooting premixed benzene/oxygen/argon flames. Dupont et al., 2003 used the kinetic model proposed by Richter & Howard, 2002 to simulate benzene depletion in a laminar premixed flat

stoichiometric low-pressure methane/air/benzene flame. The results showed good to excellent agreements between predictions and measured mole fraction profiles for reactants, intermediates and products such as methane, O_2, methyl, H, OH, CO, CO_2, and H_2O.

Tan & Frank, 1996 also proposed a detailed kinetic mechanism to model benzene/oxygen flames. They conducted reaction path flux and sensitivity analysis to model species profiles in rich benzene/oxygen/argon flames (Bittner & Howard, 1981), flame speeds (Goloniva & Fyodorov, 1956) and ignition delay data (Burcat et al., 1986). A satisfactory agreement was obtained between the model predictions and experimental data, except for the reactions involving C_5 species. Davis et al., 1996 measured flame speeds of benzene/air in an atmospheric pressure counter-flow flame within an equivalence ratio range of $0.8 \leq \varphi \leq 1.4$, and compared the experimental data to model predictions from mechanisms due to Emdee et al., 1991a, 1992 and Lindstedt & Skevis, 1994. They also proposed modification to the mechanism of Emdee, 1991a to achieve better comparison with the experimental data. The modified mechanism gave good agreement with the flame speeds, while providing good fit to atmospheric pressure flow reactor data for benzene oxidation at temperatures of 1000 to 1200K.

Alzueta et el., 2000 examined benzene oxidation in a plug-flow reactor at 900-1450K and residence times in the order of 150ms. They reacted 107ppm of benzene with 830 to 491000ppm of O_2 in the presence of 0.5 to 2% H_2O, and proposed a detailed kinetic model for benzene oxidation. The detailed kinetic model was used to simulate experimental data from turbulent flow (Lovell et al., 1988) and jet-stirred

reactors (Chai & Pfefferle, 1998). It was conjectured that the flow and stirred reactor data are incompatible. Zhang & McKinnon, 1995 developed an elementary reaction mechanism, containing 514 reactions without any adjustment to the parameters for low-pressure rich combustion of benzene. This mechanism accounted for pressure-dependent unimolecular and bimolecular reactions and included phenyl radical oxidation and pyrolysis reactions. They compared the predicted data with species profiles measured by Bittner & Howard, 1981. The mechanism captured stable species and free radical profiles in the flame, and the computed profiles of small free radicals, such as H-atom or OH, match the data quite well. However, phenyl radical and phenoxy radical concentrations showed large discrepancies.

The detailed kinetic models for benzene oxidation, proposed by Ristori et al., 2001 and Da Costa et al., 2003, which were developed on the basis of stirred reactor data, have proved to be capable of adequately simulating the Bittner and Howard flame data. Ristori et al., 2001 studied benzene oxidation in a jet-stirred reactor at atmospheric pressure and temperatures of 1010-1295K for a range of equivalence ratio ($0.3 \leq \varphi \leq 2$). They modelled shock tube and flame experiments (Davis et al., 1996), well-mixed reactor data (Chai & Pfefferle, 1998) and their own perfectly stirred reactor data at 9.7atm. The kinetic mechanism showed good comparison with the benzene/air flame speed data. Sensitivity analysis revealed the importance of reactions involving cyclopentadienyl, phenyl and phenoxy radicals. Da Costa et al., 2003 reported experimental results for the oxidation of benzene in a jet-stirred reactor at a temperature of 923K and in a shock tube at temperatures between 1230 and 1970K. They proposed a detailed mechanism that reproduced their experimental data

and previously published experimental data obtained from a flow reactor and in a near-sooting laminar flame reported by Bittner & Howard, 1981 and Lovell et al., 1988.

Detilleux and Vandooren, 2009a&b used the kinetic model proposed by Ristori et al., 2001and Richter & Howard, 1981 to simulate their experimental data from rich and sooting benzene flames. They examined one-dimensional laminar premixed benzene-oxygen-argon flames with equivalence ratios of 2, 1 and 0.7, stabilized at low pressure (45mbar) on a flat flame burner. Gas speciation and analysis was conducted using gas chromatography. The detailed kinetic mechanisms reproduced rich benzene flame data, but were unable to reproduce measurements performed in stoichiometric and lean flames. The phenyl production rate and its opening into the linear form of C_6H_5 was the major difference between both mechanisms. In Richter & Howard's 1981 mechanism, the high rate of linear C_6H_5 production was not coherent with experimental data, as this resulted in high overestimation of the diacetylene formation.

Shandross et al., 1996 used the model proposed by Lindstedt & Skevis, 1994 for benzene combustion in premixed flames, to model their experimental data. Shandross et al., 1996 examined a flat, laminar, premixed $H_2/O_2/Ar$ flame, seeded with C_6H_6. The results were used to investigate the C_6H_6 and C_6H_5OH reaction networks proposed in kinetic models reported by Emdee et al., 1992, Zhang & McKinnon, 1995 and Lindstedt & Skevis, 1994. Large errors in the predictions of important reaction pathways limited the usefulness of simple mole fraction comparisons or reaction path analysis. A technique called net rate analysis was

developed from existing mechanism screening techniques and modified reaction path analyses. The net rate analysis proved that benzene destruction is well predicted by existing mechanisms, especially when fall-off effects were included. However, problems with the fit of the coupled phenyl chemistry raised critical concerns about C_6H_6 chemistry and it was suggested that models contain reactions for C_6H_7 and C_6H_8 in hydrogen-rich environments, as addition of H and H_2 becomes more important.

Sivaramakrishnan et al., 2006b examined the high temperature pyrolysis of benzene under elevated pressures of 30 and 50bars in high pressure single pulse shock tube. These authors were the first to report species profiles for the decay of benzene and formation of the primary products, C_2H_2 and C_4H_2 under such extreme conditions. The data was used to test existing mechanisms and models proposed by Laskin &Lifshitz, 1996 and the Wang et al., 2000. The primary difference in these two models was in the description of the decay of phenyl radical, which governs the formation of two primary products C_2H_2 and C_4H_2. Laskin & Lifshitz's model consists of 22 elementary reactions and 17 species, whereas Wang et al.'s model has 16 reactions and 13 species. Neither model matched the experimental data. Kinetic model earlier proposed by same authors was then modified (Sivaramakrishnan et al., 2005). The modified model was able to match the experimental benzene and C_2H_2 profiles.

Vourliotakis et al., 2011 addressed certain uncertainties that still exist regarding benzene combustion features, despite the numerous experimental and numerical investigations. They evaluated experimental data on benzene oxidation and pyrolysis and validated detailed kinetic mechanisms. Speciation data from phenol and

benzoquinone pyrolysis and oxidation were additionally used as validation targets. Vourliotakis & co-workers re-evaluated the phenyl radical oxidation, phenol/phenoxy chemistry, and proposed a cyclopentadiene submechanism. A direct comparison of a single, thoroughly validated, detailed kinetic mechanism against recent experimental data from a total of six laminar premixed benzene flames, as well as data from shock tubes and stirred and flow reactors was performed. This provided the opportunity for critical assessment of benzene oxidation and combustion chemistry under a broad range of operating conditions (temperature, pressure, and stoichiometry). Phenol and benzoquinone pyrolysis and oxidation were adequately captured. They also revealed that linearization reaction of C_5 and C_6 species largely determines ring rupture, leading to C_1-C_4 hydrocarbon formation was reproduced by the model.

From above literature review, the following can be extracted:

1. The decomposition of xylene occurs through initiation reactions with a colliding molecule which yield two major pathways; either results to removal of methyl group from the aromatic ring or H-abstraction. Once initiated, toluene is formed through the 4-methyl phenyl reaction pathways. Toluene decomposes in similar manner, eventually yielding benzene as shown in figure 2-2.

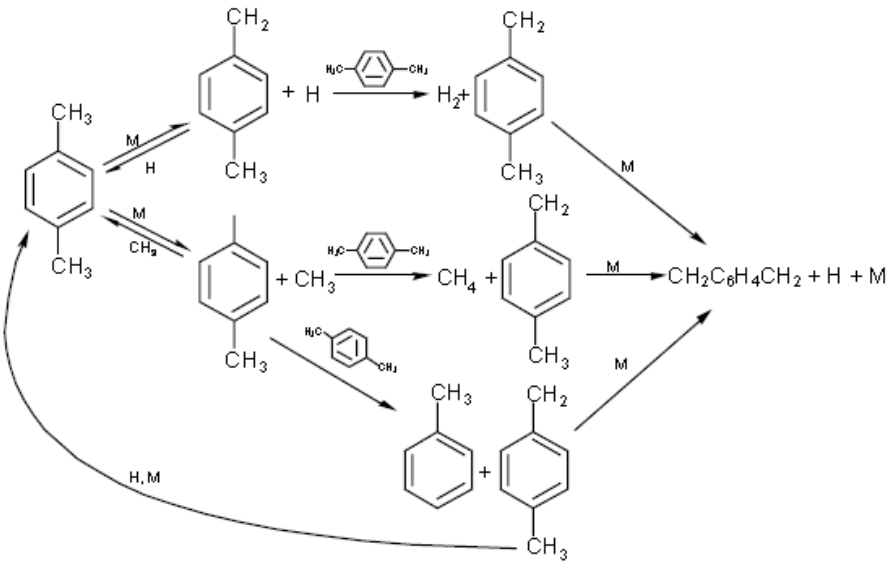

Figure 2-2. Thermal Decomposition Pathways of p-Xylene, Adapted (Hippler et al., 1990; Norman et al., 2002)

2. Studies on the thermal oxidation and pyrolysis of benzene, toluene and xylene were conducted under different reactor configurations and flame structures, but studies under hydrogen sulfide flame environment are still lacking.
3. The chemical pathways associated with hydrogen sulfide combustion in the presence of BTX are expected to be more complex due to the additional radicals BTX will generate in the reaction zones and there subsequent interactions with sulfur species present in the reaction pool. The reaction kinetics of the first few intermediates formed in the BTX thermal oxidation and pyrolysis process that follows the initial fuel consumption is critical. The chemistry of COS and CS_2 is expected to play prominent role.
4. For improved operation of the Claus reactor, the understanding of the complex gas phase chemistry of hydrogen sulfide combustion in the presence of trace

amounts of BTX and other feed contaminants, as well as reactor conditions that promotes the formation/destruction of CS_2 and COS requires better understanding. So, further studies are required to examine the chemistry of hydrogen sulfide combustion in the presence of trace amounts of BTX and other associated acid gas feed contaminants. The chemistry associated with formation and destruction of COS and CS_2, including reactor conditions that promote there destruction can also be better understood. Such studies will also assist in the assembly of important reaction pathways to be included in simulation models.

5. The high content of CO_2 in most acid gas cause flame stabilization problems that result in insufficient reactor temperature for complete BTX destruction in Claus reactors. These often promote production of CO and other lower hydrocarbons in the reactor that deposit on the surface of the catalysts to cause faster deactivation to necessitate frequent change of catalysts. Thus, it is desirable to provide sufficient temperature at the thermal stage reactor to completely eliminate BTX and other contaminants for improved performance of Claus reactors. This requires process modifications that permit the manipulation of temperature, residence time and/or mixing in the reactor. Temperature and residence time are the most important parameters that offers more favorable destruction of contaminants such as BTX.

Chapter 3 Experimental Facility

A description of the experimental facility used to achieve the research objectives of this dissertation is presented. The experimental facility was designed to facilitate the flame characterization and understanding of the detailed chemistry of acid gas and BTX (in trace quantities) combustion in a simulated thermal stage Claus reactor. The geometry and configuration of the experimental setup was designed to provide controlled flame and steady laminar flow of gases in the reactor, which favored the understanding of sulfur chemistry during the combustion process. The experimental setup also allowed favorable investigation of the role of trace quantities of BTX on sulfur chemistry in the simulated thermal stage Claus reactor, while ensuring safe operation in the laboratory vicinity. Detailed description of the experimental setup is given below.

3.1 Experimental Setup

The experimental setup consisted of a burner, quartz reactor, sampling system, flow meters, diagnostics and safety gas monitors. A schematic of the experimental setup is shown in figure 3-1. To achieve the research objectives, there was need to choose a burner and reactor configuration that produces a short and stable flame in which the hot core remains narrow along the reactor central axis. This prevented impingement of the flame on the reactor wall. A tip-mixed burner design was chosen to provide enhanced process safety during the combustion process. The burner consisted of a double concentric tube with a bluff body stabilizer located immediately

downstream of the burner exit. Depending on the desired gas stream composition, hydrogen sulfide and/or hydrogen, carbon dioxide was premixed with benzene, toluene or xylene and injected into the central tube of the burner, while oxygen and/or nitrogen was introduced into the outer annulus. This burner allowed the examination of wide range of experimental conditions. A quartz tube reactor was used for complete optical access to the test region for gas sampling and analysis. The reactor had a dimension of 190mm in length and a diameter 40mm. Two steel bases were fabricated with proper dimensions for housing the reactor from both ends of the quartz tube. The burner and reactor configuration favored a steady laminar flow of gasses in the reactor.

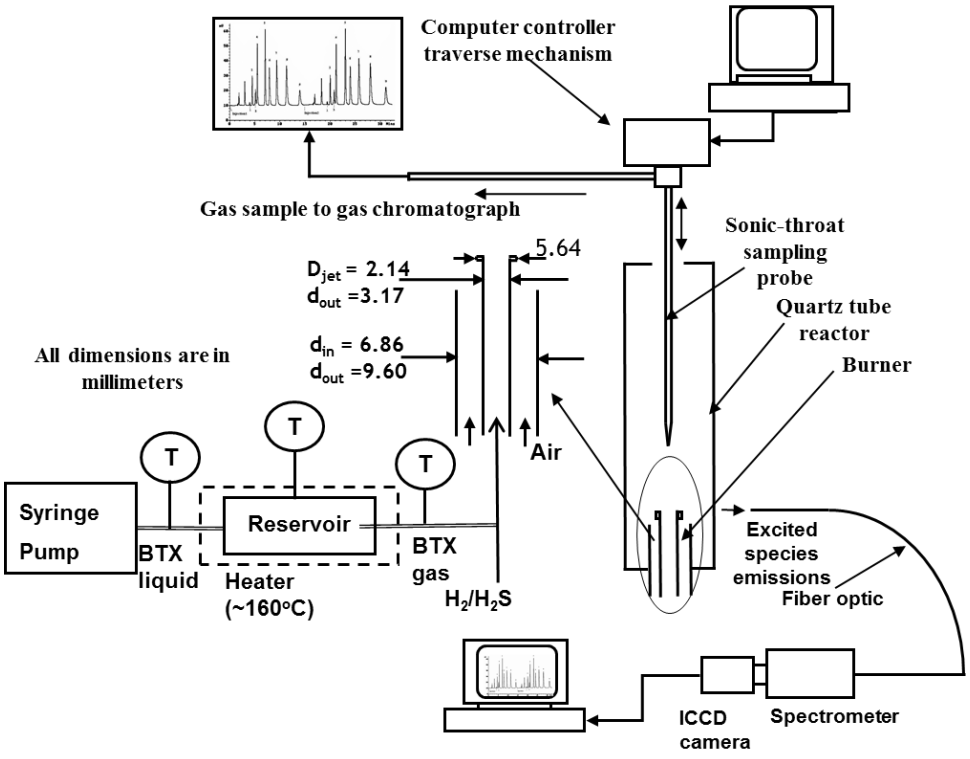

Figure 3-1. Schematic of experimental facility

3.2 Flow Meters

Thermal flow meters/controllers, from AALBORG High Quality Flow Instrumentation, were used to deliver the required flow rates of each gas (such as oxygen, hydrogen sulfide and hydrogen) into the reactor. Since a wide range of flow rates have been examined, flow controllers were changed accordingly in each experiment in order to supply the required flow rates with the least possible error. A syringe pump (PHD 2000 from Harvard apparatus) was used for the injection of liquid benzene, toluene or xylene through the evaporator tube into the burner. Temperature in the evaporator tube was allowed to attain a steady-state of 463K. The preheated tube ensured the evaporation of liquid benzene, toluene or xylene into gas. A reservoir tank was connected to the evaporator tube for accumulation of benzene, toluene or xylene vapors to ensure steady flow injection into the burner. Thermocouples were installed at three different locations in the evaporator tube to monitor the progress of temperature in the evaporator. The resulting flow rate of gaseous benzene, toluene or xylene was calculated through the density of liquid and gaseous BTX at the corresponding temperature measured upon injection.

3.3 Gas Sampling Probe

Gas sampling from the reactor was conducted using a quartz sampling probe with a fine tip (0.2 x 0.4 mm in diameter). The fine tip allowed gas sampling with negligible flow field disturbances. Sampled gas accelerated along the fine tip passage of the probe so as to freeze the chemical reactions instantaneously. Sampling probe was mounted on a traverse mechanism, which allowed axial movement along the

reactor centerline axis. The traverse mechanism has a resolution of about 25 microns. Moisture separator was also installed along the sampling line to separate water from the sampled gas prior to analysis. This also served as a reservoir tank to ensure steady flow of sampled gas into the gas analyzer. A suction pump was connected to the sampling line for suction of the sampled gas from the reactor. The pump provided flow rates in the range of 0.3 to 8 lit/min.

3.4 Diagnostics and Safety Gas Detectors

The major diagnostics adopted in this research was gas chromatography and flame spectroscopy. Gas chromatograph (GC) was used to obtain analysis of stable combustion products in the reaction pool. The sampled gas was split into two streams and injected into the GC simultaneously. First stream was injected into Inficon micro GC 3000 model, which has four different columns equipped with thermal conductivity detectors (TCD). The columns were suitable for the separation of permanents gases (such as carbon dioxide, hydrogen and nitrogen) and hydrocarbons. The TCD was responsible for the analysis of carbon monoxide, carbon dioxide, oxygen, hydrogen, nitrogen and hydrocarbons. Second stream was injected into Agilent GC 7890A that was equipped with flame photometric detector (FPD). The column condition was suitable for efficient separation of trace and high quantities of sulfur compounds, which was connected to the FPD, and was used for gas analysis of stable sulfur compounds (hydrogen sulfide, carbonyl sulfide, carbon disulfide, and sulfur dioxide).

Flame emission spectroscopy was conducted to examine the spectra from non-stable species within the flame zone in the reactor. A spectrometer (SpectraPro 300i) coupled with an ICCD camera (from Princeton Instrument) was used for the detection of chemiluminescence signal from the excited species of combustion products in the reactor. The spectrometer slit was set at 10 microns. Signal from the flame region was passed to the spectrometer through a fiber optic cable. Two gratings were used for different resolutions of the spectrum. Coarse grating was used to obtain coarse resolution of the spectrum (~270nm), while fine resolution of the spectrum (~70nm) was obtained with the fine grating. A mercury lamp was used for the re-calibration of spectrometer after changing the grating or in case of change in spectrum of interest.

Gas leakages and monitoring of toxic gases in the laboratory were carefully observed using three different safety gas detectors. Volatile organic compounds that include, benzene, toluene, xylene and ammonia were monitored using Gas Alert Micros series. Hazardous gas lame detector was used for the monitoring of hydrogen, methane, propane and carbon dioxide, and hydrogen sulfide was monitored using Crowcon gas monitor. The entire experimental facility was placed in a fume hood and exhaust system.

3.5 Systematic Error

Sources of systematic error in this research were expected from traverse mechanisms, thermocouple, gas chromatograph (TCD and FPD), spectrometer grating and flow meters. The error in all apparatuses used in this research is shown in table 3.1. The maximum estimated error for all measurements of species profile did

not exceed ±0.11%. One can see that, error ranges are very minimal, so that they all lay within the experimental data point symbols represented in figures.

All experiments were repeated three times and good data repeatability was achieved. The maximum repeatability error of the measured species concentration in all experiments did not exceed 2.3% for all the results reported in this dissertation. Radiation correction in thermocouple measurements was conducted, and the maximum correction for all temperature measurements was 85K.

Table 3.1. Error associated with experimental measurements

Device	Measured quantity	Error
FPD	H_2S, SO_2, COS, CS_2	<± 0.1 % of measured concentration
TCD	CO, H_2, C_2H_2, CO_2, CH_4	<± 0.1 % of measured concentration
Thermocouple	temperature	± 2.8 K at T=1600 K
Traverse mechanisms	distance	± 0.0762mm/254mm
Spectrometer grating	Wavelengths	± 0.9 nm for 150 grove/mm grating ± 0.25 nm for 600 grove/mm grating
Flow Controllers	volumetric flow	1.5% at full scale
Syringe Pump	Volumetric flow	0.35% of flow

The systematic error associated with metering of liquid and gaseous fuels impacted the accuracy of equivalence ratio calculations. The maximum error associated with the calculation of equivalence ratio (Φ=3) was ±4.98% for all the test conditions.

Chapter 4 Results and Discussion

The results presented in this chapter are divided into four sections (4-1 to 4-5). The first section contains results on the role of xylene, toluene or benzene addition to H_2S/O_2 flames. In the second and third sections, results are presented on the destruction of different composition of acid gas (H_2S, CO_2 and BTX) in Claus reactors using H_2/O_2-N_2 flames. And in the fourth section, results on the reaction pathways of H_2S and BTX destructions is presented, followed by combined effect of CO_2 and toluene or xylene to H_2S combustion in H_2/air flame that is provided in the fifth section.

4.1 Benzene, Toluene or Xylene Addition Effects to H_2S Combustion

Investigations were conducted to examine the combustion chemistry of H_2S and BTX. The goal was to understand the effect of each aromatic contaminant (benzene, toluene or xylene) on the product speciation of H_2S combustion in a Claus reactor. It has been reported that xylene has the greatest effect on catalysts deactivation and hence reduced process efficiency and increased emissions in Claus plants (Crevier et al., 2001). However, plant data were reported that suggested that benzene has the greatest impact on sulfur emissions in Claus process plants (Clark et al., 2000). Therefore, it necessary to examine the individual effect of benzene, toluene and xylene on the product speciation in thermal stage Claus reactors. The results are presented in three sub-sections. The effect of toluene addition is presented first (sub-

section 4-1.1), followed by results on effect of benzene (sub-section 4-1.2) and xylene addition (sub-section 4-1.3) to H_2S combustion.

4.1.1 Toluene Addition Effects to H_2S/O_2 Flame

Experiments were conducted to examine the effect of toluene addition on the combustion of H_2S and the evolution of gas-phase combustion generated species. Table 4-1 shows the test matrix for the experimental conditions reported. Combustion of 100% H_2S gas stream was first investigated followed by the addition of trace amounts of toluene. During operation after the addition of toluene, oxygen flow rate was adjusted to achieve the targeted equivalence ratio of three with respect to H_2S and complete combustion of toluene. The equivalence ratio was defined as actual fuel/air ratio normalized by the stoichiometric fuel/air ratio. Toluene gas flow rates were calculated based on their densities: liquid toluene has a density of 0.866 g cm^{-3} while the gas toluene had a density of 0.003 g cm^{-3} (at the injection temperature).

Table 4-1. Experimental test matrix

Case #	H_2S (cm^3/min)	O_2 (cm^3/min)	C_7H_8 (gas) (cm^3/min)
1	150	75	0
2	150	81.8	0.75
3	150	88.5	1.5
4	150	142.5	7.5

The resulting concentrations of toluene in the H_2S gas stream examined represented 0%, 0.5% and 1%. Gas sampling and analysis of local species was conducted along the centerline axis of the reactor. Dimensionless axial distance (W= axial distance/D_{jet}) was used for all the results presented. Inner jet diameter of the

burner (D_{jet}=2.14mm) and was used to transform the linear distances into dimensionless quantity for wider application of the results.

Figure 4-1 shows the temperature of the reactor measured experimentally. It is observed that temperature increased to a maximum as H_2S reacted with O_2 and then subsequently decreased due to heat losses to the reactor wall. Toluene addition resulted in an increased reactor temperature. This is attributed to the large heating value associated with toluene chemical decomposition. Toluene has a lower heating value (LHV) of 43.5 MJ/Kg while that of hydrogen sulfide is15.2 MJ/Kg. Mean temperature decreased with distance beyond the flame region further downstream of the reactor (at W~7), which is attributed to heat loss to the reactor walls.

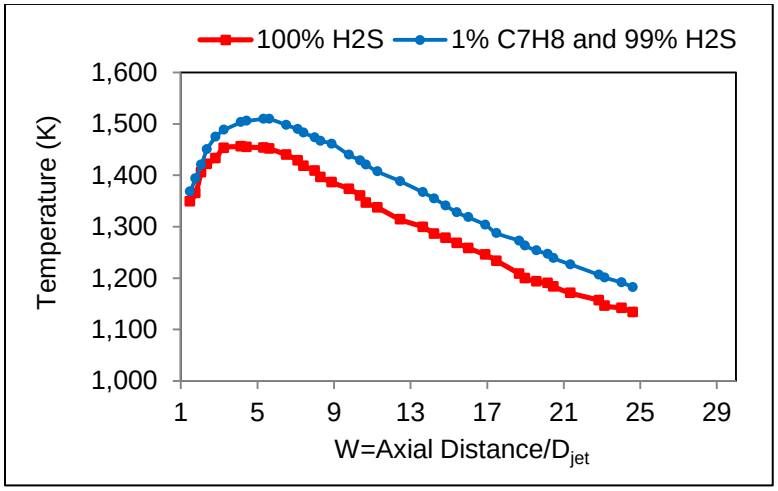

Figure 4-1. Temperature profile of H_2S/O_2 and $H_2S/C_7H_8/O_2$ flame at Φ=3.

4.1.1.1 Analysis of Combustion Products

Effect of toluene addition was examined under different concentrations in the H_2S gas stream and, the results compared with the baseline case of 100% H_2S gas combustion with oxygen. Toluene concentration of 0%, 0.5% and 1% in the gas stream is presented. Figure 4-2 shows the trends of H_2S, H_2 and SO_2 along centerline

of the reactor with 100% H_2S gas stream composition. Hydrogen sulfide mole fraction decreased monotonically to an asymptotic minimum value. The decay of H_2S was due to the chemical and thermal decomposition and is divided into two stages as illustrated in the following chemical reactions, 4-1 to 4-11 (Cerru et. al., 2005, 2006, Leeds Universiy, 2012 and Selim et. al, 2012c). In the first stage, H_2S undergoes thermal and chemical decomposition (reactions 4-1 to 4-3), while H_2S oxidation occurs in the second stage, as shown in reactions 4-4 and 4-15 (Leeds Universty, 2012). Marginal amount of H_2 was observed as shown in figure 4-3, which provided direct support to reactions 4-1 and 4-3.

$$H_2S + M \Leftrightarrow S + H_2 + M \quad (4\text{-}1)$$

$$H_2S + S \Leftrightarrow 2HS \quad (4\text{-}2)$$

$$H_2S + H \Leftrightarrow HS + H_2 \quad (4\text{-}3)$$

$$H_2S + O \Leftrightarrow HS + OH \quad (4\text{-}4)$$

$$H_2S + OH \Leftrightarrow HS + H_2O \quad (4\text{-}5)$$

$$S + OH \Leftrightarrow SO + H \quad (4\text{-}6)$$

$$HS + O_2 \Leftrightarrow SO + OH \quad (4\text{-}7)$$

$$HS + O_2 \Leftrightarrow HSO + O \quad (4\text{-}8)$$

$$S + OH \Leftrightarrow SO + H \quad (4\text{-}9)$$

$$HS + O_2 \Leftrightarrow SO + OH \quad (4\text{-}10)$$

$$H_2 + OH \Leftrightarrow H_2O + H \quad (4\text{-}11)$$

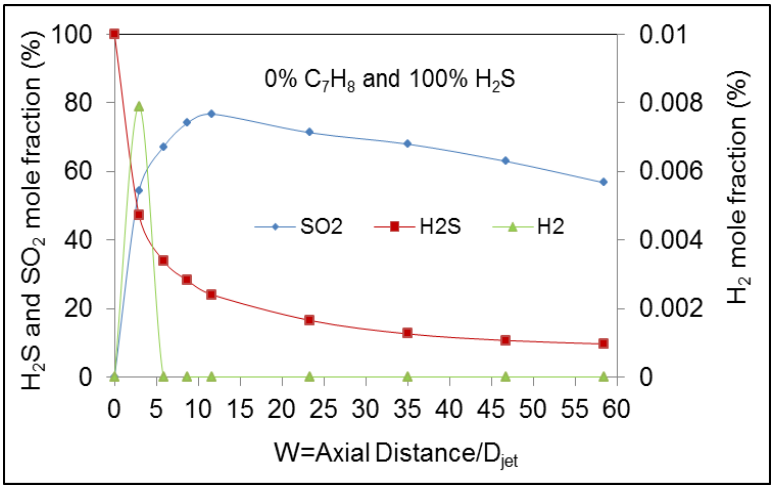

Figure 4-2. Hydrogen sulfide, hydrogen and sulfur dioxide mole fractions.

Flame conditions: H_2S/O_2, Φ=3.0

Mole fraction of SO_2 increased until it reached a maximum value, and afterwards decreased monotonically to a minimum value. The formation of SO_2 is attributed to the oxidation of sulfur radicals formed from H_2S in the primary stage of reaction (see reactions 4-12 to 4-14). With limited amount of oxygen, reaction between H_2S and SO_2 occurs to result in the formation of elemental sulfur. This occurs in elementary reactions steps that include reactions 4-15 to 4-17 (Selim et al., 2012a).

$$HSO + O_2 \Leftrightarrow SO_2 + OH \quad (4\text{-}12)$$

$$SO + OH \Leftrightarrow SO_2 + H \quad (4\text{-}13)$$

$$SO + O_2 \Leftrightarrow SO_2 + O \quad (4\text{-}14)$$

$$SO + HS \Leftrightarrow S_2 + OH \quad (4\text{-}15)$$

$$SO + S + M \Leftrightarrow S_2 + O \quad (4\text{-}26)$$

$$HS + S \Leftrightarrow S_2 + H \quad (4\text{-}17)$$

Figures 4-3 to 4-5 show the trends of H_2S, H_2, SO_2, CO CO_2 and COS mole fractions along centerline of the reactor for 99.5% H_2S and 0.5% C_7H_8 gas stream composition. Compared to the 100% H_2S gas stream case, the conversion of H_2S decreased, as mole fractions of H_2S decomposed to a higher asymptotic minimum value. This is because toluene addition stimulated production of higher amounts of hydrogen, which provides oxidation competition to H_2. The mole fraction of H_2 increased to a peak value and then decayed with distance but was never completely consumed in the reactor. This is attributed to increased reactor temperature with toluene addition, which enhanced the thermal decomposition of H_2S (reactions 4-5 and 4-7). Also, combustion of toluene can result in the production of additional amounts of H_2 (Yuan et. al., 2014).

Mole fraction of SO_2 increased until it reached to a maximum value and then decayed with distance. The peak value of SO_2 was found to be lower and the rate of decay was faster in the case of 99.5% H_2S and 0.5% C_7H_8 gas stream composition than the baseline case of 100% H_2S. The decrease in the peak value of SO_2 mole fraction is partly due to the oxidation competition provided by H_2, which is supported from the increase in asymptotic mole fraction value of H_2S in the reactor. Moreover, toluene addition triggered formation of CO and COS which seems to have enhanced the rate of decay of SO_2. Significant reactions involved are depicted in reactions 4-18 through 4-25 (Karan et. al. 1998 and Clark and co-workers, 2000).

$$2CO + SO_2 \Leftrightarrow 0.5S_2 + 2CO_2 \qquad (4\text{-}18)$$

$$CO + SO_2 \Leftrightarrow SO + CO_2 \qquad (4\text{-}19)$$

$$CO + SO \Leftrightarrow COS + O \qquad (4\text{-}20)$$

$$COS + SO_2 \Leftrightarrow SO + 0.5S_2 + CO_2 \quad (4\text{-}21)$$

$$COS + SO \Leftrightarrow S_2 + CO_2 \quad (4\text{-}22)$$

$$CO + S \Leftrightarrow COS \quad (4\text{-}23)$$

$$COS + M \Leftrightarrow CO + S + M \quad (4\text{-}24)$$

$$COS + H_2O \Leftrightarrow H_2S + CO_2 \quad (4\text{-}25)$$

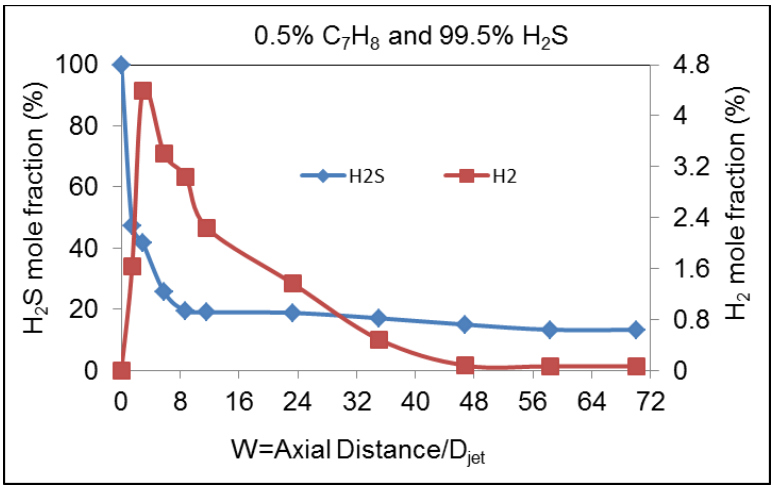

Figure 4-3. Hydrogen sulfide and hydrogen mole fractions. Flame conditions: $H_2S/C_7H_8/O_2$ flame, Φ=3.0

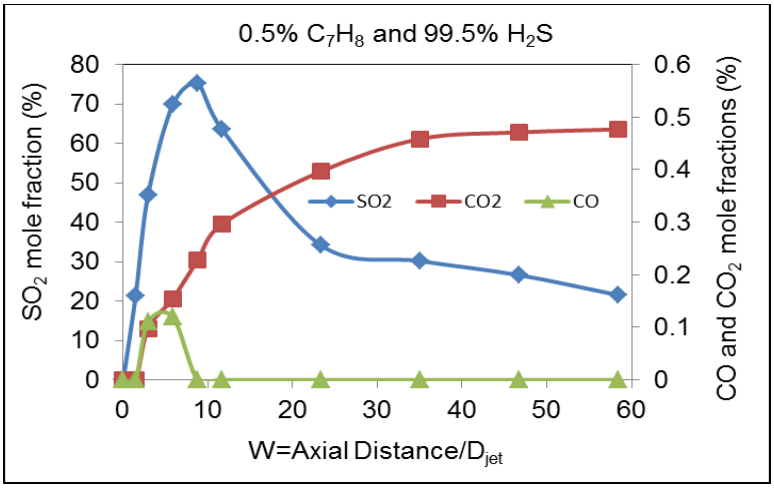

Figure 4-4. Sulfur dioxide, carbon monoxide and carbon dioxide mole fractions. Flame conditions: $H_2S/C_7H_8/O_2$ flame, Φ=3.0

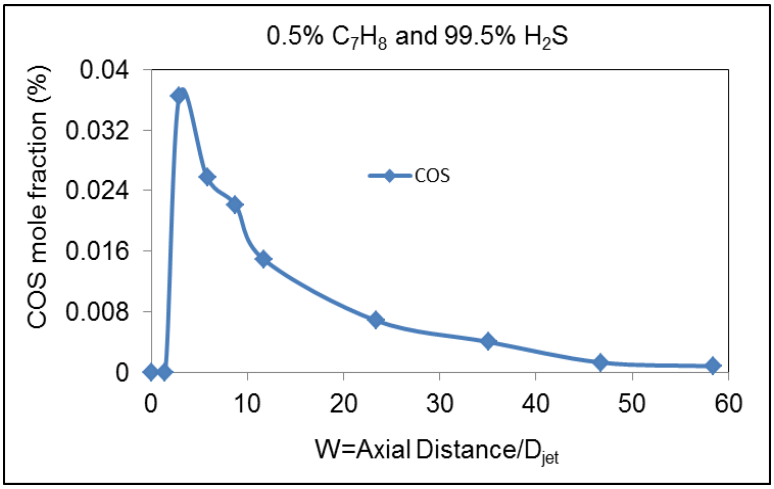

Figure 4-5. Carbonyl sulfide mole fractions. Flame conditions: $H_2S/C_7H_8/O_2$ flame, Φ=3.0

The formation of CO is due to toluene decomposition, while oxidation of CO to zero value could be due to the oxidation of CO by sulfur radicals to form COS and CO_2 simultaneously. The formation of COS is strongly dependent on the presence of CO in the reaction pool. Significant reactions involved are given in reactions 4-18 to 4-25 to elucidate the chemistry of CO, COS and other sulfur radicals in the reactor. Reaction 4-25 is expected to have played a part in the increased asymptotic minimum mole fractions of H_2S. This is also supported by the fact that mole fractions of produced CO_2 increased throughout the reactor centerline axis.

Figures 4-6 to 4-8 show the mole fractions of H_2S, H_2, CO, COS and CO_2 along the centerline of the reactor for 99% H_2S and 1% C_7H_8 gas stream composition. Compared to the previous two cases of 100% H_2S and 99.5% H_2S/0.5% C_7H_8 gas stream composition, the conversion of H_2S further decreased, as the asymptotic value of H_2S decay and maximum mole fraction of H_2 in the reactor further increased.

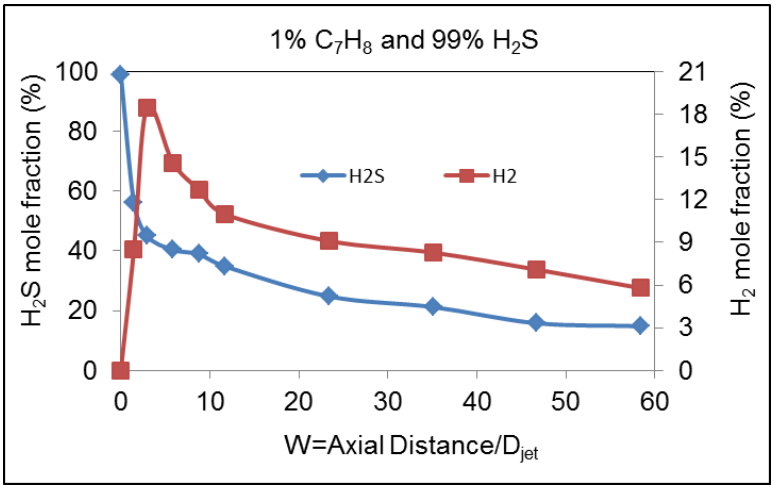

Figure 4-6. Hydrogen sulfide and hydrogen mole fractions. Flame conditions: $H_2S/C_7H_8/O_2$ flame, Φ=3.0

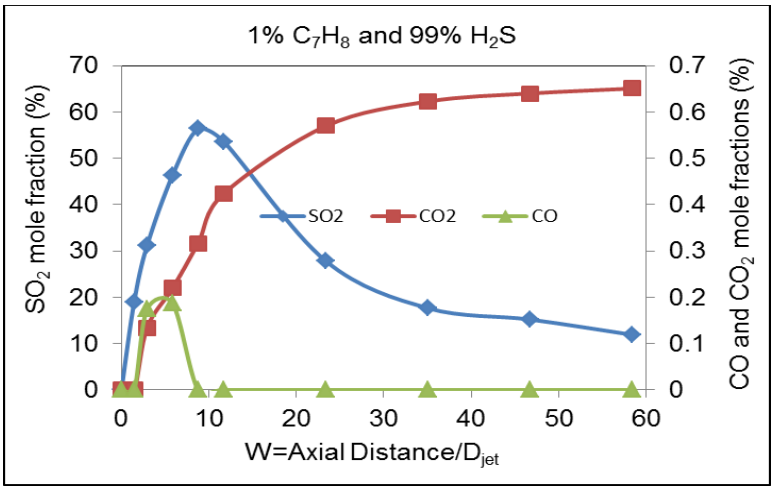

Figure 4-7. Sulfur dioxide, carbon monoxide and carbon dioxide mole fractions. Flame conditions: $H_2S/C_7H_8/O_2$ flame, Φ=3.0

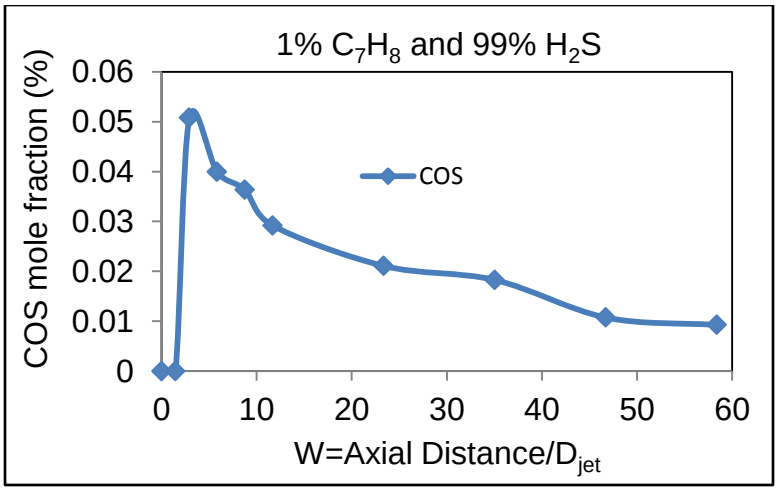

Figure 4-8. Carbonyl sulfide mole fractions. Flame conditions: $H_2S/C_7H_8/O_2$ flame, Φ=3.0

This supports the aforementioned interpretation that toluene addition stimulated production of higher amounts of hydrogen, which provided oxidation competition to H_2S. The peak value of SO_2 mole fraction further reduced and its rate of decay was faster than the other two previous cases. Moreover, reaction 4-25 could also have contributed to the production of additional H_2S as the mole fractions of COS and CO_2 increased throughout the reactor due to increased amounts of toluene addition. Mole fraction of CO increased to a maximum value and then decreased down to zero value, while that of CO_2 increased along the reactor centerline. On the other hand, COS increased to a peak value and then decomposed until it reached to an asymptotic value. The mole fractions of CO, CO_2 and COS were found to be higher than those with 99.5% H_2S/0.5% C_7H_8 gas stream composition. This is attributed to the increased toluene concentration in the gas stream.

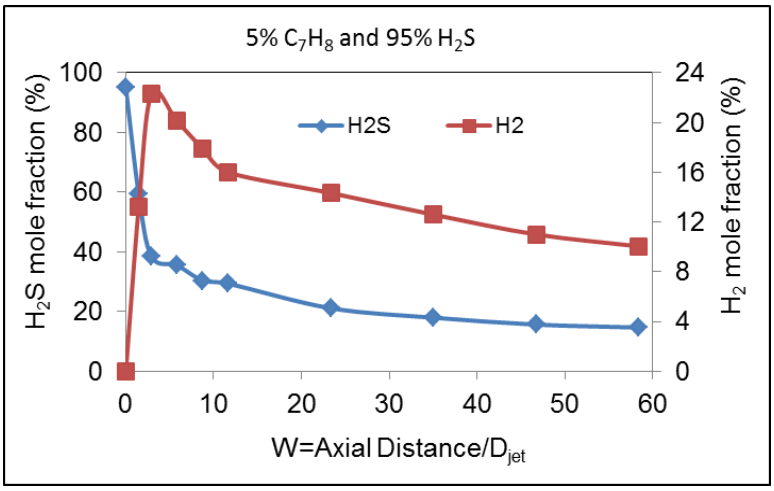

Figure 4-9. Hydrogen sulfide and hydrogen mole fractions. Flame conditions: $H_2S/C_7H_8/O_2$ flame, Φ=3.0

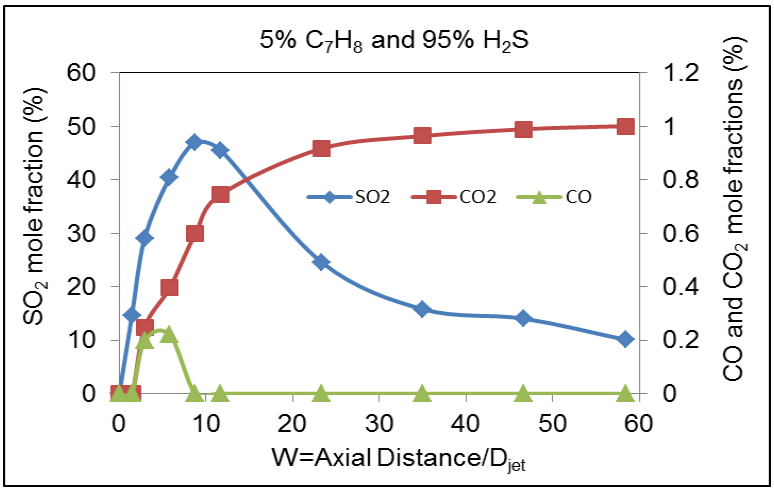

Figure 4-10. Hydrogen sulfide and hydrogen mole fractions. Flame conditions: $H_2S/C_7H_8/O_2$ flame, Φ=3.0

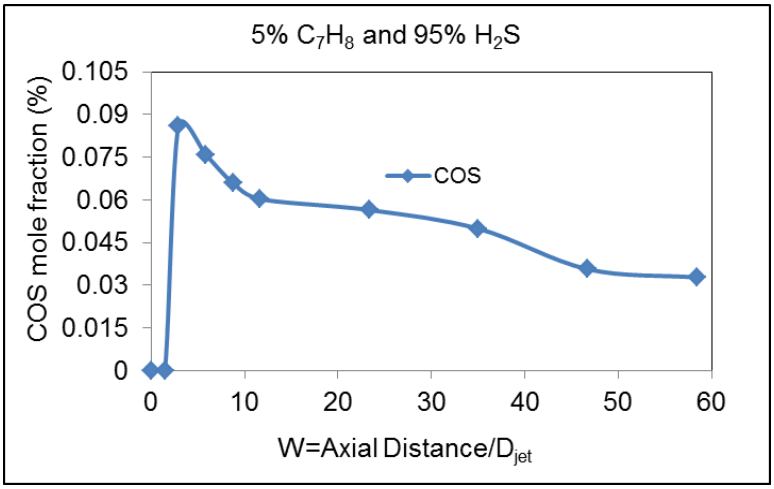

Figure 4-11. Hydrogen sulfide and hydrogen mole fractions. Flame conditions: $H_2S/C_7H_8/O_2$ flame, Φ=3.0

Further increase in the concentration of toluene (95% H_2S and 5% C_7H_8) did not alter the observed trends as shown in figures 4-9 to 4-11. This further justified interpretation of the results.

4.1.1.2 Summary

The role of toluene to H_2S combustion has been examined. Concentrations of toluene (0%, 0.5%, 1% and 5%) addition to H_2S gas were presented and the results compared with the baseline case of 100% H_2S gas stream. Addition of toluene triggered the formation of H_2, which increased with increase in toluene addition. The formed H_2 inhibited the oxidation of H_2S as evidenced from the increased amounts of H_2S at the reactor exit. Addition of toluene also resulted in the formation of CO and COS, which is attributed to the reactions of CO with SO_2 or S_2 and radicals. The mole fractions of both SO_2 and COS increased to a maximum then decayed with distance further downstream of the reactor. The maximum mole fraction of SO_2 and its rate of decay increased with increased toluene concentration in the gas stream. This supports

the possible reaction of SO_2 with COS to form elemental sulfur. Therefore, the presence of toluene, even in trace amounts can hinder the conversion of H_2S to S_2.

4.1.2 Benzene Addition Effects to H_2S/O_2 Flame

The effect of benzene to hydrogen sulfide combustion was also conducted. Benzene has higher thermal stability and lower reactivity, compared to toluene and xylene (Ji et al., 2011), and it is important to understand the relative effect of benzene, xylene and toluene during thermal decomposition in Claus reactors. Characterizing the individual effect of each contaminant (CO_2, N_2, benzene, toluene and xylene) on the composition of combustion generated species of hydrogen sulfide provides significant implications for operators, designers and program developers of sulfur plants. This will also facilitate modeling efforts and justifiable assumptions for practical applications.

Table 4-2 shows the test matrix for all experiments reported. The gas phase combustion generated species were quantified and analyzed. Combustion of 100% H_2S gas stream was first examined followed by a mixture of hydrogen sulfide and benzene (in small concentrations) combustion at equivalence ratio of three with respect to hydrogen sulfide and complete combustion of benzene.

Table 4-2. The test matrix

Run #	H_2S (cm^3/min)	O_2 (cm^3/min)	C_6H_6 (gas) (cm^3/min)	Gas Composition
1	150	75.00	0.00	100% H_2S
2	150	78.34	0.45	99.7%H_2S/ 0.3% C_6H_6
3	150	80.63	0.75	99.5% H_2S/ 0.5% C_6H_6
4	150	86.25	1.5	99.0% H_2S/ 1.0% C_6H_6

Benzene gas flow rates were calculated based on their densities: liquid benzene (0.876 g cm^{-3}) and gas benzene (0.00242 g cm^{-3}). Gas sampling and analysis of local species was conducted along the centerline of the reactor longitudinal axis.

4.1.2.1 Temperature Measurements

Mean temperatures were measured along the longitudinal axis of the reactor centerline using a K-type thermocouple. Figure 4-12 shows temperature profile in H_2S/O_2 and $H_2S/C_6H_6/O_2$ flame. In both cases, mean temperature increased to a peak value as the H_2S reacted with the surrounding oxygen. A decrease in temperature further downstream the reactor, is due to the heat losses from the reactor walls. However, addition of benzene into H_2S/O_2, even in trace amounts, favored an increase in flame temperature throughout the central axis of the reactor. This is due to the direct effect of energy release from benzene oxidation.

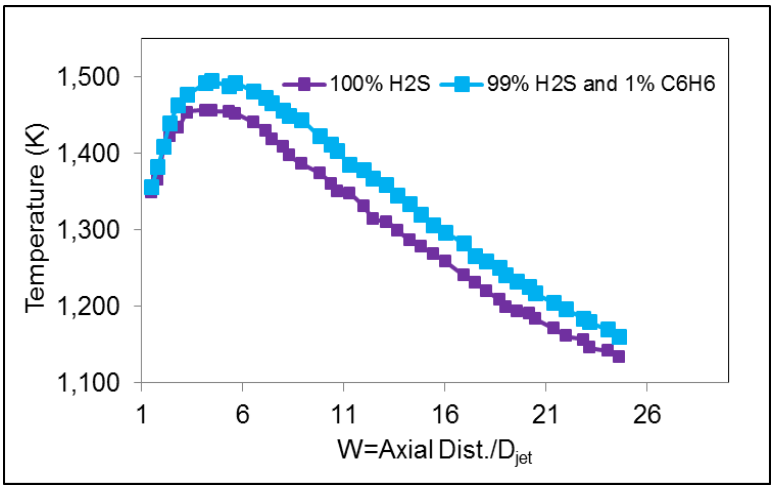

Figure 4-12. Temperature profiles from H_2S/O_2 and $H_2S/C_6H_6/O_2$ flame, Φ=3.0

4.1.2.2 Product Speciation and Analysis

Results from combustion of H_2S and 0.3%, 0.5 % and 1% of benzene in the H_2S/C_6H_6 mixtures are presented and evaluated. Combustion of H_2S is known to occur through pyrolysis at the initial stage (characterized by the formation of H_2 and sulfur radicals), followed by oxidation of H_2 and other formed radicals in the later stages (Selim et. al., 2011b).

Compared to neat H_2S combustion, pyrolysis reactions played a more prominent role as trace amounts of benzene (0.3%, 0.5% and 1%) were introduced alongside with H_2S into the burner. Combustion of neat H_2S is already discussed in the previous sub-section (4.2.1.1). Benzene altered the chemical kinetic pathways of H_2S reactions during combustion. It was observed that mole fractions of produced H_2 increased at each reactor centerline axis examined (figure 4-13). Increase in the amounts of benzene into the inlet H_2S stream further increased the mole fractions of produced H_2 in the reactor. This is partially attributed to the increased pyrolysis reactions of H_2S as a result of increased reactor temperature due to benzene addition. Detailed and reduced reaction pathways of H_2S pyrolysis/combustion have been examined by previous investigators (Raymont, 1974, Hawboldt et. al., 2000, maneta et. al., 2013).

It is also noted that H_2S reacts much faster with oxygen as compared to benzene due to difference in their bond energies and this stimulated increased pyrolysis reactions of both H_2S and benzene in the reactor. Increased formation of H_2 also caused oxidation competition between H_2S and formed H_2 in the reactor. It was observed that the rate of H_2S decomposition decreased slightly with increased

amounts of benzene addition downstream of the reactor (figure 4-14). However, the slight increase in the rate of H_2S decomposition observed at the initial stage of combustion is attributed to the increase in reactor temperature that enhanced H_2S pyrolysis (reactions 4-1 and 4.2).

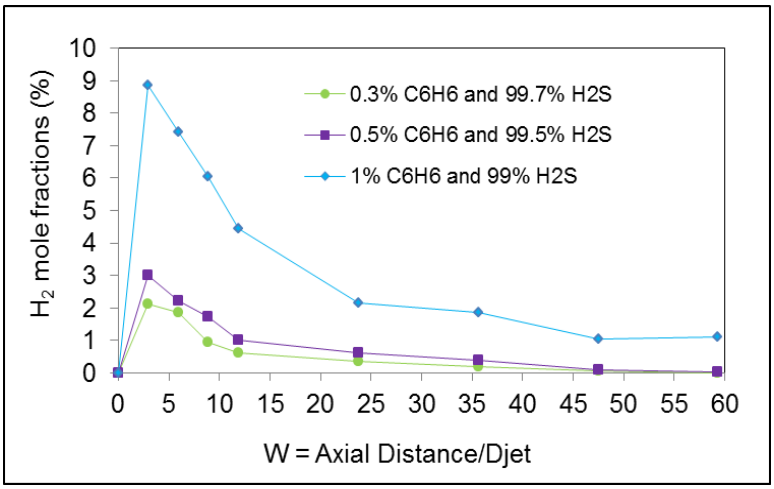

Figure 4-13. Mole fraction of hydrogen. Flame conditions: $H_2S/C_6H_6/O_2$ flame, Φ=3.0

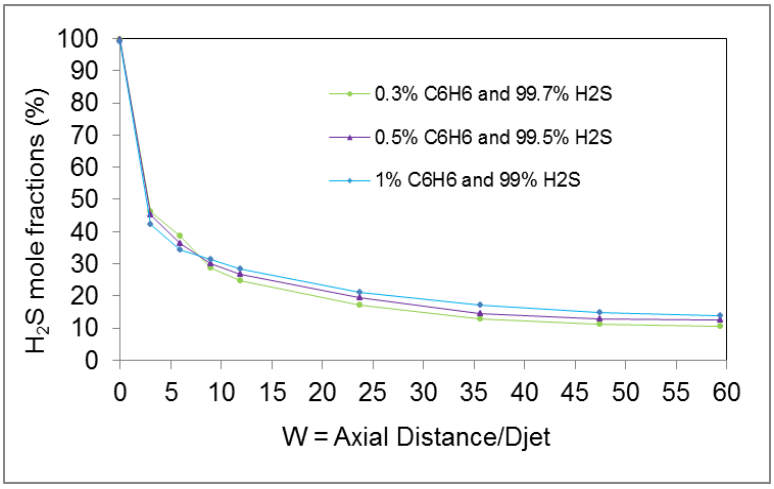

Figure 4-14. Mole fraction of hydrogen sulfide. Flame conditions: $H_2S/C_6H_6/O_2$ flame, Φ=3.0

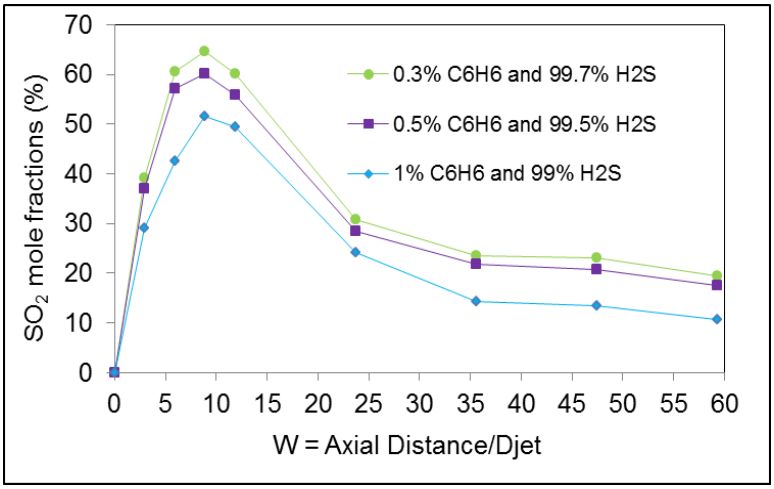

Figure 4-15. Mole fraction of sulfur dioxide. Flame conditions:

$H_2S/C_6H_6/O_2$ flame, Φ=3.0

Benzene reduced the maximum mole fraction of SO_2 (see figure 4-15) and its subsequent rate of decomposition was faster during H_2S/benzene mixture combustion as compared to combustion of neat H_2S. This observation corresponded to the formation of COS, which emanated from the formed CO in the reactor (see mole fractions of CO and COS results shown in figures 4-16 and 4-17). Thus, the observed trends of SO_2 mole fractions is attributed to oxidation of formed CO and other hydrocarbon radicals by SO_2, SO and other sulfur radicals in the reactor. The abundance of SO and other sulfur radicals have been shown in previous studies (Selim et. al., 2011b).

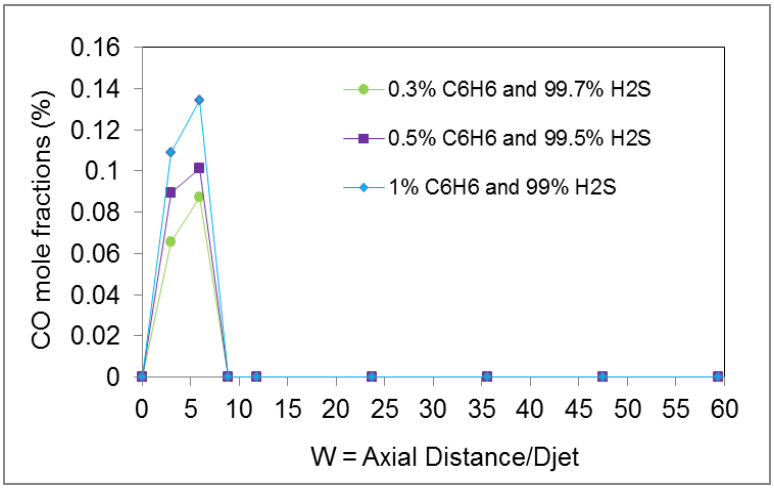

Figure 4-16. Mole fraction of carbon monoxide. Flame conditions:

$H_2S/C_6H_6/O_2$ flame, Φ=3.0

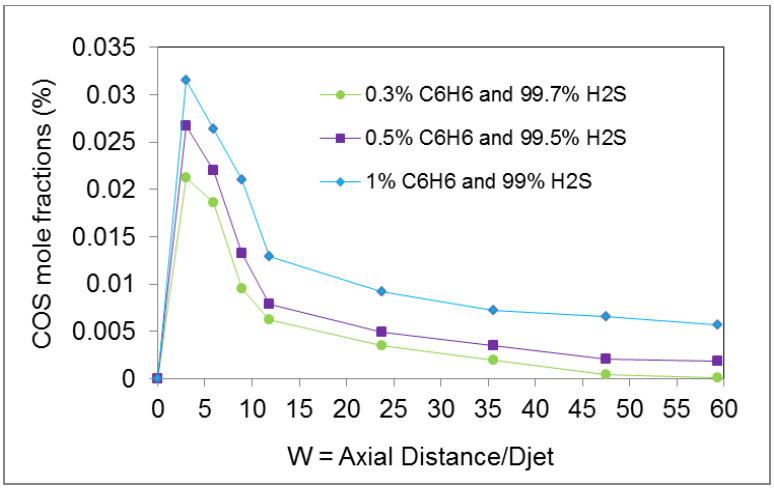

Figure 4-17. Mole fraction of carbonyl sulfide (COS). Flame conditions:

$H_2S/C_6H_6/O_2$ flame, Φ=3.0

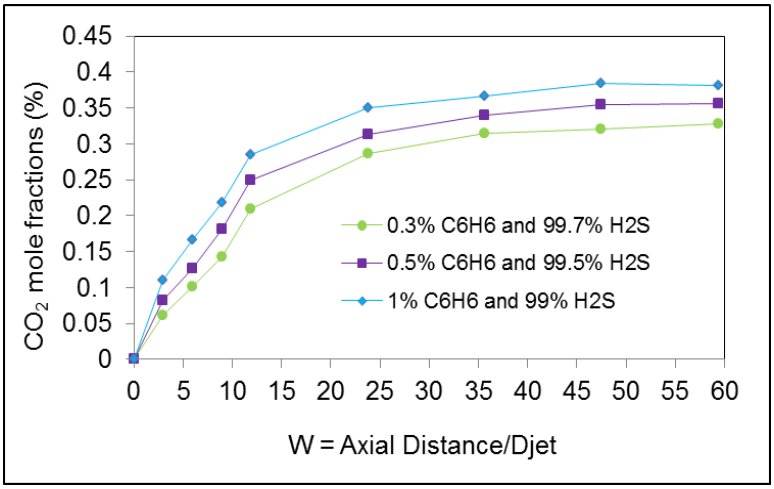

Figure 4-18. Mole fraction of carbon dioxide. Flame conditions: $H_2S/C_6H_6/O_2$ flame, Φ=3.0

Mole fraction of produced CO_2 is shown in figure 4-18, which revealed increased production with increase in residence time along the reactor centerline axis. Increased amounts of benzene injection further increased the mole fractions of CO and COS but reduced the amounts of formed SO_2 in the reactor to impact elemental sulfur production. Benzene showed a more severe impact, compared to toluene addition to H_2S. However, mole fractions of produced COS and H_2S at reactor exit reduced with benzene than with toluene. This is attributed to the lower amounts of H_2 and CO formation with benzene. Both toluene and benzene did not show any evidence of aromatic ring rupture due to the absence of acetylene in the sampled gas. This suggests that CO formation from benzene occurred through cyclopentadienyl and phenoxyl radicals, and in the case of toluene, methyl radical is easily formed, which yielded CO through HCO radicals. The work of Sagesse et al., 2013 supports this interpretation.

Benzene also had direct impact on the quality of produced sulfur as the sulfur deposit was observed to contain carbon/soot. These results highlight the significant impact of introducing small amounts of benzene on stable gas phase products during H_2S combustion. The formation of H_2, CO and COS in the reactor provides severe impact on the performance and efficiency of Claus reactors for sulfur capture from acid gases. The benzene addition can also favor increased emissions from sulfur recovery plants to increase environmental burden.

4.1.2.3 Summary

The direct effect of trace amounts (0.3%, 0.5% and 1%) of benzene to H_2S combustion was presented. A comparison of results with baseline case of neat H_2S combustion was also made. Benzene increased the amounts of H_2S at reactor exit, triggered significant H_2 production while reducing the amounts of SO_2 formed. Benzene also served as a precursor on the formation of CO and COS, as it favored CO production that provided the mechanistic pathways for COS formation due to the reactions of CO with SO_2 and other sulfur radicals in the reactor. Compared to toluene, benzene showed more severe impact on SO_2 formation in the reactor to reduce elemental sulfur production.

4.1.3 Xylene Addition Effects to H_2S Combustion

The role of xylene to H_2S combustion was examined and the formation/decomposition of selected gas phase products of combustion was evaluated. Xylene, unlike toluene and benzene, behaves much differently during thermal oxidation. The combustion properties of xylene are much different from those of benzene and toluene (Battin-Leclerc et al., 2006). Xylene exhibits a higher

reactivity than toluene and benzene during thermal oxidation, and flames of aromatic compounds are highly sensitive to fuel-specific chemistry (Ji et al., 2012). The reaction kinetics of the first few intermediates formed in the thermal oxidation and pyrolysis process that follows the initial fuel consumption is critical (Gail and Dagaut, 2005). Xylene is expected to have more severe impact on sulfur chemistry in the Claus reactor than toluene or benzene, due to higher reactivity and generation of intermediate products. Therefore, the role of trace amounts of xylene to H_2S combustion is examined under Claus condition. The evolutionary behavior of gas phase species evolved during combustion are determined and analyzed.

Table 4-3 shows the test matrix for all experiments to be presented. Combustion of neat H_2S gas stream is compared to mixture of H_2S and xylene combustion at equivalence ratio of three with respect to H_2S and complete combustion of xylene. Xylene gas flow rates were calculated based on their densities: liquid xylene (0.879 g cm-3) and gas xylene (0.0032 g cm-3). Gas sampling and analysis of local species was conducted along the centerline axis of the reactor.

Table 4-3. The test matrix

Run #	H_2S (cm^3/min)	O_2 (cm^3/min)	C_8H_{10} (gas) (cm^3/min)	Gas Composition
1	150	75	0	100% H_2S
2	150	82.9	0.75	99.5%H_2S/ 0.5% C_8H_{10}
3	150	90.8	1.5	99%H_2S/1% C_8H_{10}
4	150	106.5	3.0	98%H_2S/2% C_8H_{10}

Temperature profiles along centerline axis of the reactor are presented first followed by a discussion on speciation of stable gas phase products with xylene

addition. Dimensionless axial distance (W) was used for all the results presented here. Inner jet diameter of the burner was used to transform the linear distances into dimensionless parameters (W= axial distance/D_{jet}) for generalization of the results.

4.1.3.1 Temperature Measurements

Mean temperatures were measured along the centerline axis of the reactor using a K-type thermocouple. Figure 4-19 shows temperature profile in H_2S/O_2 flame both without and with the addition of xylene. During neat H_2S combustion, mean temperature increased to a peak value as the H_2S was oxidized by the surrounding oxygen, and decrease in temperature further downstream the reactor was due to heat loss to the reactor walls. On the other hand, combustion of H_2S/C_8H_{10} mixture caused the flame temperature to increase throughout the centerline axis of the reactor.

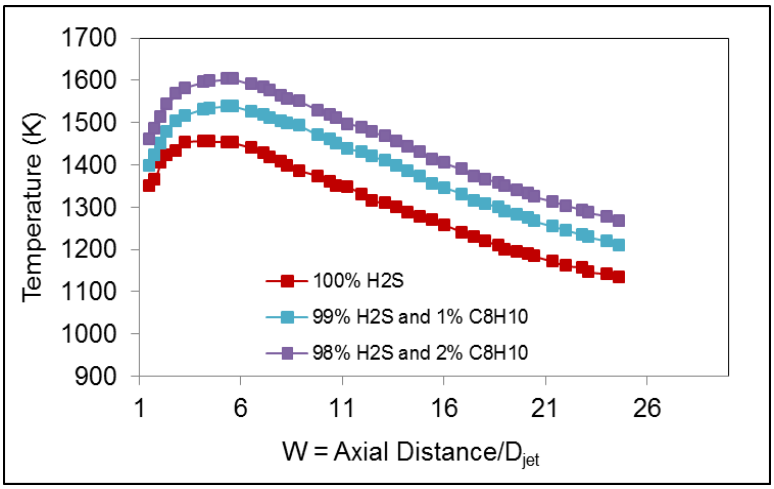

Figure 4-19. Temperature profile of H_2S/O_2 and $H_2S/C_8H_{10}/O_2$ flame, Φ=3.0

This is attributed to the direct effect of energy release from xylene combustion; increase in the amounts of xylene addition to 2% further increased the temperature at all distances along longitudinal centerline of the reactor. Compared to toluene and benzene, the magnitude of temperature increase was proportional to the

carbon number in the BTX, as xylene showed the highest magnitude of temperature increase in the reactor.

4.1.3.2 Product Speciation and Analysis

Different amounts of xylene addition (0.5%, 1% and 2%) into H_2S gas stream are presented. Results from combustion of H_2S and xylene mixtures are compared with the baseline case of 100% H_2S gas combustion. Combustion of H_2S was presented in previous sub-section 4.2.1.1. Addition of different amounts (0.5%, 1% and 2%) of xylene into H_2S gas stream altered the chemical kinetics and product distribution of H_2S reactions during combustion.

Figures 4-20 and 4-21 show the distribution of H_2S and H_2 mole fractions along centerline of the reactor for different gas mixture combustion. Xylene addition increased the initial decomposition of H_2S, but slowed down further downstream the reactor centerline axis to slightly increase the mole fraction of H_2S at the reactor exit. Further increase in xylene addition showed similar trends. Increase in the initial consumption of H_2S is attributed to increase in reactor temperature. In addition, formation of CO and CH_4 from xylene decomposition created additional pathways on H_2S consumption. Example of such reactions is shown in reactions 4-26 through 4-29 (Clark et. al., 2000 and Chin et. al. 2000, 2001). Further downstream the reactor, H_2S decomposition decreased due to the possible formation of H_2S from oxidation of formed COS and CS_2, as well as oxidation competition between formed H_2 and H_2S in the reactor. Xylene stimulated increased formation of H_2 in the reactor, which increased to a maximum and then decreased until reaching to a minimum value. Mole fractions of produced H_2 increased with increase in the amounts of xylene addition

into the inlet H_2S. Formation of H_2 emanated from the pyrolysis of both H_2S and xylene. Hydrogen is known to be an intermediate product formed during combustion/pyrolysis of xylene (Binoist et. al., 2003 and Ji et. al., 2014). Moreover, H_2 formation could be enhanced from increased pyrolysis of H_2S (such as, reaction 4-1 and 4-3) at initial stage of combustion due to higher reactor temperatures with xylene addition. It was noted that H_2S reacts with oxygen much faster than xylene and pyrolysis of xylene is expected to be dominant during combustion of H_2S and xylene mixture.

$$CH_3 + H_2S \Leftrightarrow CH_4 + SH \quad (4\text{-}26)$$

$$CH + 2H_2S \Leftrightarrow CS_2 + 2.5H_2 \quad (4\text{-}27)$$

$$CH_2 + S \Leftrightarrow CS + H_2 \quad (4\text{-}28)$$

$$CH_4 + 2S \Leftrightarrow CS_2 + 2H_2 \quad (4\text{-}29)$$

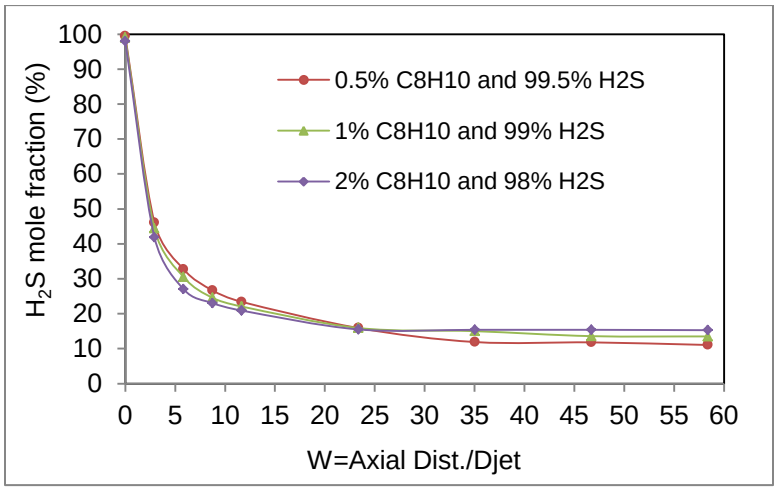

Figure 4-20. Mole fraction of hydrogen sulfide. Flame conditions: $H_2S/C_8H_{10}/O_2$ flame, Φ=3.0

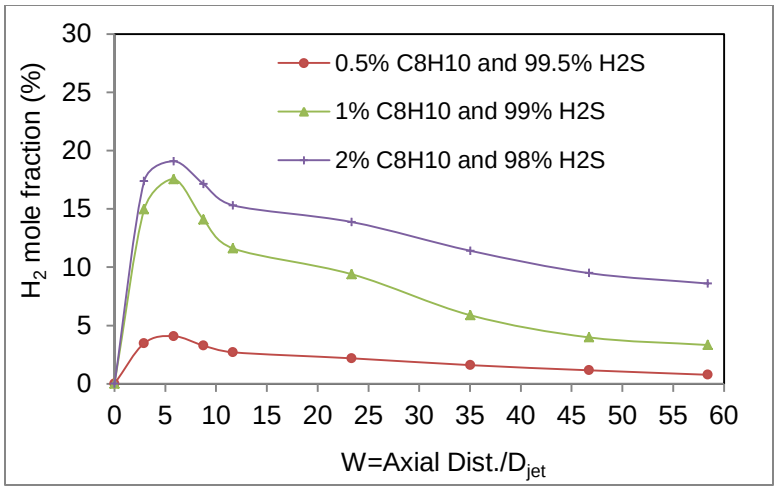

Figure 4-21. Mole fraction of hydrogen. Flame conditions: $H_2S/C_8H_{10}/O_2$ flame, Φ=3.0

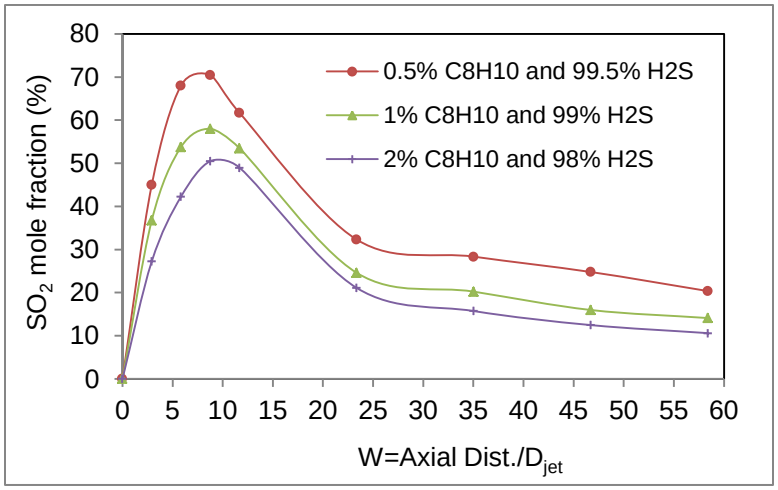

Figure 4-22. Mole fraction of sulfur dioxide. Flame conditions: $H_2S/C_8H_{10}/O_2$ flame, Φ=3.0

Mole fraction of SO_2 (shown in figure 4-22) increased to a maximum value as H_2S reacted with oxygen, and then decomposed with increase in axial distance (residence time in the reactor) due to reaction of H_2S with SO_2 to form elemental sulfur. The maximum SO_2 mole fraction was observed to be lower and the subsequent rate of decomposition was faster compared to combustion of neat H_2S. The behavior

of SO_2 mole fraction could be attributed to the possible reaction of SO radicals or SO_2 with CO, CH_4 or hydrocarbon radicals in the reactor to form COS and CS_2, such as reactions 4-30 to 4-33 (Chin et al., 2001). Arutyunov and co-workers, 1992 & 1993, showed that abundance of SO_2 favors the oxidation of CH_4 in the reactor, and this supports interpretation of the presented data. Mole fractions of CO and CH_4 increased to a maximum and then decomposed at further downstream position along the centerline axis of the reactor.

Xylene decomposed to foster the formation of CO and CH_4, and the formed CO and CH_4 were subsequently oxidized by SO, SO_2 and other radicals to form COS and CS_2 in the reactor. The abundance of SO and other sulfur radicals have been shown in the work of Selim et al., 2011b. However, increased xylene addition lowered the maximum mole fraction of formed of SO_2 but increased the subsequent rate of decomposition of SO_2 further downstream the reactor. This is because increased xylene addition further increased the reactor temperature that enhanced the rate of reactions between SO radicals or SO_2 with CO, CH_4 or hydrocarbon radicals in the reactor to form mercaptans (COS and CS_2) and elemental sulfur.

$$CH_4 + 2SO_2 \Leftrightarrow CO_2 + S_2 + 2H_2O \quad (4\text{-}30)$$

$$CS_2 + SO \Leftrightarrow COS + S_2 \quad (4\text{-}31)$$

$$COS + SO_2 \Leftrightarrow SO + 0.5S_2 + CO_2 \quad (4\text{-}32)$$

$$CS_2 + H_2O \Leftrightarrow COS + H_2S \quad (4\text{-}33)$$

Mole fractions of produced CO_2 increased throughout the reactor centerline axis (see figure 4-23), which support the possible reactions for SO_2 reduction and those of COS and CS_2 formation and decomposition. It was noted that CO mole

fractions did not decompose to zero value, as observed with toluene and benzene in the inlet H_2S gas stream. The incomplete oxidation of CO can be attributed to the role of SO_2, H_2S and H_2 as possible inhibitors to CO oxidation. Since the amounts of CO were very low with toluene and benzene, the inhibition effect was not noticeable. Another potential factor is the amounts of formed CH_4 in the reactor, which increases oxidation competition in the reactor to alter the local equivalence ratio. The enhanced fuel rich condition of the reactor can then increase the rate of CO inhibition by SO_2.

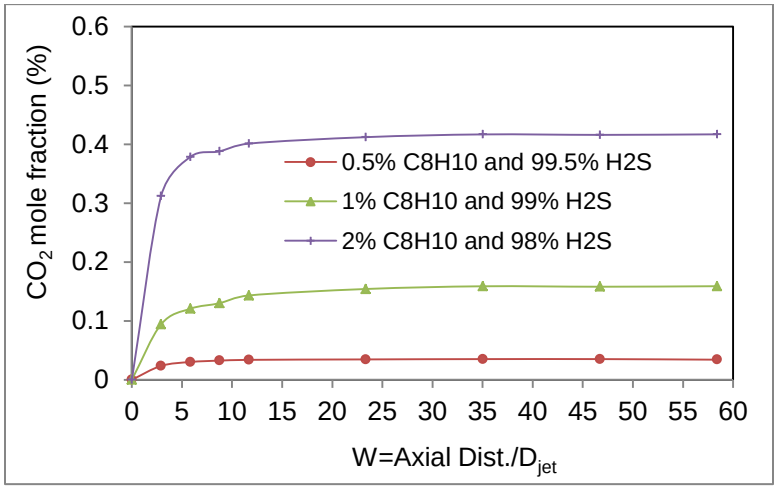

Figure 4-23. Mole fraction of carbon dioxide. Flame conditions:

$H_2S/C_8H_{10}/O_2$ flame, Φ=3.0

Moreover, Dagaut et al., 2003 also suggested the inhibition effect of SO_2 in CO-H_2 flames. Also, higher amounts of SO_2 were formed with xylene as compared to toluene and benzene, and this has significant impact on elemental sulfur formation.

$$CH_3C_6H_5CH_3 + M \Leftrightarrow CH_3C_6H_5CH_2 + H + M \quad (4\text{-}34)$$

$$CH_3C_6H_5CH_3 + M \Leftrightarrow C_6H_5CH_3 + CH_3 + M \quad (4\text{-}35)$$

$$C_6H_5CH_3 + M \Leftrightarrow C_6H_5CH_2 + H + M \quad (4\text{-}36)$$

$$C_6H_5CH_3 + M \Leftrightarrow C_6H_6 + CH_3 + M \quad (4\text{-}37)$$

$$C_6H_6 + M \Leftrightarrow C_6H_5 + H + M \qquad (4\text{-}38)$$

Mole fractions of CH_4 and CS_2 are shown in figures 4-24 and 4-25. Formation of CH_4 and CS_2 is attributed to the interaction of CH_4 and other hydrocarbon radicals with sulfur species in the reactor. The formed radicals from initial xylene decomposition played prominent role in H_2S oxidation. Thermal decomposition of xylene occurs through thermal or chemical initiation by active radicals (such as H, OH, S and HS) in the reactor. This results in H-abstraction or methyl radical formation, which leads to H_2 and CH_4 formation in the reactor.

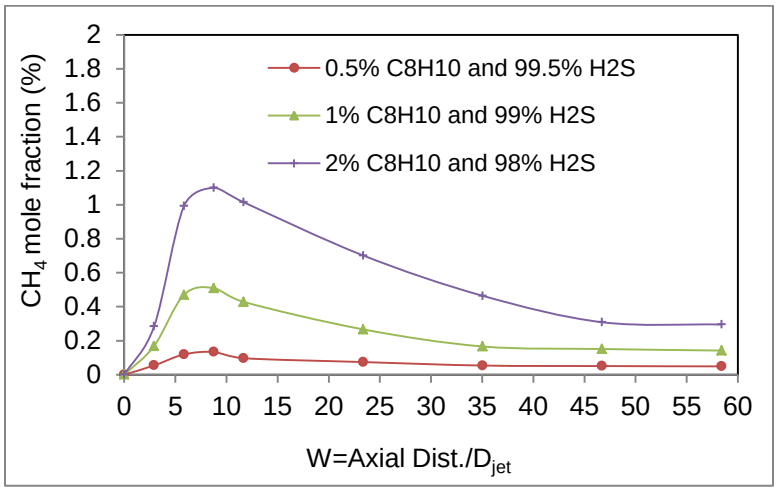

Figure 4-24. Mole fraction of methane. Flame conditions: $H_2S/C_8H_{10}/O_2$ flame, Φ=3.0

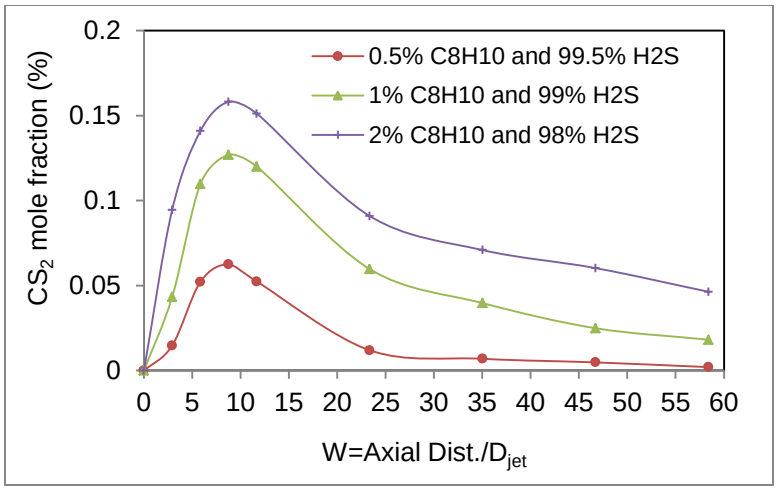

Figure 4-25. Mole fraction of carbon disulfide. Flame conditions: $H_2S/C_8H_{10}/O_2$ flame, Φ=3.0

A summary of reactions involved in initial decomposition of xylene is shown in reactions 4-34 through 4-38 (Hippler et al., 1994; Ji et al., 2012). This resulted in the formation of toluene and CH_4 from radical recombination reaction. Increase in the amounts of xylene addition further increased CH_4 formation that resulted in increased production of CS_2 at each location examined in the reactor. The oxidation of both CH_4 and CS_2 could be attributed to the availability of SO_2 in the reactor, which favored production of CO_2, H_2, S_2 and additional amounts of H_2S. It was observed that H_2S and H_2 mole fractions increased further downstream the reactor exit. Mole fractions of COS and CO are shown on figures 4-26 and 4-27.

$$C_6H_5CH_2 + O \Leftrightarrow C_6H_5CHO + H + M \quad (4\text{-}39)$$

$$C_6H_5CHO + O \Leftrightarrow C_6H_5CO + H \quad (4\text{-}40)$$

$$C_6H_5CO + M \Leftrightarrow C_6H_5 + CO + M \quad (4\text{-}41)$$

$$C_6H_6 + M \Leftrightarrow C_6H_5 + H + M \quad (4\text{-}42)$$

$$C_6H_5 + O \Leftrightarrow C_5H_4 + CO \quad (4\text{-}43)$$

$C_6H_5CHO + H \Leftrightarrow C_6H_6 + HCO$ (4-44)

$HCO + M \Leftrightarrow CO + H + M$ (4-45)

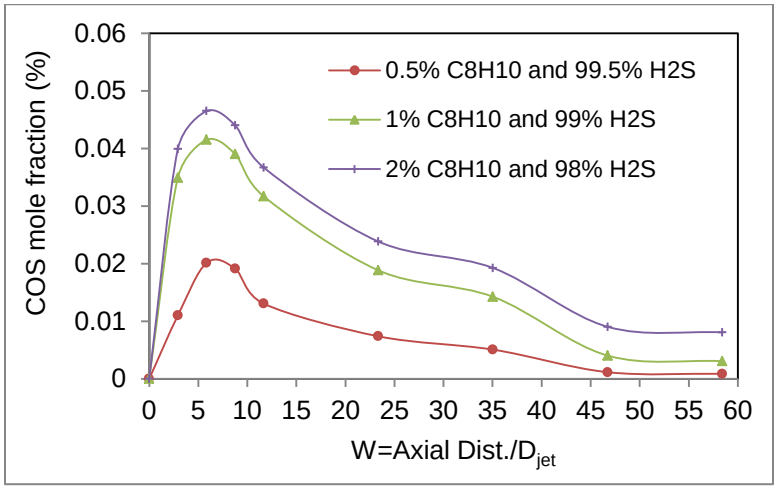

Figure 4-26. Mole fraction of carbonyl sulfide. Flame conditions:

$H_2S/C_8H_{10}/O_2$ flame, Φ=3.0

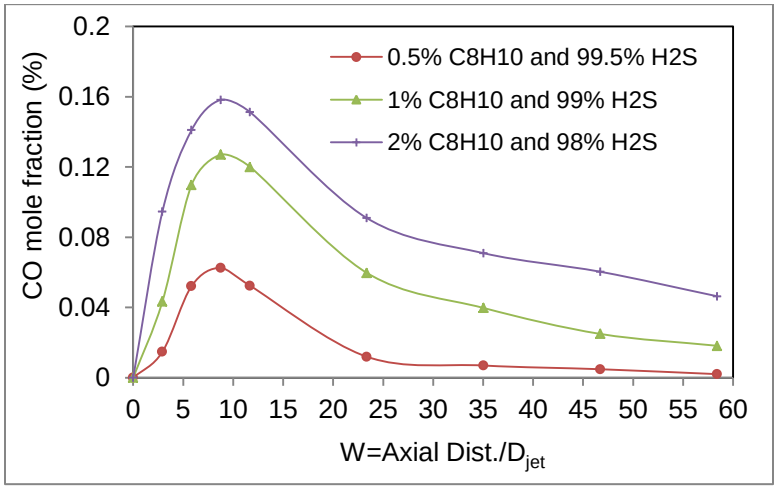

Figure 4-27. Mole fractions of carbon monoxide. Flame conditions:

$H_2S/C_8H_{10}/O_2$ flame, Φ=3.0

The formation of CO is due to xylene decomposition in the reactor, and this involves occurrence of reactions 4-39 through 4.45 (Ji et al., 2012). The first few radicals formed from xylene initial decomposition contributed to CO, COS and CS_2

formation in the reactor. Production of CO occurred through the oxidation of methyl radical and through phenoxy species from methylbenzyl, benzyl and phenyl radical oxidation. The results did not suggest aromatic ring rupture from xylene decomposition or its intermediates (toluene and benzene) as acetylene was absence in the sampled gas. Acetylene is known to be the major product of aromatic ring opening reactions, particularly in rich flames. Formation of CO then provided the pathway on COS formation. The oxidation of COS and CO further supports the observed reduction in the mole fractions of produced SO_2 in the reactor, and also contributed to the observed increase in the asymptotic minimum mole fractions of H_2S.

Compared to the previous data with toluene or benzene, these results showed quantitative difference in the amounts of H_2, H_2S and SO_2 produced in the reactor. Gas speciation at the reactor exit is compared for the H_2S and mixtures of H_2S and benzene, toluene or xylene (figures 4-28 to 4-31). Xylene showed less severe impact on H_2S conversion and SO_2 formation, with subsequent impact on elemental sulfur production, compared to toluene and benzene. Benzene had a more severe impact on SO_2 production in the Claus reactor. The higher amount of H_2S production with toluene was attributed to the chemistry of intermediate species formed in the combustion process. The two methyl group radicals released from xylene, compared to one methyl radical from toluene and non in benzene, created additional pathways on H_2S consumption. The chemistry of intermediates species (COS, CS_2, CO and H_2) played significant role in H_2S conversion.

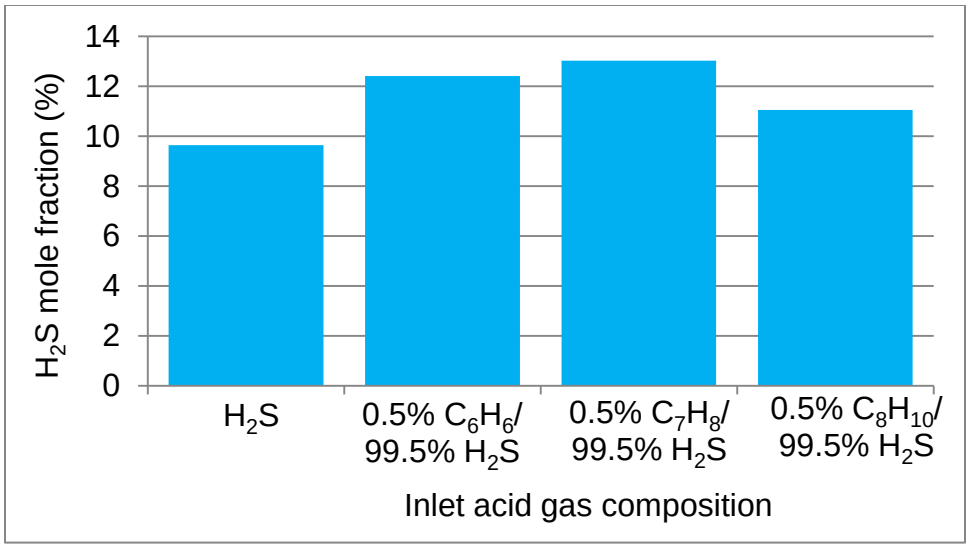

Figure 4-28. Hydrogen sulfide production at the exit of thermal stage reactor without/with benzene, toluene or xylene addition

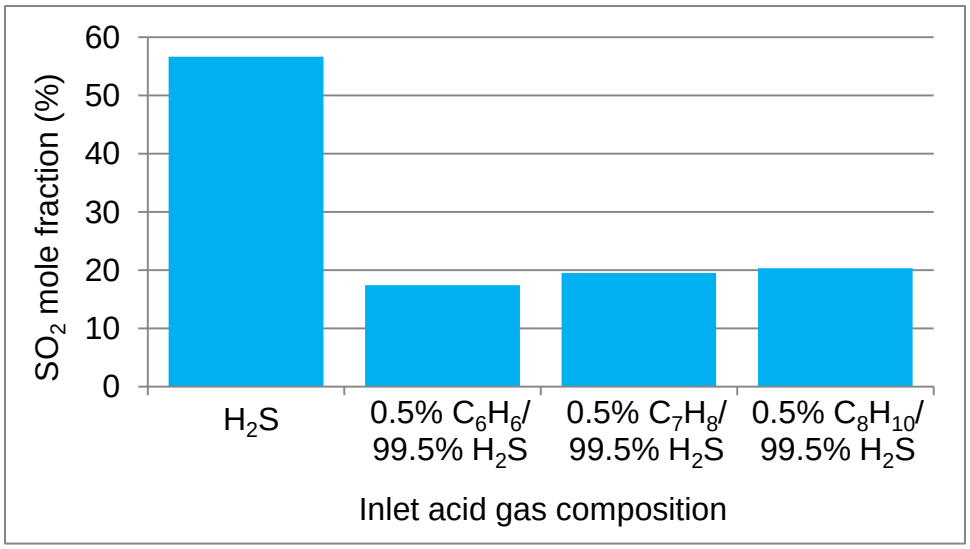

Figure 4-29 Sulfur dioxide production at the exit of thermal stage reactor without/ with benzene, toluene or xylene addition

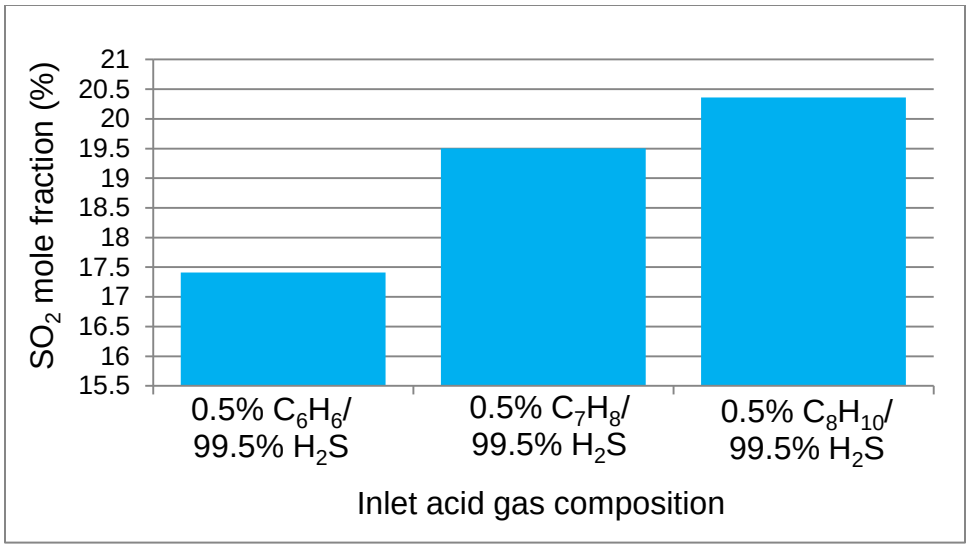

Figure 4-30 Sulfur dioxide production at the exit of thermal stage reactor with benzene, toluene or xylene addition

It was noted that the oxidation of COS and CS_2 formed in the reactor favored additional amounts of H_2S production. The reaction between COS and H_2O resulted in increased H_2S and CO_2 formation (reactions 4-25), and production of COS was higher with toluene addition than with benzene or xylene (figure 4-31). In addition to reaction 4-25, there was also oxidation of CS_2 to form additional amount of H_2S and CO_2 (reaction 4-33), and reaction of COS with H_2S to form CO and elemental sulfur (reaction 4-46). However, since CO formation was higher with xylene addition, one will expect higher production of COS. The lower amounts of COS production with xylene is attributed to the occurrence of competing reaction 4-46 in the Claus reactor. This reaction played a more prominent role due to the higher magnitude of temperature increase favored by xylene addition, compared to benzene and toluene.

$$COS + H_2S \Leftrightarrow CO + 0.5S_2 \qquad (4\text{-}46)$$

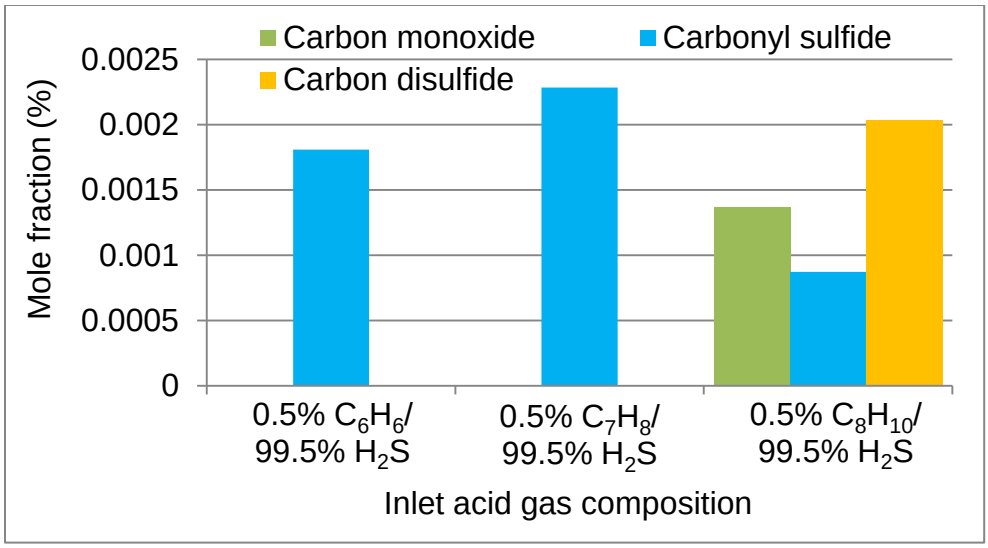

Figure 4-31 Carbonyl sulfides, carbon disulfide and carbon monoxide production at the exit of thermal stage reactor with benzene, toluene or xylene

The faster reactivity of xylene as compared to toluene and benzene was evident on the higher mole fractions of produced CO. Formation of CO with toluene or benzene addition occurred at the initial stage of combustion, but was rapidly oxidized further downstream in the reactor. However, CO formation significantly increased with xylene/H_2S combustion. This is directly attributed to the role of the first few intermediate radicals formed during initial stage of xylene decomposition, which increased the number of mechanistic pathways on CO formation. This favored production of higher amounts of toxic compounds (CO, COS and CS_2), to increase the processing load in catalytic stages. This offers more insight on why previous researchers have observed faster catalyst deactivation with xylene than with benzene or toluene. Benzene showed the greatest effect on SO_2 production to hinder elemental sulfur formation in the thermal stage Claus reactor, and the effect decreases from toluene to xylene.

These results highlight the formation of combustion intermediates (CO, CH_4, H_2, COS and CS_2) with trace amounts of xylene addition into H_2S flames. These compounds have direct impact on performance and efficiency of Claus reactors for sulfur capture from acid gases, as well as the increased production of mercaptans (COS and CS_2) under the prevailing conditions with trace quantities of xylene. Although H_2 is not considered an environmental hazard, it affects oxidation of H_2S and also acts as a diluent in Claus reactor. So, increased formation of H_2 could necessitate an increase in the volume of Claus reactors for sulfur capture from acid gases.

4.1.3.3 Summary

Results have been presented on the effect of trace amounts (0.5%, 1% and 2%) of xylene addition into inlet H_2S gas during combustion and compared with the baseline case of neat H_2S combustion. Xylene addition increased the amounts of H_2S at the exit of thermal stage reactor, stimulated production of H_2, CH_4, CO, COS and CS_2. The methyl radicals in the xylene molecule played significant role in the formation of these intermediate compounds. The oxidation of CH_4 and CO by SO_2 and other sulfur radicals reduced the maximum mole fraction of SO_2 but increased the subsequent rate of SO_2 decomposition to favor elemental sulfur formation. Xylene showed less severe impact on H_2S conversion and SO_2 formation, compared to toluene and benzene. Benzene had a more severe impact on SO_2 production in the Claus reactor, to hinder elemental sulfur production. The observed differences are attributed to the higher flame temperatures observed with xylene addition, compared to toluene and benzene, as well as the chemistry of intermediate species formed in the

combustion process. Initial chemistry of xylene decomposition had a distinct mark on the production of CO in the reactor. The produced CO was not completely oxidized in the reactor due to inhibition effects by SO and SO_2. The results also showed higher production of hydrogen with xylene, and the produced H_2 inhibits conversion of H_2S. This can necessitate increase in the size of Claus reactors due to the increase in volume of processing gases. The results highlight the need for efficient destruction of BTX and other formed impurities under high temperature conditions to enhance sulfur production while minimizing emissions.

4.2 BTX Destruction in Claus Reactors

Presence of impurities in acid gas (such as BTX, COS and CS_2) leads to serious operational issues that reduce the process plant efficiency. The efficiency of Claus process is a function of acid gas composition and reactor operational conditions. These impurities, especially BTX causes loss in catalyst activity due to the deposition of carbon/soot on the catalyst surfaces, corrosion of downstream equipment leading to decreased sulfur recovery efficiency, to increase maintenance cost and higher sulfur emissions. Therefore, destruction of BTX and other impurities at the thermal stage of Claus process is the solution. However, acid gas can contain considerable amounts of carbon dioxide (lean acid gas) that makes it difficult to achieve high furnace temperature (Rameshni, 2010). The presence of high concentration of carbon dioxide causes problems of flame instability and reduced temperatures in the reactor. This does not provide high enough furnace temperatures to burn the higher hydrocarbons (BTX) that exist in the acid gas. It has been reported

that the reaction pathways responsible for BTX destruction are kinetically controlled, and the rate of BTX destruction increases with increase in the temperature of gases in the reactor (Norman et al., 2002). High localized flame temperatures are essential for complete destruction of BTX in the thermal stage reactors. Other parameters that enhance destruction of impurities (including BTX) are residence time and mixing. Temperature and residence time have greater effect on BTX destruction (Norman et al., 2002). It is therefore necessary to seek reactor conditions that enhance flame temperatures and increase gas residence time in the thermal stage reactor.

4.2.1 Investigation of Optimum Reactor Temperature

A parametric study was conducted using equilibrium sulfur conversion in CHEMKIN PRO to investigate optimum reactor temperature for enhanced sulfur capture from mixtures of H_2S, toluene and CO_2. The use of equilibrium sulfur conversion is favorable due to the high temperature condition of the thermal stage of Claus process, which favors faster rate of chemical reactions. Equilibrium modeling can also be representative of product compositions, and this is most significant in fast chemical kinetic processes.

4.2.1.1 Experimental and Numerical Comparison of Data

Experiments were carried out to quantify the sulfur conversation efficiency of a thermal stage Claus reactor. Simulations were conducted using equilibrium analysis mode in CHEMKIN PRO. Table 4-4 shows the gas composition injected into the reactor. To validate the trends observed from simulations, experiments were conducted to quantify conversion efficiency. The simulations were carried out at selected temperature of 1495K for comparison with experimental data (conversion

efficiency vs. toluene concentration) due to the existence of temperature variation in the experiments. Sulfur conversion efficiency used to compare the reactor performance under different operational conditions is defined as:

$$Conversion\,Efficiency = \frac{Mass\,of\ recovered\ sulfur}{Mass\,of\ sulfur\,in\,inlet\ H_2S}$$

Table 4-4.The test matrix

Run #	H_2S (cm^3/min)	O_2 (cm^3/min)	C_7H_8 (gas) (cm^3/min)	Acid gas composition (%)
1	150	75	0	0% C_7H_8, 100%H_2S
2	150	81.75	0.75	0.5%C_7H_8, 99.5%H_2S
3	150	88.5	1.5	1%C_7H_8, 99%H_2S
4	150	102	3.0	2%C_7H_8, 98%H_2S
5	150	115.5	4.5	3%C_7H_8, 97%H_2S

The major goal of this comparison was to validate experimentally the trends of predicted conversion efficiency with different amounts of toluene addition into acid gas stream, so that this model can then be used to investigate optimum reactor temperature for enhanced sulfur recovery. Figure 4-32 depicts the experimental and numerical trends of conversation efficiency with change in the amounts of toluene addition into the H_2S acid gas stream. The figure shows a near linear relationship of conversion efficiency with different amounts of toluene addition. Deviation between the simulation and experiment increased with increase in toluene addition. Nevertheless, predicted results fairly agree with experimentally observed trends qualitatively, most especially at low toluene concentrations, but quantitatively, showed significant deviation from experiments.

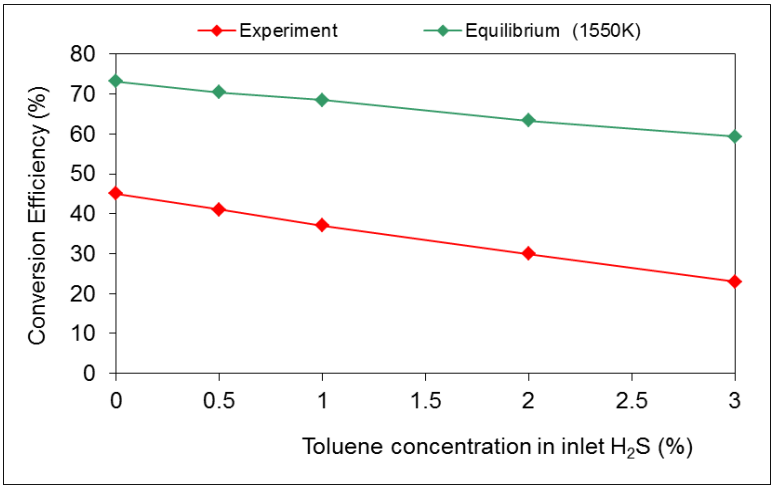

Figure 4-32. Equilibrium prediction vs. experimental comparison of conversion efficiency with change in toluene addition to inlet H_2S

This observed deviation could be attributed to the assumptions involved in equilibrium mode of analysis and, the temperature variation in the experiments. Nevertheless, the major emphasis from this comparison is on understanding the qualitative trends of conversion efficiency with change in acid gas composition. Conversion efficiency decreases with increase in the amounts of toluene addition into H_2S gas stream. Toluene was observed to stimulate formation of significant amounts of H_2 in the reactor, which reduced rate of H_2S decomposition due to oxidation competition between H_2S and formed H_2 in the reactor. Toluene also triggered formation of CO and the formed CO was oxidized by SO_2 and other sulfur radicals to form COS in the reactor.

4.2.1.2 Toluene and Acid Gas (H_2S) Combustion

Numerical simulations were conducted to seek the role of toluene on the optimum reactor temperature for enhanced sulfur conversion efficiency at the thermal stage of Claus reactor. The temperature range of 800-2000K was examined over a

wide range of toluene (0-3%) and carbon dioxide (0-70%) concentration in inlet H_2S gas stream. Figure 4-33 shows change in conversion efficiency with increase in temperature for different amounts of toluene in H_2S acid gas. This graph revealed existence of optimum temperature that corresponds to maximum amount of sulfur recovery from acid gas. Conversion efficiency increased at lower temperatures due to the formation of elemental sulfur (reactions 4-47 and 4-48) and this resulted in lower amounts of SO_2 formation.

$$H_2S + 1.5O_2 \rightarrow H_2O + SO_2 \quad (4\text{-}47)$$

$$2H_2S + SO_2 \rightarrow 1.5\ S_2 + 2H_2O \quad (4\text{-}48)$$

In contrast, conversion efficiency decreased at higher temperatures due to change in the chemical kinetics of H_2S reactions that enhanced continuous SO_2 production rather than elemental sulfur. However, toluene addition decreased the conversion efficiency due to reduced amounts of sulfur formation, as it altered the chemical kinetics and product speciation of H_2S reactions. This could be attributed to the formation of several intermediate products that altered the product distribution of H_2S reactions. The optimum reactor temperature was constant when less than 1% of toluene was present in acid gas, but addition of higher amounts of toluene caused the optimum reactor temperature to increase (see figure 4-34).

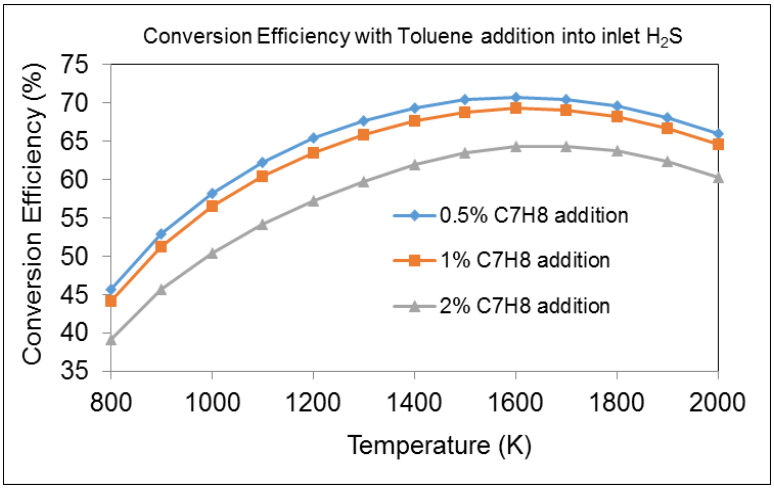

Figure 4-33. Conversion efficiency vs. reactor temperature with change in toluene addition to H_2S

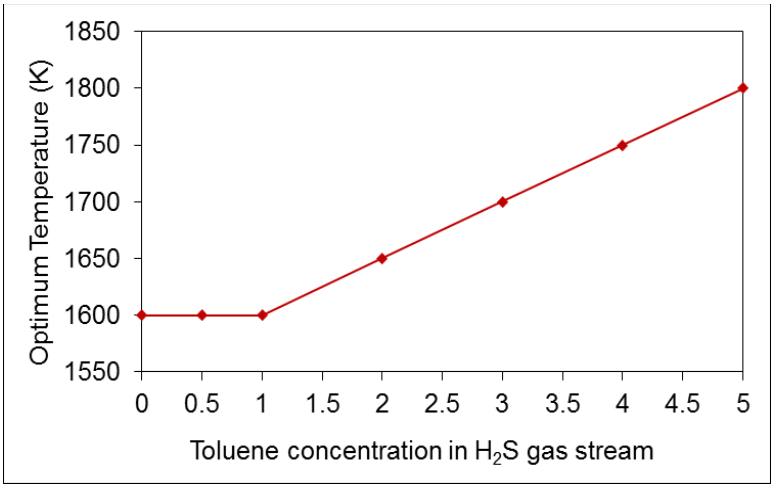

Figure 4-34. Optimum reactor temperature vs change in toluene addition to inlet H_2S in mole percentages

4.2.1.3 Toluene, CO_2 and H_2S Combustion

A parametric study was also carried out to examine the effect of both CO_2 and toluene addition into inlet H_2S and see if this would also pose similar effects as toluene addition alone. Similar temperature range of 800-2000K and toluene concentration between 0 - 3% in the inlet H_2S acid gas was examined. Figure 4-35

shows change in conversion efficiency with increase in temperature for different amounts of toluene and CO_2 in inlet H_2S acid gas. Amount of toluene was kept constant at 0.5% and that of CO_2 was changed between 0-70% in the inlet H_2S acid gas. The results showed similar trends as the conversion efficiency increased at lower temperatures to a peak value and decreased at higher temperature. In comparison to toluene addition alone, both CO_2 and toluene addition caused significant decrease in conversion efficiency at higher reactor temperature and, this increased with higher amounts of CO_2 addition. This also resulted in a decrease in the optimum temperature for enhanced sulfur recovery. Figure 4-36 shows the optimum reactor temperature with different amounts of toluene and CO_2 addition into the inlet H_2S. It was observed that presence of CO_2 resulted in lower optimum reactor temperature for all amounts of toluene present in inlet acid gas mixture ($H_2S/C_7H_8/CO_2$).

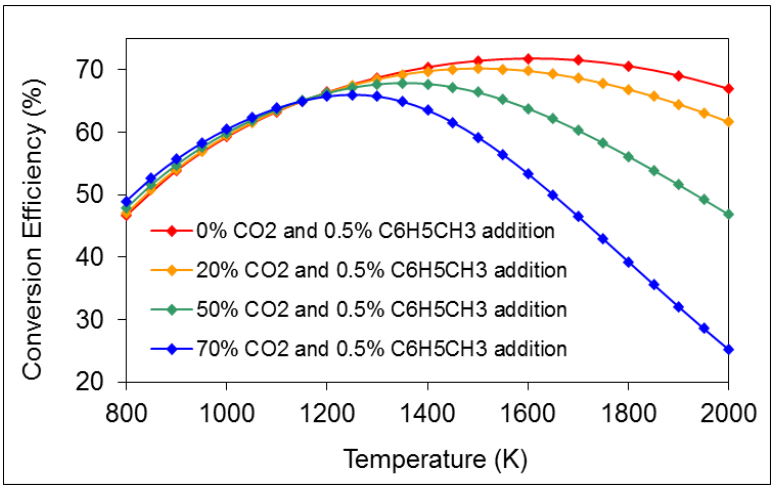

Figure 4-35. Conversion efficiency vs. reactor temperature change in CO_2 and C_7H_8 addition to inlet H_2S

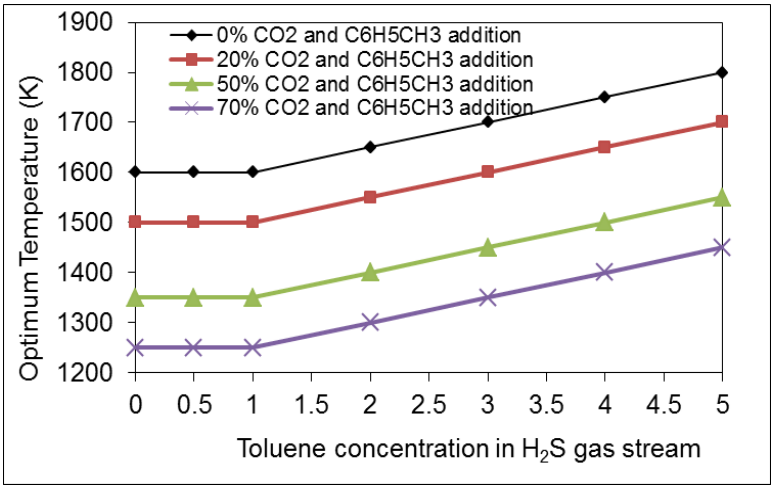

Figure 4-36. Optimum reactor temperature vs different amounts of toluene and carbon dioxide addition to inlet H_2S acid gas in mole percentages

At high temperatures, CO_2 dissociates to release oxidizer into the reaction pool, reactions 4-49 and 4-50. Reaction 4-49 is endothermic.

$$CO_2 + M \Leftrightarrow CO + O + M \qquad (4\text{-}49)$$

$$CO_2 + H \Leftrightarrow CO + OH \qquad (4\text{-}50)$$

The equilibrium analysis demonstrated the role of reactor temperature and acid gas composition on the sulfur recovery in Claus reactors. However, it is necessary to further conduct experiments to characterize the combustion of different acid gas composition under high temperature conditions.

4.2.1.4 Summary

The effect of toluene and CO_2 (accompanying H_2S in acid gases) on conversion efficiency and optimum reactor temperature, within a temperature range of 1000-2000K has been examined. Quantitative and qualitative trends of conversion efficiency for different concentration of toluene and CO_2 in H_2S acid gas were conducted using equilibrium simulations. The results revealed a decrease in

conversion efficiency with increase in toluene and CO_2/toluene addition into the inlet H_2S gas stream. It was observed that toluene increases the optimum reactor temperature for enhanced sulfur recovery, whereas it reduces the optimum operating temperature in the presence of CO_2. Both toluene and CO_2 in the acid gases alters the optimum temperature of the reactor and decreases the sulfur recovery efficiency.

4.2.2 Techniques for Increasing Thermal Stage Reactor Temperature

Reactor temperature and gas residence time are crucial parameters in ensuring complete BTX destruction in the thermal stage of Claus process. Some modifications to Claus plants have been proposed to mitigate the impact of other impurities (such as NH_3, COS, CS_2, CH_4) in acid gases. The major parameters used in these techniques are temperature and residence time. These techniques are evaluated with respect to suitability for BTX destruction.

4.2.2.1 Acid Gas Bypass

In order to achieve high reaction furnace temperature, a portion of the lean acid gas is bypassed around the furnace (figure 4-37).

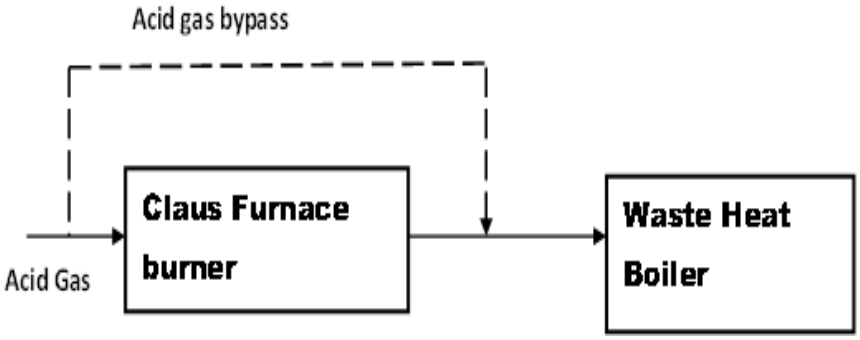

Figure 4-37. Schematic representation of acid gas bypass in Claus process

The amount of oxygen fed to the burner is the total amount required to burn the entire acid gas stream. The bypassed acid gas stream is mixed with the burner

effluent prior to its introduction into the waste heat boiler. The technique of acid gas bypass is most effective for ammonia destruction (ZareNezhad & Hosseinpour, 2008). It increases the reaction furnace temperature, high enough for ammonia destruction. However, the technique is not recommended when processing acid gas feeds containing BTX. This is because the presence of BTX in the bypass stream may cause serious operational problems and deactivation of catalysts downstream in the catalytic converters.

4.2.2.2 Feed Preheat

This techniques involves preheating of the acid gas and/or combustion air stream entering the reaction furnace (figure 4-38), which is possible using steam heat exchangers. This increases the reaction furnace temperature, which then promotes BTX destruction. The amount of steam used for preheating is largely compensated by the increased steam production in the waste heat boiler. Depending on the heating medium, it is possible to achieve maximum of 335-375K increase in reaction furnace temperature. However, combustion air preheating is limited to nominally 645K due to metallurgical constraint in the sulfur recovery unit, and indirect steam preheaters generally will not allow acid gas preheat to temperature beyond 535K (Rameshni, 2010; ZareNezhad & Hosseinpour, 2008).

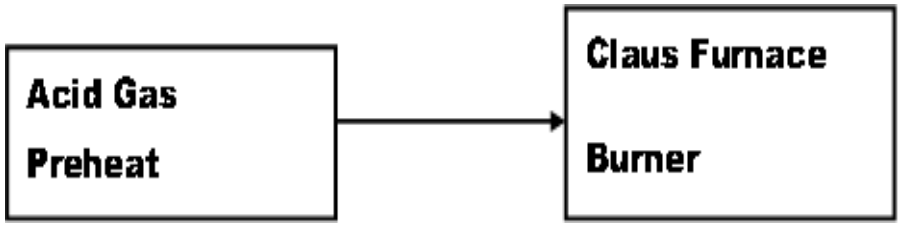

Figure 4-38. Schematic Representation of Acid gas Preheat in Claus Process

Selection of preheating type is determined by economic factors, conditions of the feed gas and availability of utilities. Feed preheat can increase the reaction furnace temperature without significant impact on the equipment size or sulfur recovery efficiency. However, preheat increases operational cost and the total pressure drop across the unit, in addition to increase in capital investment through installation of preheaters (ZareNezhad & Hosseinpour, 2008).

4.2.2.3 Fuel Gas Supplement

In this technique, the reaction furnace temperature is increased by co-firing a portion of fuel (such as methane) with acid gas in the reaction furnace (figure 4-39). The use of fuel gas with constant composition is important in order to maintain the desired combustion condition necessary for optimum Claus reactions. Generally a temperature increase of about 305K can be obtained for every volumetric percent of fuel added ((ZareNezhad & Hosseinpour, 2008).

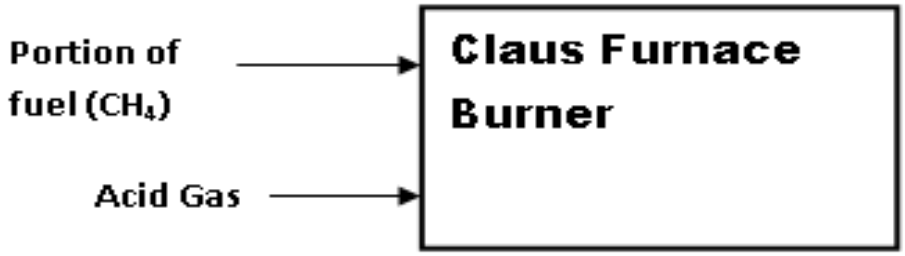

Figure 4-39. Schematic representation of fuel gas supplement in Claus Process

However, it is difficult to implement co-firing especially when the acid gas contains BTX. This is also accompanied by undesirable side reactions, leading to formation of COS and CS_2. In the downstream Claus converters and hydrolysis/hydrogenation reactors, considerable amounts of COS and CS_2 are converted to H_2S, but are not completely eliminated. Dilution effect caused by the

additional water formed from hydrocarbon combustion and inert gas cause unfavorable Claus reactions, resulting in low Claus process efficiency. Moreover, this technique requires an increase in the size of Claus furnace to handle the increased process gas flow leading to higher operational cost (Rameshni, 2010).

4.2.2.4 Oxygen Enrichment to Combustion Air

Oxygen enrichment to combustion air is an effective Claus burner modification used to increase the Claus reaction furnace temperature. In this technique, the nitrogen in air is partly or entirely replaced with oxygen (figure 4-40). Nitrogen act as diluents in the Claus reaction furnace absorbing some heat released in the combustion process which lowers the entire reaction furnace temperature. Therefore, by replacing all or part of the nitrogen present in air helps augment the reactor temperature.

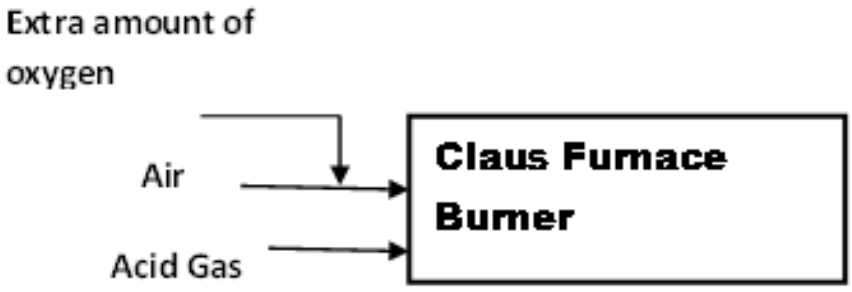

Figure 4-40. Schematic representation of Oxygen enrichment in Claus Process

Reduction in the concentration of nitrogen in the combustion air leads to significant decrease in the total amount of process gas flowing through the unit. This also increases the residence time and provides the basis for design of more compact equipment, which leads to significant savings in capital investment. The high furnace temperature resulting from oxygen enrichment to combustion air significantly

enhances flame stability and the tolerance of reaction furnace to inevitable process disturbances, thus providing a more stable operation and improving sulfur recovery efficiency (Norma et al., 2002). However, economical source of oxygen need to be available otherwise oxygen enrichment technology could be prohibitively expensive.

4.2.2.5 Summary

Processing acid gas, containing high amounts of CO_2 (lean acid gas) causes problems of low flame stability in the reaction furnace that results in incomplete destruction of contaminants (such as BTX, NH4, COS and CS_2). These also promote undesired side reactions that promote COS and CS_2 formation in the Claus unit.

From the process modifications for handling the processing of acid gases containing various impurities evaluated above, oxygen enrichment to combustion air appears to be an excellent technique that helps increase the reaction furnace temperature while increasing the residence time. This favors the processing of feed gases containing BTX and ammonia. It also enhances flame stability and enables the design of more compact equipment, resulting in significant savings in capital investment. Once sufficient temperature is provided for BTX destruction, other contaminants including CS_2, COS and NH_3 can also destroyed.

4.3 BTX Destruction with Oxygen Enriched Air

Oxygen enrichment to combustion air was examined to investigate experimentally the reactor conditions that favor BTX destruction. This was conducted by reducing the flow of nitrogen in the oxidizer stream (air) to vary the concentration of oxygen in air. This caused two simultaneous effects:

1. Increase in temperature of gases in reactor
2. Reduction in the total volumetric flow of gases (from decrease in nitrogen flow rate) in the Claus reactor resulting in a change in mixing characteristics (decreases average gas flow velocity and Reynolds number). This increases the average residence time in the reactor.

The reduction in the flow of nitrogen which acts as a diluent in the reactor is capable of increasing feed processing capacity of Claus plants and enables the design of more compact Claus reactors that can result in capital savings. Destruction of BTX in the thermal stage of Claus reactors is crucial for improved process efficiency. The effect of oxygen enrichment on the combustion of different composition of acid gas (H_2S, BTX and CO_2) in H_2/O_2-N_2 flames was examined.

The flames of H_2/O_2-N_2 are different from H_2S/O_2 in terms of temperature distribution, intermediate species and reaction rates, and the chemical kinetics of H_2/O_2-N_2 is well understood. This allowed accurate understanding of the role of BTX on the chemical kinetic pathways of the H_2S combustion, as BTX was the only source of carbon in the reactor. This helped to understand the chemical kinetic pathways on BTX destruction and formation of COS and CS_2. It was also noted that H_2S and H_2 combustion practically occur in Claus process from the thermal decomposition of H_2S (at initial stages of combustion) and hydrocarbons present in the acid gas. Also, the separation of acid gas using current desulfurization techniques, such hydro-desulfurization uses hydrogen, which results in higher hydrogen content in the separated acid gases. The available hydrogen in the Claus reactor tends to provide oxidation competition to hydrogen sulfide. Therefore, operating the Claus reactor

with H_2/O_2-N_2 flame helped to extract more information on H_2S and BTX chemical kinetic pathways with respect to different reactor input and operational conditions.

The destruction of BTX in H_2/O_2-N_2 flames was carried out with defined amounts of H_2S and BTX or carbon dioxide under fuel-rich mixture conditions at equivalence ratio of Φ=3 (Claus conditions). The oxygen enriched air allowed variation in temperature of the reactor while maintaining the same equivalence ratio at Claus condition. The speciation of gas phase species during combustion is presented at different concentrations of oxygen in air (0%, 19.5% and 69.3%). The results are presented in three sub-sections: effect of oxygen enrichment of air on toluene/H_2S combustion in sub-section 4.3.1, xylene/H_2S in sub-section 4.3.2 and carbon dioxide/H_2S in sub-section 4.3.3.

Xylene and toluene were chosen in further investigations of BTX destruction. It was noted that xylene has the greatest impact on intermediate products production and sulfur emissions. Moreover, xylene decomposition is a hierarchical process in which toluene and benzene are eventually formed, which means that benzene and toluene will also be present in the reactor during xylene and H_2S combustion.

4.3.1 Toluene and H_2S Destruction in Oxygen Enriched Air

Experiments were conducted to examine the effect of oxygen enriched air on combustion of H_2S and H_2S/C_7H_8 in H_2/O_2-N_2 flames under Claus condition. Table 4-5 shows the experimental test matrix of each gas introduced into the burner. The gas flow characteristics in the burner tubes are shown in table 4-6. The first case represents gas stream consisting of 100% H_2S, while in the second case gas mixture of 99% H_2S and 1% C_7H_8 is examined. In order to achieve the required experimental

condition, H_2/O_2-N_2 mixture was combusted under slightly fuel-lean conditions. Based on the flow rate of the excess oxygen, hydrogen sulfide and toluene were injected to achieve the targeted equivalence ratio of Φ=3.0 for the Claus condition, based on hydrogen sulfide or hydrogen sulfide and toluene mixture for all the experiments reported. Gas flow rate of toluene was calculated based on densities: liquid toluene has a density of 0.866 g cm^{-3} while that of gaseous toluene is 0.0030 g cm^{-3}. Gas sampling and analysis of local species were conducted along the longitudinal axis of the reactor. Dimensionless axial distance (W=axial distance/D_{jet}) was used for all the results presented. Inner jet diameter of the burner was used to transform the linear distances into dimensionless parameters for generalization of the results. Due to the high flow rates of reactant gases, the burner diameter was changed. The burner inner tube had a dimension of 3.58mm and the outer tube was 9.94mm. A bluff body was also used to stabilize the flame, and this burner was used for all experiments conducted with H_2/O_2-N_2 flames.

Table 4-5. The Test Matrix

Flow Rate (cm^3/min)						
Gas stream	%O_2 Enrichment in air	H_2	O_2	N_2	H_2S	C_7H_8
100% H_2S	0	2000	1165	4380	330	0
	19.5	2000	1165	3476	330	0
	69.3	2000	1165	2112	330	0
99%H_2S /1%C_7H_8	0	2000	1175	4418	330	3.30
	19.5	2000	1175	3507	330	3.30
	69.3	2000	1175	2130	330	3.30

Table 4-6. Cold Gas Flow Characteristics

Cold Gas Flow Velocity (m/s)		Reynolds number	
Oxidizer (O_2/N_2)	Fuel	Oxidizer (O_2/N_2)	Fuel
2.00	3.901	34.54	66.14
1.69	3.901	29.13	66.14
1.21	3.901	20.86	66.14
2.01	3.904	34.6	66.19
1.70	3.904	29.18	66.19
1.21	3.904	20.86	66.19

The accuracy of the results reported in this paper was estimated by considering the inaccuracy from gas chromatography (GC), flow rates and traverse mechanism. The GC used is known to have an accuracy of ±0.1%, estimated flow rate accuracy of 1.5% at full scale and a traverse mechanism accuracy of 0.01%. These errors were found to be within the experimental data point symbols presented in the figures.

4.3.1.1 Temperature Measurements

Mean temperature of the reactor was measured along the longitudinal centerline of the reactor using K-type thermocouple. A traverse mechanism was used to move the thermocouple incrementally along the reactor centerline. Three test cases presented here are with 0% (normal air) and 69.3% oxygen enriched combustion air. These test cases represent the lowest and highest temperature effects of all the six test cases presented. Figure 4-41 shows temperature profile for 0% and 69.3% oxygen enrichment in H_2/O_2-N_2 flame with 100% H_2S and 99% H_2S/1% C_7H_8 gas addition to the burner. Similar trends were observed in all conditions as evident in the figure with major difference being the magnitude of temperatures.

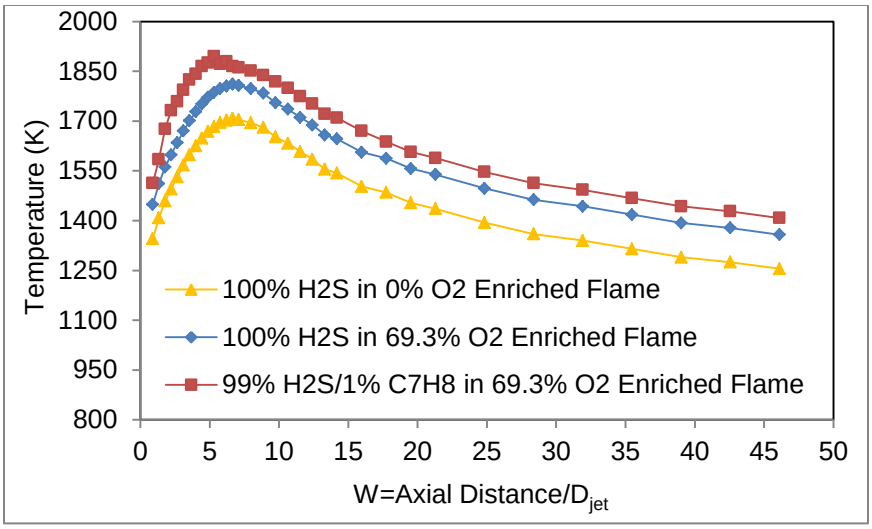

Figure 4-41. Temperature profile of H_2/O_2-N_2 flame with 100% H_2S and 99% H_2S/1%C_7H_8 gas mixture at Φ=3.0.

Under all conditions, temperature increased to a maximum due to chemical reaction between hydrogen, hydrogen sulfide and the surrounding air. Decrease in temperature beyond W~5 is attributed to the heat loss to reactor walls. In comparison to 100% H_2S case, addition of 99% H_2S/1% C_7H_8 mixture caused flame temperature to increase throughout the reactor. This is directly attributed to the effect of increased heating value associated with toluene decomposition as compared to H_2S.

4.3.1.2 Combustion of 100% H_2S

Combustion of 100% H_2S acid gas resulted in the production of SO_2 and other sulfurous compounds and intermediate radicals. Figures 4-42 and 4-43 show the mole fraction of H_2S and H_2 along the longitudinal centerline of the reactor at different oxygen enrichments to air (0%, 19% and 69%). Results revealed increase in the rate of H_2S decomposition with increase in percentage of oxygen enrichment to air and is attributed to increased flame temperature. At Claus condition, H_2S combustion takes

place in stages. The first stage involves thermal and chemical decomposition to form radical species and hydrogen. In the second stage, H_2S oxidation takes place. The significant reactions include reactions 4-1 through 4-5.

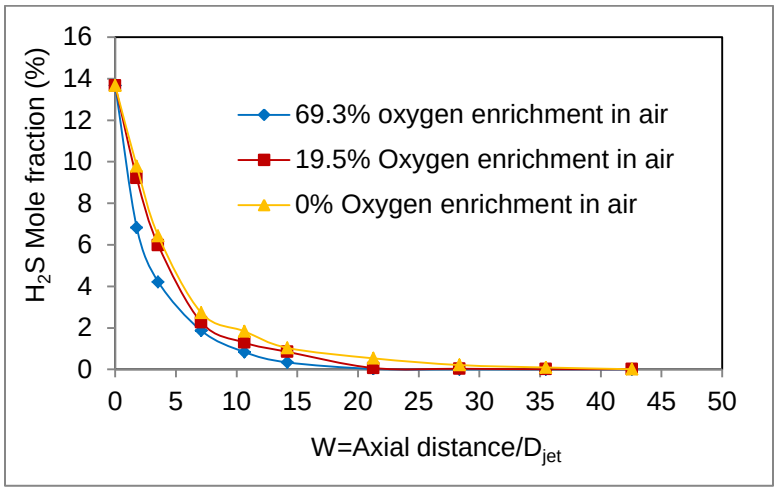

Figure 4-42. Hydrogen sulfide mole fraction. Flame condition: H_2/O_2-N_2 with 100% H_2S addition at Φ=3.0

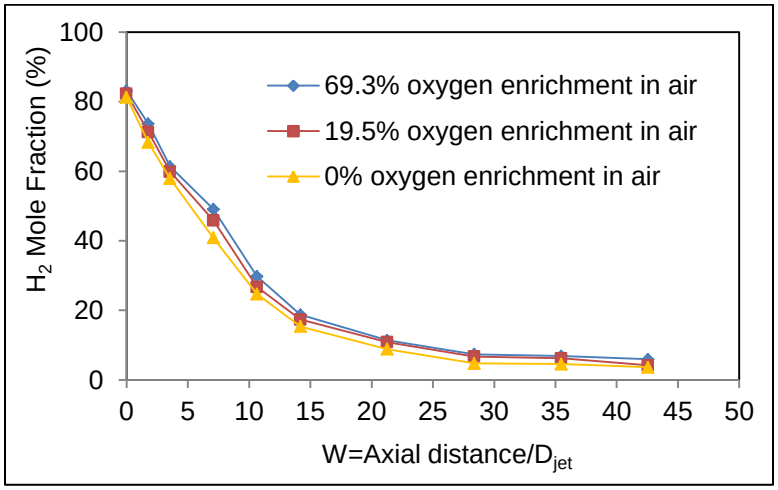

Figure 4-43. Hydrogen mole fraction. Flame condition: H_2/O_2-N_2 with 100% H_2S addition at Φ=3.

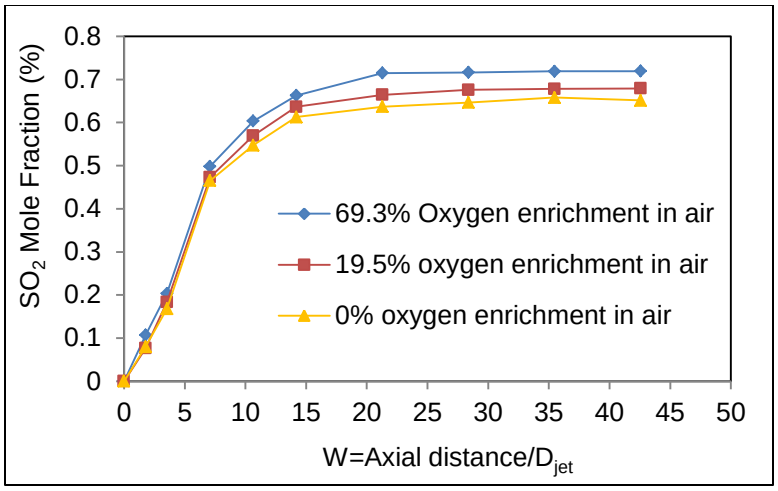

Figure 4-44. Sulfur dioxide mole fraction. Flame condition: H_2/O_2-N_2 with 100% H_2S addition at Φ=3.0

Increase in oxygen enrichment of air promotes greater contribution from reaction 4-1, due to increased reactor temperature, which results in greater decomposition of H_2S. This interpretation is further supported in figure 4-43, which shows the mole fraction of hydrogen. It is observed that hydrogen mole fraction increased minimally with increase in oxygen enrichment of air. This is attributed to the direct increase in amounts of hydrogen produced from reactions, such as 4-1 and 4-3. Hydrogen mole fractions did not decompose to zero value due to the oxidation competition between H_2S and H_2. Several investigators have reported that H_2S acts as an oxidation inhibitor to H_2 and this is in good agreement with previous findings (Azatyan et al., 1969, Bernez-Cambot et al., 1981, Selim et al., 2011, 2012c). Mole fraction of SO_2 increases monotonically until it reaches to a maximum value and this coincided with other species reaching their steady-state minimum (figure 4-44). The increase in oxygen enrichment to combustion air increased the rate of sulfur dioxide

formation and the magnitude of asymptotic value due to greater rate of H_2S oxidation at higher temperatures.

4.3.1.3 Combustion of 99%H_2S and 1%C_7H_8 Mixture

Figures 4-45 and 4-46 depict the mole fractions of hydrogen sulfide and sulfur dioxide respectively along the centerline axis of the reactor at different percentages of oxygen enrichment to combustion air. In comparison with the case of 100% H_2S, similar trends can be observed for H_2S mole fraction, with the only noticeable difference being the rate of decay. The rate of decay of hydrogen sulfide was faster in the gas mixture than with H_2S alone. The faster consumption of H_2S could be due to a number of factors. Firstly, the presence of toluene helps to increase the reactor temperature due to high heating value associated with toluene decomposition. Secondly, hydrocarbon radicals formed from toluene decomposition tend to react with hydrogen sulfide to form intermediate species, such as CS_2.

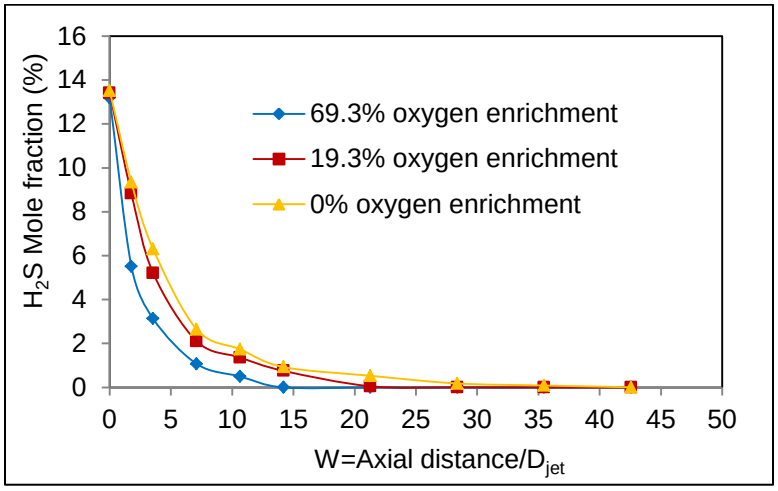

Figure 4-45. Hydrogen sulfide mole fraction. Flame condition:

H_2/O_2-N_2 with 99% H_2S/1%C_7H_8acid gas at Φ=3.0

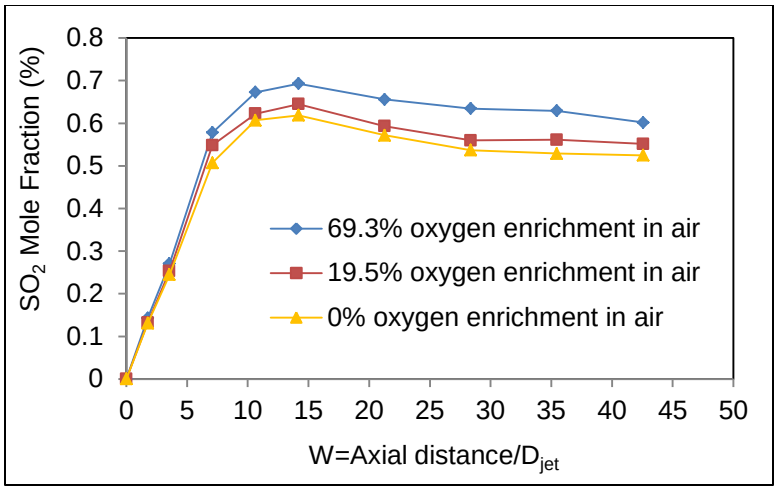

Figure 4-46. Sulfur dioxide mole fraction. Flame condition: H_2/O_2-N_2 with 99% H_2S/1%C_7H_8 acid gas at Φ=3.0

Possible pathways are shown in reactions 4-27 to 4-29 (Chin et al., 2000), and these reactions are supported from the observed trends of methane, carbon disulfide and hydrogen. On the other hand, faster rate of sulfur dioxide production was observed until it reached a peak mole fraction value at axial distance of W~15 in the reactor, and subsequently decayed to an asymptotic minimum value further downstream the reactor centerline (figure 4-46). The faster rate of SO_2 formation is attributed to the tendency of H_2S to react faster with O_2 as compared to toluene. The presence of toluene in the inlet gas stream resulted in SO_2 reduction at higher reactor distances (higher residence time) as compared to 100% H_2S gas stream case. This could be explained by the following reasons. Firstly, some amounts of oxygen is consumed by toluene, which could reduce the amounts of SO_2 formed, even though H_2S reacts with oxygen much faster than toluene. Secondly, it is possible for hydrocarbon radicals to react with H_2S or sulfur containing radicals to form carbon disulfide or other radical species such as in reaction 4-27 to 4-30 (Chin et al., 2000).

Thirdly, toluene seems to enhance the rate of elemental sulfur formation as oxygen was depleted much faster when toluene was present in the reaction pool. This enhanced the rate of SO and SO_2 reactions with other available sulfur containing radical species to form elemental sulfur further downstream the reactor, as shown in reactions 4-30 to 4-33 (Clark et al., 2000). Moreover, the formed hydrocarbons (such as methane) in the reaction pool could also be oxidized by the abundant SO and SO_2 species to form elemental sulfur and carbon dioxide.

The observed decrease in SO_2 mole fractions with toluene addition suggests an increased possibility of sulfur formation. Selim et al., 2012a examined elemental sulfur formation. They conjectured that formation of elemental sulfur involves the recombination of elementary reactions from products of H_2S decomposition (such as HS and HS_2) and S, SO or SO_2. In the case of 100% H_2S combustion, most of the H_2S was transformed into SO_2 and this reduces the rate of elemental sulfur formation. Figure 4-47 shows the mole fractions of hydrogen along the centerline of the reactor at different percentages of oxygen enrichment to air. Compared to the 100% H_2S gas stream combustion, the observed trends were similar, but the rate of H_2 oxidation was slower in the H_2S-C_7H_8 mixture case. This observation is attributed to the fact that toluene decomposition produces additional amounts of hydrogen in the reaction pool.

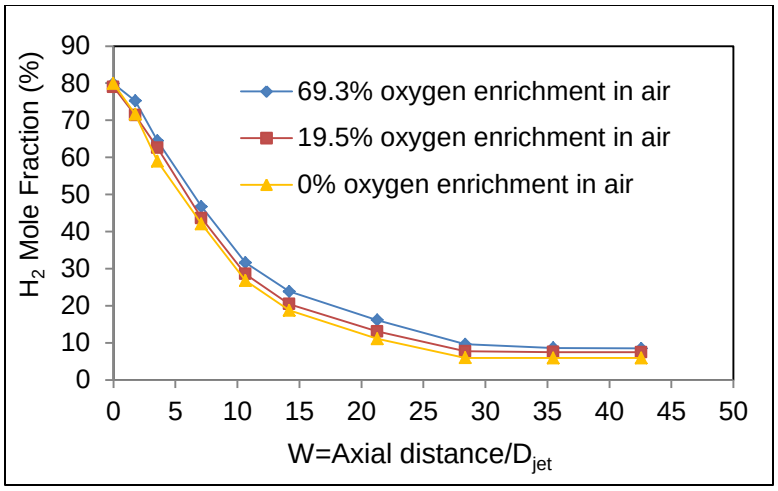

Figure 4-47. Hydrogen mole fraction. Flame condition: H_2/O_2-N_2 with 99% H_2S/1%C_7H_8 acid gas at Φ=3.0

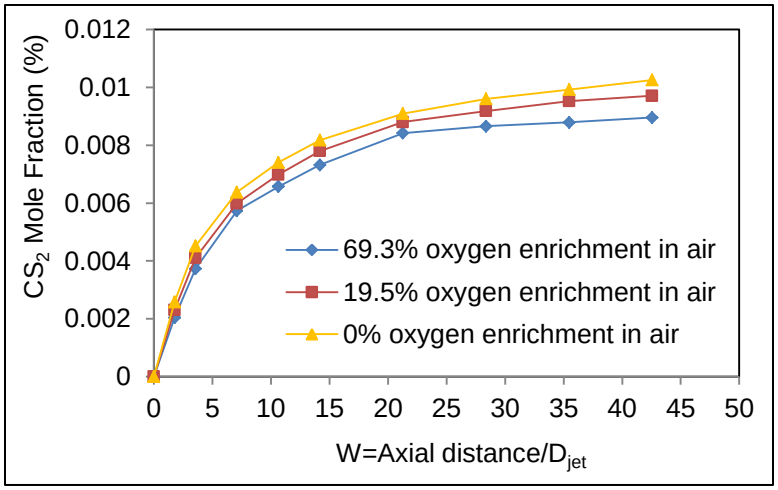

Figure 4-48. Carbon disulfide mole fraction. Flame condition: H_2/O_2-N_2 with 99% H_2S/1%C_7H_8 acid gas at Φ=3.0

The presence of toluene in gas stream triggered the formation of carbon disulfide. Figure 4-48 illustrates the trends of carbon disulfide mole fraction for the examined conditions. Mole fractions of carbon disulfide increased to a maximum value. Oxygen enrichment of air caused a decrease in the rate of carbon disulfide formation. This is attributed to the faster decomposition of hydrocarbons in the

reactor at higher temperatures. Moreover, the mole fractions of acetylene and methane downstream the reactor was lower with increase in oxygen enrichment to combustion air.

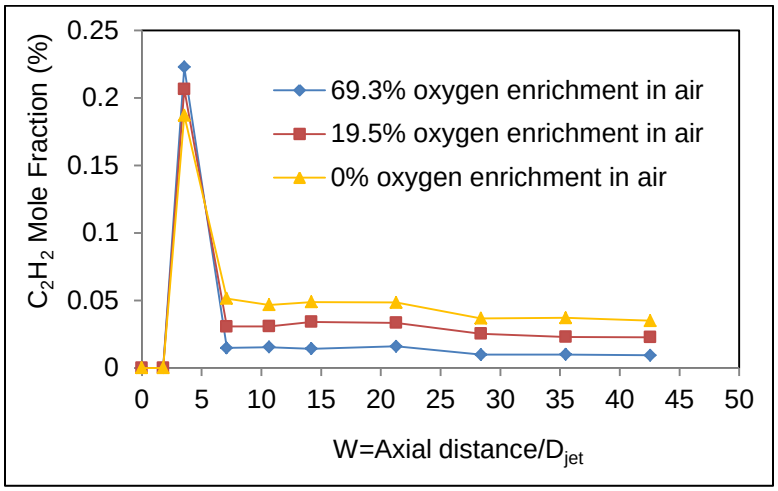

Figure 4-49. Acetylene mole fraction. Flame condition: H_2/O_2-N_2 with 99% H_2S/1%C_7H_8 acid gas at Φ=3.0

Toluene provided the pathways on hydrocarbons formation in the reactor. Figure 4-49 depicts mole fraction of acetylene along the reactor centerline at different concentrations of oxygen enrichments to combustion air. Mole fraction of acetylene increased to a peak value at reactor distance W~4 and rapidly decreased to a minimum value. Rate of decrease in mole fractions of acetylene from reactor distance, W~7 was found to be very slow and did not reach to zero value. This could be attributed to decrease in reactor temperature in the post flame zone of the reactor as well as possible recombination of hydrocarbon radicals to form acetylene (such as reaction 4-65 (Liu et al., 2011). The kink in acetylene mole fractions at W~29 is attributed to some experimental instability.

Figure 4-50 and 4-51 show mole fractions of methane and carbon dioxide along the reactor centerline at different percentages of oxygen enrichment to combustion air. Methane mole fraction increased to a peak value at reactor distance W~14 and then decayed with increase in axial distance to an asymptotic value. The occurrence of peak mole fraction of acetylene at W~4 and that of methane at W~14 suggest the possible decomposition of acetylene to methane. It is to be noted that with increase in oxygen enrichment of air, peak value of methane mole fraction increased but subsequent rate of decomposition was observed to be faster. This is possibly because of increased temperatures due to oxygen enrichment which enhanced decomposition of toluene.

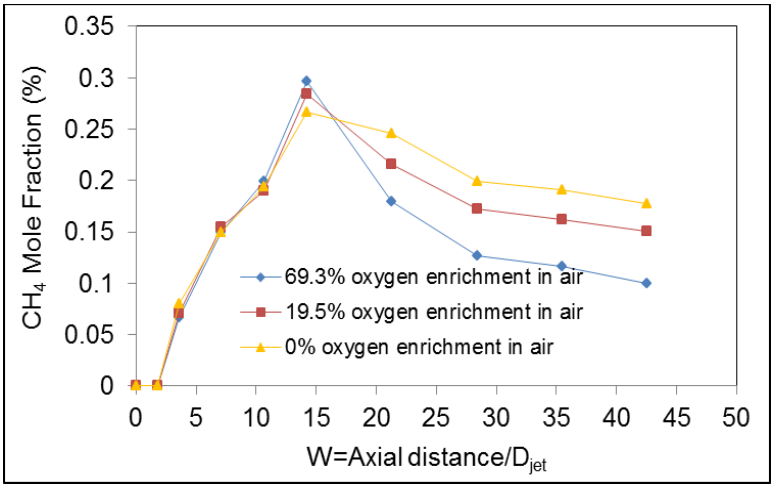

Figure 4-50. Methane mole fraction. Flame condition: H_2/O_2-N_2 with 99% H_2S/1%C_7H_8acid gas at Φ=3.0

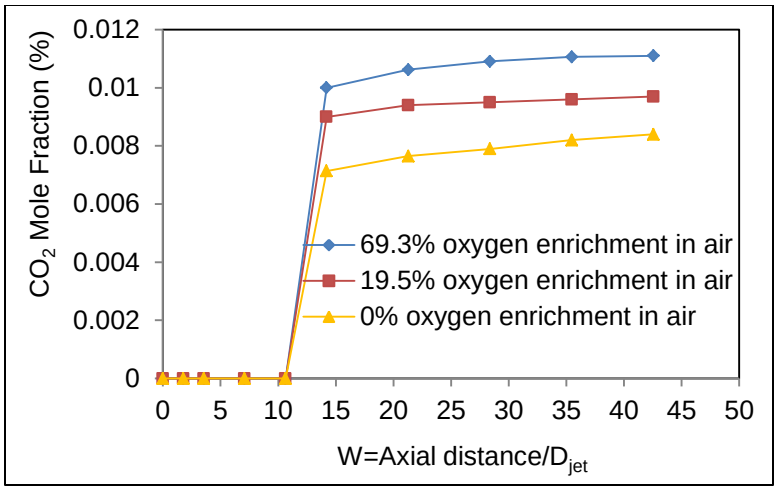

Figure 4-51. Carbon dioxide mole fraction. Flame condition: H_2/O_2-N_2 with 99% H_2S/1%C_7H_8acid gas at Φ=3.0

Increase in mole fractions of CO_2 (figure 4-51) and decrease in mole fractions of SO_2 in the second half of the reactor supports the occurrence of reaction 4-34. It is also observed that CO_2 mole fractions increased with increase in oxygen concentration to air. This further substantiates the faster rate of hydrocarbons oxidation by oxygenated species such as SO and SO_2 further downstream the reactor.

4.3.1.4 Summary

Results on the combustion of 100% H_2S and 1% C_7H_8 / 99% H_2S acid gas streams in hydrogen-oxygen enriched air (H_2/O_2-N_2) flames were presented and compared. Three different percentages of oxygen enrichment to air have been examined (0%, 19.5% and 69.3%) for the two gas streams of H_2S and H_2S/toluene gas mixtures. Combustion of 100% H_2S gas stream resulted in the formation of SO_2. Oxygen enrichment to the combustion air increased the rate of SO_2 formation due to increased H_2S oxidation and decreased H_2 oxidation. These trends are attributed to increases in temperatures with increased concentration of oxygen in air. Similar

trends were observed with addition of toluene into the gas stream for H_2 and H_2S mole fraction profiles. However, the rate of H_2 decomposition was observed to be slower and oxidation of H_2S was faster. The addition of toluene to H_2S helped reduce the amounts of SO_2 formed while simultaneously increasing the formation of more desired elemental sulfur. Presence of toluene also resulted in the formation of methane and acetylene. These hydrocarbons were precursors to carbon disulfide formation. However, oxygen enrichment to the combustion air increased rate of hydrocarbon decomposition which also had direct impact on the amounts of CS_2 formed. This was evident from the decreased rate of CS_2 formation at higher concentrations of oxygen in the combustion air. Formation of CS_2 and hydrocarbons has a severe impact on Claus process performance. Oxygen enrichment showed enhanced destruction of hydrocarbons while minimizing the formation of carbon disulfide. These results will help to improve Claus process efficiency for sulfur capture.

4.3.2 Xylene and H_2S Destruction with Oxygen Enriched Air

The effect of oxygen enriched air on combustion of xylene and H_2S mixture combustion in H_2/O_2-N_2 flames was also examined under (fuel-rich) Claus condition. Table 4-7 depicts the experimental test matrix of each gas introduced into the burner. The resulting flow properties of the cold gas, along the burner tube are given on table 4-8. However, the experimental procedure was similar to the one used in the previous sub-section 4.3.1. The combustion of H_2S/C_8H_{10} mixture was examined and compared to the case of 100% H_2S combustion. Gas flow rate of xylene was calculated based on densities: liquid xylene has a density of 0.879 g cm^{-3} while that of

gaseous xylene is 0.0032 g cm^{-3}. Gas sampling and analysis of local species were conducted along the longitudinal axis of the reactor.

Table 4-7. The Test Matrix

Flow Rate (cm^3/min)						
Gas composition	% O_2 Enrichment in air	H_2	O_2	N_2	H_2S	C_8H_{10}
99% H_2S/ 1%C_8H_{10}	0	2000	1176.6	4426	330	3.30
	19.5	2000	1176.6	3512	330	3.30
	69.3	2000	1176.6	2133	330	3.30

Table 4-8. Cold Gas Flow Properties

Cold Gas Flow Velocity (m/s)		Reynolds number	
Oxidizer (O_2/N_2	Fuel	Oxidizer (O_2/N_2	Fuel
2.01	3.904	34.6	66.19
1.70	3.904	29.18	66.19
1.21	3.904	20.86	66.19

The product gas speciation along the reactor centerline for the combustion of 99% H_2S/1% C_8H_{10} gas stream is presented. Dimensionless axial distance (W=axial distance/D_{jet}) was used for all the results presented here. Inner jet diameter (D_{jet}=3.58mm) of the burner was used to transform the linear distances into dimensionless parameters for generalization of the results.

4.3.2.1 Results and Discussions

The results showed formation of several sulfurous and hydrocarbon species in the reactor. Figures 4-52 to 4-57 show the mole fractions of H_2S, H_2, C_2H_2, CH_4, SO_2 and CS_2 along the longitudinal centerline of the reactor, at different percentages of oxygen enrichment to combustion air. Oxygen enrichment of air caused faster decomposition of H_2S and H_2, while promoting formation of CS_2 and SO_2, as well as

destruction of C_2H_2 and CH_4 in the reactor. Oxygen enrichment to combustion air increased the rate of SO_2 formation due to increased H_2S oxidation and decreased H_2 oxidation. These trends were similar to those observed during toluene destruction in oxygen enriched air. Xylene also triggered the formation of methane and acetylene to favor formation of carbon disulfide.

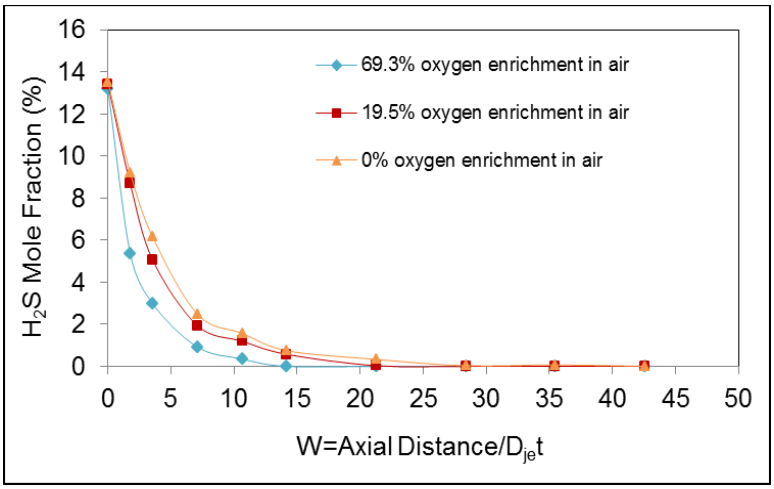

Figure 4-52. Hydrogen sulfide mole fraction. Flame condition: H_2/O_2-N_2 with 99% H_2S/1%C_8H_{10} acid gas at Φ=3.0

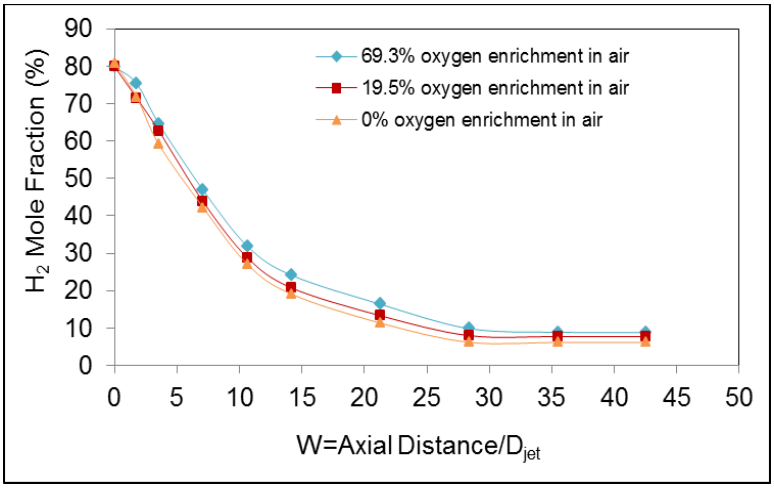

Figure 4-53. Hydrogen mole fraction. Flame condition: H_2/O_2-N_2 with 99% H_2S/1%C_8H_{10} acid gas at Φ=3.0

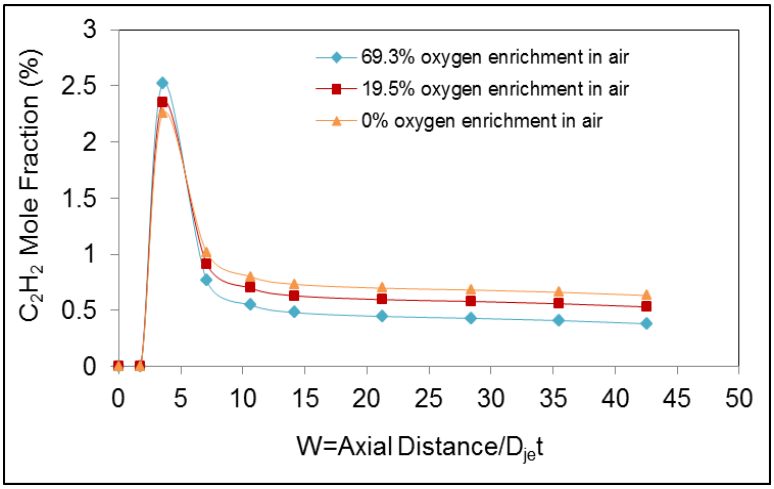

Figure 4-54. Acetylene mole fraction. Flame condition: H_2/O_2-N_2 with 99% H_2S/1%C_8H_{10} acid gas at Φ=3.0

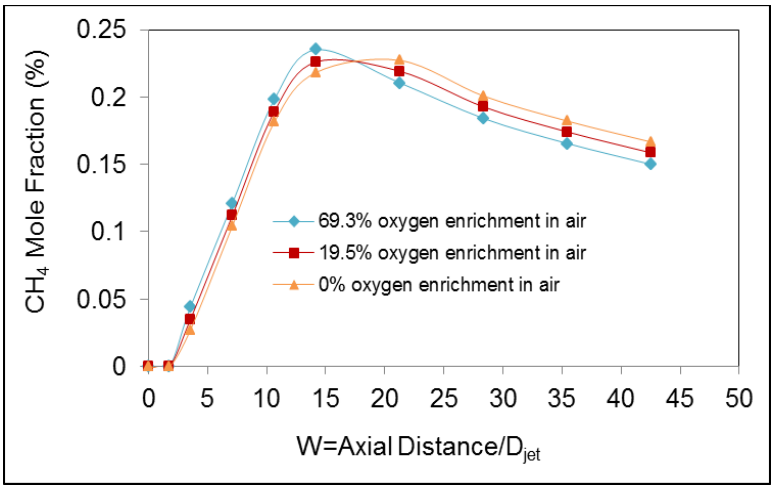

Figure 4-55. Methane mole fraction. Flame condition: H_2/O_2-N_2 with 99% H_2S/1%C_8H_{10} acid gas at Φ=3.0

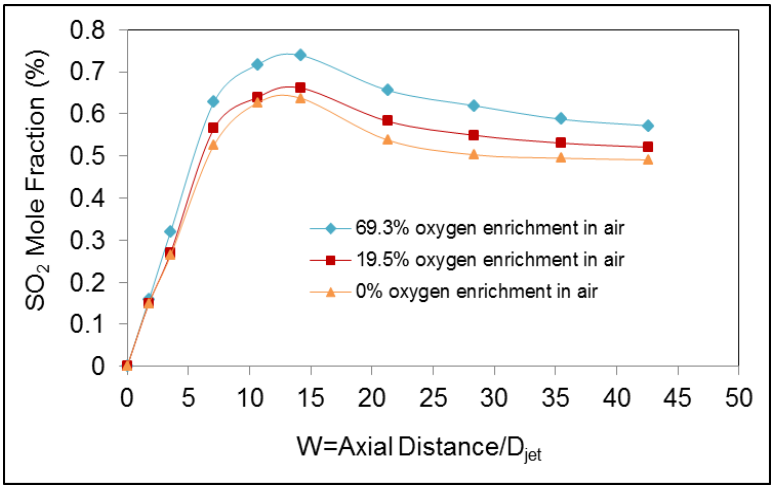

Figure 4-56. Sulfur dioxide mole fraction. Flame condition: H_2/O_2-N_2 with 99% H_2S/1%C_8H_{10} acid gas at Φ=3.0

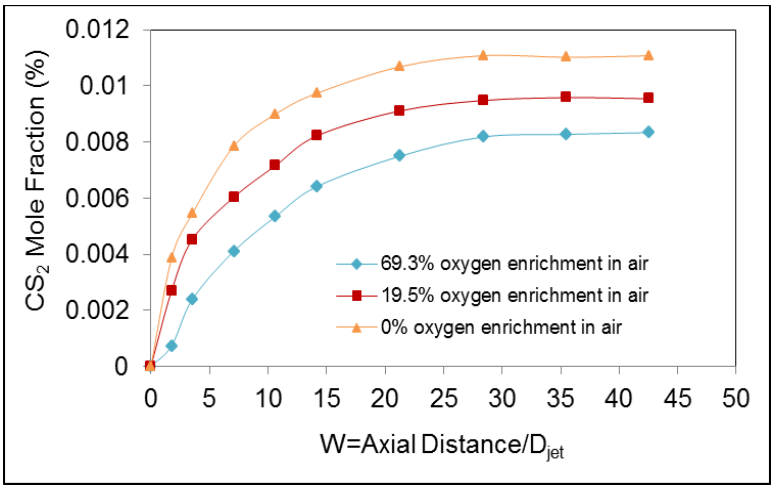

Figure 4-57. Carbon disulfide mole fraction. Flame condition: H_2/O_2-N_2 with 99% H_2S/1%C_8H_{10} acid gas at Φ=3.0

Xylene showed increased formation of acetylene, methane and carbon disulfide in the reactor, compared to the case with toluene. The amounts of produced C_2H_2 and CS_2 with xylene increased dramatically at the reactor exit (combustion of 1% C_7H_8 / 99% H_2S vs. 1% C_8H_{10} / 99% H_2S). However, mole fraction of CH_4 did not show a significant increase with xylene. Therefore, the higher production of

acetylene with xylene suggests increased formation of higher polycyclic aromatic compounds (PAH).

4.3.2.2 Summary

Results on the combustion of 1% C_8H_{10} / 99% H_2S acid gas stream in H_2/O_2-N_2 flames were presented. Oxygen enrichment to the combustion air (0%, 19.5% and 69.3%) was varied to provide suitable reactor conditions for xylene destruction. These results showed similar trends but had quantitative differences in mole fractions, when compared to the case of toluene destruction. The results demonstrate increased production of hydrocarbons with xylene in the thermal stage of Claus reactor, which has a more severe impact on thermal stage reactor as compared to toluene.

4.3.3 CO_2 and H_2S Destruction in Oxygen Enriched Air

Experiments were conducted to examine the effects of oxygen enrichment of air on acid gas (H_2S and CO_2) combustion in H_2/O_2-N_2 flames under Claus condition. Table 4-9 depicts the test matrix for all test conditions reported. In order to achieve the required experimental conditions H_2/O_2-N_2 mixture was combusted under slightly fuel-lean conditions. According to the flow rate of the excess oxygen, 50% CO_2 and 50% H_2S were injected to achieve the targeted equivalence ratio (Φ=3.0) for the Claus condition.

Table 4-9. The test matrix

Flow Rate (cm^3/min)						
	% O_2 Enrichment in air	H_2	O_2	N_2	H_2S	CO_2
50% H_2S/ 50% CO_2	0	2000	1165	4380	330	330
	19.5	2000	1165	3476	330	330
	69.3	1600	932	1690	264	264

Gas sampling and analysis of local species were conducted along the longitudinal axis of the reactor. Thus, the results reported are with 50% CO_2 and 50% H_2S addition to H_2/O_2-N_2 flames. A comparison is also made with results from 100% H_2S combustion. Temperature profile along the reactor centerline is presented first, followed by product speciation along reactor centerline for the 50% H_2S and 50% CO_2 acid gas. Dimensionless axial distance (W) was used for all the results presented here. Inner jet diameter (D_{jet} =3.58mm) of the burner was used to transform the linear distances into dimensionless parameter (W= axial distance/D_{jet}).

4.3.3.1 Temperature Measurements

Mean temperature of the reactor was measured along the reactor centerline using K-type thermocouple. A traverse mechanism was used to move the thermocouple incrementally along the reactor centerline. Two cases were considered; 0% and 69.3% oxygen enrichment in the air. Figure 4-58 shows temperature profile for 0% oxygen enrichment in H_2/O_2-N_2 flame with 100%H_2S and 50% H_2S/50% CO_2 acid gas addition to the burner. Figure 4-59 shows temperature profile for 69.3% oxygen enriched H_2/O_2-N_2 flame with 100% H_2S and 50% H_2S/50% CO_2 acid gas case. Similar trends were observed in both cases as evident in both the figures, with major difference being the magnitude of temperatures. Under all conditions, temperature increased as chemical reaction between hydrogen, hydrogen sulfide and air occurred along the reactor centerline axis.

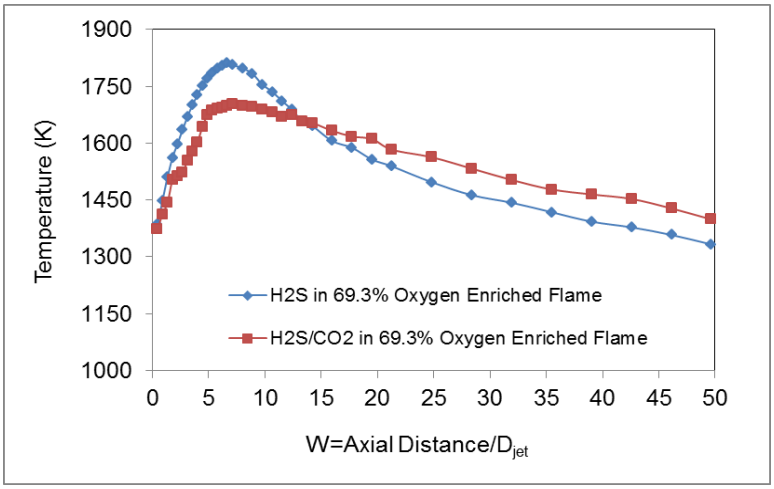

Figure 4-58. Temperature profile of H_2/O_2-N_2 flame with 100% H_2S and 50% H_2S/50% CO_2 addition at Φ=3.0.

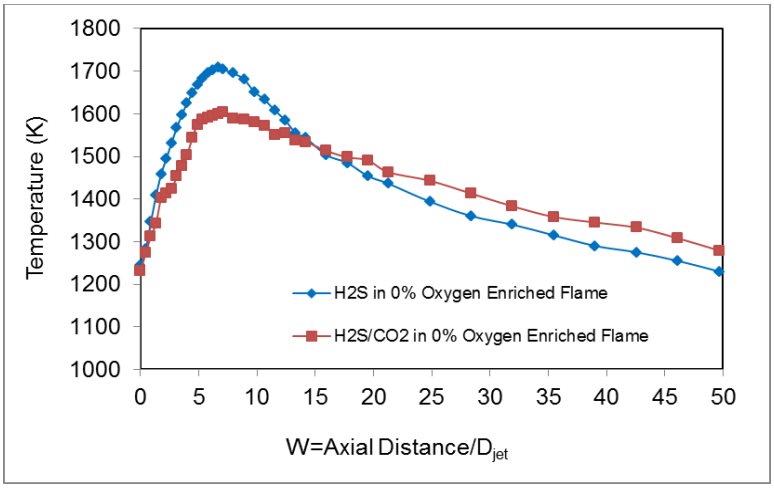

Figure 4-59. Temperature profile of H_2/O_2-N_2 flame with 100% H_2S and 50% H_2S/50% CO_2 addition at Φ=3.0.

Beyond W~15, temperature decreased and it is attributed to the heat loss to reactor walls. Addition of CO_2 caused flame temperature to decrease immediately upon injection. This is attributed to the endothermic decomposition of H_2S and CO_2. Further downstream the reactor, temperature increase was observed. This is possibly due to the fact that CO_2 helped to enhance the oxidizing medium.

4.3.3.2 Analysis of Combustion Products

Figures 4-60, 4-61 and 4-62 describe the mole fractions of hydrogen sulfide, sulfur dioxide and hydrogen, along the centerline of the reactor at different percentages of oxygen enrichment to air. Similar trends were observed for case of 50% H_2S and 50% CO_2 mixture as compared to 100% H_2S combustion alone. However, the rate of decay of hydrogen sulfide and hydrogen were faster in case of 50% H_2S and 50% CO_2 mixture combustion. Similarly, rate of sulfur dioxide production was slightly faster for the gas mixture. The faster rates of production/decomposition are attributed to the fact that carbon dioxide releases oxidizer into the reaction pool.

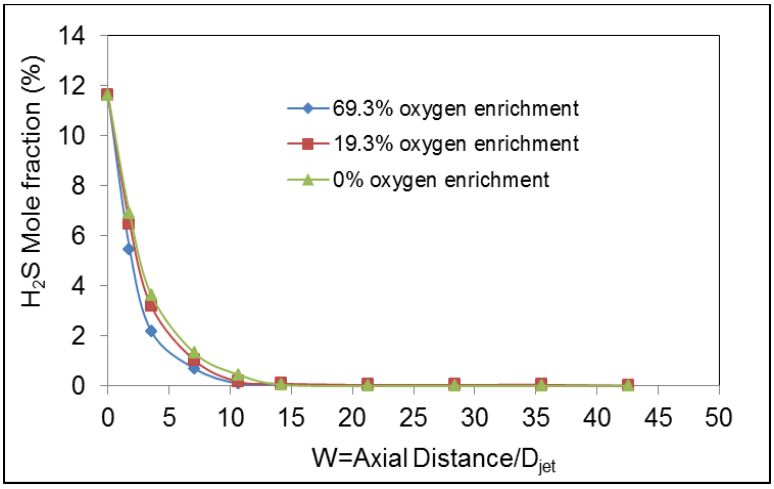

Figure 4-60. Hydrogen sulfide mole fraction. Flame conditions: H_2/O_2-N_2 with 50% H_2S/50% CO_2 acid gas at Φ=3.0

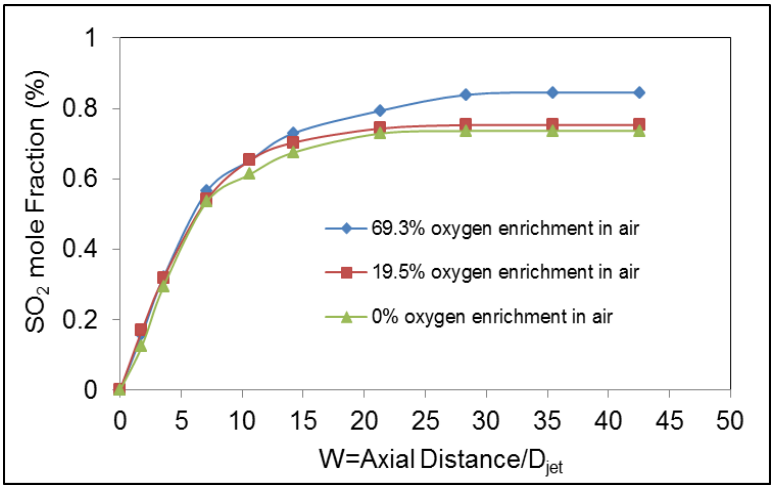

Figure 4-61. Sulfur dioxide mole fraction. Flame conditions: H_2/O_2-N_2 with 50% H_2S/50% CO_2 acid gas at Φ=3.0

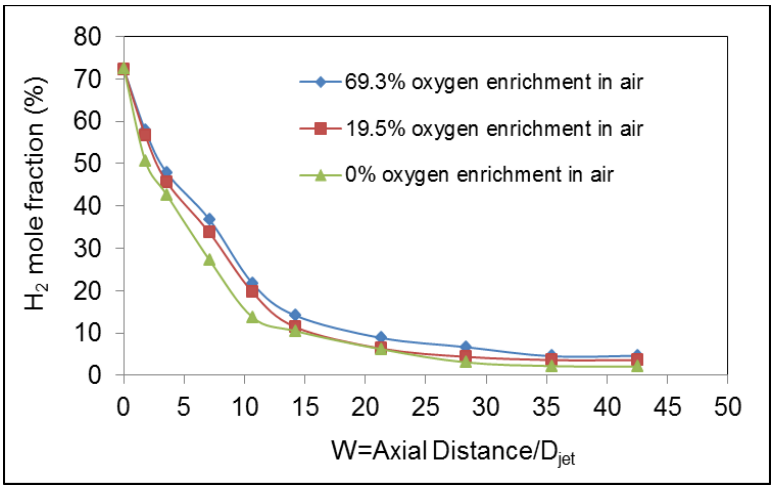

Figure 4-62. Hydrogen mole fraction. Flame conditions: H_2/O_2-N_2 with 50% H_2S/50% CO_2 acid gas at Φ=3.0

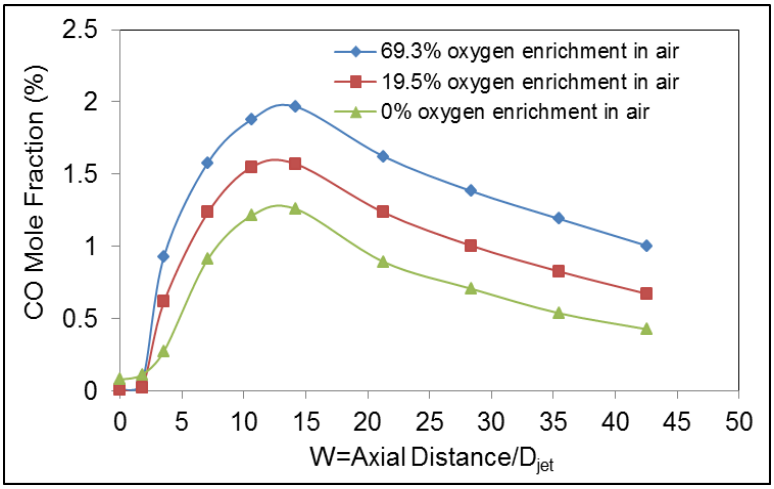

Figure 4-63. Carbon monoxide mole fraction. Flame conditions: H_2/O_2-N_2 with 50% H_2S/50% CO_2 acid gas at Φ=3.0

Figure 4-63 depicts mole fraction of carbon monoxide along the reactor centerline. The presence of carbon dioxide triggered the formation of carbon monoxide. Mole fraction of carbon monoxide increases at higher percentage of oxygen enrichment in air because of higher temperatures. Formation of carbon monoxide can occur through CO_2 thermal or chemical decomposition (see reactions 4-49 and 4-50). At 0% oxygen enrichment in air, reaction 4-49 is expected to be more dominant since CO_2 thermal oxidation occurs at significantly high temperatures. Moreover, the significant dominance of hydrogen radical in H_2/O_2-N_2 combustion enhances the rate of reaction 4-50. However, at higher percentage of oxygen enrichment, contribution from reaction 4-49 is expected to be significant due to higher temperatures. This was evident in the noticeable increase of carbon monoxide mole fraction with the increase in percentage of oxygen enrichment to air. On the other hand, carbon monoxide mole fraction decreased at higher reactor distances (higher residence times) due to the formation of COS and CS_2 in the reactor.

However, the incomplete oxidation of CO is attributed to the role of SO and SO_2 as oxidation inhibitor to CO. The abundant SO radicals in the Claus reactor compete with CO for oxidizer. This then hinders CO oxidation to CO_2, such as reaction 4-51, which favors the reaction of CO with S, HS or SO to form CS and CS_2. Figure 4-64 shows the behavior of carbon disulfide mole fraction under the investigated conditions.

$$CO + S \Leftrightarrow CS + O \quad (4\text{-}52)$$

$$CO + SO \Leftrightarrow CS + O_2 \quad (4\text{-}53)$$

$$CO + S_2 \Leftrightarrow CS_2 + O \quad (4\text{-}54)$$

$$CS + SO \Leftrightarrow CS_2 + O \quad (4\text{-}55)$$

$$CS + S_2 \Leftrightarrow CS_2 + S \quad (4\text{-}56)$$

$$CS + SO_2 \Leftrightarrow CS_2 + O_2 \quad (4\text{-}57)$$

$$CS + O_2 \Leftrightarrow COS + O \quad (4\text{-}58)$$

$$CS_2 + O \Leftrightarrow COS + S \quad (4\text{-}59)$$

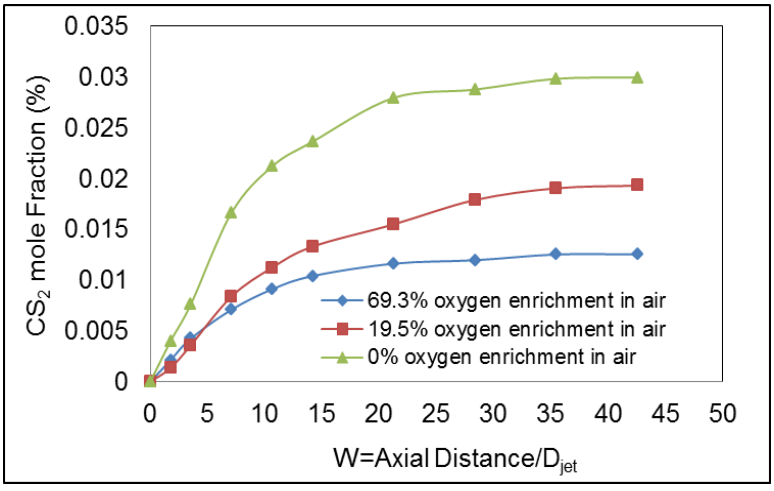

Figure 4-64. Carbon disulfide mole fraction. Flame conditions: H_2/O_2-N_2 with 50% H_2S/50% CO_2 acid gas at Φ=3.0

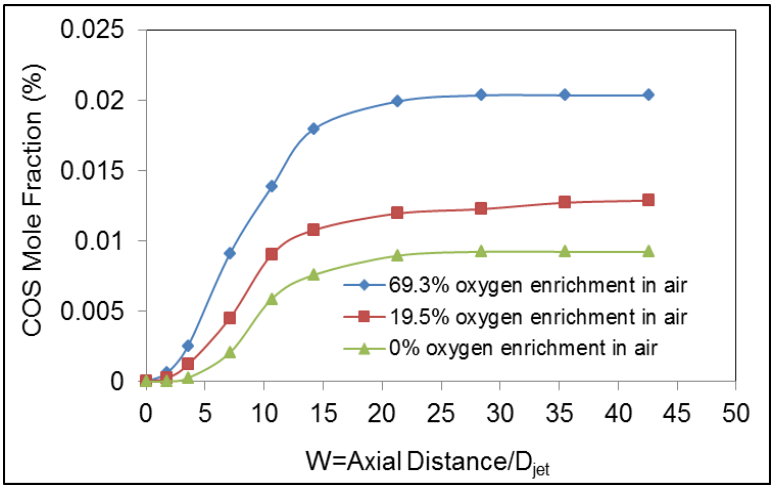

Figure 4-65. Carbonyl sulfide mole fraction. Flame conditions: H_2/O_2-N_2 with 50% H_2S/50% CO_2 acid gas at Φ=3.0

Formation of carbon disulfide is dependent on the presence of carbon monoxide in the reaction pool. The significant reactions involved are shown in equations 4-42 through 4-59 (Clark et al., 2001; Murakami et al., 2001).

Figure 4-65 shows the distribution of carbonyl sulfide mole fraction along reactor centerline at different percentages of oxygen enrichment to air. However, increase in mole fraction of COS with oxygen enrichment in air is attributed to the increased amounts of CO present and higher reactor temperatures. Moreover, release of atomic and molecular oxygen, from increased activity of CO_2, at higher temperatures substantiates the role of reactions 4-58 and 4-59. This interpretation is supported by the fact that CS_2 mole fraction decreased with oxygen enrichment to air.

4.3.3.3 Summary and Comparative Analysis

Acid gas (H_2S and CO_2) combustion was examined in H_2/O_2-N_2 flame at different percentages of oxygen enrichment to combustion air. Three different percentages of oxygen enrichment of air (0%, 19.5% and 69.3%) were presented. The

rate of oxidation of hydrogen was faster in case of 50% H_2S/50% CO_2 than 100% H_2S due to higher amounts of oxidizer released from the carbon dioxide present in the reaction pool. Oxygen enrichment in air decreased the rate of hydrogen oxidation. Hydrogen sulfide reacted with oxygen to form SO_2 rather than more favorable S_2. This supports the increase in SO_2 mole fraction until it reached to an asymptotic maximum value. Increase in oxygen enrichment to air increased the rate of SO_2 production. Carbon dioxide proved to contribute as an oxidizer provider into the reaction pool, in particular at higher temperatures. Presence of carbon monoxide also triggered the formation of other sulfurous-carbonaceous compounds, such as COS and CS_2. With oxygen enriched air, rate of COS production increased while that of CS_2 decreased. This is attributed to increase in the mole fraction of CO and amount of oxygen released into the reaction pool. A summary of the oxygen enrichment effects on major species with respect to different acid gas mixtures is given in table 4-10 below.

Table 4-10. Summary of Oxygen Enrichment Effects

<table>
<tr><td colspan="6">Effect of Oxygen Enrichment of Combustion air
(Temperature and Residence time)</td><td></td></tr>
<tr><td>Composition</td><td colspan="5">Major Species composition at reactor exit</td><td></td></tr>
<tr><td></td><td>H_2S</td><td>SO_2</td><td>H_2</td><td>COS</td><td>CS_2</td><td>C_1-C_2</td></tr>
<tr><td>H_2S/C_7H_8
H_2S/C_8H_{10}
H_2S/CO_2</td><td>Conversion Increases</td><td>Production Increases</td><td>Conversion Decreases</td><td>Not formed

Production Increase</td><td>Production Decreases</td><td>Decreases

Not formed</td></tr>
</table>

4.4 Reaction Pathways of BTX and H_2S Destruction

Characterization of xylene and H_2S combustion in H_2/O_2-N_2 flames under (fuel-rich) Claus condition was examined. Xylene was chosen as the representative of BTX in the reactor, since toluene and benzene are produced at the initial stage of xylene decomposition. This means that benzene, toluene and xylene will all be present in the rector. Table 4-11 shows flow rates of each gas introduced into the burner. The inlet gas stream consisted of 0.5%, 0.75 and 1% xylene with H_2S making up the remaining gas mixture composition. The experimental procedure was the same as those discussed previously in section 4.3. Gas flow rate of xylene was calculated based on the respective densities: liquid xylene has a density of 0.879 g cm^{-3} while that of gaseous xylene is 0.0032 g cm^{-3}. Gas sampling and analysis of local species were conducted along the longitudinal centerline of the reactor axis. The results are compared and discussed below. Dimensionless axial distance (W= axial distance/D_{jet}) was used for all the results presented. Inner jet diameter (D_{jet}=3.58mm) of the burner was used to transform the linear distances into dimensionless parameters for broader application of the results.

Table 4-11. The Test Matrix

	flow rate: cm^3/min				
Gas composition	H_2	O_2	N_2	H_2S	C_8H_{10}
0.5% C_8H_{10} and 99.5% H_2S	1600	936.6	1705	264	1.32
0.75% C_8H_{10} and 99.25% H_2S	1600	938.9	1709	264	1.98
1% C_8H_{10} and 99% H_2S	1600	941.2	1713	264	2.64

4.4.1 Product Speciation

Combustion of xylene and hydrogen sulfide mixture in H_2/O_2-N_2 flame resulted in the formation of hydrocarbons, sulfurous compounds and several other hydrocarbon and sulfur radicals (stable and unstable species) in the reactor. Mole fractions of H_2S, H_2, CH_4 and SO_2 along the longitudinal centerline axis of the reactor are shown in figures 4-66 to 4-71. Both H_2S and H_2 decomposed with high conversion as the residence time in the reactor increased, but H_2 was not completely consumed. The incomplete decomposition of hydrogen is directly attributed to the additional amounts of hydrogen formation from initial decomposition of hydrogen sulfide and xylene. In addition, the fierce oxidation competition between H_2S, H_2, xylene and other formed hydrocarbons in the reactor also contributed. Similar observation was also made with toluene and H_2S combustion in H_2/O_2-N_2 flames.

Combustion of H_2S occurs through thermal and chemical decomposition to form radical species and H_2 in the primary reaction zone. This is followed by oxidation of H_2S, formed H_2 and other radicals in the secondary stage; under partially oxidizing conditions of Claus reactors. The formed radicals further recombine to produce SO_2 as shown in the global reactions 4-47, before the occurrence of global reaction 4-48 that is dominant under Claus condition. It is noteworthy that global reactions 4-47 and 4-48 occur through series of elementary reaction steps, where formed sulfur radicals and SO_2 recombine to yield elemental sulfur at higher residence times in the reactor, as depicted in reactions 4-1 to 4-17 (Cerru et al., 2005). It was evident in figure 4-69 that the mole fractions of SO_2 formed a peak at W~15 in the reactor. The formation of hydrocarbon radicals from xylene also favored SO_2 and

SO reduction to produce other compounds, such as CS_2. This is supported by the decrease in mole fractions of methane while that of CS_2 simultaneously increased. Significant reactions involved are illustrated in reactions 4-26 through 4-29 and 4-55 to 4-57, to provide better interpretation of the experimental data. These reactions have been carefully adapted from studies obtained under partially oxidizing conditions, as well as reduced mechanism of H_2S oxidation (Leeds University, 2012, Chin, 2000, Clark et al., 2001). The mole fraction of C_2H_2 along the reactor axial distance is shown in figure 4-71. The formation of lower series of hydrocarbons, CH_4 and C_2H_2 in the reactor is attributed to xylene decomposition. It was observed that C_2H_2 formation occurred very rapidly in the flame zone of the reactor, but subsequently decomposed until it reached a steady state minimum mole fraction at higher residence time in the post flame zone (higher reactor axial distance).

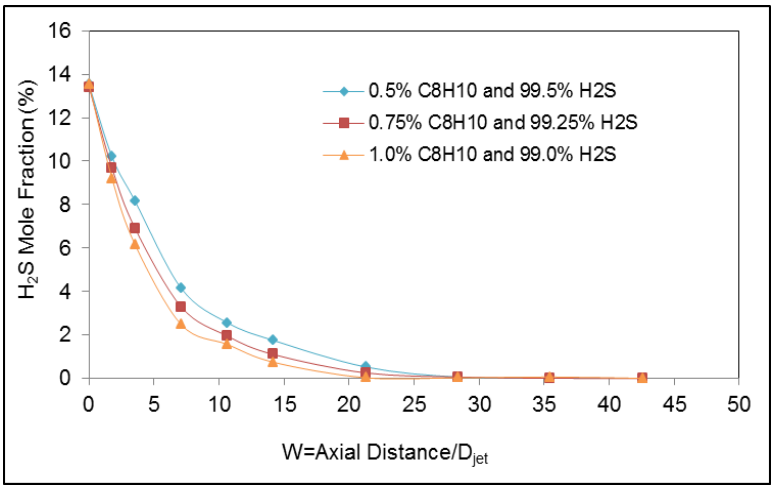

Figure 4-66. Hydrogen sulfide mole fractions. Flame condition: H_2/O_2-N_2 with H_2S/C_8H_{10} acid gas at Φ=3.0.

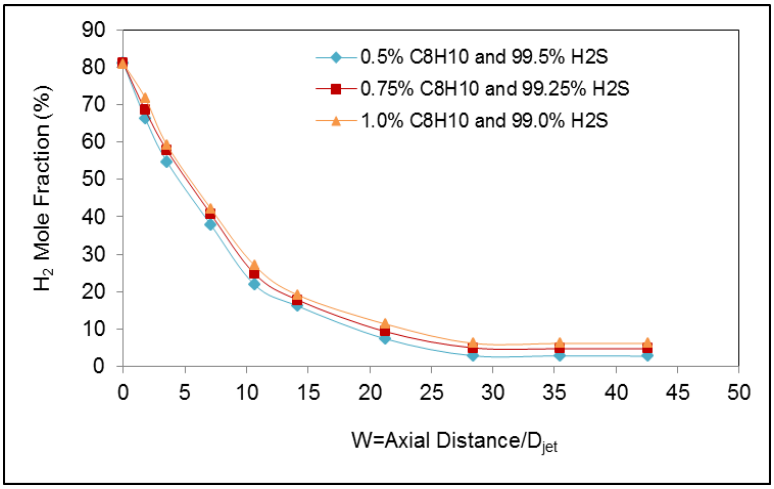

Figure 4-67. Hydrogen mole fractions. Flame condition: H_2/O_2-N_2 with H_2S/C_8H_{10} acid gas at Φ=3.0

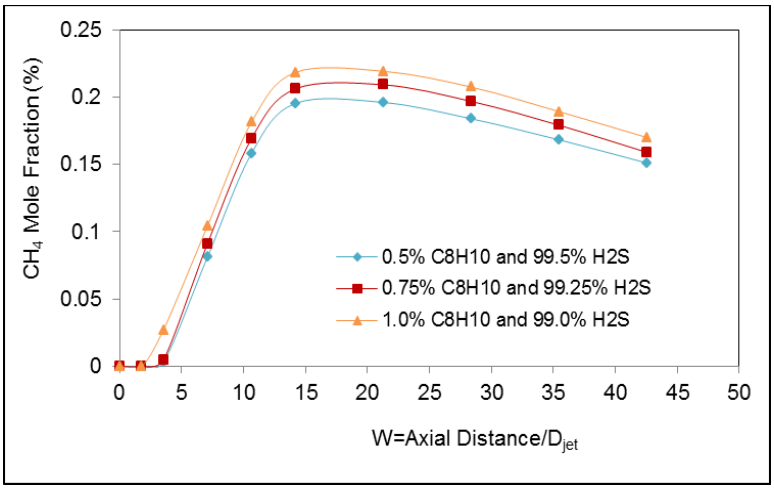

Figure 4-68. Methane mole fraction. Flame condition: H_2/O_2-N_2 with H_2S/C_8H_{10} acid gas at Φ=3.0

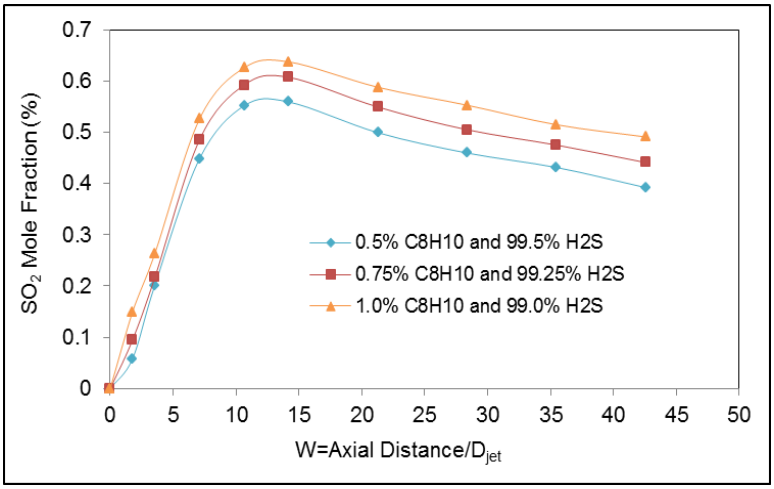

Figure 4-69. Hydrogen sulfide mole fraction. Flame condition: H_2/O_2-N_2 with H_2S/C_8H_{10} acid gas at Φ=3.0

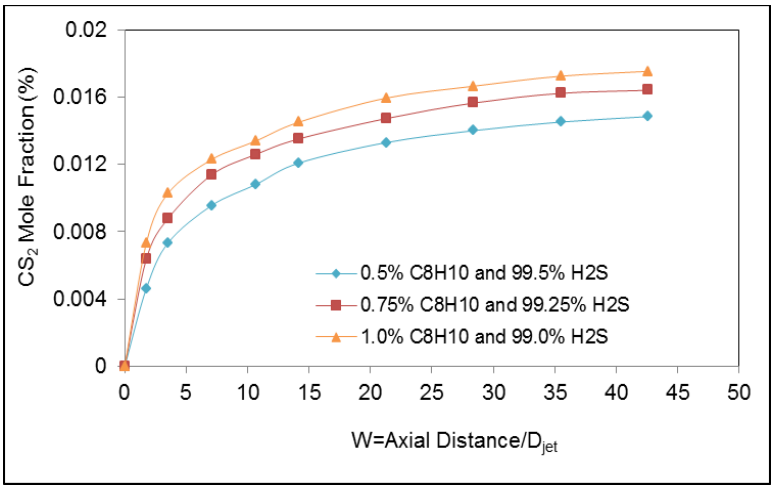

Figure 4-70. Hydrogen sulfide mole fraction. Flame condition: H_2/O_2-N_2 with H_2S/C_8H_{10} acid gas at Φ=3.0

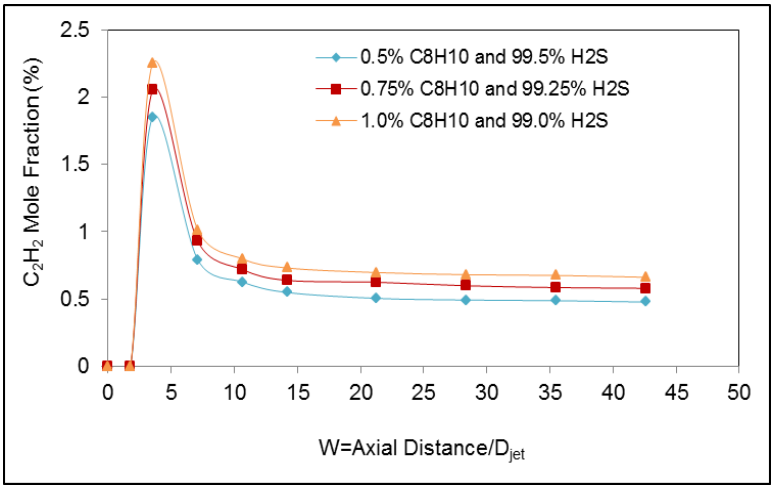

Figure 4-71. Acetylene mole fraction. Flame condition: H_2/O_2-N_2 with H_2S/C_8H_{10} acid gas at Φ=3.0

Formation of acetylene suggested aromatic ring rupture in the xylene molecules and its intermediates (benzene and toluene). On the other hand, CH_4 mole fraction increased steadily to a peak value at reactor distance of W~15, much higher than that of acetylene that occurred at W~5. This suggests increased decomposition of xylene and rupture of the aromatic ring to yield C_2H_2 and other hydrocarbon radicals. Xylene decomposition is initiated from collision with another molecule (M and/or H, S, SH, SH, O and OH) in the reactor, see reactions 4-60 to 4-65 (Emdee et al., 1991, Saggese et al., 2013, Zhenyu et al., 2011).

$$CH_3C_6H_4CH_3 + M \Leftrightarrow CH_3C_6H_4CH_2 + H \quad (4\text{-}60)$$

$$CH_3C_6H_4CH_3 + H \Leftrightarrow CH_3C_6H_4CH_2 + H_2 \quad (4\text{-}61)$$

$$CH_3C_6H_4CH_3 + H + M \Leftrightarrow CH_3C_6H_4 + CH_4 \quad (4\text{-}62)$$

$$C_6H_5CH_3 + H \Leftrightarrow C_6H_5CH_2 + H_2 \quad (4\text{-}63)$$

$$C_6H_5CH_3 + H \Leftrightarrow C_6H_5 + CH_4 \quad (4\text{-}64)$$

$$C_6H_6 + H \Leftrightarrow C_6H_5 + H_2 \quad (4\text{-}65)$$

This results in methyl radical formation or, more favorably, hydrogen atom removal from xylene (H-abstraction). Eventually, toluene is formed via a radical-radical recombination once xylene decomposition is initiated and, likewise, benzene is formed from toluene. Benzene also undergoes H-abstraction to produce C_6H_5 radical (Emdeeet al., 1991; Saggesse et al., 2013). A radical recombination of CH_3 with another radical can also yield CH_4. This contributed to the observed increase in CH_4 mole fractions at lower residence times (reactor axial distance) in the reactor. Methyl-benzyl ($CH_3C_6H_4CH_2$), benzyl ($C_6H_5CH_2$) and phenyl (C_6H_5) radicals are long-lived in a combustion process because they are resonantly more stabilized than other radical isomers (Blanksby and Ellison, 2003). Therefore, they play dominant roles in the initial decomposition of BTX. In high-temperature decomposition of straight-chain alkanes (such as C_1-C_5), reactions of alkyl radicals (such as CH_3) formed from CH_4 decomposition, occur rapidly. But in the case of BTX, the reactions of alkylated-benzyl, benzyl and phenyl radicals from xylene, toluene and benzene respectively occur slowly (You et al., 2009 and Ji et al., 2009). Therefore, these reactions could be rate-limiting in the overall decomposition rate of BTX in Claus reactors.

$$C_6H_5 + M \Leftrightarrow C_2H_2 + C_4H_3 \quad (4\text{-}66)$$

$$C_6H_5 + M \Leftrightarrow 2C_2H_2 + C_2H \quad (4\text{-}67)$$

$$C_6H_6 + O \Leftrightarrow C_6H_5O + H \quad (4\text{-}68)$$

$$C_6H_5O + O \Leftrightarrow C_5H_5 + CO_2 \quad (4\text{-}69)$$

$$C_5H_5 + M \Leftrightarrow C_2H_2 + C_3H_3 \quad (4\text{-}70)$$

$$C_2H_2 + H \Leftrightarrow C_2H + H_2 \quad (4\text{-}71)$$

$$C_2H_2 + OH \Leftrightarrow C_2H + H_2O \quad (4\text{-}72)$$

$$C_2H_2 + S \Leftrightarrow CH_2 + CS \quad (4\text{-}73)$$

$$C_2H_2 + CH_3 \Leftrightarrow CH_4 + C_2H \quad (4\text{-}74)$$

$$CH_2 + CH_2 \Leftrightarrow C_2H_2 + H_2 \quad (4\text{-}75)$$

Further decomposition of phenyl radical results in the formation of acetylene, and significant reactions include 4-66 to 4-75 (Saggese et al., 2013 and Zhenyu et al., 2011). Cyclopentadienyl (C_5H_5) is one important radical widely observed in BTX oxidation and pyrolysis at equivalence ratio of 1-2 (Saggese et al., 2013). Reaction 4-70 is a major reaction pathway on acetylene formation and it involves reactions 4-68 and 4-69. The formed acetylene then undergoes pyrolysis and oxidation via reaction with the abundant hydrocarbon and sulfur radicals, such as S, SH and SO in the reactor. Since it is known that C_2H_2 is a precursor to soot and formation of polycyclic aromatic hydrocarbons (PAH), other potential pathways on C_2H_2 consumption are those leading to PAH formation. The reaction pathways illustrated here were adapted from studies conducted under partially oxidizing condition, but are not meant to be exhaustive. It is understood that other pathways are also possible. Benzene may also be oxidized through its chemically activated reaction with oxygen atom to form phenol, phenoxy or other oxygenates. However, the fuel rich condition in the Claus reactor means that the likelihood of xylene molecules or product of its radicals reacting with O and OH, at the expense of H_2S and its radicals is minimal. The higher bond energy of xylene molecules and C-H radicals when compared to H_2S and S-H suggests the later are preferentially oxidized in the Claus reactor. Since the GC did not favor detection of radical species, some of the short-lived combustion generated

species (unstable species) in the reactor were further examined using flame chemiluminescence of excited species.

4.4.2 Xylene and H_2S Spectra in H_2/air Flame

The spectra of H_2S and xylene mixture in H_2-air flame was examined to identify the unstable (radical) species formed in the reactor. The flame spectra were obtained at the same experimental run to allow easier data analysis and coupling with the data obtained from gas analyzer for stable combustion products. Figure 4-72 and 4-73 show spectrums of H_2S and xylene in hydrogen/air flame between 230nm and 490nm at two different locations in the reactor. A fine grating of the spectrometer was used to examine the flame spectra at two locations, corresponding to low residence time and primary reaction zone of the reactor (W = Axial Distance/D_{jet} = 1.77 and 3.55). This was achieved by positioning the fiber optic cable, mounted on a traverse mechanism at each desired location to collect the emitted light from species in the desired reactor location.

Series of peaks were identified at the initial stage of reaction as seen in figure 4-72. At this point, the amount of formed SO_2 was very minimal (see figure 4-74), but as the fiber optic was moved to a higher reactor distance/residence time, the concentration of SO_2 increased and the spectrum showed a stronger continuum band between 280-460nm (see figure 4-73). Also, the intensity of several peaks decreased and, the peaks were superimposed on the continuum band. This is attributed to the increase in radical pool of sulfurous and hydrocarbon intermediates. The observed continuum matches fairly well with that of SO_2 afterglow observed by other previous investigators, who also pointed out that SO_2 afterglow causes increase in the

background signal of the spectrum between 260nm and 490nm (Gaydon, 1934, Selim et al., 2011 and Mulcahy and Williams, 1970). Mulcahy and Selim attributed the formation of SO_2 afterglow to excited singlet and triplet states of SO_2* within wavelengths of 350nm and 420nm.

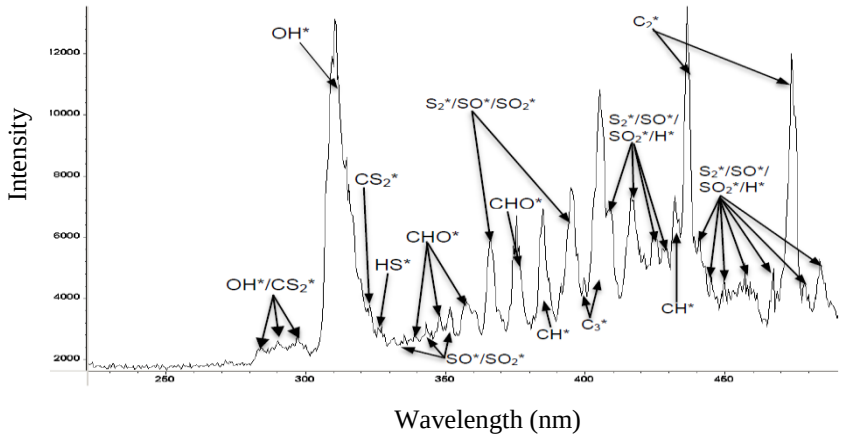

Figure 4-72. Emission spectrum between 230nm-500nm at W=Axial Distance/D_{jet}=1.77. Flame condition: 99.5% H_2S/0.5% C_8H_{10} in H_2/O_2-N_2 at Φ=3.0.

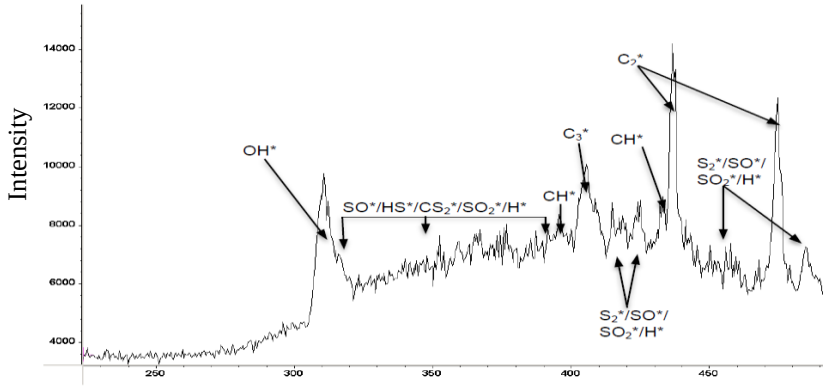

Figure 4-73. Emission spectrum between 230nm-500nm at W= Axial Distance/D_{jet} = 3.55. Flame condition: 99.5% H_2S/0.5% C_8H_{10} in H_2/O_2-N_2 at Φ=3.0.

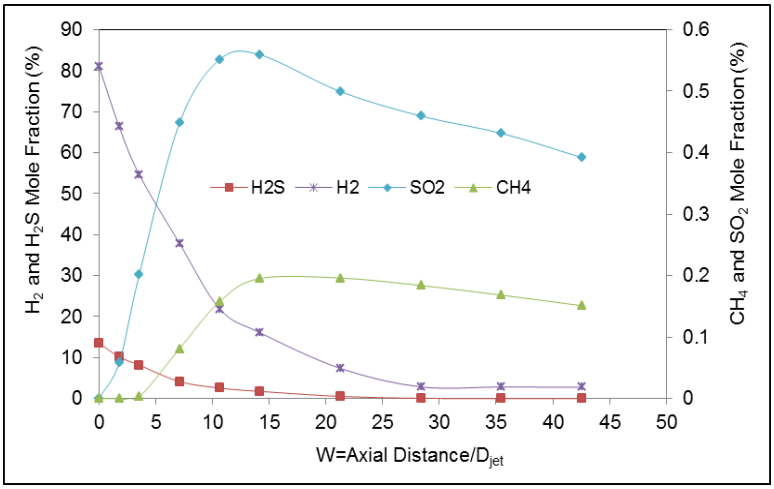

Figure 4-74. Hydrogen, hydrogen sulfide, methane and sulfur dioxide mole fractions. Flame condition: 99.5% H_2S/0.5%C_8H_{10} in H_2/O_2-N_2 at Φ=3.0.

A coarse grating was used to elaborate on the peaks observed between 280 – 490nm in figure 4-72, and the resulting flame spectra are shown in figures 4-75 to 4-80. Figures 4-75 and 4-76 show the spectra between 230nm to 350nm. Weak peaks were discernible between 282-296nm, above the background of the global OH* peaks that appeared at wavelengths of 306.6, 309.67nm and 314nm. These weak peaks could be attributed to OH* and CS_2*. The work of Toyota and co-workers, 1974, wherein they reported bands of CS_2* at 282nm and 285nm supports this interpretation. Peaks of OH* could also extend from 310nm to 280nm (Gaydon, 1934 and Selim et al., 211), so that observed peaks are attributed to both OH* and CS_2* bands. Moreover, the presence of CS_2 in the sampled gas (GC analysis) also justifies this interpretation (See figure 4-77). The bands of CS_2 have also been reported in literature to appear at 320nm (Toyota et al., 1974) and SH bands at 323.5nm and 327.8nm (Muller et al., 1979 and Selim et al., 2011). Absorption bands were the suitable way to distinguish them and our results showed the presence of CS_2 at

319.9nm and SH bands at 324.4 and 328.8, where the lowest magnitude of light intensity was observed.

Several peaks were also observed beyond 310nm. These bands could be attributed to the emission from sulfurous species, SO* (Gaydo and Whittingham, 1947), SO_2* (Mulcahy and Williams, 1970), S_2* (Fowler and Vaidya, 1931 and Dagnall et al., 1969) and SO_3* (Gaydon, 1934), hydrocarbon radicals CHO*, C_3*, CH* and C_2* (Dagnall et al., 1969 and Pearse and Gaydon, 1963)) and H* Balmer series (Wood, 1920 and Dagnall et al., 1969). It has been suggested that SO_3* is responsible for the peaks beyond 350nm by Gaydon et al., 1934, 1947, 1963 and Dooley et al., 1946. The formation of SO_3 can occur in the Claus reactor through reactions with O or OH group, such as reactions 4-76 to 4-77 (Gaydon, 1934). The formation of SO_3, shown in Reaction 4-67 is more favorable under fuel lean conditions, where oxygen is in excess and OH radicals are abundant. Therefore, the likelihood of SO_3* being responsible for peaks beyond 320nm is minimal due to the fuel rich condition of the flame and fierce oxidation competition between H_2, H_2S and C_8H_{10} molecules.

$$SO + OH \Leftrightarrow SO_2^* + H \qquad (4\text{-}76)$$

$$SO_2 + OH \Leftrightarrow SO_3^* + H \qquad (4\text{-}77)$$

Conversely, the likelihood of SO* bands being present beyond 310nm is very high because SO is an important radical that play prominent role in the pathways leading to SO_2, CS_2 and S_2 in Claus reactors (Leeds University, 2012). The spectrum of SO* exhibits over 40 peaks occurring between 244nm - 394nm and are more

common in rich flames, albeit unlikely to occur under single set of conditions (Gaydon and Whittingham, 1947).

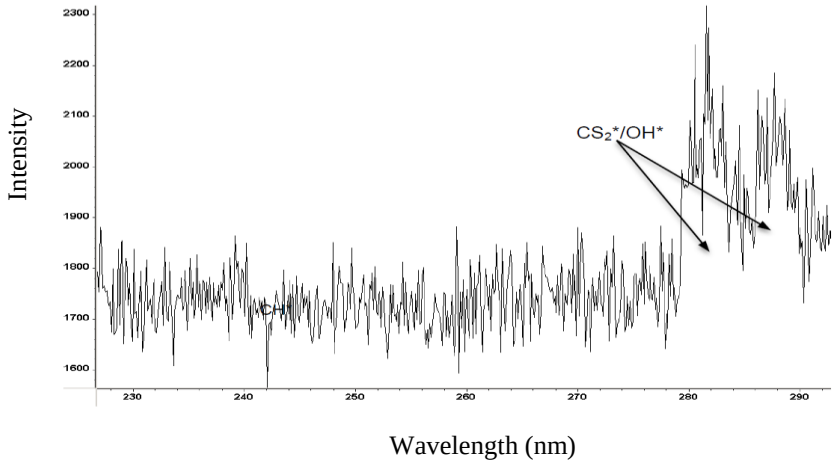

Figure 4-75. Emission spectrum between 230nm-290nm at W= Axial Distance/D_{jet} = 1.77. Flame condition: 99.5% H_2S/0.5% C_8H_{10} in H_2/O_2-N_2 at Φ=3.0.

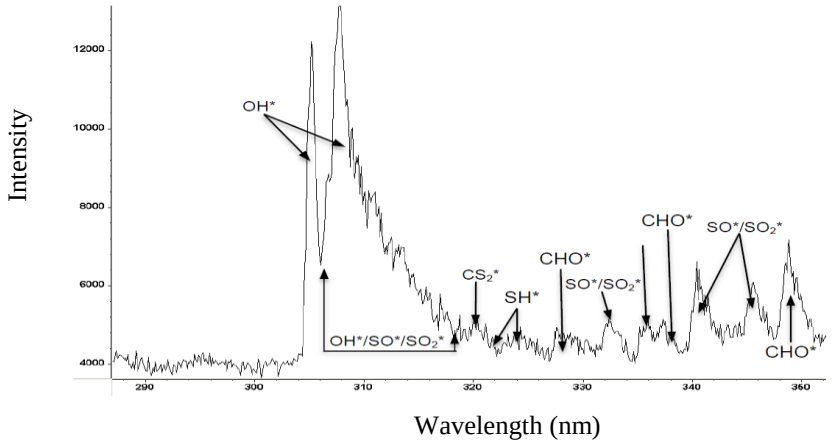

Figure 4-76. Emission spectrum between 290nm-350nm at W=Axial Distance/D_{jet} =1.77. Flame condition: 99.5% H_2S/0.5% C_8H_{10} in H_2/O_2-N_2 at Φ=3.0.

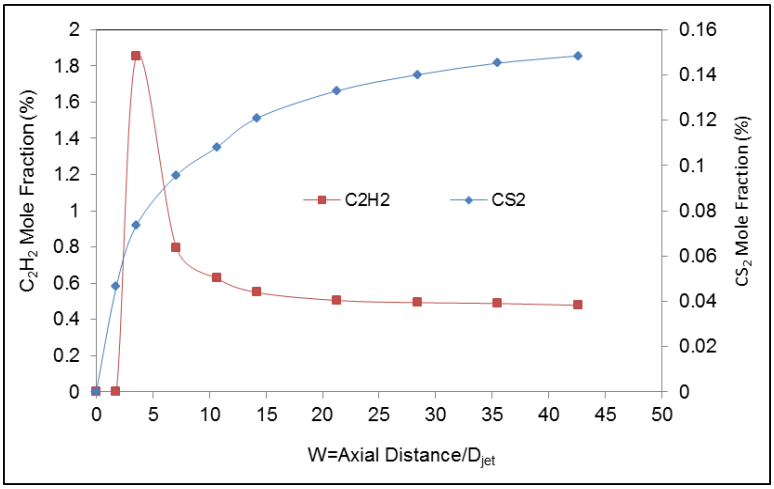

Figure 4-77. Acetylene and carbon disulfide mole fractions. Flame condition: 99.5% H_2S/0.5%C_8H_{10} in H_2/O_2-N_2 at Φ=3.0.

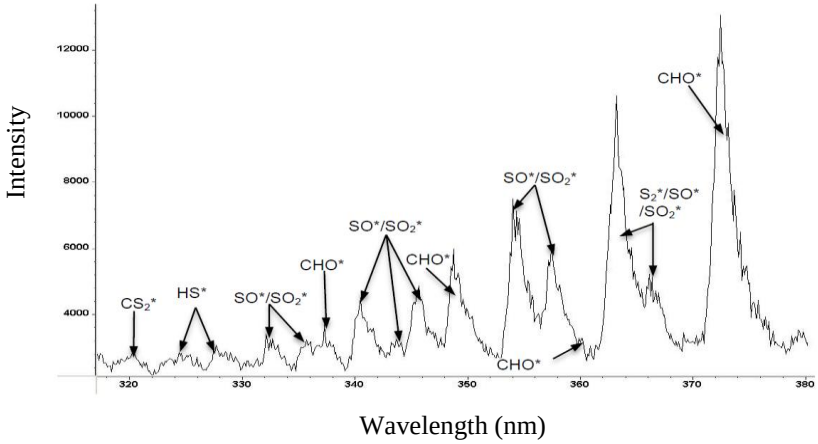

Figure 4-78. Emission spectrum between 320nm-380nm at W= Axial Distance/Djet =1.77. Flame condition: 99.5% H_2S/0.5% C_8H_{10} in H_2/O_2-N_2 at Φ=3.0

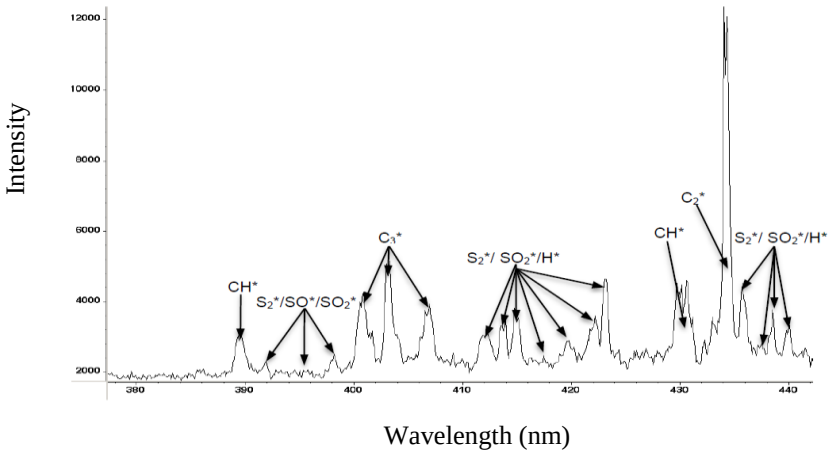

Figure 4-79. Emission spectrum between 380nm-440nm at W=Axial Distance/D_{jet} =1.77. Flame condition: 99.5% H_2S/0.5% C_8H_{10} in H_2/O_2-N_2 at Φ=3.0.

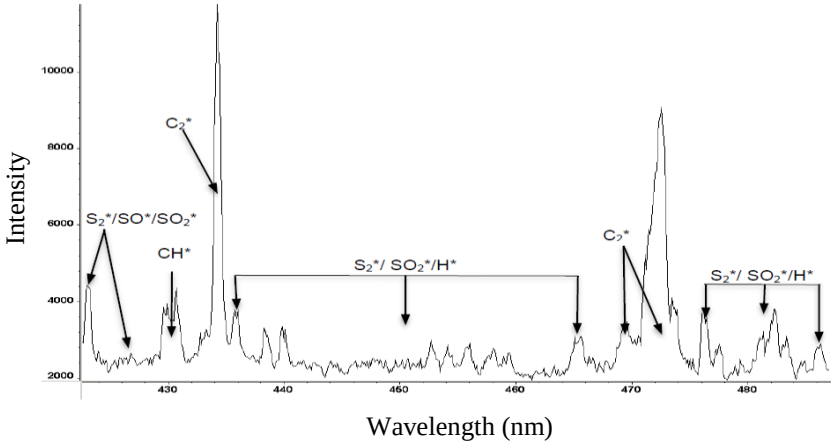

Figure 4-80. Emission spectrum between 430nm-490nm at W= Axial Distance/Djet =1.77. Flame condition: 99.5% H_2S/0.5% C_8H_{10} in H_2/O_2-N_2 at Φ=3.0.

The occurrence of SO_2 afterglow means peaks of SO_2* could also be present, so that some of the observed peaks between 316-355nm could be attributed to SO* and SO_2* bands. Bands of S_2* are also very likely due to the fuel rich condition of the Claus reactor that favor S_2 formation (Selim et al., 2012c). These bands are known to occur between 360-490nm (Fowler and Vaidya, 1931, Pearse and Gaydon, 1963) and

sulfur formation was visibly observed on the walls of the reactor during the experiments. Balmer series of H*, commonly observed between 389-490nm (Wood, 1920) also play significant role in both H_2S and hydrocarbon flames. This makes it very difficult to establish any justifiable distinction amongst SO_2*, S_2* and H* bands. Therefore, peaks between 360-486nm are attributed to bands of SO_2*, S_2* and H* Balmer series. The work of Gaydon and co-workers (Pearse and Gaydon, 1963) supports this interpretation. A summary of all the identified peaks is shown in table 4-12. However, distinct bands of hydrocarbon radicals were also identified between 330-475nm. Bands of CHO* (Vaidya's bands) were observed at 338nm, 350nm and 359nm, C_3*: 400nm, 404nm and 407nm, CH*: 389nm and 431.9 and Swan bands of C_2*: 434, 470-474nm (Pearse and Gaydon, 1963, Dagnall et al., 1969). These bands have been observed in hydrocarbon flames consistently, but bands of C_3* are mostly favorable in fuel rich hydrocarbon flames. Another possible radical is CH_2* and has been provisionally assigned bands at 405nm in literature, but this is doubtful as most authors observed that C_3* is responsible for emission at 405nm (Pearse and Gaydon, 1963).

Table 4-12. Spectrum of H_2S and C_8H_{10} in H_2/O_2-N_2 Flame

Wavelength (nm)	Species		Wavelength (nm)	Species	
280-296	OH* and CS_2*	Sulfur Dioxide Afterglow	412.11	S_2*,SO_2* and H* bands	Sulfur Dioxide Afterglow
306-314	OH* bands		420.23		
316.59	SO* and SO_2* bands		422.42		
319.86	CS_2 (absorption) bands		424.88		
322.74	SO* and SO_2* bands		431.98	CH* band	
324.44	SH (absorption) band		434.50	C_2* band	
326.99	SO* and SO_2* bands		436.08	S_2*, SO_2* and H* bands	
328.82	SH (absorption) bands		438.65		
332.23	SO* and SO_2* bands		440.25		
336.87			447.90		
338.28	CHO* band		452.68		
342.28	SO* and SO_2* bands		454.38		
346.65			456.08		
350.26	CHO* band		458.23		
355.43	SO* and SO_2* bands		459.24		
359.76	CHO* band		465.24		
363.69	S_2*, SO_2* and H* bands		470-474	C_2* band	
367.74			478.04	S_2*,SO_2* and H* bands	
374.32	CHO* band		482.21		
389.34	CH* band		484.79		
394.52	S_2*, SO_2* and H* bands		486.17		
398.42					
400.51	C_3* bands				
404.17					
407.57					

4.4.3 Summary

Gas chromatograph (GC) analysis and Spectra of excited species were used to characterize the combustion generated products of hydrogen sulfide and xylene mixtures in hydrogen-air flame under Claus Condition. GC analysis showed oxidation of H_2S with very high conversion. This resulted in SO_2 formation to a maximum mole fraction and subsequent decomposition of formed SO_2 to produce S_2 and CS_2. The formed acetylene and methane were not completely oxidized in the reactor, even

though SO_2 proved to be a source of oxidizer. Examination of emission spectra of excited species proved interaction between hydrocarbon and sulfur species to form CS_2. The bands observed between 280nm-490nm were attributed to C_3*, C_2* (swan bands), CHO* (Vaidya's flame bands), H* (Balmer series), CH* and other sulfurous species, SO, SH, S_2* and SO_2*. The existence of SO_2 afterglow was also observed. These results demonstrate the role of xylene in formation of lower hydrocarbon in a Claus reactor. The produced methane and acetylene could be a value added chemicals. The results are also of significant interest to operators and designers of sulfur plants and policy-makers on emission control.

4.5 Role of BTX to Acid Gas (H_2S/CO_2) Combustion

In the previous sections, the role of individual contaminant (xylene, benzene, toluene or CO_2) addition into H_2S/O_2 and H_2/Air flames were examined under Claus condition. Destruction of BTX is more favorable under high reactor temperature condition and presence of CO_2 reduces the operating temperature of the reactor. It is therefore, necessary to characterize and evaluate the combustion of H_2S, CO_2 and BTX mixtures, which represents a more practical acid gas composition. More than one contaminant is always present in acid gas stream, so that examination of combined effect of CO_2 and toluene or xylene mixtures to H_2S combustion is of scientific and practical value. This can help provide guidelines for improved operation of Claus reactors and mitigate emissions from sulfur recovery plants.

4.5.1 Role of Toluene to Acid Gas (H_2S/CO_2) Combustion

Combined effect of toluene and CO_2 on the combustion of H_2S in H_2/O_2-N_2 flames under (fuel-rich) Claus condition was examined. Table 4-13 shows the flow rates of each gas introduced into the burner. Three gas stream compositions were examined and compared to isolate the combined role of toluene and CO_2. The effect of gas stream compositions (H_2S, H_2S/C_7H_8, or $H_2S/C_7H_8/CO_2$) on product gas distribution was evaluated. The first case represents inlet gas stream consisting of 100% H_2S, while second case represent gas mixture of H_2S/C_7H_8 and third case represent $H_2S/CO_2/C_7H_8$.

Table 4-13. The Test Matrix

	flow rate: cm^3/min					
Gas composition	H_2	O_2	N_2	H_2S	C_7H_8	CO_2
100% H_2S	1600	932	1690	264	0	0
99.5% H_2S/0.5% C_7H_8	1600	936	1697	264	1.32	0
49.75%H_2S/49.75%CO_2/0.5%C_7H_8	1600	876	1578	132	1.32	132
49.5% H_2S/49.5%CO_2/ 1% C_7H_8	1600	878	1578	132	2.64	132

In order to achieve the required experimental conditions, H_2/O_2-N_2 mixture was combusted under slightly fuel-lean conditions. Based on the flow rate of the excess oxygen, hydrogen sulfide and toluene were injected to achieve the targeted fuel-rich equivalence ratio (Φ=3.0), for the Claus condition. The equivalence ratio was calculated based on the combustion of hydrogen sulfide and toluene mixture. Equivalence ratio is defined as actual fuel to oxidizer ratio normalized by stoichiometric fuel to oxidizer ratio. It was assumed that addition of CO_2 did not impact the equivalence ratio of the flame. Gas flow rate of toluene was calculated

based on the respective densities: liquid toluene has a density of 0.866 g cm^{-3} while that of gaseous toluene is 0.003 g cm^{-3}. Gas sampling and analysis of local species were conducted along the longitudinal centerline of the reactor axis.

The temperature profiles along the longitudinal centerline axis of the reactor centerline are presented first followed by an analysis of species distribution along centerline of the reactor for the combustion of 100% hydrogen sulfide gas stream. The gas speciation and analysis for the combustion of H_2S/C_7H_8 and $H_2S/CO_2/C_7H_8$ gas stream is then presented. Dimensionless axial distance (W= axial distance/D_{jet}) was used for all the results presented here. Inner jet diameter of the burner was used to transform the linear distances into dimensionless parameters for broader application of the results.

4.5.1.1 Temperature Measurements

Mean temperature profiles along the reactor were measured along the longitudinal centerline of the reactor using K-type thermocouple. A traverse mechanism was used to move the thermocouple incrementally along the reactor centerline. Figure 4-81 shows temperature profile for H_2/O_2-N_2 flame with 100% H_2S, 99.5% H_2S/0.5% C_7H_8 and 49.75% H_2S/49.75% CO_2/ 0.5% C_7H_8 gas addition to the burner. Similar trends were observed under all other conditions examined here. However, major differences were observed in the magnitude of temperatures. Temperature increased to a maximum value, and it is attributed to the energy release from the reaction of hydrogen and hydrogen sulfide with the surrounding air. Decrease in temperature further downstream the reactor is due to heat loss to the reactor walls. In comparison to 100% H_2S acid gas combustion, addition of 0.5%

C_7H_8 to 99% H_2S caused flame temperature to increase throughout the reactor. This is directly attributed to the effect of increased heating value associated with toluene during combustion.

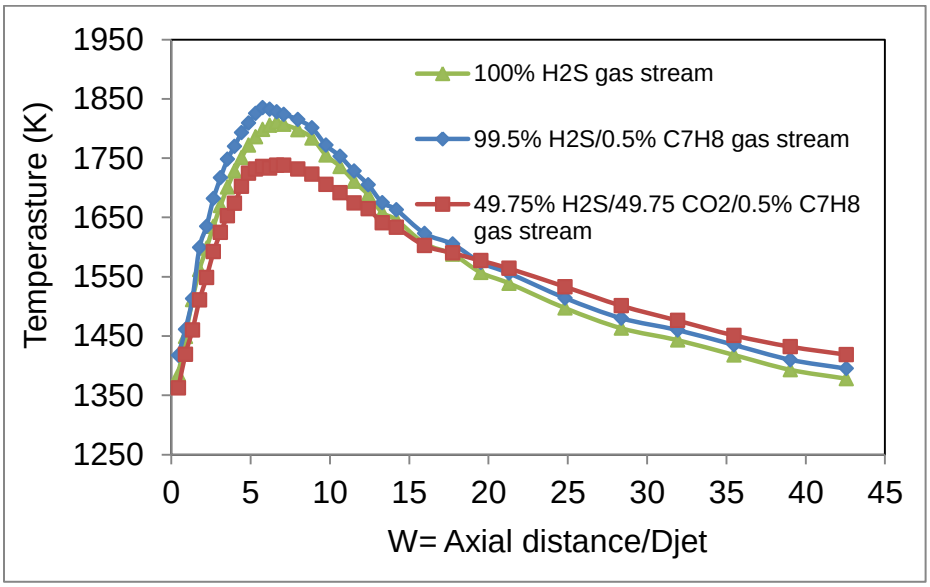

Figure 4-81. Temperature profiles of H_2/O_2-N_2 flame with different acid gas and acid gas mixture addition at Φ=3.0.

On the contrary, addition of both CO_2 and toluene into H_2S (mixture of 49.75% H_2S/49.75% CO_2/ 0.5% C_7H_8) decreased the temperature upon injection. This is attributed to dilution effect and the endothermic dissociation of CO_2 into carbon monoxide and atomic oxygen. Temperature increased further downstream the reactor as CO_2 decomposed to provide additional oxidizing medium to further promote toluene and H_2S combustion and pyrolysis in the reactor.

4.5.1.2 Product Speciation and Analysis

The product speciation for the different acid gas mixtures (H_2S, CO_2 and toluene) are presented and evaluated to isolate the combined role of CO_2 and toluene in the acid gas.

4.5.1.3 Combustion of 100% H2S

Combustion of 100% H_2S and H_2S/C_7H_8 mixtures are evaluated to isolate the role of toluene on hydrocarbon formation under the examined conditions. Combustion of 100% H_2S acid gas resulted in the formation of SO_2 and other intermediate species and radicals. Figure 4-82 shows mole fractions of H_2, H_2S and SO_2 along the reactor centerline respectively.

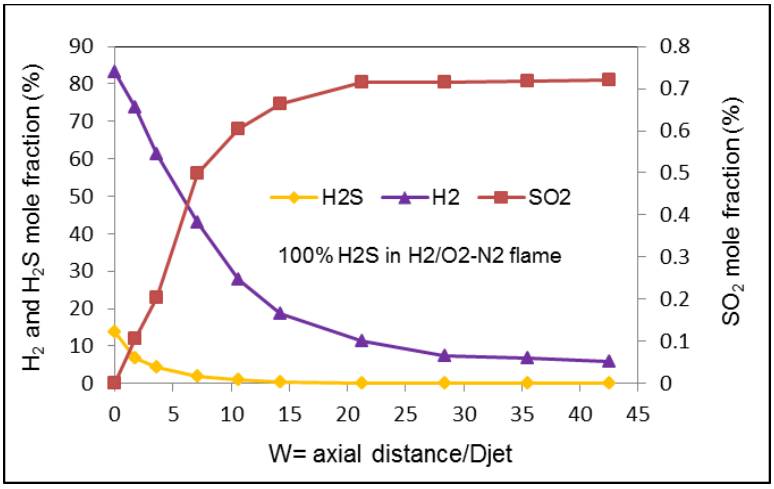

Figure 4-82. Hydrogen, Hydrogen sulfide and sulfur dioxide mole fractions.

Flame condition: H_2/O_2-N_2 with 100% H_2S acid gas at Φ=3.0

Mole fraction of H_2 decreased monotonically until it reached to a minimum value, while that of H_2S decreased until it was almost oxidized completely. The decrease in H_2S mole fractions corresponds to an increase in SO_2 mole fraction due to the reaction of H_2S with O_2 to form SO_2.

4.5.1.4 Toluene /H_2S Acid Gas Combustion

Combustion of H_2S/C_7H_8 mixture resulted in the formation of hydrocarbons, sulfurous compounds and intermediate species in the reactor (Figure 4-89 and 4-90). The mole fraction of H_2, H_2S and SO_2 along the centerline axis of the reactor is shown in figure 4-83. Comparing these results with those from 100% H_2S gas stream combustion (see figure 4-82), the mole fractions of H_2 and H_2S showed similar trends, but are in contrast to that of SO_2. The rate of H_2S decomposition was observed to be faster while that of H_2 was slower. Faster rate of H_2S decomposition is attributed to the increased reactor temperature due to energy release from toluene combustion to enhance pyrolysis and oxidation reactions of H_2S. In addition, hydrocarbon radicals formed from toluene pyrolysis/combustion created additional pathways on H_2S consumption. Toluene pyrolysis was expected to be more dominant over oxidation because H_2S is more reactive as compared to hydrocarbons when reacted with oxygen (Pierucci and co-workers, 2004).

Initial decomposition of toluene occurs through methyl radical formation and H- abstraction (reactions 4-36, 4-37, 4-63 and 4-64). The formed radicals then create additional channels on consumption of H_2S. The observed trends of CH_4, CS_2 and H_2 (figures 4-83 and 4-84) support the possible occurrence of the shown reactions. It is established that CH, CH_3, SH, H, OH radicals are formed during combustion of H_2S and toluene in H_2/air flames (Dagnall et al., 1969, Gaydon et al., 1934 and Selim et al., 2011b). It was noted that hydrogen mole fractions decreased monotonically along the reactor centerline but was not completely oxidized. This could be attributed to two

simultaneous effects. Firstly, there could be possible formation of hydrogen from initial consumption of H_2S.

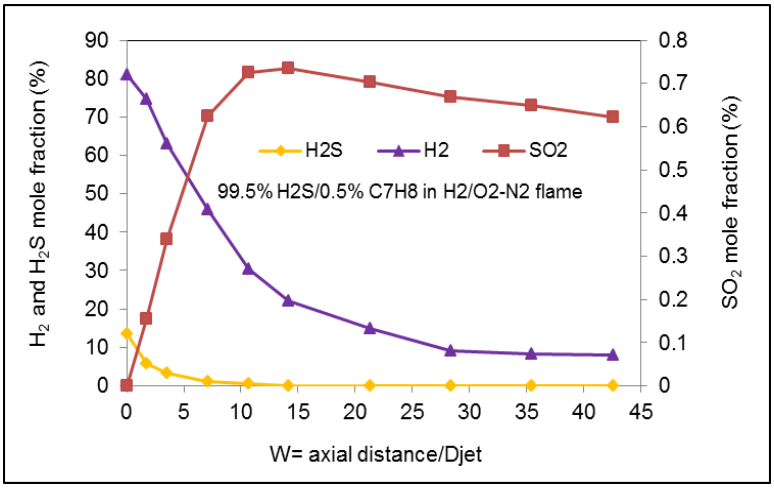

Figure 4-83. Hydrogen, Hydrogen sulfide and sulfur dioxide mole fractions.

Flame condition: H_2/O_2-N_2 with 99.5% H_2S/0.5%C_7H_8 acid gas at Φ=3.0

Consumption of H_2S occurs via pyrolysis at the initial stage followed by oxidation at later stages (Cerru et al., 2005). Secondly, there exists an oxidation competition between H_2S and H_2 that could prevent complete H_2 decomposition as observed. Previous findings support this interpretation of the data, particularly the work of Pierucci and co-workers, 2004, where these authors compared contact times against conversion from stoichiometric combustion of an equimolar mixture of H_2S, H_2 and CH_4 at reactor temperature of 1500K. They found that H_2S was more reactive than H_2 and CH_4. The rate of H_2 decomposition was observed to be slower due to the formation of additional amounts of H_2 from both H_2S and toluene pyrolysis.

Conversely, SO_2 formation was observed to be faster until it reached to a peak value at axial distance of W~15 in the reactor, but subsequently decomposed to an asymptotic value further downstream in the reactor. Faster initial formation of SO_2 is

attributed to the increased reactor temperature from toluene pyrolysis, while decomposition of formed SO_2 is due to reactions of SO and SO_2 with other sulfur containing radical species to form elemental sulfur. Possible reactions include 4-78 and 4-79 (Chin, 2000). In addition, hydrocarbons (CH_4 and C_2H_2) and its radicals from toluene pyrolysis could react with SO_2 to form S_2 and other products (such as reaction 4-30 and 4-31).

$$SO_2 + M \Leftrightarrow SO + O + M \qquad (4\text{-}78)$$

$$SO_2 + H \Leftrightarrow SO + HSO \qquad (4\text{-}79)$$

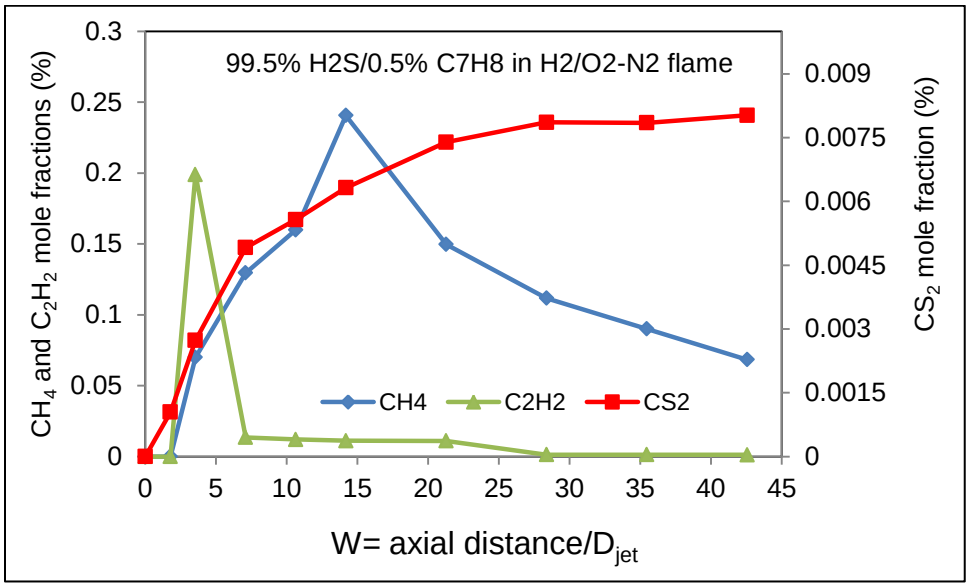

Figure 4-84. Methane, acetylene and carbon disulfide mole fractions. Flame condition: H_2/O_2-N_2 with 99.5% H_2S/0.5%C_7H_8 acid gas at Φ=3.0

The formation of C_2H_2, CH_4 and CS_2, was triggered by the presence of toluene in inlet H_2S gas (see figure 4-84). Mole fraction of acetylene increased to a peak value at reactor distance of W~4 and rapidly decreased to an asymptotic minimum value. However, rate of decomposition of C_2H_2 from within the reactor at distance of

W~7 was observed to be slow and did not reach to zero value due to possible recombination of hydrocarbon radicals to form acetylene. Similarly, CH_4 mole fraction increased to a peak value at reactor distance of W~14 and then subsequently decomposed with increase in axial distance until it reached an asymptotic minimum.

The rate of methane formation/decomposition was observed to be slower than that of acetylene in the reactor. Formation of hydrocarbons in the reactor favored increased formation of CS_2 throughout the reactor along the centerline. This is due to the interaction of methane, acetylene and other hydrocarbon species and radicals with sulfur species in the reactor. The results of Karan et al., 1998a&b and Arutyunov et al., 1991, 1992 and 1993, who both examined oxidation of methane with SO_2, support this interpretation.

4.5.1.5 Toluene/CO_2/H_2S Acid Gas Combustion

The results from the combustion of $H_2S/C_7H_8/CO_2$ mixture are presented and compared with those from H_2S and H_2S/C_7H_8 gas cases discussed above. Figures 4-85 and 4-86 compare the mole fractions of H_2S and H_2 from combustion of different acid gas mixtures along the reactor centerline. In the case of $H_2S/C_7H_8/CO_2$ mixture, initial mole fraction of H_2S was lower in the inlet acid gas as compared to other test cases due to the dilution effect of CO_2. Therefore, H_2S was oxidized much faster. In addition, the presence of CO_2 could also have contributed because it proved to enhance the oxidizing medium by releasing oxidizer into the reaction pool.

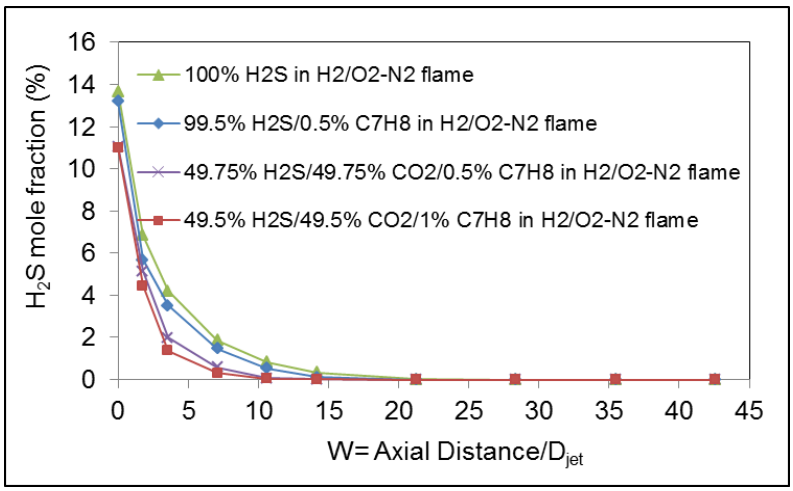

Figure 4-85. Hydrogen sulfide mole fraction with combustion of different acid gas mixtures in H_2/O_2-N_2 at Φ=3.0

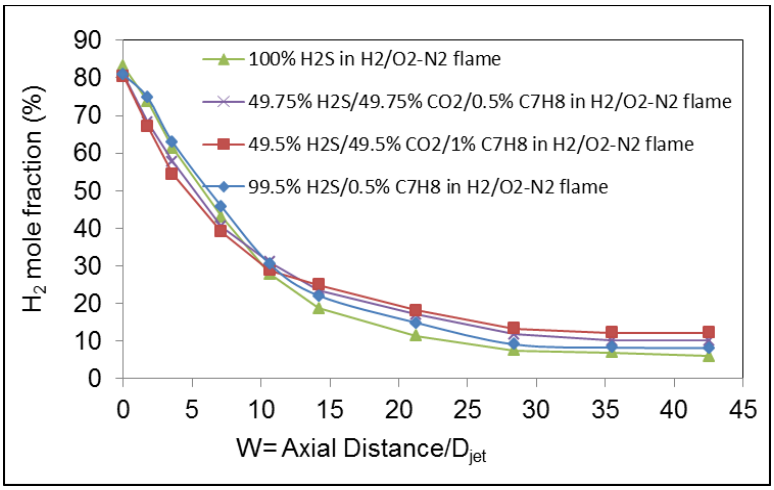

Figure 4-86. Hydrogen mole fraction with combustion of different acid gas mixtures in H_2/O_2-N_2 at Φ=3.0

Hydrogen mole fraction decomposed faster up to a reactor axial distance of W~10 and subsequently slowed down, resulting to increased amounts of H_2 produced at the reactor exit with the examined $H_2S/C_7H_8/CO_2$ mixture. This is attributed to increased reactor temperature due to the oxidizing role of CO_2, which possibly

enhanced pyrolysis and combustion of toluene and other formed hydrocarbons in the reactor.

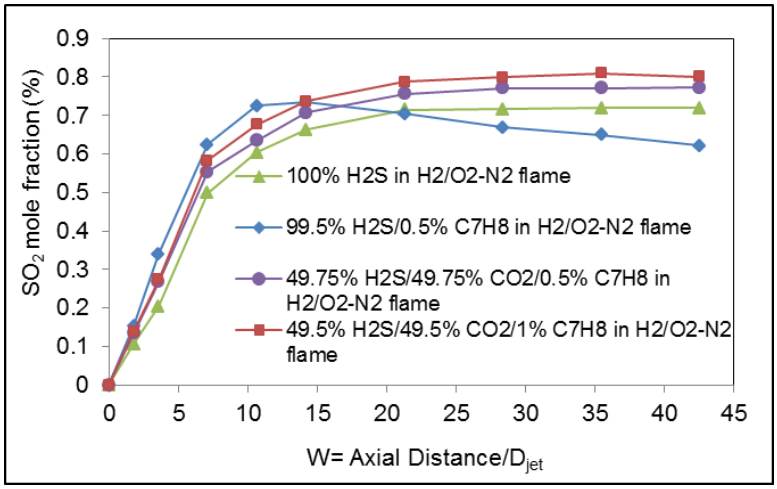

Figure 4-87. Sulfur dioxide mole fraction with combustion of different acid gas mixtures in H_2/O_2-N_2 at Φ=3.0

The formation of CO was a distinct mark on the role of CO_2 as an oxidizer provider in the reaction pool and this supports previous observation. A comparison of SO_2 mole fractions in figure 4-87 revealed faster production of SO_2 as compared to 100% H_2S combustion, and is due to the higher reactor temperature and the release of oxidizer by CO_2 in the reactor. However, initial SO_2 formation was slower (up to reactor axial distance W~14) when compared to the case H_2S/C_7H_8 gas mixture. This is because addition of CO_2 decreased the flame temperature upstream the reactor. Then, further downstream the reactor, the formed SO_2 did not show noticeable decay, as CO_2 enhanced the oxidizing medium that continually supported SO_2 formation. This has the potential implications on reduced sulfur recovery since most of the H_2S is transformed to SO_2.

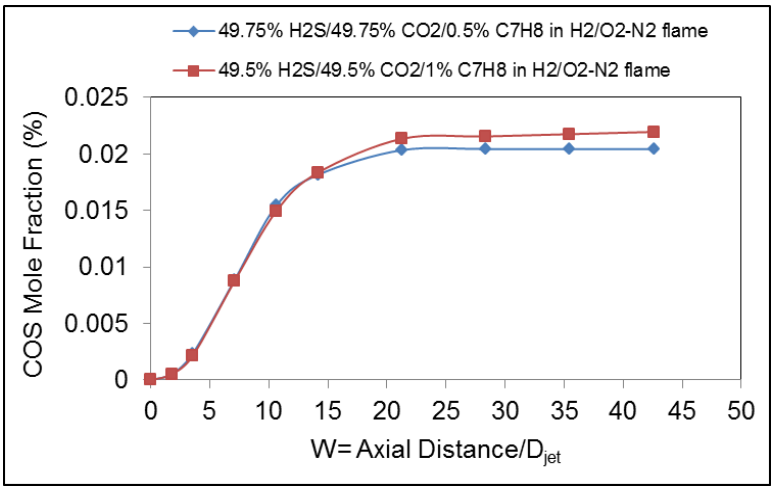

Figure 4-88. Carbonyl sulfide mole fraction from the combustion of different acid gas streams in H_2/O_2-N_2 at Φ=3.0

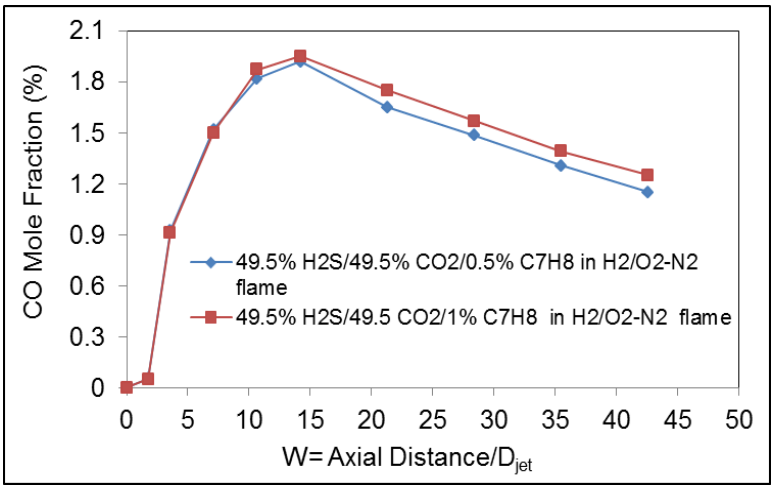

Figure 4-89. Carbon monoxide mole fraction with the combustion of acid gas mixture in H_2/O_2-N_2 at Φ=3.0

It was reported in previous studies that depletion of O_2 in the reactor favors S_2 formation, as this causes several elementary reactions to form S_2 rather than SO_2 (Selim et al., 2011a). Thus, it is necessary to keep control of availability of oxygen in the reaction pool to enhance sulfur recovery. Presence of toluene and CO_2 triggered formation of hydrocarbons and mercaptans (COS and CS_2) in the reactor.

Figures 4-88 and 4-89 illustrate mole fractions of COS and CO along the reactor centerline. Mole fractions of CO increased to a maximum value as CO_2 decomposed to release oxidizer into the reactor (reactions 4-49 and 4-50). However, decrease in CO mole fractions further downstream the reactor is attributed to COS and CS_2 formation (figure 4-90), as well as possible recombination of CO to form CO_2 (reaction 4-51). The incomplete oxidation of CO is due to the inhibition effect by SO and SO. Both COS and CS_2 mole fractions increased monotonically until they reached a maximum value. It was noted that COS formation was not observed in the absence of CO and CO_2 in the reaction pool. Formation of CO promotes both COS and CS_2 production in the reactor.

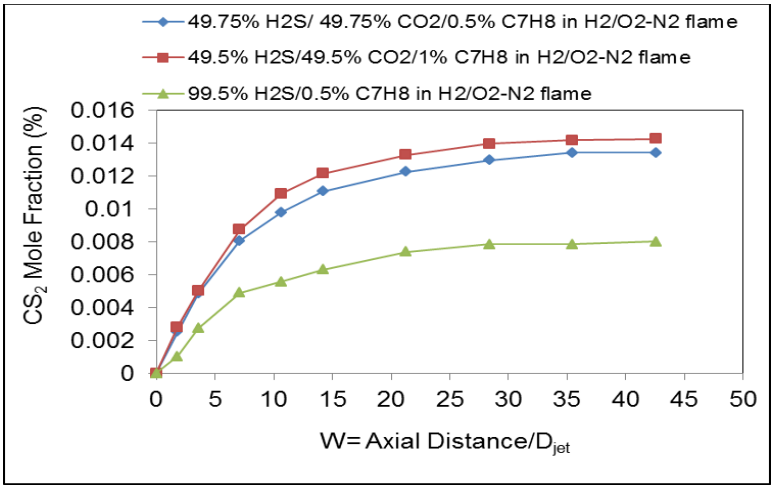

Figure 4-90. Carbon disulfide mole fraction with the combustion of acid gas mixture in H_2/O_2-N_2 at Φ=3.0

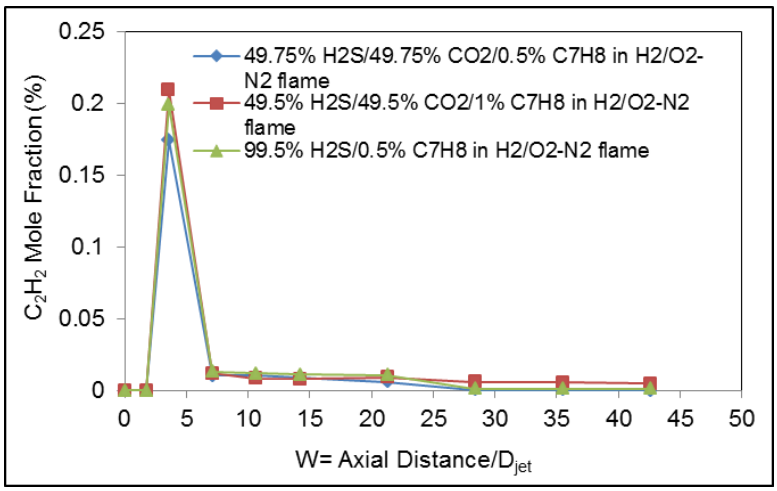

Figure 4-91. Acetylene mole fraction from the combustion of different acid gas stream in H_2/O_2-N_2 at Φ=3.0

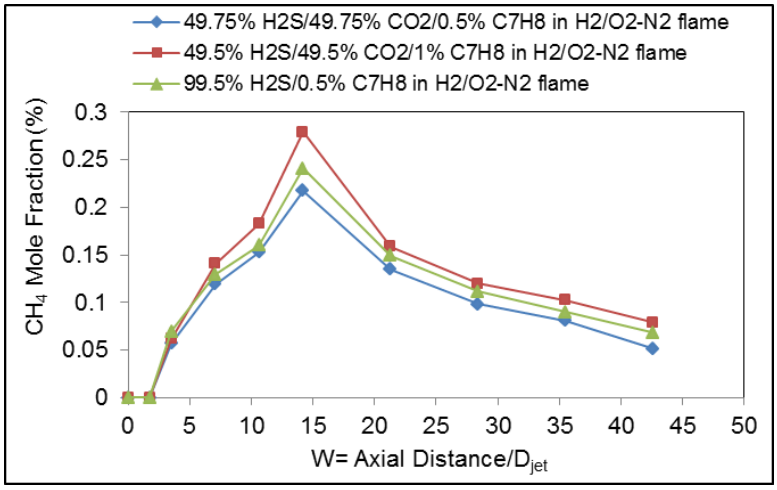

Figure 4-92. Methane mole fraction from the combustion of different acid gas streams in H_2/O_2-N_2 at Φ=3.0

The formation of hydrocarbons (methane and acetylene) in the reactor is attributed to the presence of toluene in the acid gas stream. Mole fractions of acetylene (4-91) increased to a maximum value but subsequently decreased until it completely consumed downstream the reactor. Conversely, methane mole fractions (4-92) increased to a maximum value and then decomposed to an asymptotic

minimum. In comparison, the rates of methane and acetylene decomposition were observed to be faster and the maximum mole fractions were lower than the case of H_2S/C_7H_8 mixture. Presence of CO_2 supported enhanced methane and acetylene destruction, and this was evident in the increased mole fractions of produced hydrogen at the reactor exit (see figure 4-86). Presence of CO_2 could help reduce the impact of hydrocarbons during sulfur capture from acid gases.

4.5.1.6 Summary

Results on the combustion of H_2S, H_2S/C_7H_8 and $H_2S/CO_2/C_7H_8$ gas mixtures in H_2/O_2-N_2 flame are presented. The combined effect of CO_2 and toluene that often accompany H_2S gas stream has been examined. Combustion of H_2S gas resulted in the formation of SO_2. Addition of toluene into acid gas (H_2S or H_2S and CO_2 mixture) enhanced or reduced the rate of reactants/product decomposition and formation. Combustion of toluene and H_2S mixture caused faster SO_2 formation, but the formed SO_2 decomposed to increase the possibility of elemental sulfur formation. In contrast, combustion of toluene and acid gas (H_2S and CO_2) mixture showed increased formation of SO_2 formation throughout the reactor, as CO_2 enhanced the oxidizing medium. Toluene alone, directly contributed to the formation of CH_4, C_2H_2 and CS_2 in the reactor, while both toluene and CO_2 caused increased formation of mercaptans (CS_2 and COS), but enhanced destruction of formed hydrocarbons (CH_4 and C_2H_2). These results support the formation of hydrocarbons and mercaptans that hinders the efficiency of sulfur capture efficiency from acid gases. These results show conditions under which hydrocarbons and mercaptans are formed during combustion of acid

gases in the presence of toluene, and these results help to establish suitable gas treatment conditions for enhanced sulfur capture and efficiency.

4.5.2 Role of Xylene to Acid Gas (CO_2/H_2S) Combustion

The role of xylene to acid gas (H_2S and CO_2) was examined to characterize the gas phase combustion products. The decomposition of xylene is a hierarchical process that involves formation of toluene and benzene (Ji et al., 2011). This means that benzene and toluene are also present in the Claus reactor during examination of xylene combustion. It is important to investigate the combined role of xylene to acid gas due to the higher carbon number of xylene as compared to benzene and toluene. Once sufficient temperature and residence time is supplied for xylene destruction in the Claus reactor, toluene and benzene destruction is also favorable. Therefore, experiments were conducted to examine the effect of xylene and CO_2 on the combustion of H_2S in H_2/O_2-N_2 flames under (fuel-rich) Claus condition. Table 4-14 shows the flow rates of each gas introduced into the burner.

Table 4-14. The Test Matrix

	flow rate: cm^3/min					
Gas composition	H_2	O_2	N_2	H_2S	C_8H_{10}	CO_2
100% H_2S	1600	932	1690	264	0	0
99% H_2S/1% C_8H_{10}	1600	941	1713	264	2.64	0
49.5% H_2S/49.5% CO_2/ 1% C_8H_{10}	1600	875	1592	132	2.64	132

Three gas stream compositions were examined and compared to isolate the combined role of toluene and CO_2. The effect of gas stream compositions (H_2S, H_2S/C_8H_{10}, or $H_2S/C_8H_{10}/CO_2$) on product gas distribution was examined. The experimental conditions and procedures were similar to those in the previous sub-

section. Dimensionless axial distance (W= axial distance/D_{jet}) was used for all the results presented here. Inner jet diameter of the burner was used to transform the linear distances into dimensionless parameters for broader application of the results.

4.5.2.1 Product Speciation and Analysis

Gas sampling and analysis of local species were conducted along the longitudinal centerline of the reactor axis. The gas speciation and analysis for the combustion of 100%H_2S, 99% H_2S/1% C_8H_{10} and 49.5% H_2S/49.5% CO_2/1% C_8H_{10} gas stream are presented. The mole fractions of H_2, SO_2 and H_2S are shown in figures 4-93 to 4-99. The presence of CO_2 enhanced destruction of H_2S, which resulted in faster SO_2 production, with subsequent impact on the rate of elemental sulfur formation. This also enhanced CS_2 and COS formation in the reactor. The formation of COS and CS_2, shown in figures 4-100 and 4-101, was higher with CO_2 in the acid gas.

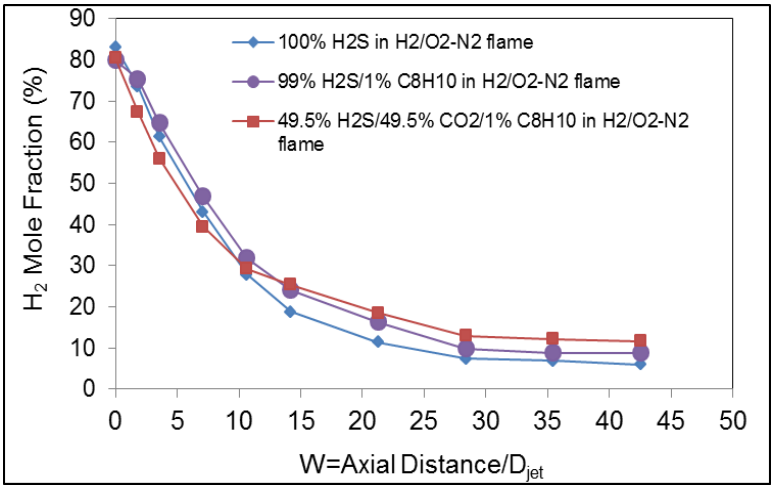

Figure 4-93. Hydrogen mole fraction from the combustion of different acid gas streams in H_2/O_2-N_2 at Φ=3.0

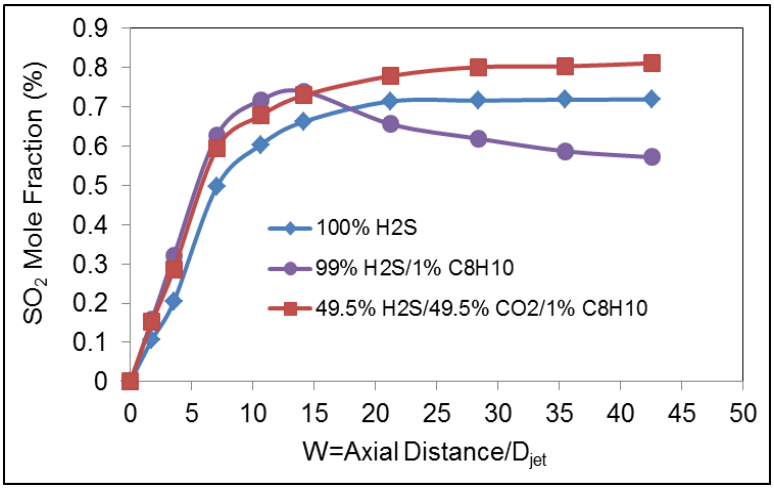

Figure 4-94. Sulfur dioxide mole fraction from the combustion of different acid gas streams in H_2/O_2-N_2 at Φ=3.0

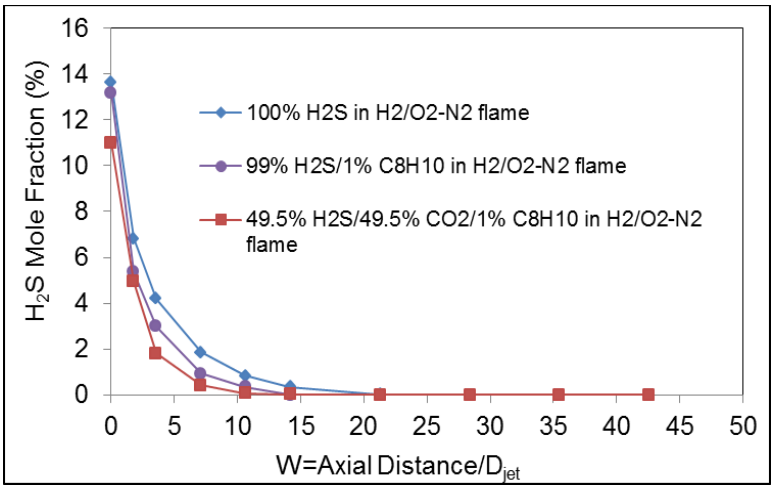

Figure 4-95. Hydrogen sulfide mole fraction from the combustion of different acid gas streams in H_2/O_2-N_2 at Φ=3.0

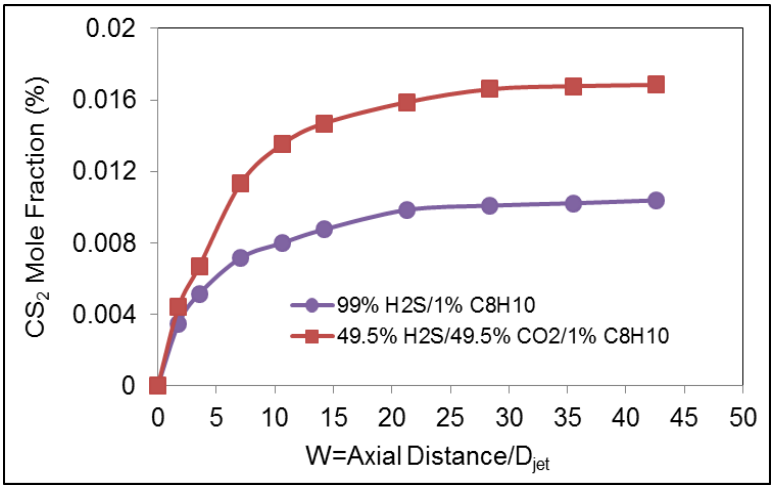

Figure 4-96. Carbon disulfide mole fraction from the combustion of different acid gas streams in H_2/O_2-N_2 at Φ=3.0

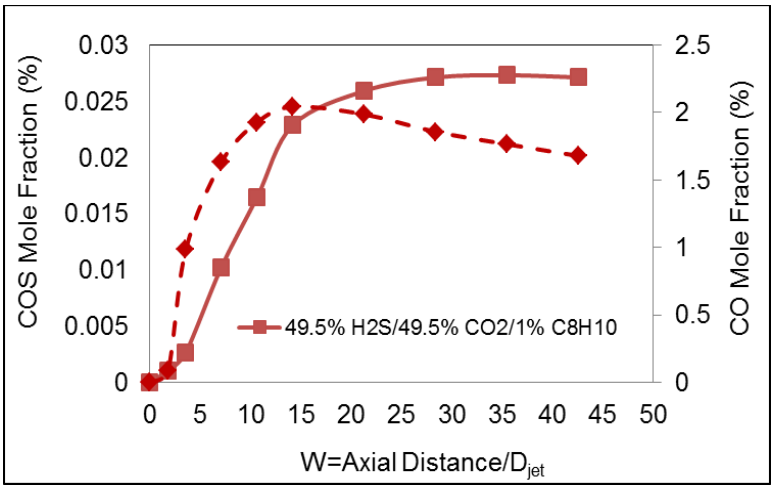

Figure 4-97. Carbonyl sulfide and carbon monoxide mole fraction from the combustion of different acid gas streams in H_2/O_2-N_2 at Φ=3.0

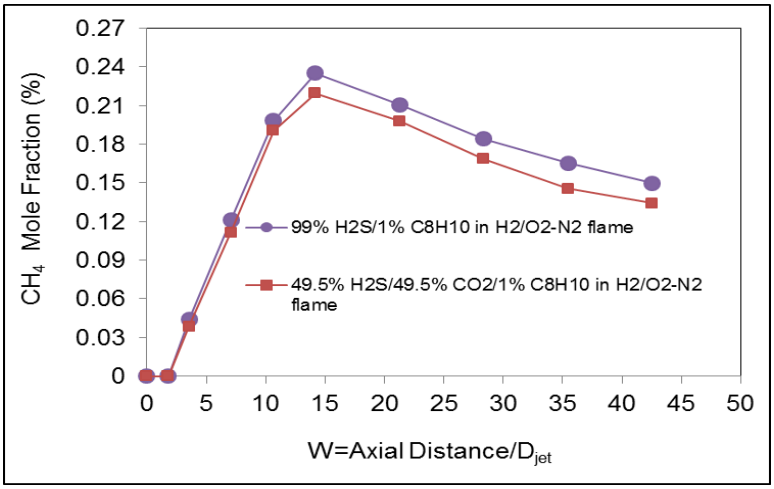

Figure 4-98. Methane mole fraction from the combustion of different acid gas streams in H_2/O_2-N_2 at Φ=3.0

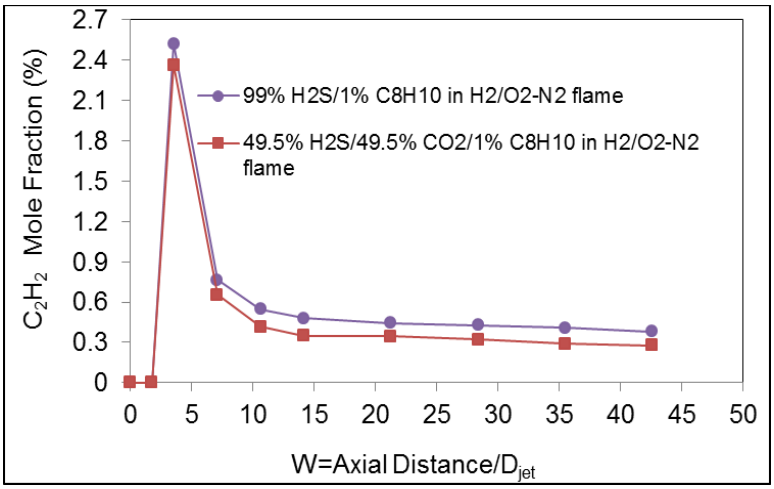

Figure 4-99. Methane mole fraction from the combustion of different acid gas streams in H_2/O_2-N_2 at Φ=3.0

The results showed quantitative different for some species (CO, CH_4, H_2, C_2H_2 and CS_2), but mostly showed similar qualitative trends when compared to toluene (figures 4-100 to 103). Mole fractions of H_2 and SO_2 at the reactor exit were higher with xylene in the inlet acid gas. The two methyl group radicals in xylene, as opposed to one methyl group in toluene played significant role in the higher mole

fractions of CS_2. This also caused increased production of carbon monoxide, methane and acetylene. There was significant increase in the amounts of acetylene and methane formation, which highlights serious operational problems to the Claus reactor with xylene in the acid gas. These differences are directly attributed to the effect of two methyl group radicals in xylene molecule, compared to one methyl group in toluene. Xylene favored higher number of radical species at the initial stage of decomposition. Although, CO_2 enhanced hydrocarbon destruction in the Claus reactor, it significantly increased COS and CS_2 production.

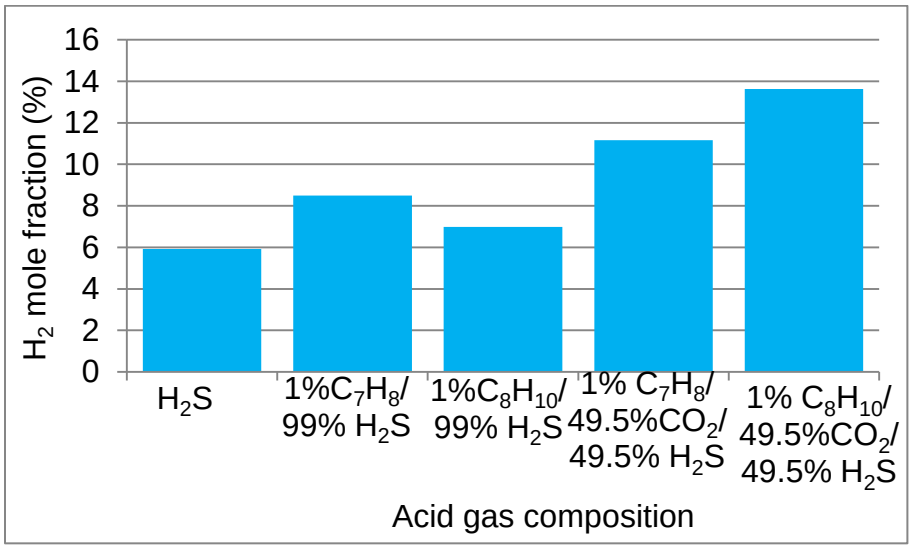

Figure 4-100. Hydrogen mole fractions at reactor exit with addition of different composition of acid gas in H_2/O_2-N_2 flames

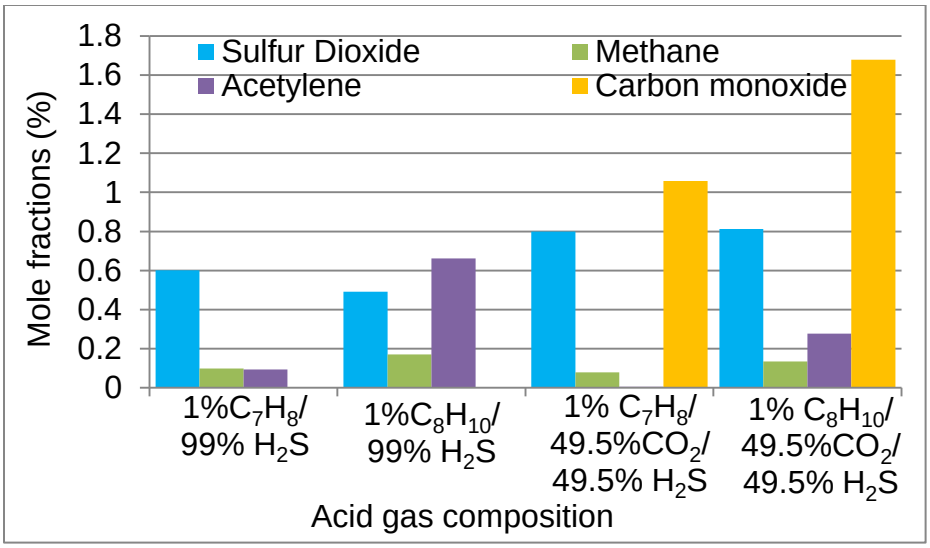

Figure 4-102. Sulfur dioxide, carbon monoxide, methane and acetylene production at reactor exit with addition of different composition of acid gas in H_2/O_2-N_2 flames

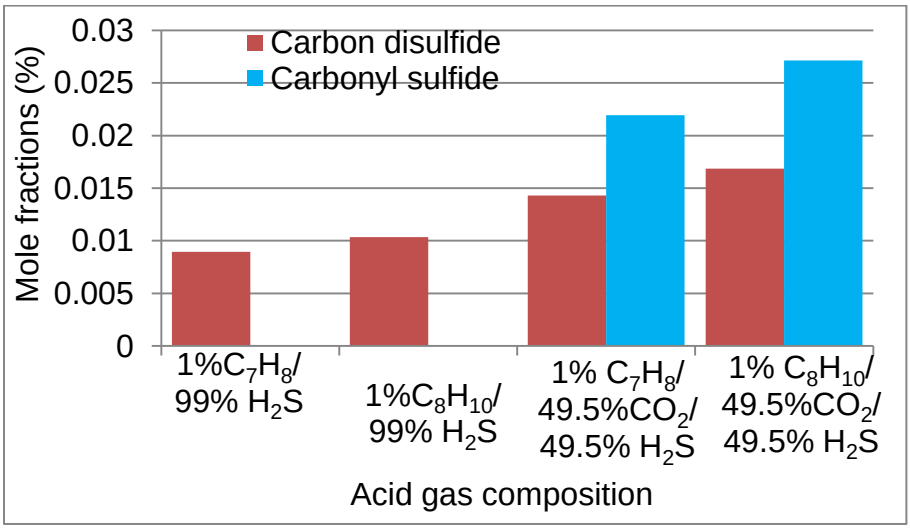

Figure 4-103. Carbon disulfide and carbonyl sulfide production at reactor exit with addition of different composition of acid gas in H_2/O_2-N_2 flames

The increased production of acetylene also suggests increased production of polycyclic aromatic hydrocarbons and soot. There was evidence of soot observed

during the experiments. However, there is need to explore the use of novel membranes for further separation of lower series of hydrocarbons at the exit of thermal stage reactor, so that these hydrocarbons can then be used as value added products from Claus reactors.

4.5.2.2 Summary

The role of xylene to acid gas (H_2S and CO_2) combustion was examined under Claus condition. The results showed significant quantitative difference compared to those observed during toluene, H_2S and CO_2 mixture combustion, but the global trends of species profile were similar. Xylene generated higher amounts of mercaptans (COS and CS_2), acetylene and methane in the thermal stage reactor, compared to the case with toluene. This was attributed to the higher reactivity of xylene and the effect of two methyl group radical xylene. These results demonstrated the potential for production of value added chemicals, such as methane from the exit of thermal stage reactor through the use of suitable separation techniques.

Chapter 5 Conclusions and Research Contributions

5.1 Conclusions

Results on the role of benzene, toluene or xylene (BTX) in H_2S in thermal stage of a simulated Claus recovery process have been presented. The focus of this investigation was to characterize the combustion of H_2S with trace amounts of benzene, toluene or xylene, so that more favorable operating conditions of Claus reactors can be established for improved efficiency, better quality of sulfur and reduced environmental burden. Flame characterization with the addition of trace amounts of benzene, toluene or xylene addition to H_2S/O_2 flames substantiated the need for high reactor temperature conditions. The role of oxygen enriched air on the destruction of BTX in acid gas has been investigated using hydrogen/air flames. Flame emission spectroscopy and GC analysis were used to help evaluate the reaction pathways on the formation of lower series of hydrocarbons during BTX and H_2S thermal destruction. The combined effect of CO_2 and BTX to H_2S combustion was investigated. The formation/destruction of sulfurous compounds (such as COS and CS_2) with different acid gas mixtures under various operational conditions were evaluated.

5.1.1 Effect of BTX on H_2S Combustion in Flames

Effect of trace amounts of toluene (0%, 0.5%, 1% and 5%), benzene (0.3%, 0.5% and 1%) or xylene (0.5%, 1% and 2%) addition to H_2S/O_2 flames was investigated at an equivalence ratio of three (i.e., under Claus condition). Addition of toluene, benzene or xylene to H_2S increased the reactor temperature and altered the

product speciation of H_2S combustion that resulted in decreased sulfur conversion efficiency of H_2S in thermal stage of the Claus reactor. The product speciation revealed significant production of H_2 that hindered H_2S conversion and decreased SO_2 production with subsequent impact on reduced formation of elemental sulfur in the thermal stage. The amounts of H_2S at the reactor exit were higher with toluene addition as compared to benzene and xylene, which was attributed to the chemistry of intermediate byproducts formed in the combustion process. Additionally, produced SO_2 had the tendency to provide oxidizer for the oxidation of intermediate species, such as CO, COS, CS_2 and CH_4 in the Claus reactor that varied with the trace amounts of aromatic components (BTX) in the feed stream.

The relative effect of benzene, toluene and xylene on sulfur recovery was dependent on the production of intermediate species in the combustion process. Toluene addition promoted higher amounts of H_2, CO and COS production when compared to benzene, and formation of CO was via phenoxy radicals at the early stage of combustion (i.e., at low residence times). Benzene showed more severe impact on SO_2 reduction to directly hinder the formation of elemental sulfur. Xylene had the least impact on SO_2 reduction. Production of SO_2 was higher with xylene as compared to toluene and benzene, to favor elemental sulfur production. The relative effect of benzene, toluene and xylene on sulfur conversion in thermal stage of Claus reactor decreases in the order: xylene < toluene < benzene. However, xylene will cause faster deactivation of Claus catalyst in catalytic stage reactors, compared to toluene and benzene due to the increased processing load, from significant production of byproducts (H_2, CH_4, CO, COS and CS_2) in the thermal stage. The significant

amounts of hydrogen produced with the presence of benzene, toluene or xylene, and also methane production with xylene offers potential to recover value added products during sulfur recovery under favorable conditions.

5.1.2 Destruction of BTX in Thermal Stage Claus Reactors

Investigation was further conducted to identify reactor conditions that ensured efficient destruction of BTX, while mitigating the formation of mercaptans (COS and CS_2). Oxygen enrichment to combustion air (reduction of nitrogen concentration in air) provided suitable increase in reactor temperature and enhanced gas residence time in the reactor. Role of oxygen enrichment to combustion air on the destruction of different acid gas mixtures in H_2/O_2-N_2 flames was investigated. Three different percentages of oxygen enrichment of air were examined (0%, 19.5% and 69.3%) for different acid gas composition that consisted of 100% H_2S, 1% C_7H_8 / 99% H_2S, 1% C_8H_{10} / 99% H_2S and 50% H_2S/50% CO_2 gas mixtures.

Combustion of 100% H_2S acid gas using oxygen enriched air resulted in increased SO_2 formation that corresponded to increase in H_2S and decrease in H_2 oxidation. These trends are attributed to increase in temperatures with increased oxygen concentration in the combustion air. Examination of toluene and H_2S mixtures showed faster rate of H_2S and slower rate of H_2 decomposition with increase in the percentage of oxygen enrichment to air. Addition of toluene enhanced SO_2 production while increasing the possibility of sulfur recovery. Oxygen enrichment to air showed enhanced destruction of hydrocarbons while minimizing the formation of carbon disulfide (CS_2). Combustion of xylene and H_2S mixture revealed quantitative differences in mole fractions of combustion products, but the trends of species

concentration profiles were similar when compared to those observed with toluene. Increase in oxygen enrichment to combustion air also favored xylene destruction to minimize CS_2 production. The amounts of hydrocarbons, SO_2, CS_2 and H_2 production at the reactor exit increased with xylene as compared to toluene. This was attributed to the fact that xylene decomposition is a hierarchical process that occurs via toluene and benzene formation.

Acid gas (H_2S and CO_2) combustion also showed increased rate of H_2S and H_2 oxidation for the different concentrations of oxygen in combustion air. Carbon dioxide decomposed at high temperature to form CO and atomic oxygen, and this favored formation of SO_2 at the expense of more desirable elemental sulfur. Formation of SO_2 also hindered CO oxidation due the preferential oxidation of SO radicals to SO_2, which then favored COS and CS_2 production. Higher percentage of oxygen enrichment to air further promoted CO production, but significantly decreased CS_2, while promoting COS formation. In addition, the formed SO and SO_2 also provided oxidation competition for CO that resulted in significant quantities of CO production at the reactor exit. These results demonstrated the effectiveness of oxygen enriched air in mitigating the role of trace impurities in H_2S and also sulfur emissions from sulfur recovery plants.

5.1.3 Reaction Pathways of BTX and H_2S Destruction

The reaction pathways for the destruction of xylene and H_2S mixtures under high temperature condition provided by hydrogen-air flame were examined using emission spectroscopy of excited species and Gas chromatograph (GC). Xylene was chosen for this investigation because it generates higher amounts of byproducts in

Claus process than benzene or toluene, and it decomposes hierarchically through formation of toluene and benzene in the reactor. The results revealed interaction of sulfur radicals with hydrocarbons to form CS_2 in the Claus reactor. The pathways leading to acetylene and methane formation were evaluated, which provided strong evidence of aromatic ring rupture in the xylene molecule that resulted in the formation of acetylene in the reactor. However, the formed acetylene and methane were not completely oxidized in the reactor, even though SO_2 showed to be a source of oxidizer. Formation of SO_2 increased to a maximum mole fraction, but the formed SO_2 subsequently decomposed to promote S_2 and CS_2 production. The spectra of excited species provided interaction between hydrocarbon and sulfur species to form CS_2. The bands observed between 280nm-490nm were attributed to C_3*, C_2* (swan bands), CHO* (Vaidya's flame bands), H* (Balmer series), CH* and other sulfurous species, CS_2*, SO, HS, S_2* and SO_2*. These results revealed a potential on the formation of hydrocarbons in thermal stage of Claus reactors.

5.1.4 Combined Effect of BTX and CO_2 to H_2S Combustion

Combustion of different acid gas composition (H_2S, CO_2, C_7H_8 and C_8H_{10}) in H_2/O_2-N_2 flame was characterized and evaluated to isolate the combined effect of CO_2 and BTX to H_2S. This represented a more practical acid gas composition. Formation of COS and CS_2 with change in acid gas composition was also evaluated. Combustion of H_2S gas resulted in the decomposition of H_2S to increase SO_2 mole fractions to an asymptotic maximum value. Combustion of toluene and H_2S mixture caused faster H_2S oxidation and SO_2 formation, but the formed SO_2 decomposed to increase the possibility of elemental sulfur formation. In contrast, combustion of

toluene and acid gas (H_2S and CO_2) mixture showed increased formation of SO_2 throughout the reactor, as CO_2 enhanced the oxidizing medium. Toluene alone, directly contributed to the formation of CH_4, C_2H_2 and CS_2 in the reactor, while both toluene and CO_2 caused increased formation of mercaptans (CS_2 and COS), but enhanced destruction of formed hydrocarbons (CH_4 and C_2H_2). There was significant amount of CO production, which was attributed to the oxidation competition between CO and SO radicals and SO_2.

Combustion of xylene, H_2S and CO_2 mixtures, showed similar qualitative trends in species concentration profiles, but significant quantitative differences were observed when compared to those with toluene. Xylene showed a more significant impact on the increased production of methane, acetylene, COS and CS_2 in the reactor. This was attributed to the faster reactivity of xylene and increased radical production during the initial stage of decomposition, due to the two methyl group radicals present in xylene. Increased production of acetylene and methane with xylene can cause severe problems in the downstream catalytic stages of Claus process. Therefore, it beneficial to separate out these hydrocarbons at the exit of thermal stage reactor since they can be utilized as value added products.

5.2 Research Contributions

The research work presented in this dissertation resulted in both academic and practical contributions, mostly in the areas of combustion chemistry of H_2S, CO_2, benzene, toluene and xylene, as well as enhanced sulfur recovery and other chemicals in thermal energy processes.

- Comprehensive characterization of BTX in acid gas (H_2S and CO_2) flames
- Quantified the relative effect of BTX on toxic gases emissions and sulfur recovery from acid gases
- Demonstrated the effectiveness of oxygen enriched air in mitigating trace impurities (BTX) in H_2S and also sulfur emissions from sulfur recovery plants
- Defined reactor conditions for enhanced destruction of different acid gas composition (H_2S, CO_2, N_2 and BTX) in thermal stage of Claus reactors
- Determined the chemical kinetic pathways of BTX destruction under high temperature conditions of thermal stage reactor in Claus process
- Identified reactor conditions that promote/mitigate unwanted byproducts (such as CO, COS and CS_2) in the presence of trace amounts of BTX, during combustion of H_2S in the presence of CO_2
- Defined the region of optimum operating conditions with respect to acid gas composition
- Revealed formation of methane and acetylene with BTX in thermal stage of Claus reactors
- Demonstrated increased potential of hydrogen formation with BTX in thermal stage of sulfur recovery process

Chapter 6 Recommendations for Future Work

The role of BTX to sulfur recovery in thermal stage of Claus reactors was investigated in this research. Reactor conditions and detailed reaction pathways of BTX and H_2S destruction was examined. In addition, formation of sulfurous compounds (COS and CS_2) with different composition of acid gas was evaluated under high temperature condition of Claus reactors. This provided significant insight into reactor conditions that promote BTX destruction and mitigate/promote COS and CS_2 production with respect to different composition of acid gas.

However, there is a need to further explore a unified reactor condition that provides a reasonable trade-off between BTX destruction and formation of COS, CS_2 and sulfur (with improved sulphur quality). Note that good quality sulfur is important as poor quality sulfur offers no value. This requires a systematic approach that couples the detailed chemistry of H_2S, BTX, CO_2, CS_2 and COS along with a fluid dynamic model to provide an effective optimization tool for the Claus process. The investigations on the destruction of BTX contaminants have demonstrated significant formation of intermediate product species (secondary contaminants) that include methane, acetylene, COS and CS_2. In addition to less harmful hydrogen, other trace species could also be present. Some of the process conditions that help to promote or mitigate the impact of these impurities have been identified. However, the mitigation of one contaminant could favor formation of other contaminants in significant quantities that is now known to hinder the efficiency of the Claus process. For instance, processing of H_2S, CO_2 and BTX in a Claus furnace at higher temperatures

(above 1550K), ensures efficient destruction of BTX and reduces CS_2 formation. However, higher temperatures promotes COS formation significantly, while lower temperatures can reduce both COS and CS_2 formation, but promotes formation of lower series of hydrocarbon and H_2.

There are separate kinetic mechanisms available for BTX and H_2S oxidation and pyrolysis. These kinetic models were developed for neat fuels under different conditions and applications. A reaction mechanism for the combustion of toluene and H_2S were combined and the resulting kinetic model was used in Chemkin Pro to simulate the experimental data. More details on the combined mechanism are given in section 4.2-1. The mechanism over-predicted the experimental data (see figures 6-1 to 6-3), which shows the need for more detailed evaluation and optimization.

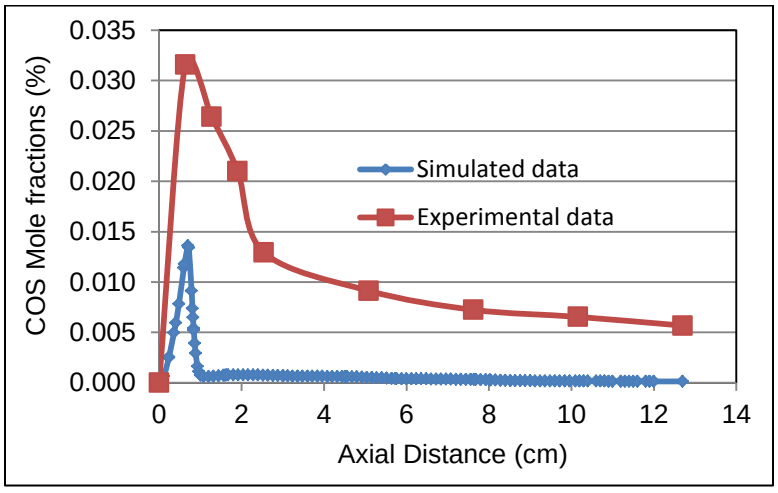

Figure 6-1. Comparison of experimental and simulated mole fraction of carbonyl sulfide. Flame condition: 99% H_2S/1% C_6H_6/O_2 at Φ=3

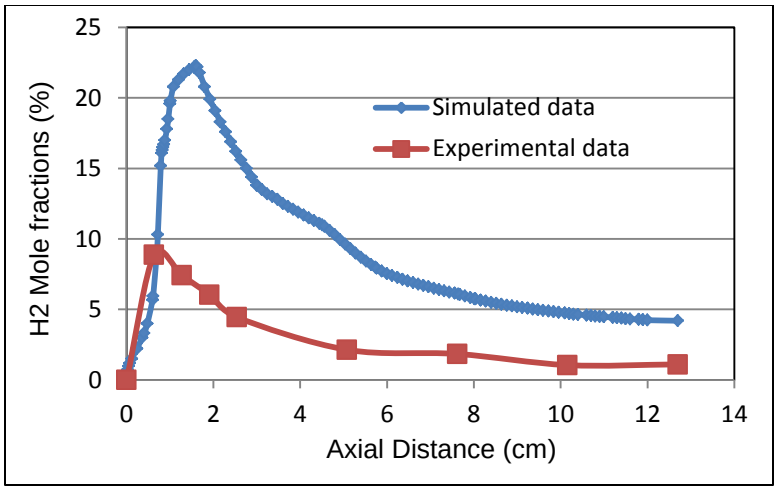

Figure 6-2. Comparison of experimental and simulated mole fraction of hydrogen. Flame condition: 99% H_2S/1% C_6H_6/O_2 at Φ=3

Therefore, development of highly efficient optimization tool that couples fluid dynamics with detailed kinetic model will be highly beneficial for further understanding of the chemistry involved as well as its direct benefit to industry. Moreover, this will help in exploring a near isothermal condition of the Claus reactor. The operation of Claus reactor under near isothermal condition enhances the efficiency of Claus process and minimizes emission of sulphurous compounds. This will ensure more efficient treatment of acid gas and associated impurities, which will then reduce the processing load in the catalytic stages and number of catalytic reactors, as well as significant reduction in operational cost.

BTX showed significant impact on SO_2 reduction in the thermal sage reactor. And given the significance of SO_2 chemistry in Claus process, it is important to investigate the kinetics of BTX oxidation by SO_2 under Claus reactor condition. This will result in better understanding of the BTX and SO_2 chemistry to help in the development of robust optimization tools for the Claus process plants.

The potential for hydrocarbon and hydrogen formation with BTX in the thermal stage reactors was observed in the results presented in this dissertation. The lower series of hydrocarbons formed in the reactor can be harnessed to provide value added products from the Claus plant. This can be achieved by separating out the hydrocarbons, especially methane at the exit of the thermal stage using novel gas separation techniques. This can then provide value added products that can be used to boost energy generation. Separation of these hydrocarbons or methane can be achieved using suitable polymeric membranes or novel graphene technology that offers significant benefits over other methods as it can be used for a range of gases. This approach will help reduce the number catalytic reactors with significantly improved efficiency of the Claus process plant and environmental burden, in addition to the direct benefits of providing value added products and clean syngas.

Alternative utilization and more efficient treatment of acid gas are also required to preserve our environment from sulfur-bearing fuels while simultaneously enhancing energy generation. This study has shown that both syngas and sulfur can be produced from acid gas under certain reactor operational conditions. This is an attractive alternative since the large volume of CO_2 in acid gas can be captured from the produced syngas. Moreover, sulfur recovery from lean acid gas that contains higher CO_2 content than H_2S as well as hydrocarbon impurities in a Claus process pose severe technical and environmental issues. Therefore, acid gas pyrolysis will also be well suited for the treatment of lean acid gas. The H_2 and CO produced (syngas) can then be used in industry for energy and power applications. This can be achieved with minimal adverse effect to the environment, human health and building

aesthetics. Syngas can be used as a fuel for gas engines, or to produce valuable chemicals, such as ammonia and liquid fuels. Note that Siemens energy gas plants require syngas ratio of H_2 to CO between 0.33 and 1.2 for successful operation and similar ratio is required in ammonia production plants.

Appendix A: List of Publications

Journal papers published

- Ibrahim S., AlShoaibi A. and Gupta A.K., (2013). Role of Toluene in Hydrogen Sulfide Combustion under Claus Condition. Applied Energy, 112, 60-66.
- Selim H., Ibrahim S., AlShoaibi A. and Gupta A.K., (2013). Effect of Oxygen Enrichment on Acid Gas Combustion in Hydrogen/Air Flames under Claus Condition. Applied Energy, 109, 119-124.
- Ibrahim S., AlShoaibi A. and Gupta A.K., (2014). Toluene Destruction in Thermal Stage of Claus Reactor with Oxygen Enriched Air. Applied Energy, 115, 1-8.
- Selim H., Ibrahim S., AlShoaibi A. and Gupta A.K., (2014). Investigation of Sulfur Chemistry with Acid Gas Addition in Hydrogen/Air Flames. Applied Energy, 113, 1134-1140.
- Ibrahim S., AlShoaibi A. and Gupta A.K., (2015). Effect of Benzene on Product Evolution in a H2S/O2 Flame under Claus Condition. Applied Energy, (APEN-D-14-03965R1). Applied Energy, 145, 21-26.
- Ibrahim S., AlShoaibi A. and Gupta A.K., (2015). Xylene Addition Effects to H_2S Combustion under Claus Condition. Fuel, 150, 1-7.
- Ibrahim S., Al Shoaibi A. and Gupta A.K., (2015). Role of Toluene to Acid Gas (H_2S and CO_2) Combustion in H2/O2-N2 Flame under Claus Condition. Applied Energy, 147, 62-68.

Journal papers submitted

- Ibrahim S., AlShoaibi A. and Gupta A.K., (2014). Xylene and H2S Destruction in High Temperature Flames under Claus Condition. Applied Energy. August, 2014.

Conference papers presented

- Selim H., Ibrahim S., AlShoaibi A.S., & Gupta A. K. (2013, July). Effect of Acid Gas (H2S and CO2) Addition in Hydrogen/Air Flames. ASME 2013 Power Conference. American Society of Mechanical Engineers.
- Ibrahim S., AlShoaibi A.S., & Gupta A.K. (2013, July). Effect of Toluene Addition on Hydrogen Sulfide Combustion under Claus Condition. ASME 2013 Power Conference. American Society of Mechanical Engineers.
- Ibrahim S., Selim H., Al Shoaibi A.S., & Gupta, A. K. (2013, July). Effect of Oxygen Enrichment in air on Acid Gas Combustion under Claus Conditions. 11th International Energy Conversion Engineering Conference (AIAA 2013-3738).
- Ibrahim, S., AlShoaibi, A., & Gupta, A. K., (2014, January). Hydrocarbon Formation with Toluene in Thermal Stage of Claus Process. AIAA SciTech (AIAA 2014-1068), 52nd Aerospace Sciences Meeting.
- Ibrahim S., Chardonneau M., AlShoaibi A.S. and Gupta A.K. (2014, July). Role of Toluene and Carbon Dioxide on Sulfur Recovery Efficiency in Claus Process. ASME 2014 Power Conference. American Society of Mechanical Engineers.

- Ibrahim S., AlShoaibi A.S., & Gupta A.K. (2014, July). Xylene Addition Effects in Thermal Stage of Claus Reactors. ASME 2014 Power Conference. American Society of Mechanical Engineers.
- Ibrahim S., AlShoaibi A.S., & Gupta A. K., (2015, January). Role of Benzene on Thermal Stage Performance in a Claus Process. AIAA SciTech (AIAA 2015-2018709). 53nd Aerospace Sciences Meeting.
- Groisil M., Ibrahim S., AlShoaibi A.S. and Gupta A.K. (2015, March). Numerical Examination of Acid Gas for Syngas and Sulfur Recovery. The 7th International Conference on Applied Energy - ICAE2015, paper No. 25.
- Ibrahim S., Chardonneau M., AlShoaibi A.S. and Gupta A.K. (2015, March). Role of Toluene and Carbon Dioxide on Sulfur Recovery Efficiency in Claus Process. The 7th International Conference on Applied Energy - ICAE2015, paper No. 24.

Conference Papers to be presented

- Groisil M., Ibrahim S., AlShoaibi A.S. and Gupta A.K. (2015, July). Acid Gas Simulation for Recovering Syngas and Sulfur. Proceedings of the ASME 2015 Power & Energy Conference (POWERENERGY2015-49014). American Society of Mechanical Engineers. Accepted.
- Ibrahim S., Al Shoaibi A., & Gupta A. K., (2015, May). Effect of BTX on H_2S Chemistry in Thermal Stage of Claus Process. Abu Dhabi International Research and Development Conference & Exhibition (ADRAC).

References

Adesina A.A., Meeyoo V. and Foulds G., (1995). Thermolysis of Hydrogen Sulphide in an Open Tubular Reactor. Int. J. Hydrogen Energy, 20:777-783.

Al-Shahrani F., Xiao T.C., Llewellyn S.A., Barri S., Jiang Z., Shi H.H., Martinie G. and Green M.L.H., (2007). Desulfurization of Diesel via H_2O_2 Oxidation of Aromatic Sulfides to Sulfones Using a Tungstate Catalyst. Appl. Catal. B-Environ., 73:311-316.

Alzueta M.U., Glarborg P., Dam-Johansen K., (2000). Experimental and Kinetic Modelling Study of the Oxidation of Benzene. International Journal of Chemical Kinetics, 32:498-522.

Alzueta M. U., Bilbao R. and Glarborg, P., (2001). Inhibition and Sensitization of Fuel Oxidation by SO_2. Combustion and Flame, 127(4):2234-2251.

Andrae J, Johansson D, Björnbom P, Risberg P. and Kalghatgi G., (2005). Co-Oxidation in the Auto-Ignition of Primary Reference Fuels and N-Heptane/Toluene Blends. Combustion and Flame, 140:267–86.

Andrae J.C.G., Brinck T. and Kalghatgi G.T., (2008). HCCI Experiments with Toluene Reference Fuels Modeled By a Semi-Detailed Chemical Kinetic Model. Combustion and Flame, 155:696–712.

Andrae J.C.G., (2011). A Kinetic Modeling Study of Self-Ignition of Low Alkylbenzenes at Engine-Relevant Conditions. Fuel Proc. Technol., 92:2030–2040.

Andrae J.C.G., (2013). Comprehensive Chemical Kinetic Modeling of Toluene Reference Fuels Oxidation. Fuel, 107:740–748.

Armstrong S. M., Sankey B. M. and Voordouw G., (1995). Conversion of Dibenzothiophene to Biphenyl by Sulfate Reducing Bacteria Isolated from Oil Field Production Facilities. Biotechnol. Lett., 17:1133–1136.

Arutyunov V. S., Baserich V. Ya., Vedeneev V. I., Ushakov V. A., Chernysheva A. V., (1991). Kinetics of Sulfur Dioxide Reduction II. Reduction by Carbon Monoxide. Kinetika I Kataliz, 31:919.

Arutyunov V. S., Basevich V. Y. and Sokolov O. V., (1992). Kinetics of Formation of Products of the Reaction of Sulfur Dioxide with Methane. Kinetika I Kataliz, 32(6):1295-1301.

Arutyunov V., S., Vedeneev V, I, Nikisha L, V., Polyak S. S., Romanovich L. E., Sokolov O. V., (1993a). Kinetic Studies of Methane and Hydrogen Sulfide Cooxidation, in Kinetics and Catalysis, 194-197.

Arutyunov V.S., Basevich V.Y. and Sokolov O.V., (1993b). Kinetics of Formation of Products of the Reaction of Sulfur Dioxide with Acetylene. Kinetika I Kataliz, 34(4):515-517.

Aynsley E. E.; Pearson T. G.; Robinson P. L., (1935). The Kinetics of the Reaction between Hydrogen and Sulphur. Part I. J. Chem. Soc., 58-68.

Azatyan V. V., Gershenson U.M., Sarkissyan E.N., Sachyan G. A. and Nalbandyan A.B., (1969). Investigation of Low-Pressure Flames of a Number of Compounds Containing Sulfur by the ESR Method. Symposium (International) on Combustion, 12(1):989-994.

Babich V.I. and Moulijn J.A., (2003). Science and Technology of Novel Processes for Deep Desulfurization of Oil Refinery Streams: A review. Fuel, 82.

Barnard J.A., Sankey B.M., (1968a). The Slow Combustion of the Isomeric Xylenes: Meta- and Para-Xylene, Combustion and Flame 12:345-352.

Barnard J.A. and Sankey B.M., (1968b). The Slow Combustion of the Isomeric Xylenes: II: Ortho-Xylene. Combustion and Flame, 12:353-359.

Battin-Leclerc F., Bounaceur R., Fournet R. and Glaude P. A. (2004). Deliverable 28 Report on Ongoing Progress of Aromatic Hydrocarbons Detailed Kinetic Model Development: Bibliographic Review and Modelling of the Auto-ignition and Oxidation of Toluene. Project SAFEKINEX, Project No. EVG1-CT-2002-00072

Battin-Leclerc F., Bounaceur R. and Glaude P. A. (2005). Deliverable 36 Validated Detailed Kinetic Models for Aromatic Hydrocarbons. Project SAFEKINEX, Project No. EVG1-CT-2002-00072

Battin-Leclerc F., Bounaceur R., Belmekki N. and Glaude P.A., (2006). Experimental and Modeling Study of the Oxidation of Xylenes. International Journal of Chemical Kinetics, 38:284-302.

Bernez-Cambot J., Vovelle C. and Delbourgo R., (1981). Flame Structures of H_2S–Air Diffusion Flames. Symposium (International) on Combustion, 18(1):777-783.

Bezverkhyy I., Ryzhikov A., Gadacz G. and Bellat J.P., (2008). Kinetics of Thiophene Reactive Adsorption on Ni/SiO2 and Ni/ZnO Catal. Today, 130:199–205

Binoist M., Labegorre B., Monnet F., Clark, P.D., Dowling, N.I., Huang M., Archambault D., Plasari E. and Marquaire P.M., (2003). Kinetic Study of the Pyrolysis of H2S. Industrial & Engineering Chemistry Research, 42:3943-3951.

Bishara A., Salman O. A., Khraishi N. and Marafi A., (1987). Thermochemical Decomposition of Hydrogen Sulfide by Solar Energy," International Journal of Hydrogen Energy, 12(10):679-685.

Bittker D. A., (1991). Detailed Mechanism for Oxidation of Benzene. Combustion Science and Technology, 79(1-3), 49-72.

Bittner J.D. and Howard J.B., (1981). Composition Profiles and Reaction Mechanisms in a near-sooting Premixed Benzene/oxygen/argon Flame. Symposium (International) on Combustion. The Combustion Institute, 18(1):1105-1116.

Blitz M.A., McKee K.W. and Pilling M.J., (2000). Temperature Dependence of the Reaction of OH with SO. Proceedings of the Combustion Institute, 28(2):2491-2497.

Bonde S.E., Gore W., Dolbear G.E. and Skov E.R., (2000). Selective Oxidation and Extraction of Sulfur-Containing Compounds to Economically Achieve Ultra-Low Diesel Fuel Sulfur Requirements. Am. Chem. Soc., Div. Petrol. Chem. Prepr., 45:364.

Borgne S. L. and Quintero R., (2003). S. Review: Biotechnological Processes for the Refining of Petroleum. Fuel Process Technol., 81:155–169.

Bounaceur R., Da Costa I., Fournet R., Billaud F. and Battin-Leclerc F., (2005). Experimental and Modeling Study of the Oxidation of Toluene. Int. J. Chem. Kin., 37:25-49.

BP., (2012). Natural Gas Reserves. Retrieved from British Petroleum. http://www.bp.com/sectiongenericarticle800.do?categoryId=9037178&contentId=7068624

Braun-Unkhoff M., Frank P. and Just T., (1988). A Shock Tube Study on the Thermal Decomposition of Toluene and Of the Phenyl Radical at High Temperatures. Proceedings of the Combustion Institute, 22:1053–1061

Brezinsky K., (1986). The High-Temperature Oxidation of Aromatic Hydrocarbons. Progress in Energy and Combustion Science, 12(1), 1-24.

Brezinsky K., Emdee J.L. and Glassman I., (1996). A Kinetic Model for the Oxidation of Toluene near 1200 K. J. Phys. Chem. A, 2151.

Burcat A., Farmer R. C., Espinoza R. L. and Matula R. A., (1979). Comparative Ignition Delay Times for Selected Ring-Structured Hydrocarbon. Combustion and Flame, 36:313.

Burcat A., Snyder C. and Brabbs T., (1986). Ignition Delay Times of Benzene and Toluene With Oxygen in Argon Mixtures, NASA TM-87312.

Cerru F.G., Kronenburg A. and Lindstedt R.P., (2005). A Comparison of Detailed and Reduced Chemical Mechanism for Sulphur Oxidation. Proceeding of the European Combustion Meeting, 30:1227.

Cerru F.G., Kronenburg A. and Lindstedt R.P., (2006). Systematically Reduced Chemical Mechanism for Sulfur Oxidation and Pyrolysis. Combustion and Flame, 146(3):437-455.

Chai Y. and Pfefferle L.D., (1998). An Experimental Study of Benzene Oxidation at Fuel-Lean and Stoichiometric Equivalence Ratio Conditions. Fuel, 77:313-320.

Chen M.S.K., Hegarty W. P. and Sampat D.J., (1986) Production of Sulfur from an Oxygen-Enriched Claus System, U.S. Patent 4,632,818.

Chernysheva A.V., Basevich V.Ya., Vedeneev V.I. and Arutyunov V.S., (1990). Mechanism of Gas-Phase Oxidation of Hydrogen Sulfide at High Temperatures. Translated from Izvestiya Akademii Nauk SSSR, 9:1956.

Chevron Phillips Chemical Company L.P., (2011). Product Stewardship Summary Benzene, Toluene, Xylene Mixture (BTX)/Hydrotreated Pygas (HPG). http://www.cpchem.com/en-us/ehs/Documents/BTX%20HPG.pdf.

Chin H.S.F., (2000). The Fate of Methane in the Reaction Furnace of a Modified Claus Plant, in Chemical and Petroleum Engineering, University of Calgary, Calgary, MSc Thesis University of Calgary, Calgary.

Chin H.S.F., Karan K., Mehrotra. A. K. and Behie L.A., (2001). The Fate of Methane in a Claus Plant Reaction Furnace, Canadian Journal of Chemical Engineering, 482-490.

Chivers T., Hyne J. B. and Lau C., (1980). The Thermal Decomposition of Hydrogen Sulfide over Transition Metal Sulfides. Int. J. Hydrogen Energy, 5:499-506.

Clark P.D., Dowling N.I., Hyne J.B. and Moon D.L., (1995). Production of Hydrogen and Sulphur from Hydrogen Sulphide in Refineries and Processing Plants. Proceedings of Sulphur, 95 International Conferences, Abu Dhabi, British Sulphur Publishing: London, October 15-18; 33-48.

Clark P.D., Dowling N.I. and Huang M., (1997). Mechanisms of CS_2 Formation in the Claus Front End Reaction Furnace. Proceedings of the 47th Annual Laurance Reid Gas Conditioning Conference; College of Continuing Education, The University of Oklahoma, Norman, OK, March 2-5, 321.

Clark P.D., Dowling N.I. and Huang M., (1998). Understanding Claus Furnace Chemistry: Development of a "Modified" Claus for Low H_2S-Content Acid Gases. Proceedings of the 48th Annual Laurance Reid Gas Conditioning Conference; College of Continuing Education, The University of Oklahoma, Norman, OK, March 1-4, 241-263.

Clark P.D., Dowling N.I., Huang M., Svrcek W.Y. and Monnery W.D., (2000). Mechanisms of CO and COS Formation in the Claus Furnace, in Industrial & Engineering Chemistry Research, American Chemical Society, 497-508.

Colket M. and Seery D., (1994). Reaction Mechanisms for Toluene Pyrolysis. Proceedings of the Combustion Institute, 25:883–891

Costa I.D., Fournet R., Billaud F. and Battin-Leclerc F., (2003). Experimental and Modeling Study of the Oxidation of Benzene. International Journal of Chemical Kinetics, 35(10):503-524.

Crutzen P.J., (1976). The Possible Importance of COS for the Sulfate Layer of the Stratosphere. Geophysical research letters, 3(2):73-76.

Crevier P. P., Clark P. D., Dowling N. I. and Huang M., (2001). Quantifying the Effect of Individual Aromatic Contaminants on Claus Catalysts. Saudi Aramco Journal of Technology, 47-54.

Da Silva G., Bozzelli J.W., (2010). On the Reactivity of Methylbenzenes. Combustion and Flame, 157:2175-2183.

Dagaut P., Lecomte F., Mieritz J. and Glarborg P., (2000). Experimental and Kinetic Modeling Study of the Effect of NO and SO_2 on the Oxidation of CO–H_2 Mixtures. International Journal of Chemical Kinetics, 35(11):564-575.

Dagaut P., Pengloan G. and Ristori A., (2002). Oxidation, Ignition and Combustion of Toluene: Experimental and Detailed Chemical Kinetic Modelling. Phys. Chem. Phys., 4:1846-1854.

Dagnall R.M., Smith D.J., Thompson K.C. and West T.S., (1969). Emission Spectra Obtained from the Combustion of Organic Compounds in Hydrogen Flames. Analyst, 94:871-878.

Dames E. and Wang H., (2013). Isomerization Kinetics of Benzylic and Methylphenyl Type Radicals in Single-Ring Aromatics. Proceedings of the Combustion Institute, 34(1), 307-314.

Davidson D.F., Gauthier B.M. and Hanson R.K., (2005). Shock Tube Ignition Measurements of Iso-Octane/Air and Toluene/Air at High Pressures, Proceedings of the Combustion Institute, 20:1175-1182.

Davis S.G., Wang H., Breinsky K. and Law C.K., (1996). Laminar Flame Speeds and Oxidation Kinetics of Benzene-Air and Toluene-Air Flames. Proceedings of Combustion Institute, 26:1025-1033.

Davis S.G. and Law C.K., (1998). Determination of and Fuel Structure Effects on Laminar Flame Speeds of C1 to C8 Hydrocarbons. Combust. Sci. Technol., 140:427-449.

De Souza W.F., Guimaraes I.R., Guerreiro M.C. and Oliveira L.C.A., (2009). Catalytic Oxidation of Sulfur and Nitrogen Compounds from Diesel Fuel. Appl. Catal. A-Gen., 360:205-209

Deixonne M. and Sharma A., (2010). Reduction of Benzene, Toluene and Xylene Emissions by Co-firing Fuel Gas and Acid Gas in the US11 (Claus Unit) Sulfur Production Unit Reaction Furnace at Total Lacq. Sulphur. Prague November.

Detilleux V. and Vandooren J., (2009a). Experimental and Kinetic Modeling Evidences of a C_7H_6 Pathway in a Rich Toluene Flame. J. Phys. Chem. A., 113:10913–10922.

Detilleux V. and Vandooren J., (2009b). Experimental Study and Kinetic Modeling of Benzene Oxidation in One-dimensional Laminar Premixed Low-Pressure Flames. Combustion, Explosion and Shock Waves, 45(4):392-403.

Detilleux V. and Vandooren J., (2011). Experimental and Kinetic Modeling Investigation of Toluene Combustion in Premixed, One-Dimensional and Laminar Toluene-Oxygen-Argon Flames. Proceedings of Combustion Institute, 33:217-224.

Dowling N.I., Hyne J. B. and Brown D.M., (1990). Kinetics of the Reaction between Hydrogen and Sulfur under High-Temperature Claus Furnace Conditions. Ind. Eng. Chem. Res., 29: 2327-2332.

Dupont L., El Bakali A., Pauwels J.F., Da Costa I., Meunier P. and Richter, H. (2003). Investigation of Stoichiometric Methane/Air/Benzene (1.5%) and Methane/air Low Pressure Flames. Combustion and Flame, 135(1):171-183.

El Bakali A., Dupont L., Lefort B., Lamoureux N., Pauwels J.F. and Montero M., (2007). Experimental Study and Detailed Modeling of Toluene Degradation in a Low-Pressure Stoichiometric Premixed $CH_4/O_2/N_2$ Flame. J.of Phys. Chem. A, 111(19):3907-3921.

El-Bishtawi R. and Haimour N.M., (2004). Claus Recycle with Double Combustion Process. Fuel Processing Technology, 86(3):245-60.

Emdee J.L., Brezinsky K. and Glassman I., (1990). Oxidation of o-Xylene, Proceedings of the Combustion Institute, 23:77-84.

Emdee J.L., (1991a). An Experimental and Modeling Study of the High temperature Oxidation of the Xylenes. PhD Thesis, Department of Mechanical and Aerospace Engineering, Princeton University.

Emdee J.L., Brezinsky K. and Glassman I., (1991b). High Temperature Oxidation Mechanisms of m- and p-Xylene. J. of Phys. Chem., 95:1626-1635.

Emdee J.L., Brezinsky and Glassman I., (1992). A Kinetic Model for the Oxidation of Toluene near 1200 K. J. Phys. Chem., 96:2151-2161.

Eng R. A., Fittschen C., Gebert A., Hibomvschi P., Hippler H. and Unterreiner A.N., (1998). Kinetic Investigations of the Reactions of Toluene and of p-Xylene with Molecular Oxygen between 1050 and 1440 K. Proceedings of the Combustion Institute, 27:211-218.

Eng R., Gebert A., Goos E., Hippler H. and Kachiani C., (2002). Incubation times, Fall-off and Branching Ratios in the Thermal Decomposition of Toluene. Experiments and Theory, Phys. Chem. Phys., 4:3989–3996.

EPA, (2001). Control of Air Pollution from New Motor Vehicles Amendment to the Tier-2/Gasoline Sulfur Regulations, US Environmental Protection Agency, April 13.

EPA, (2014). Tier 3 Vehicle Emission and Fuel Standards Program. http://www.epa.gov/otaq/tier3.htm

Farrell J.T., Johnston R.J. and Androulakis I.P., (2004). Molecular Structure Effects on Laminar Burning Velocities at Elevated Temperature and Pressure. SAE Paper 2004-01-2936.

Fowler A. and Vaidya W. M., (1931). The Spectrum of the Flame of Carbon Disulfide. Proceedings of the Royal Society of London, Series B, Biological Sciences, 132(819):310-330.

Frenklach M., Lee J.H., White, J. N. and Gardnier J.R., W. C., (1981). Oxidation of Hydrogen Sulfide, Combustion and Flame, 41:1-16.

Fukuda K., Dokiya M., Kameyama T. and Kotera Y., (1978). Catalytic Decomposition of Hydrogen Sulfide, Industrial and Engineering Chemistry Fundamentals, 17(4):243-248.

Fuwa K., and Vallee B. L., (1963). The Physical Basis of Analytical Atomic Absorption Spectrometry. Analytical Chemistry, 35(8):942-946.

Fuwa K., and Vallee B. L., (1969). Molecular Flame Absorption Spectrometry for Sulfur. Analytical Chemistry, 41(1):188-190.

Gaïl S. and Dagaut P., (2005). Experimental Kinetic Study of the Oxidation of p-Xylene in a JSR and Comprehensive Detailed Chemical Kinetic Modeling. Combustion and Flame, 141: 281-297.

Gaïl S. and P. Dagaut, (2007). Oxidation of M-Xylene in a JSR: Experimental Study and Detailed Chemical Kinetic Modeling. Combust. Sci. Technol., 179:813-844

Gaïl S., Dagaut P., Black G. and Simmie J.M., (2008). Kinetics of 1, 2-dimethylbenzene Oxidation and Ignition: Experimental and Detailed Chemical Kinetic Modeling. Combustion Science and Technology, 180:1748-1771.

Gargurevich I.A., (2005). Hydrogen sulfide combustion: Relevant issues under Claus furnace conditions. Industrial & Engineering Chemistry Research, 44: 7706-7729.

Gaydon A.G., (1934). Spectrum of the Afterglow of Sulphur Dioxide, Proceedings of the Royal Society of London. Series B, Biological Sciences, 146:859:901-910.

Gaydon A.G. and Whittingham G., (1947). The Spectra of Flames Containing Oxides of Sulphur. Proceedings of the Royal Society of London. Series B, Biological Sciences, 189: 1018:313-325.

Gaydon A.G., (1974). The Spectroscopy of Flames. Chapman and Hall Ltd., London, 2nd Edition.

Glarborg P., Kubel D. and Dam-Johansen K., (1996). Impact of SO_2 and NO on CO Oxidation under Post-Flame Conditions," International Journal of Chemical Kinetics, 28(10):773-790.

Goloniva E.S. and Fyodorov G.G., (1956). Speeds of Freely-Propagating Benzene-Oxygen-Nitrogen Flames. Proceedings of Combustion Institute, 6:88-96.

Gregory D., Jackson R.A. and Bennett P.J., (1999). Mechanisms for the Formation of Exhaust Hydrocarbons in a Single-Cylinder Spark Ignition Engine, Fueled with Deuterium-labeled Ortho-, Meta-, and Para-Xylene. Combustion and Flame, 118:459-468

Grieco W.J., Lafleur, A.L., Swallow K.C., Richter H., Taghizadeh K. and Howard J.B., (1998). Fullerenes and PAH in Low-Pressure Premixed Benzene/Oxygen Flames. Symposium (International) on Combustion. The Combustion institute, 27(2):1669-1675.

Gupta N., Roychoudhury P.K. and Deb J.K., (2005).Biotechnology of desulfurization of diesel: prospects and challenges. Appl. Microbiol. Biotechnol., 66, 356–366

Guth E. and Diaz A., (1974). Method for Removing Sulfur and Nitrogen in Petroleum Oils. US Patent 3847800

Halstead C.J. and Thrush B.A., (1966). The Kinetics of Elementary Reactions Involving the Oxides of Sulphur. II. Chemical Reactions in the Sulphur Dioxide Afterglow. Proceedings of the Royal Society of London, 295(1443):363-379.

Harvey W.S., Davidson J. H., and Fletcher E.A., (1998). Thermolysis of Hydrogen Sulfide in the Temperature Range 1350-1600K. Industrial and Engineering Chemistry Research, 37(6):2323-2332.

Hawboldt K.A., Monnery W.D. and Svrcek W.Y., (2000). New Experimental Data and Kinetic Rate Expression for H_2S Pyrolysis and Re-association. Chemical Energy Science, 55(5):957-66.

Hedley A.B., (1967). Factors Affecting the Formation of Sulphur Trioxide in Flame Gases," Journal of the Institute of Fuel, 40:142-151.

Hernandez J. and Yang R. T., (2004). New Sorbents for Desulfurization of Diesel Fuels via Π-Complexation. AIChE J., 50:791–801.

Hippler H., Reihs C. and Troe J., (1990). Elementary Steps in the Pyrolysis of Toluene and Benzyl Radicals. Zeitschrift für Physikalische Chemie, 167(Part1), 1-16.

Hirasawa T., Sung C.J., Joshi A., Yang Z., Wang H. and Law C.K., (2002). Determination of Laminar Flame Speeds Using Digital Particle Image Velocimetry: Binary Fuel Blends Of Ethylene, N-Butane, And Toluene. Proceedings of the Combustion Institute, 29:1427–1433.

Hughes K.J., Tomlin A.S., Dupont V.A., and Pourkashanian M., (2001). Experimental and Modelling Study of Sulfur and Nitrogen Doped Premixed Methane Flames at Low Pressure. Faraday Discussions, 119:337-352.

Hughes K.J., Blitz M.A., Pilling, M.J. and Robertson S.H., (2002). A Master Equation Model for the Determination of Rate Coefficients in the $H+SO_2$ Systems. Proceedings of the Combustion Institute, 29(2):2431-2437.

Hui X., Das A., Kumar K., Sung C., Dooley S. and Dryer F., (2012). Laminar Flame Speeds and Extinction Stretch Rates of Selected Aromatic Hydrocarbons. Fuel. 97:695–702.

Jackson J.L., (1951). Spontaneous Ignition Temperatures. Industrial and Engineering Chemistry, 43:2869-2870.

Jensen A.B. and Webb C., (1995). Treatment of H2S-containing Gases: A Review of Microbiological Alternatives. Enzyme and Microbial Technology, 17: (1)2-10.

Ji C., Dames E., Wang Y.L., Wang H. and Egolfopoulos F.N., (2010). Propagation and Extinction of Premixed C_5-C_{12} n-Alkane Flames. Combustion and Flame, 157:277–287.

Ji C. and Egolfopoulos F.N., (2011). Flame Propagation of Mixtures of Air with Binary Liquid Fuel Mixtures. Proceedings of the Combustion Institute, 33:955–961.

Ji C., Dames E., Wang H. and Egolfopoulos F. N., (2012). Propagation and Extinction of Benzene and Alkylated Benzene Flames. Combustion and Flame, 159:1070-1081

John S.E., (2002). Recovery of Sulfur from Sour Acid Gas: A Review of the Technology. Environmental Progress, 21(3):143-162.

Johnston R.J. and Farrell J.T., (2005). Laminar Burning velocities and Markstein Lengths of Aromatics at Elevated Temperature and Pressure. Proceedings of the Combustion Institute, 30:217-224.

Kaloidas V. and Papayannakos N., (1989). Kinetics of Thermal, Non-Catalytic Decomposition of Hydrogen Sulphide. Chem. Eng. Sci., 44:2493-2500.

Karan K., (1998a). An Experimental and Modeling Study of Homogenous Gas Phase Reactions Occurring in the Modified Claus Process, in PhD Thesis,

Department of Chemical and Petroleum Engineering, University of Calgary, Calgary.

Karan K., Mehrotra A.K. and Behie L.A., (1998b). COS-Forming Reaction between CO and Sulfur: A High-Temperature Intrinsic Kinetics Study. Industrial & Engineering Chemistry Research, American Chemical Society, 4609-4616.

Karan K. and Behie L.A., (2004). CS_2 Formation in the Claus Reaction Furnace: A Kinetic Study of Methane-Sulfur and Methane-Hydrogen Sulfide Reactions. Industrial & Engineering Chemistry Research, American Chemical Society, 3304-3313.

Khudenko B.M., Gitman G.M. and Wechsler E.P., (1993). Oxygen Based Claus Process for Recovery of Sulfur from H2S Gases. Journal of Environmental Engineering, 119(6):1233- 1251.

Klotz S.D., Brezinsky K. and Glassman I., (1998). Modelling the Combustion of Toluene-Butane Blends. Proceedings of Combustion Institute, 27:337-344.

Kohl A. and Nielsen R., (1997). Gas Purification, Gulf Publishing Company, Houston TX,

Lannuzel F., Bounaceur R., Michels R., Scacchi G. and Marquaire P., (2010). An Extended Mechanism Including High Pressure Conditions (700bar) for Toluene Pyrolysis. J. Anal. Appl. Pyrolysis, 87:236–247.

Laskin A. and Lifshitz A., (1996). Thermal Decomposition of Benzene: Single Pulse Shock-Tube Investigation. Proceedings of Combustion Institute, 26:669.

Leeds University, (2002). Sulfur mechanism extension to the Leeds methane mechanism. http://www.chem.leeds.ac.uk/combustion/sox.htm.

Levy A. and Merryman E.L., (1965). The Microstructure of Hydrogen Sulphide Flames. Combustion and Flame, 9(3):229-240.

Lewis M. and White J.U., (1966). The Band Spectrum of SH. Physical Review, 55(10):894-898.

Li Y., Zhang L., Tian Z., Yuan T., Wang J., Yang B. and Qi F., (2009). Experimental Study of a Fuel-Rich Premixed Toluene Flame at Low Pressure. Energy Fuels, 23:1473–1485.

Li Y., Zhang L., Yuan T., Zhang, K., Yang J., Yang B. and Law C.K. (2010). Investigation on fuel-rich premixed flames of monocyclic aromatic hydrocarbons: Part I. Intermediate identification and mass spectrometric analysis. Combustion and Flame, 157(1), 143-154.

Li Y., Cai J., Zhang L., Yuan T., Zhang K. and Qi F., (2011). Investigation on Chemical Structures of Premixed Toluene Flames at Low Pressure. Proceedings of the Combustion Institute, 33:593–600.

Lindstedt R.P. and Maurice L.Q., (1996). Detailed Kinetic Modeling of Toluene Combustion. Combustion Science and Technology, 120(1–6):119–167.

Lindstedt R.P. and Skevis G., (1994). Detailed Kinetic Modeling of Premixed Benzene Flames. Combustion and Flame, 99(3), 551-561.

Liuti G., Dondes S. and Harteck P., (1966). The Reaction of Hydrogen Sulfide and Atomic Oxygen. Journal of the American Chemical Society, 88(14):3212-3215.

Loftus J. and Satterfield C.N., (1965). Mechanism of Homogeneous Gas-phase partial Oxidation of o-Xylene. Journal of Physical Chemistry, 69:909-918.

Lovell W.G., Campbell J.M. and Boyd T.A., (1934). Knocking Characteristics of Hydrocarbons Determined from Compression Ratios at Which Individual Compounds Begin to Knock Under Specified Conditions. Industrial and Engineering Chemistry, 26:1105-1108.

Lovell A.B., Brezinsky K. and Glassman I., (1988). Benzene Oxidation Perturbed by NO_2 Addition. Proceedings of Combust Institute, 22:1063-1074.

Luinstra E.A. and D'Haene P.E., (1989). Catalyst added to Claus Furnace reduces Sulfur Losses. Hydrocabon Processing, 68.

Manenti F., Papasidero D. and Ranzi E., (2013). Revised Kinetic Scheme for Thermal Furnace of Sulfur Recovery Units. Chemical Engineering Transactions, 1285-1290.

Merryman E.L. and Levy A., (1967). Kinetics of Sulfur-Oxide Formation in Flames: II. Low Pressure H_2S Flames. Journal of the Air Pollution Control Association, 17(12): 800-806.

Merryman E.L. and Levy A., (1969). Sulfur-Oxide Formation in Carbonyl Sulfide Flames, Environmental Science and Technology, 3(1):63-68.

Merryman E.L. and Levy A., (1971). Sulfur Trioxide Flame Chemistry-H_2S and COS Flames. Symposium (International) on Combustion, 13(1):427-436.

Merryman E.L. and Levy A., (1972). Disulfur and the Lower Oxides of Sulfur in Hydrogen Sulfide Flames. The Journal of Physical and Colloid Chemistry, 76(14):1925-1931.

Merryman E.L. and Levy A., (1979). Enhanced SO_3 Emissions from Staged Combustion. Symposium (International) on Combustion, 17(1):727-736.

Metcalfe W.K., Dooley S. and Dryer F.L., (2011). Comprehensive Detailed Chemical Kinetic Modeling Study of Toluene Oxidation. Energy Fuel, 25:4915–36.

Michael J.G. and Bruce C.C., (1991). Reactivities, Reaction Networks and Kinetics in High-Pressure Catalytic Hydroprocessing. Ind. Eng. Chem. Res., 30:2021–2058.

Mittal G. and Sung C.J., (2007). Auto-ignition of Toluene and Benzene at Elevated Pressures in a Rapid Compression Machine. Combustion and Flame, 150:355–368.

Monnery W.D., Hawboldt K.A., Pollock A. and Svrcek W.Y., (2000). New Experimental Data and Kinetic Rate Expression for the Claus Reaction. Chemical Engineering Science, 55(21):5141-5148.

Monnery W.D., Hawboldt K.A., Pollock A. and Svrcek W.Y., (2001). Ammonia Pyrolysis and Oxidation in the Claus France. Industrial and Engineering Chemistry Research, 40(1):144-151.

Montoya A., Sendt K. and Haynes B.S., (2005). Gas-Phase Interaction of H_2S with O_2: A Kinetic and Quantum Chemistry Study of the Potential Energy Surface. Journal of Physical and Colloid Chemistry, 109(6):1057-1062.

Mulcahy M.F.R. and Williams D.J., (1970). Chemiluminescent Emission from the O (3P)-SO2 System. Chemical Physics Letters, 7(4):455-458.

Muller III C.H., Schofield K., Steinberg M. and Broida H. P., (1979). Sulfur Chemistry in Flames. Symposium (International) on Combustion, 17(1): 867-879.

Muller III C.H., Schofield K. and Steinberg M., (1980). Laser-Induced Fluorescence: A Powerful Tool for the Study of Flame Chemistry. ACS Publications, Washington DC, Vol. 134, ISBN13: 9780841205703, Laser Probes for Combustion Chemistry: Chapter 2:103.

Murakami Y., Ogushi T., Hashimoto K. and Nosaka Y., (2007). Theoretical Study of the Benzyl + O_2 Reaction: Kinetics, Mechanism, and Product Branching Ratios. J. Phys. Chem. A., 111:13200-13208.

Narayanaswamy K., Blanquart G. and Pitsch H., (2010). A Consistent Chemical Mechanism for Oxidation of Substituted Aromatic Species. Combustion and Flame, 157:1879–1898.

Nasato L.V., Karan K., Mehrotra A.K. and Behie, L. A., (1994). Modeling Reaction Quench Times in the Waste Heat Boiler of a Claus Plant. Ind. Eng. Chem. Res., 33:7-13.

Natelson R.H., (2010). Pre-ignition and Auto-ignition Behavior of the Xylene Isomers, MSc. Thesis, Drexel University, Philadelphia, PA.

Natelson R.H., Kurman M. S., Johnson R. O., Cernansky N. P. and Miller, D. L. (2011). Preignition and Autoignition Chemistry of the Xylene Isomers. Combustion Science and Technology, 183(9), 897-914.

Nehlsen J.P., (2006). Developing Clean Fuels: Novel Techniques for Desulfurization. Ph.D. Dissertation, Princeton University.

Norrish R.G.W. and Zeelenberg A. P., (1957). The combustion of Hydrogen Sulphide Studied by Flash Photolysis and Kinetic Spectroscopy. Proceedings of the Royal Society of London, 240(1222):293-303.

Norrish R.G.W. and Rideal E.K., (1923). The Conditions of Reaction of Hydrogen with Sulfur. Part I. Direct Union. J. Chem. SOC1., 123,696-705.

OSHA, www.osha.gov/SLTC/etools/oilandgas/general_safety/general_safety.html

Otsuki S., Nonaka T., Takashima N., Qian W.H., Ishihara A., Imai T. and Kabe T., (2000). Oxidative Desulfurization of Light Gas Oil and Vacuum Gas Oil by Oxidation and Solvent Extraction. Energy Fuels, 14:1232-1239

Pamidimukkala K., Kern R., Patel M., Wei H. and Kiefer J., (1987). High-Temperature Pyrolysis of Toluene. J. Phys. Chem., 91:2148–2154.

Pearse R.W.B. and Gaydon A. G., (1963). The Identification of Molecular Spectra. Chapman and Hall Ltd., London, 3rd Edition.

Pengloan G., Dagaut P., Djebaıli-Chaumeix N., Paillard C.E. and Cathonnet M., (2001). Colloque Combustion Propre, Orleans, 6-8 June.

Pierucci S., Ranzi E. and Molinari L., (2004). Modeling a Claus Reaction Furnace via a Radical Kinetic Scheme. European Symposium on Computer-Aided Process Engineering, 463-468.

Rameshni. M., (2010). Dealing with Impurities in Sour Gas Field Developments. Sulfur 2010 International Conference, Prague November.

Randall M. and Bichowsky R., (1918). Equilibrium in the Reaction between Water and Sulfur at High Temperatures. The Dissociation of Hydrogen Sulfide. J. Am. Chem. SOC. 40: 368-375.

Ranzi E., Frassoldati A., Grana R., Cuoci A., Faravelli T., Kelley A. P. and Law, C.K., (2012). Hierarchical and Comparative Kinetic Modeling of Laminar

Flame Speeds of Hydrocarbon and Oxygenated Fuels. Progress in Energy and Combustion Science, 38(4):468-501.

Raymont M.E.D., (1974). The Thermal Decomposition of Hydrogen Sulphide. Ph.D. Thesis, University of Calgary, Calgary, AB, Canada.

Raymont M.E.D., (1975). Role of Hydrogen in Claus Plants. Hydrocarbon Processing, 54: 177-179.

Richter H. and Howard J.B., (2000). Formation of Polycyclic Aromatic Hydrocarbons and Their Growth to Soot-A Review of Chemical Reaction Pathways. Progress in Energy and Combustion Science, 26(4): 565-608.

Richter H. and Howard J.B., (2002). Formation and Consumption of Single-ring Aromatic Hydrocarbons and their Precursors in Premixed Acetylene, Ethylene and Benzene Flames. Physical Chemistry Chemical Physics, 4(11): 2038-2055.

Ristori A., Dagaut P., Bakali A. E., Pengloan G. and Cathonnet M., (2001). Benzene Oxidation: Experimental Results in a JDR and Comprehensive Kinetic Modeling in JSR, Shock-Tube and Flame. Combustion Science and Technology, 167(1):223-256.

Roubaud A., Minetti R. and Sochet L.R., (2000a). Oxidation and Combustion of Low Alkylbenzenes at High Pressure: Comparative Reactivity and Auto-Ignition. Combustion and Flame, 121:535-541.

Roubaud A., Lemaire O., Minetti R. and Sochet L.R., (2000b). High-Pressure Auto-Ignition and Oxidation Mechanisms of O Xylene, O-Ethyltoluene and N-Butylbenzene between 600 And 900K. Combustion and Flame, 123:561-571.

Sakai Y., Inamura T., Ogura T., Koshi M. and Pitz W.J., (2007a). Detailed Kinetic Modeling of Toluene Combustion over a Wide Range of Temperature and Pressure. SAE 2007-01-1885.

Sakai Y., Ozawa H., Ogura T., Miyoshi A., Koshi M. and Pitz W.J., (2007b). Effects of Toluene Addition to Primary Reference Fuel at High Temperature. SAE, 2007-01-4104.

Sakai Y., Miyoshi A., Koshi M. and Pitz W.J., (2009). A Kinetic Modeling Study on the Oxidation of Primary Reference Fuel–Toluene Mixtures Including Cross Reactions between Aromatics and Aliphatics. Proceedings of Combustion Institute, 32:411–418.

Sames J., Paskall A.H.C., Brown D.M., Chen M.S.K. and Sulkowski D., (1990). Field Measurements of Hydrogen Production in an Oxygen-Enriched Claus Furnace. Proc. Sulfur 1990 Intl. Conf., Cancun, Mexico,, British Sulphur Corp., UK, April 14, 89-105.

Sassi M. and Gupta A.K., (2008a). Sulfur Recovery from Acid Gas Using the Claus Process and High Temperature Air Combustion (HiTAC) Technology, American Journal of Environmental Sciences, 4 (5): 502-511.

Selim H., Gupta A.K. and Sassi M., (2008b). Variation of Optimum Claus Reactor Temperature with Acid Gas Composition. 6th International Energy Conversion Engineering Conference (IECEC), Cleveland, OH, July 28-30, AIAA-2008-5797.

Selim H., Al Shoaibi A., Gupta A.K., (2011a). Effect of H2S in Methane/air flames on Sulfur Chemistry and Products Speciation. Journal of Applied Energy, 88(8): 2593-2600.

Selim H., Al Shoaibi A., Gupta A.K., (2011b). Experimental Examination of Flame Chemistry in Hydrogen-sulfide Based Flames. Journal of Applied Energy, 88(260):2601-2611.

Selim H., Gupta A.K., and Al Shoaibi A., (2012a). Novel Error Propagation Approach for Reducing H_2S/O_2 Reaction Mechanism. Journal of Applied Energy, 116-124.

Selim H., Al Shoaibi A. and Gupta A.K., (2012b). Effect of CO_2 and N_2 Concentration in Acid Gas Stream on H2S Combustion. Journal of Applied Energy, 98: 53-58.

Selim H., (2012c). Characteristics and Chemical Kinetics of Hydrogen Sulfide Combustion in Thermal Claus Reactor, Mechanical Engineering, PhD Dissertation Thesis, University of Maryland

Selim H., Gupta A.K., AlShoaibi A., (2013). Effect of Reaction Parameters on the Quality of Captured Sulfur in Claus Process. Journal of Applied Energy, 104: 774-776.

Selim H., Ibrahim S., AlShoaibi A., Gupta A.K., (2014). Investigation of Sulfur Chemistry with Acid Gas Addition in Hydrogen/air Flames. Journal of Applied Energy, 113: 1134-11408.

Sendt K., Jazbec M., and Haynes B.S., (2002). Chemical Kinetic Modeling of the H/S Systems: H_2S Thermolysis and H_2 Sulfidation. Proceedings of the Combustion Institute, 29(2):2439-2446.

Shandross R.A., Longwell J.P. and Howard J.B., (1996). Destruction of Benzene in High-Temperature Flames: Chemistry of Benzene and Phenol. Symposium (International) on Combustion. The Combustion Institute, 26(1):711-719.

Sharma A., Padur J.P. and Warneck P., (1967). The Chemiluminescent Reactions of Atomic Oxygen with Carbonyl Sulfide and Hydrogen Sulfide. The Journal of Physical Chemistry, 71(6):1602-1607.

Shen H.P.S. and Oehlschlaeger M., (2009a). The Autoignition of C_8H_{10} Aromatics at Moderate Temperatures and Elevated Pressures. Combustion and Flame, 156:1053–1062.

Shen H.P.S., Vanderover J., Oehlschlaeger M.A., (2009b). A Shock Tube Study of the Auto-ignition of Toluene/Air Mixtures at High Pressures. Proceedings of Combustion Institute, 32:165–72.

Shukla B., Susa A., Miyoshi A. and Koshi M. (2007). In Situ Direct Sampling Mass Spectrometric Study on Formation of Polycyclic Aromatic Hydrocarbons in Toluene Pyrolysis. The Journal of Physical Chemistry A, 111(34):8308-8324.

Sileghem L., Alekseev V., Vancoillie J., Van Geem K., Nilsson E., Verhelst S. and Konnov A., (2013). Laminar Burning Velocity of Gasoline and the Gasoline Surrogate Components Iso-Octane, N-Heptane and Toluene. Fuel, 112:355–365.

Sivaramakrishnan R., Tranter R.S. and Brezinsky K., (2006a). High Pressure Pyrolysis of Toluene. I. Experiments and Modeling of Toluene Decomposition. J. Phys. Chem. A., 110:9388–9399.

Sivaramakrishnan R., Brezinsky K., Vasudevan H. and Tranter R.S., (2006b). A Shock-tube Study of the High-pressure Thermal Decomposition of Benzene. Combustion science and technology, 178(1-3):285-305.

Slavens A., Lamar J., O"Dell S. and Francoviglia L., (2010). Enhanced Sulfur Recovery from Lean Acid Gases Containing COS and Mercaptans. Laurence Reid Gas Conditioning Conference, Noman, Okhlahoma; 21-24 February.

Slimane R.B., Lau F.S., Khinkis M., Bingue J.P., Saveliev A.V. and Kennedy L.A., (2004). Conversion of Hydrogen Sulfide to Hydrogen by Superadiabatic Partial Oxidation: Thermodynamic Consideration. International Journal of Hydrogen Energy, 29(14):1471-1477.

Smith O.I., Tseregounis S. and Wang S., (1982). High-Temperature Kinetics of the Reactions of SO_2 and SO_3 with Atomic Oxygen. International Journal of Chemical Kinetics, 14(6):679-697.

Song C., (2002). Keynote: New Approaches to Deep Desulfurization for Ultra-clean Gasoline and Diesel Fuels: An Overview, Am. Chem. Soc., Div. Fuel Chem. Prepr., 47:438.

Song C.S., (2003). An Overview of New Approaches to Deep Desulfurization for Ultra-Clean Gasoline. Diesel Fuel and Jet Fuel. Catal. Today, 86:211-263.

Song C.S. and Ma X.L, (2004). Ultra-Deep Desulfurization of Liquid Hydrocarbon Fuels. Chemistry and Process. Int. J. Green Energy, 1:167-191.

Srivastava V. C., (2012). An Evaluation of Desulfurization Technologies for Sulfur Removal from Liquid Fuels. RSC Advances, 2:759–783

Sulfotech, http://sulfotech.tripod.com/claus.html

Tam P.S., Kittrell J.R. and Eldridge J.W., (2002). Desulfurization of fuel Oil by Oxidation and Extraction: Enhancement of Extraction Oil Yield. Ind. Eng. Chem. Res., 29:321-324.

Tan Y. and Frank P., (1996). A Detailed Comprehensive Kinetic Model for Benzene Oxidation using the Recent Kinetic Results. Proceedings Combustion Institute, 26:677-684.

Tawara K., Nishimura T., Iwanami H., Nishimoto T. and Hasuike T., (2001). New Hydrodesulfurization Catalyst for Petroleum-Fed Fuel Cell Vehicles and Cogenerations. Ind. Eng. Chem. Res., 40:2367–2370.

Toyoda M., Ogawa T. and Ishibashi N., (1974). Emission Spectra of Carbon Disulfide, Hydrogen Sulfide and Thoils by Controlled Electron Impact. Bulletin of the Chemical Society of Japan, 47:1:95-98.

Tsuchiya K., Kamiya K., and Matsui H., (1999). Studies on the Oxidation Mechanism of H_2S Based on Direct Examination of the Key Reactions. International Journal of Chemical Kinetics, 29(1):57-66.

Tyndall G., and Ravishankara, A. R., (1991). Atmospheric Oxidation of Reduced Sulfur Species. International Journal of Chemical Kinetics, 23(6):483-527.

Vasu S.S., Davidson D.F. and Hanson R.K., (2010). Shock-Tube Experiments and Kinetic Modeling of Toluene Ignition. Journal of propulsion and power, 26:4

Vasudevan V., Davidson D.F., and Hanson R.K., (2005a). Shock Tube Measurements of Toluene Ignition Times and OH Concentration Time Histories. Proceedings of the Combustion Institute, 30(1):1155–1163.

VasudevanV., Davidson D. F., and Hanson R. K., (2005b). High-Temperature Measurements of the Reactions of OH with Toluene and Acetone. Journal of Physical Chemistry A, 109(15):3352

Vourliotakis G., Skevis G. and Founti M.A., (2011). A Detailed Kinetic Modeling Study of Benzene Oxidation and Combustion in Premixed Flames and Ideal Reactors. Energy & Fuels, 25(5):1950-1963.

Wall D., (2013). A Higher Tier: Tier 3 Low Sulfur Gasoline Regulations and Their Effects. September, 2013 Issue of Hydrocarbon Engineering.

Wang H., Laskin A., Moriarty N.W. and Frenklach M., (2000). On Unimolecular Decomposition of Phenyl Radical. Proceedings of Combustion Institute, 28:1545.

Wayne R.O., (1985). Chemistry of Atmosphere: An Introduction to the Chemistry of the Atmosphere of Earth, the Planets, and Their Satelites. 1st edition, ISBN: 0198551754 ed. Oxford University Press, USA.

Won S.H., Dooley S., Dryer F.L. and Ju Y., (2011). Kinetic Effects of Aromatic Molecular Structures on Diffusion Flame Extinction. Proceedings of the Combustion Institute, 33:1163–1170.

Wright F.J., (1960). Gas phase Oxidation of the Xylenes: General Kinetics. Journal of Physical Chemistry 64:1944-1950.

Yuan W., Li Y., Dagaut P., Yang J. and Qi F., (2014). Investigation on the Pyrolysis and Oxidation of Toluene over a Wide Range Conditions. I. Flow Reactor Pyrolysis and Jet Stirred Reactor Oxidation, Combustion and Flame, *162*(1):3-21.

Zachariah M.R. and Smith O.I., (1987). Experimental and Numerical Studies of Sulfur Chemistry in H2/O2/SO2 Flame. Combustion and Flame, 69(2):125-139.

Zel'venskii Y.D., Nedumova E.S. and Prokopets V.E., (1961). The Preparation of Hydrogen Sulfide by the Catalytic Hydrogenation of Sulfur. Khim. Prom., 77-84.

Zhang H.Y. and McKinnon J.T., (1995). Elementary Reaction Modeling of High-Temperature Benzene Combustion. Combustion Science Technology, 107:261-300.

Zhang T., Zhang L., Hong X., Zhang K., Qi F, Law C., Ye T., Zhao P. and Chen Y., (2009). An Experimental and Theoretical Study of Toluene Pyrolysis with Tunable Synchrotron VUV Photoionization and Molecular-Beam Mass Spectrometry. Combustion and Flame, 156(11):2071-2083.

Zhang L., Cai J., Zhang T. and Qi F., (2010). Kinetic Modeling Study of Toluene Pyrolysis at Low Pressure. Combustion and Flame, 157(9):1686-1697.

Zhao L., Cheng Z., Ye, L., Zhang F., Zhang, L., Qi, F. and Li, Y. (2015). Experimental and kinetic modeling study of premixed o-xylene flames. Proceedings of the Combustion Institute, 35(2):1745-1752.